Développement d'un modèle cellulaire flexible tridimensionnel : un focus sur le cancer gastrique

George Alzeeb

THESE DE DOCTORAT DE

L'UNIVERSITE
DE BRETAGNE OCCIDENTALE

ECOLE DOCTORALE N° 605
Biologie Santé
Spécialité : Cancérologie

Par

George ALZEEB

Développement d'un Modèle Cellulaire Flexible Tridimensionnel : Un Focus sur le Cancer Gastrique

Development of a Flexible Three-Dimensional Cellular Model: Focus on Gastric Cancer

Thèse présentée et soutenue à Brest, le 28/01/2022
Unité de recherche : Génétique, Génomique Fonctionnelle et Biotechnologies Inserm UMR1078

Rapporteurs avant soutenance :

Ali BETTAIEB	Pr, EPHE, EA7269, Univ. Bourgogne Franche-Comté
Karine MAHEO	M. de Conf, Inserm 1069, Univ. Tours

Composition du Jury :

Président :	Sophie LANGOUET	DR, Inserm 1085, Irset, Univ. Rennes 1
Examinateurs :	Ali BETTAIEB	Pr, EPHE, EA7269, Univ. Bourgogne Franche-Comté
	Karine MAHEO	M. de Conf, Inserm 1069, Univ. Tours
Dir. de thèse :	Laurent CORCOS	DR, Inserm 1078, Univ. Brest, CHU Brest
Co-dir. de thèse :	Catherine LE JOSSIC-CORCOS	M. de Conf, Inserm 1078, Univ. Brest

Invité(s)

Valérie TRICHET	M. de Conf, Inserm 1238, Univ. Nantes
Yann LE GRAND	Pr, Optimag, Univ. Brest
Emmanuelle GENIN	DR, Inserm 1078, Univ. Brest, CHU Brest

Acknowledgments

First and foremost, praises and thanks to God for His showers of blessings throughout my whole life and to whom I owe my very existence. Glory to the Father, and to the Son, and to the Holy Spirit: now and ever and unto ages of ages.

Throughout the duration of this thesis, I have had the absolute honor of encountering wonderful people whom I would like to thank for partaking this journey with me.

First and foremost, I would like to thank all the members of the jury who have accepted to review my thesis, Pr. Ali Bettaieb and Pr. Karine Maheo for having accepted to be reporters of this thesis and Dr. Sophie Langouët, Dr. Valérie Trichet, Pr. Yann Le Grand and Dr. Emmanuelle Génin for having accepted the examination of the manuscript.

I would like to especially thank Dr. Laurent Corcos and Dr. Catherine Le Jossic-Corcos for their wise and concise direction of this thesis. Thank you Laurent for entrusting me with this responsibility and for being there to guide me and offer me precious advice. Thank you Cathy for the motivational boosts throughout the years. Thank you both for all your help, advices, support and kindness on a professional and personal level.

This thesis took place at the laboratory of Genetics, Functional Genomics and Biotechnologies (GGFB), which became my second home during my PhD. Therefore, I would like to thank Dr. Emmanuelle Génin, the director of GGFB, for hosting this thesis. Sophie, thanks for your help during these years.

I would like to thank all of the collaborators who have contributed fruitfully to this work through their scientific expertise: Dr. Olivier Mignen, Dr. Christophe Brigaudeau and Dr. Nelig Le Goux from the immunology lab, university of Brest. Dr. Yann Le Grand, Dr. Matthieu Dubreuil and Dr. Sylvain Rivet from the Optimag lab, university

of Brest. Dr. Stéphane Cérantola from the NMR platform, university of Brest. Dr. Floriant Bellvert, Nina Lager-Lachaud, Noémie Butin from the MetaToul lab and Dr. Matthieu Talagas from CHRU Brest.

I would like to thank everyone working at GGFB for their aid and assistance especially the members of the ECLA team: Dr. Marie-Bérengère Troadec, Dr. Eric Lippert, Dr. Délephine Bernard and Dr. Cédric Le Marechal. Thank you all for your support, advices and discussions. A special thanks to Danielle and Brigitte for the invaluable help you give us on a daily basis, for all your kind words of support and encouragement and for your scientific aid. Sévrine and Gaëlle thank you for all the interesting discussions, scientific aid and the memories shared in the break room.

I would like to thank all my current and past colleagues in the ECLA team for all their aid, support and shared memories. Tiffany, thank you for all your help throughout my thesis, and good luck in your current postdoc in London!! Special thanks to Marie and Benoit! Thanks for all your encouragement! all the memories, your humor, impulsiveness and kindness. Jian, thank you for all the hilarious moments, for your sympathy and kindness. Thank you for all your scientific and personal aid. Enora and Solène all the best for your thesis. Thank you for all the positive energy you diffuse through the lab.

This work could not have been carried out without the availability and good understanding of all members of the ECLA team. MERCI!

Thank you to Dr. Philipe Soubeyran, director of my M2 internship at CRCM-Marseille, for all the opportunities and expertise that you shared with me that eventually led me here.

I would like to thank my friends outside of the work environment.

Dr. Ghassan, thank you for being a brother of mine, supporting and helping me since 8 years now. I will cherish all the awesome adventures we've shared; the next step will be*

to explore new countries. Special thanks to Marc, Dr. George and Dr. Abir! Thank you for all the memories and good times, I hope to see you soon. Clara and Jessy, thank you for all the great times. Fabien, Johnathan and Joe, thanks for your support and your presence 'Marseille Boys'! I wish you all the best for your future ventures. A very very special thanks for Père Issam for being there for all of us and for all the great times and memories we had. Chahine & Marina, thank you for your help and support.

A very big thank you to my "Brest" friends for their help in my new city, Ramy, Ramez, Hassan, Souha, Sara!

A special thanks for all my hometown friends "Hammana" for their encouragement and support throughout the years, Amoulaa, Najo, Raymond, Mike², Fady, Sandra, George!!

I would like to thank Marie-Ange, for supporting me. Thanks for your presence!

I would like to thank my family to whom I am eternally grateful. If it weren't for their love and support, I wouldn't have reached where I am now. Thank you, my Dad Bassam and my Mom Eva, for your unconditional support, love, prayers, the consistent boosting and for your patience. I miss you and I pray to see you soon. Thank you to my sister, Siham, for your presence, support patience and help! Thank you for being my number one!

George

Remerciements

D'abord et avant tout, des louanges et des remerciements à Dieu pour ses bénédictions tout au long de ma vie et à qui je dois mon existence. Gloire au Père, et au Fils, et au Saint-Esprit. Comme il était au commencement, maintenant et toujours, et dans les siècles des siècles.

Tout au long de cette thèse, j'ai eu l'honneur absolu de rencontrer des personnes merveilleuses que je tiens à remercier d'avoir pris part de cette mission.

Tout d'abord, je tiens à remercier tous les membres du jury qui ont accepté d'examiner ma thèse, Pr. Ali Bettaieb et Pr. Karine Maheo pour avoir accepté d'être rapporteurs de cette thèse, Dr. Sophie Langouët, Dr. Valérie Trichet, Pr. Yann Le Grand et Dr. Emmanuelle Génin pour avoir accepté d'examiner ce manuscrit.

Je remercie tout particulièrement Dr. Laurent Corcos et Dr. Catherine Le Jossic-Corcos pour la direction avisée et concise de cette thèse. Merci Laurent de m'avoir confié cette responsabilité et d'être présent pour me guider et m'offrir de précieux conseils. Merci Cathy pour les coups de pouce motivants tout au long de ces années. Merci à tous les deux pour votre aide, vos conseils, votre soutien et votre gentillesse professionnelle et personnelle.

Cette thèse s'est déroulée au sein de laboratoire de Génétique, Génomique Fonctionnelle et Biotechnologies (GGFB), qui est devenu ma seconde maison durant mon doctorat. Je tiens à remercier Dr. Emmanuelle Génin, directrice du GGFB, pour m'avoir accueilli. Sophie je te remercie pour ton aide durant ces années.

Je tiens à remercier tous les collaborateurs qui ont contribué de manière fructueuse à ce travail par leur expertise scientifique : Dr. Olivier Mignen, Dr. Christophe Brigaudeau et Dr. Nelig Le Goux du laboratoire d'immunologie de l'université de Brest. Dr. Yann Le Grand, Dr. Matthieu Dubreuil et Dr. Sylvain Rivet du laboratoire Optimag de l'université de Brest. Dr Stéphane Cérantola de la plateforme RMN de

l'université de Brest. Dr. Floriant Bellvert, Nina Lager-Lachaud, Noémie Butin du laboratoire MetaToul. Dr. Matthieu Talagas du CHRU de Brest.

Je tiens à remercier tous ceux qui travaillent au labo GGFB pour leur aide et leur assistance, en particulier les membres de l'équipe ECLA : Dr. Marie-Bérengère Troadec, Dr. Eric Lippert, Dr. Délephine Bernard et Dr. Cédric Le Marechal. Merci à tous pour votre soutien, vos conseils et vos discussions. Un merci particulier à Danielle et Brigitte pour l'aide précieuse que vous m'avez apporté au quotidien, pour tous vos mots de soutien et d'encouragement et pour votre aide scientifique. Sévrine et Gaëlle merci pour toutes les discussions intéressantes, l'aide scientifique et les souvenirs partagés dans la salle de pause.

Je tiens à remercier tous mes collègues de l'équipe ECLA pour leur aide, leur soutien et les souvenirs partagés. Dr. Tiffany, merci pour ton aide tout au long de ma thèse, et bonne chance dans ton postdoc actuel à Londres ! Un grand merci à Marie et Benoit ! Merci pour tous vos encouragements, tous les souvenirs, votre humour, votre impulsivité et votre gentillesse. Jian, merci pour tous les moments hilarants, pour ta sympathie et ta gentillesse. Merci pour votre aide scientifique et personnelle. Enora et Solène, bonne chance pour votre thèse. Merci pour l'énergie positive que vous diffusez dans le laboratoire.

Ce travail n'aurait pas pu être mené à ce niveau sans la disponibilité et la bonne entente de tous les membres de l'équipe ECLA. MERCI !

Merci Dr. Philipe Soubeyran, directeur de mon stage de M2 au CRCM-Marseille, pour toutes les opportunités et l'expertise que vous avez partagées avec moi et qui m'ont finalement conduit ici.

Je tiens à remercier mes amis en dehors du milieu professionnel.

Dr Ghassan, merci d'être mon frère, de me soutenir et de m'aider depuis 8 ans maintenant. Je chérirai toutes les aventures géniales que nous avons partagées ; la*

prochaine étape sera d'explorer de nouveaux pays. Un grand merci à Marc, au Dr. George et au Dr. Abir ! Merci pour tous ces souvenirs et ces bons moments, j'espère vous revoir bientôt. Clara et Jessy, merci pour tous ces bons moments. Fabien, Johnathan et Joe, merci pour votre soutien et votre présence 'Marseille Boys' ! Je vous souhaite le meilleur pour vos futurs projets. Un remerciement très très spécial au Père Issam pour avoir été là pour nous et pour les bons moments et souvenirs que nous avons eus. Chahine & Marina, merci pour votre aide et votre soutien.

Un très grand merci à mes amis "brestois" pour leur aide dans ma nouvelle ville, Ramy, Ramez, Hassan, Souha, Sara !

Un merci spécial pour tous mes amis de ma ville natale "Hammana" pour m'encourager et me soutenir tout au long de ces années, Amoulaa, Najo, Raymond, Mike, Fady, Sandra !!!

Je voudrais remercier Marie-Ange, de m'avoir soutenu. Merci pour ta présence !

Je voudrais remercier ma famille à qui je suis éternellement reconnaissant. Sans leur amour et leur soutien, je ne serais jamais arrivé là où je suis maintenant. Merci, mon père Bassam et ma mère Eva, pour votre soutien inconditionnel, votre amour, vos prières, vos encouragements constants et votre patience. Vous me manquez et je prie de vous voir bientôt. Merci ma sœur, Siham, pour ta présence, ton soutien, ta patience et ton aide ! Merci d'être mon numéro un!

George

Abbreviations

2D	Two-Dimensional
3D	Three-Dimensional
ACRG	Asian Cancer Research Group
AEG	Adenocarcinomas of the Esophagogastric Junction
AJCC	American Joint Committee on Cancer
APC	Adenomatous Polyposis Coli
ASR	Age-Standardized
αSMA	Alpha Smooth Muscle Actin
BMDC	Bone Marrow-Derived Cells
CAF	Cancer-Associated Fibroblasts
CCL	Cancer Cell Line
CDH1	Cadherin-1
CIN	Chromosomal Instable
CSC	Cancer Stem Cells
CTLA	Cytotoxic T Lymphocyte Antigen-4
DMEM	Dulbecco's Modified Eagle's Medium
DMSO	Dimethyl-Sulfoxide
EBV	Epstein-Barr Virus
ECM	Extracellular Matrix
EGF	Epidermal Growth Factor
eGFP	enhanced Green Fluorescent Protein
EMT	Epithelial-Mesenchymal Transition
FAP	Fibroblast Activation Protein
FBS	Fetal Bovine Serum
FDA	Food and Drug Administration
FGF	Fibroblast Growth Factor
GAC	Gastric Adenocarcinomas
GAPDH	Glyceraldehyde-3-Phosphate Dehydrogenase
GC	Gastric Cancer
GEJ	Gastroesophageal Junction
GGPP	Geranylgeranyl Pyrophosphate
GS	Genomically Stable
HDGC	Hereditary Diffuse Gastric Cancer
poly-HEMA	Poly-2-Hydroxyethyl Methacrylate
HER2	Human Epidermal Growth Factor Receptor-2
HMG-CoA Red	3-Hydroxy-3-Methyl-Glutaryl-Coenzyme A Reductase

IARC	International Agency for Research on Cancer
ICI	Immune Checkpoint Inhibitors
IGF	Insulin-like Growth Factor
IL	Interleukin
ITG	Integrin
MCTS	Multicellular Tumor Spheroids
MDSC	Myeloid-Derived Suppressor Cells
MLH1	MutL Homolog 1
MMR	Mismatch Repair
MSC	Mesenchymal Stem Cells
MSH2	MutS Homolog 2
MSI	Microsatellite Instable
MSS	Microsatellite Stable
MTT	3-(4,5-dimethylthiazol-2-yl)-2,5-diphenyltetrazolium bromide
NCI	National Cancer Institute
NK	Natural Killer
NTC	No Template Control
PBO	Placebo
PD-1	Programmed Cell Death-1
PDGF	Platelet-Derived Growth Factor
PD-L1	Programmed Cell Death-Ligand1
PDTO	Patient-Derived Tumor Organoids
PDX	Patient-Derived Xenograft
hPSC	Human Pluripotent Stem Cells
ROS	Reactive Oxygen Species
SHG	Second Harmonic Generation
TCGA	The Cancer Genome Atlas
TGF-ß	Transforming Growth Factor-β
TME	Tumor Microenvironment
TNF	Tumor Necrosis Factor
TNM	Tumor, Nodes, and Metastases
TP53	Tumor Protein P53
TPEF	Two-Photon Excitation Fluorescence
ULA	Ultra-Low Attachment
VEGF	Vascular Endothelial Growth Factor
VEGFR	Vascular Endothelial Growth Factor Receptor
WHO	World Health Organization

Foreword

With over 19.3 million new cases diagnosed worldwide and almost 10 million deaths in 2020, cancer remains a particularly deadly disease that imposes a global health burden (Figure i). Currently, lung cancer is the leading cause of all cancer deaths (25.1%) [1]. According to the report of the International Agency for Research on Cancer (IARC) on February 4th 2020, cancer is now the most common form of death worldwide only second to heart disease [2]. The World Health Organization (WHO) estimates that cancer deaths will see a 60% increase over the next two decades to reach around 16 million deaths in 2040, if current trends continue [3].

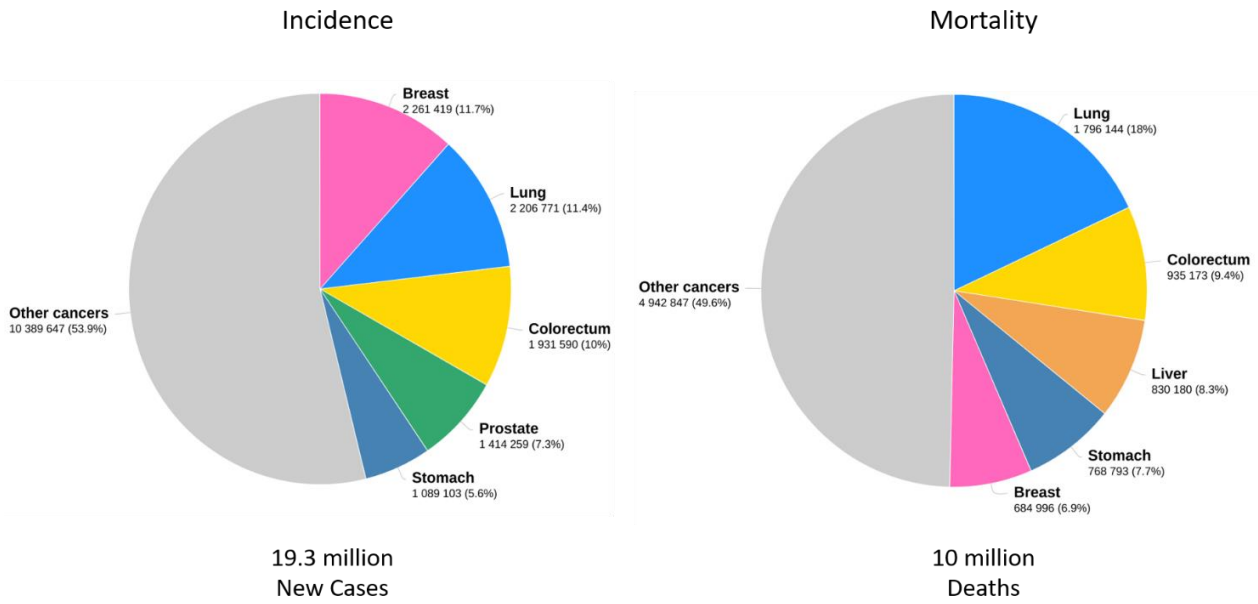

Figure i. The top 5 cancers with highest incidence and mortality worldwide in 2020. Estimated percentages of new cancer cases and cancer deaths cover all ages, all cancers and both sexes. From http://gco.iarc/survival/survmark

To minimize the risk of cancer, changes in lifestyle are highly recommended. These include abandoning smoking, adopting a healthy diet, maintaining a recommended body-mass index, avoiding excessive UV exposure and acquiring appropriate vaccinations [4]. Early and accurate diagnoses are vitally important to improve the survival rate. Once a patient has been diagnosed with cancer, eight possible treatment options are available listed by the National Cancer Institute (NCI): surgery, chemotherapy, radiation therapy, immunotherapy, targeted therapy, stem cell transplant, hormone therapy and precision medicine [5]. However, most cancer patients experience symptoms at late stages of the disease, with a delay in the diagnosis, which narrows the range of treatment options and their efficacy. Such is the case of gastric cancer (GC), to which this thesis is dedicated [6].

Currently, only one potential anti-cancer agent out of 5 000 to 10 000 is approved by the Food and Drug Administration (FDA) and only 5% of therapeutic molecules entering phase I clinical trials are ultimately approved [7]. One of the major challenges in the development of new cancer treatments is the transfer of important advances from «bench to bedside» [8].

This thesis is dedicated to GC, also named stomach cancer. I mainly discuss the development of a flexible three-dimensional (3D) culture system named spheroid as a complex GC model. During the thesis, this model was first characterized and next served to study cancer cells toxicity of an adjuvant drug candidate for repurposing in the treatment of GC. Such a 3D culture model will also be used to understand the organization of distinct cell types cohabitating within 3D structures using laser microscopy.

References

[1] H. Sung *et al.*, "Global cancer statistics 2020: globocan estimates of incidence and mortality worldwide for 36 cancers in 185 countries," *CA. Cancer J. Clin.*, vol. 71, no. 3, pp. 209–249, May 2021, doi: 10.3322/caac.21660.

[2] [Book] C. P. Wild, E. Weiderpass, and B. W. Stewart, *World Cancer Report: Cancer Research for Cancer Prevention*, vol. 199. 2020.

[3] "WHO outlines steps to save 7 million lives from cancer," Feb. 2020. https://www.who.int/news/item/04-02-2020-who-outlines-steps-to-save-7-million-lives-from-cancer.

[4] "Cancer prevention: 7 tips to reduce your risk - Mayo Clinic." https://www.mayoclinic.org/healthy-lifestyle/adult-health/in-depth/cancer-prevention/art-20044816.

[5] "Types of Cancer Treatment - National Cancer Institute." https://www.cancer.gov/about-cancer/treatment/types.

[6] E. C. Smyth, M. Nilsson, H. I. Grabsch, N. C. van Grieken, and F. Lordick, "Gastric cancer," *The Lancet*, vol. 396, no. 10251. Lancet Publishing Group, pp. 635–648, Aug. 29, 2020, doi: 10.1016/S0140-6736(20)31288-5.

[7] Z. Zhang *et al.*, "Overcoming cancer therapeutic bottleneck by drug repurposing," *Signal Transduct. Target. Ther.*, vol. 5, no. 1, pp. 1–25, Jul. 2020, doi: 10.1038/s41392-020-00213-8.

[8] A. Ocana, A. Pandiella, L. L. Siu, and I. F. Tannock, "Preclinical development of molecular-targeted agents for cancer," *Nat. Rev. Clin. Oncol.*, vol. 8, no. 4., pp. 200–209, Apr. 2011, doi: 10.1038/nrclinonc.2010.194.

Chapter I
Gastric Cancer

I.1. Epidemiology, Incidence and Risk Factors

Gastric cancer (GC) is an important contributor to the global burden of cancer [1]. Less than a century ago, it was the most common cancer in the world [2]. According to data from Global Cancer Statistics in 2020, GC is the fifth most commonly diagnosed cancer (1 089 109 new cases) and the fourth leading cause of cancer-related deaths (768 793 deaths) worldwide [3]. The decreasing trend of GC incidence in most populations is due to the decline in *Helicobacter pylori (H. pylori)* infection rates [4] in addition to lifestyle modifications of dietary and environmental risk factors, especially in developed countries. The incidence rates are almost twice as high in men than in women. There is a marked geographical variability in the incidence of GC, where it is highest in Central and East Asia followed by Latin America and Eastern Europe [5]. Although Western Europe has intermediate to low rates of GC with 28 490 new cases in 2020, the mortality rate is still high with around 18 000 deaths in 2020 (mortality rate: 63%) [6] (Figure I.1 and Figure I.2).

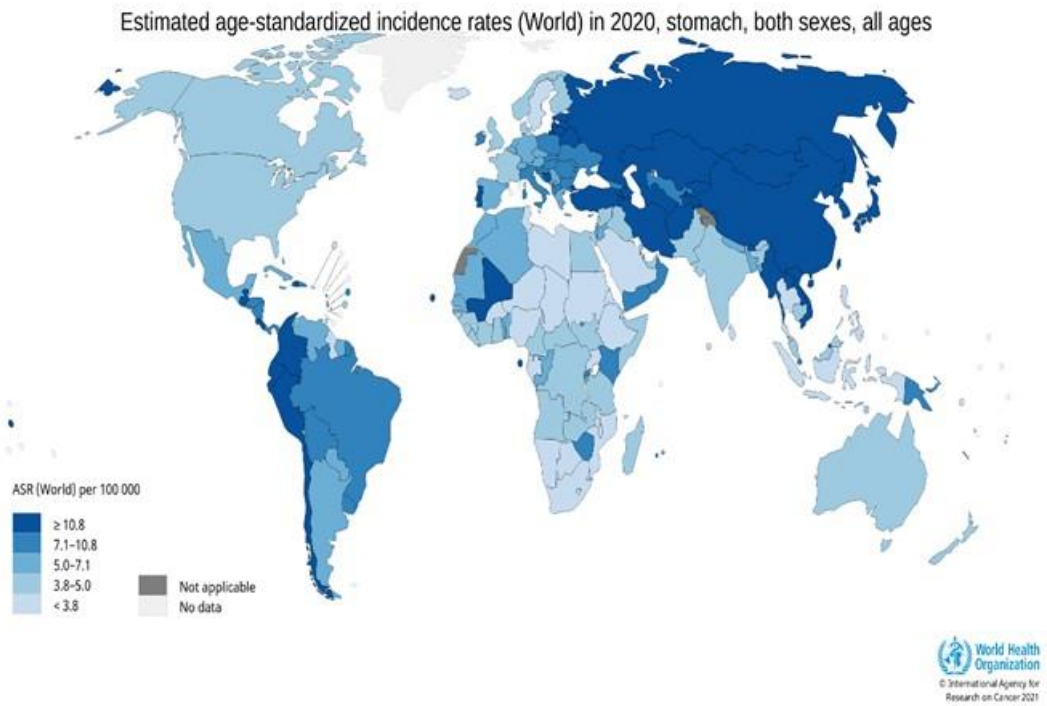

Figure I.1. Worldwide estimated age-standardized (ASR) incidence of gastric cancer in 2020.
From http://gco.iarc/survival/survmark

Mortality rates from GC are higher in areas of high incidence such as Central and East Asia and Latin America (Figure I.2).

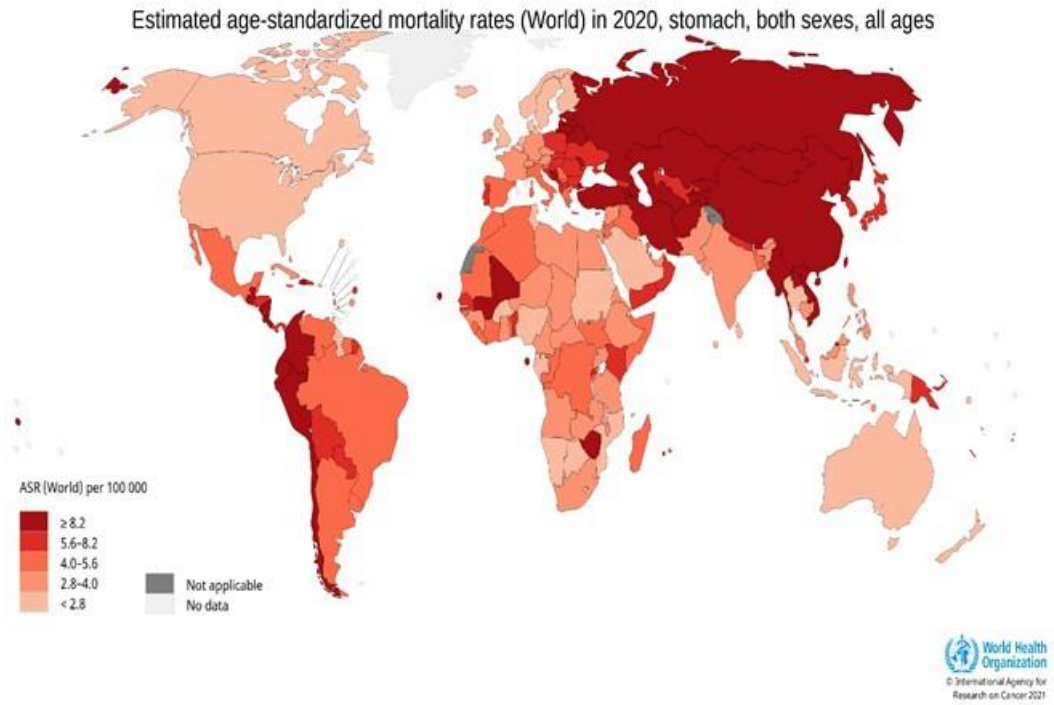

Figure I.2. Worldwide estimated age-standardized (ASR) mortality of gastric cancer in 2020.
From http://gco.iarc/survival/survmark

Survival rates in GC are highly dependent on the stage at time of diagnosis as well as on the surgical intervention [7]. The overall case fatality rate of GC is 71% compared to 48% for colorectal cancer and 94% for pancreatic cancer. Advanced GC have a 5-year survival of less than or equal to 5% [8].

H. pylori infection is the main risk factor of GC (associated with 78% of all GC) inducing inflammation of the gastric mucosa. It carries an odds ratio of 6 for the development of GC within 10 years of infection [9, 10]. GC and *H. pylori* infection association is likely related to the geographical distribution and to the socio-economic levels of countries, where it is stronger in certain regions of the world (East Asia) [11, 12]. In contrast, in other areas of the world (Taiwan, India), *H. pylori* infection is high but GC incidence is low. Such differences could be related to the interactions between *H. pylori* and different environmental factors as well as the different geographical distribution of *H. pylori* strains [13]. Dietary factors (e.g. salted, smoked, or chemically preserved foods) [14], smoking and alcohol consumption [15], Epstein-

Barr virus (EBV) infection [16, 17], are all considered as GC risk factors.

In addition, 1 to 3% of GC are related to familial syndromes [18], and inherited mutations of certain genes have been found to increase the risk of GC. Hereditary diffuse GC (HDGC) is an autosomal dominantly inherited condition caused by a germ line mutation in the *cadherin-1* (*CDH1*) gene [19], a gene that encodes a cell adhesion protein: E-cadherin. The average age of GC diagnosis in patients carrying a pathogenic variant of *CDH1* is 37 years [20]. Lynch syndrome has also been identified to increase the incidence of GC [21]. It is an autosomal dominant disease with a germ line mutation in one allele of one of the genes of the DNA mismatch repair (MMR) system; mainly *MutL Homolog 1 (MLH1) and MutS Homolog 2 (MSH2)*, the second event causing the malfunction of this system will be somatic [22]. Another syndrome is the familial adenomatous polyposis, an autosomal-dominant colorectal cancer syndrome caused by germ line mutations in the *adenomatous polyposis coli (APC)* gene, a tumor suppressor gene [23, 24]. Patients carrying these mutations have a high risk of other neoplasia, in addition to GC [25]. *p53* germline mutation (*R158G, G→C471*), in one family, was also associated with a cluster of predominant GC [26]. GC risk factors are summarized in Figure I.3.

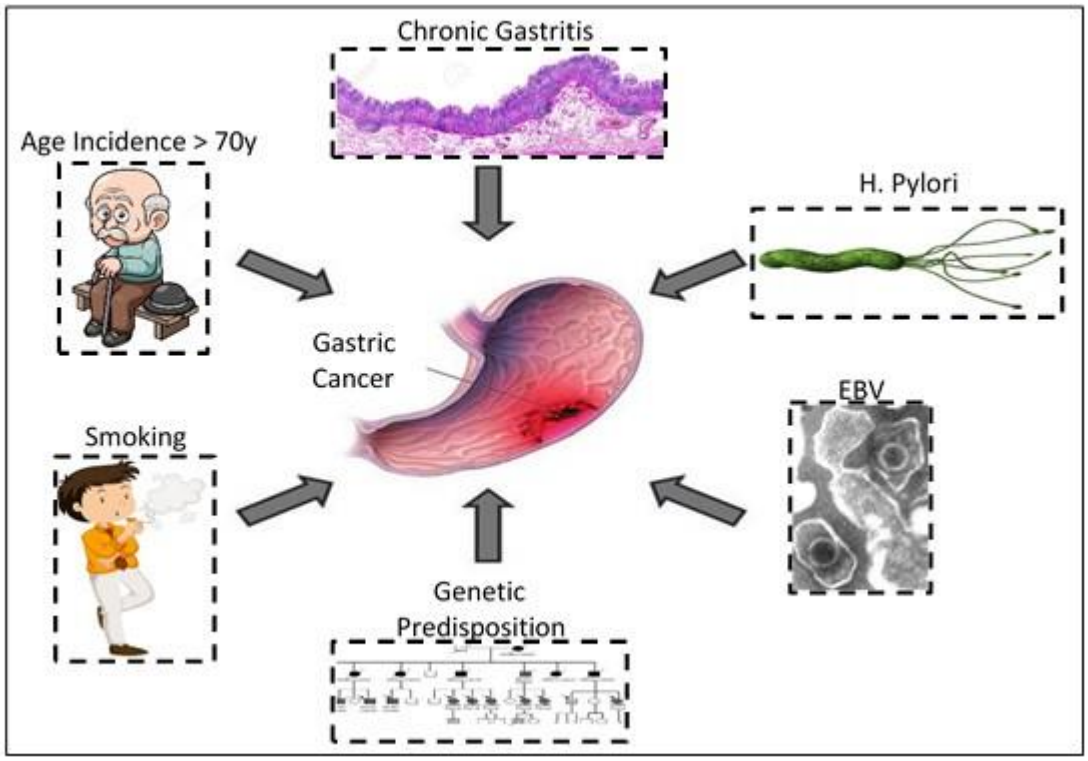

Figure I.3. Gastric cancer risk factors.

I.2. Gastric Cancer Classification

The vast majority of GC are adenocarcinomas (approximately 95%). Less frequent variants include lymphoproliferative, mesenchymal and neuroendocrine tumors [27]. Primary adenocarcinomas of the stomach develop from the epithelial cells of the gastric mucosa. Based on their anatomic location, they can be primarily classified into two subtypes: i) cardia cancers arising in the upper cavity of the stomach adjoining the gastroesophageal junction (GEJ) and ii) non-cardia cancers arise from the antrum (Figure I.4).

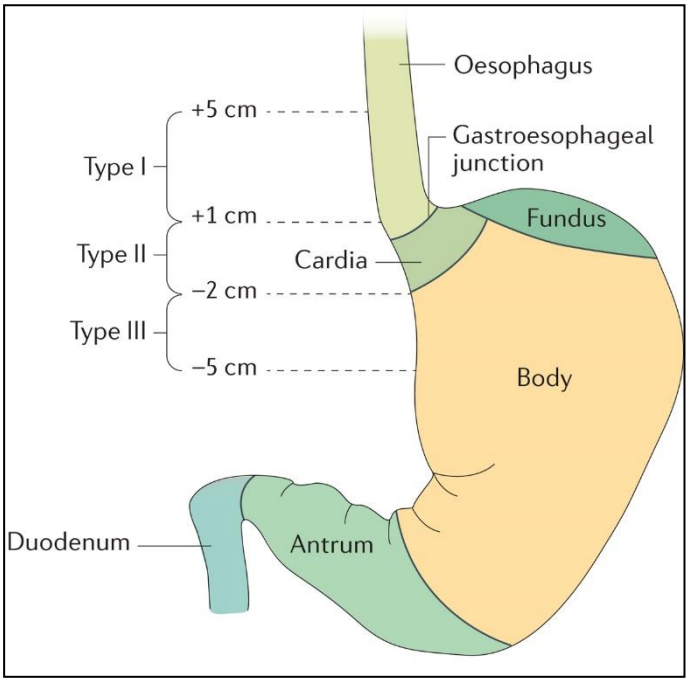

Figure I.4. The Siewert–Stein classification of gastroesophageal region cancers.
Type I gastric adenocarcinomas (GAC) are located within 1–5 cm above the anatomical gastroesophageal junction (GEJ). Type II tumors are arising from the short segment between 1 cm above and 2 cm below the GEJ. Type III adenocarcinoma are located 2 to 5 cm below the GEJ. From: Ajani, 2017 [27].

In the 1980s, Siewert-Stein established a classification system that differentiates tumors arising at the distal esophagus type I from those arising at the GEJ type II or subcardial type III [28] (Figure I.4). Lauren's criteria are widely used to classify gastric adenocarcinomas (GAC), differentiating them histologically into intestinal and diffuse types [29] (Table I.1). The intestinal subtype is characterized by visible glands and cohesion between tumor cells. The diffuse subtype comprises poorly cohesive cells, diffusely infiltrating the gastric wall with little or no gland formation (Figure I.5).

Table I.1. Differences between Lauren's intestinal and diffuse types.
Adapted from: Assumpção, 2020 [30].

	Lauren's Types Gastric Adenocarcinoma	
Characteristic	**Intestinal**	**Diffuse**
Incidence trend	Declining	Stable
Prevalence in endemic areas	Higher	Lower
Environmental influence	Strong	Weak
Age of occurrence	Old	Young
Genetic factors	Weak	Strong
Location of tumor	Distal	Proximal
Macroscopic growth pattern	Growth into the lumen	Tumor spreads along the gastric wall
Carcinogenesis	Well known	Unknown
Prognosis	Better	Worse

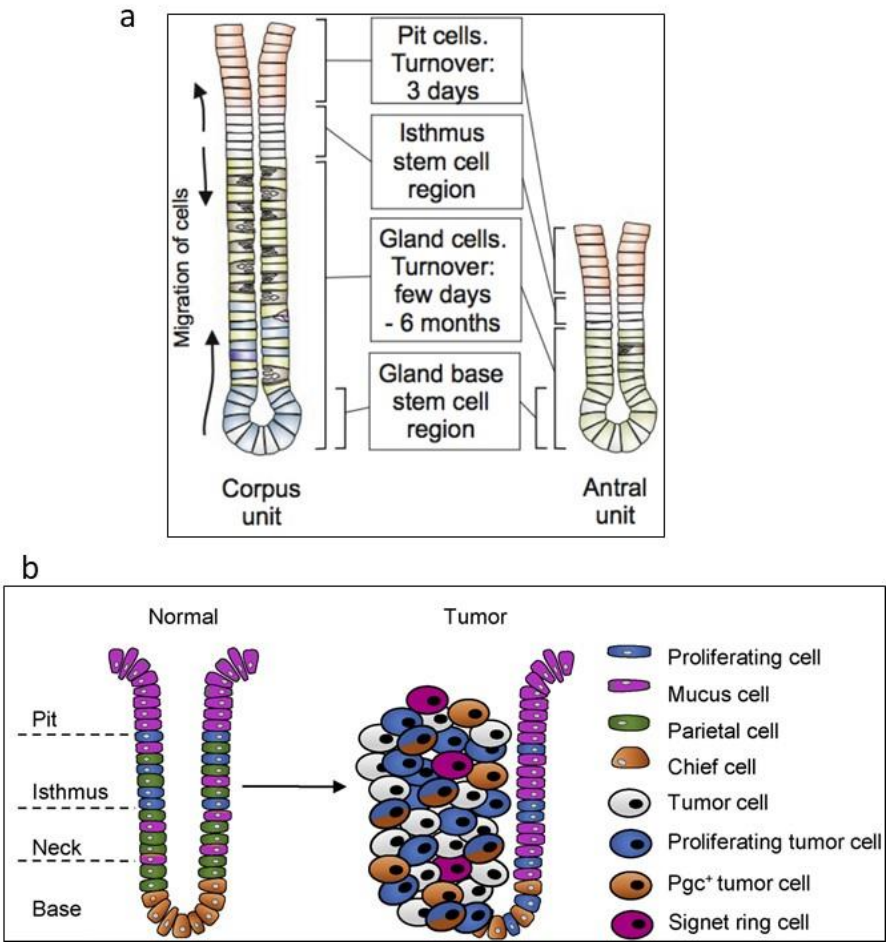

Figure I.5. Organization of gastric glands.
a: Each gland is divided into four regions: the pit, isthmus, gland neck and gland base. Stem cells reside in the isthmus and gland base where they divide and differentiate, renewing the various cell types of the gland. From: Pompaiah, 2017 [31]. b: Diffuse GC model, representation of the cell-type distribution in tumors. From: Seidlitz, 2019 [32].

The 2019 edition of the American Joint Committee on Cancer (AJCC) specified that any tumor with a distance > 2 cm from the GEJ (type III), even if it involves the junction, should be staged according to the TNM (tumor, nodes, and metastases) of GC system [33]. This international TNM classification evaluates the extension of the tumor and thus defines the tumor stage. This classification is important in management of the patient, both for the establishment of prognosis and for adapting therapeutic strategies [34] (Figure I.6).

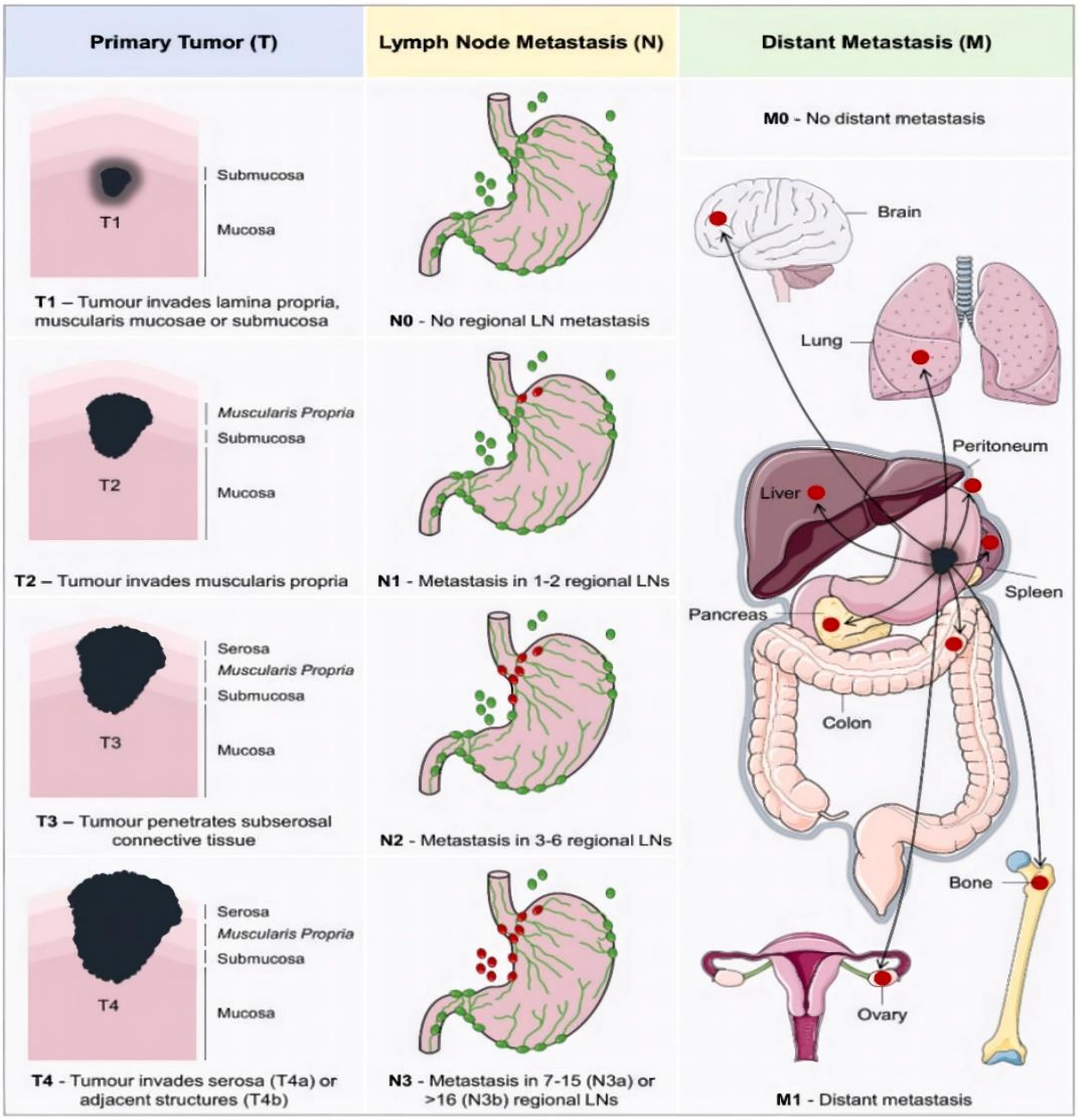

Figure I.6. TNM (tumor, nodes, and metastases) staging system of gastric cancer according to the 8th edition of American Joint Committee on Cancer (AJCC).
From: Cancer Research UK [35].

The Cancer Genome Atlas (TCGA) research network separated GAC into four different molecular subgroups: i) positive for the EBV, ii) a genomically stable (GS) subtype displaying diffuse histology, iii) a chromosomal instable (CIN) subtype and iv) a microsatellite instable (MSI) subtype [36] (Figure I.7).

The molecular characterization of GEJ revealed their high similarity to the CIN subtype of GC [37].

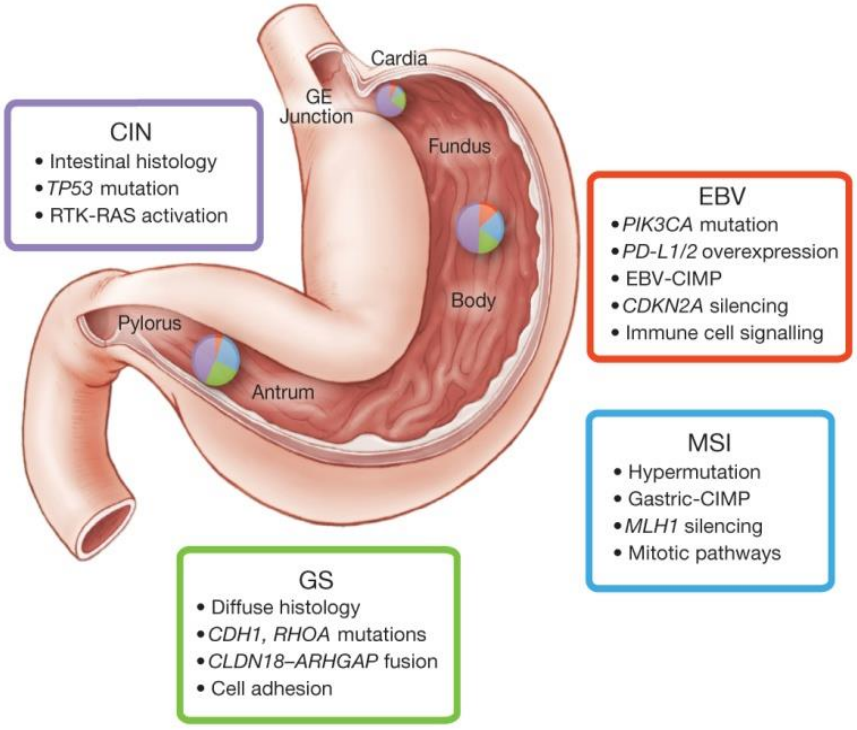

Figure I.7. Molecular classification of gastric cancer (GC).
Comprehensive molecular characterization of gastric adenocarcinomas (GAC), performed by TCGA consortium in 2014 defined four major genomic subtypes of GC: EBV-infected tumors, tumors with microsatellite instability (MSI), genomically stable tumors (GS) and chromosomally instable tumors (CIN). From: GC Genome Atlas, 2014 [36].

Epstein Barr Virus (EBV)-infected subtype

The EBV-positive subtype accounts for about 10% of GC. It is associated to the pathogenicity of the virus and shows the presence of chromosomal aberrations and epigenetic modifications: methylation of promoter regions of tumor suppressor genes. TCGA studies have demonstrated a deregulation of the phosphoinositide 3-kinases (PI3K) / serine-threonine protein kinase (Akt) and januse kinase 2 (JAK2) signaling pathways in addition to the silencing of *cyclin-dependent kinase inhibitor 2A (CDKN2A)* [38].

Genomically stable subtype (GS)

The GS subtype represents 20% of GC but accounts for nearly 75% of HDGC. This subtype is characterized by the presence of mutations in the *Ras Homolog Family Member A (RHOA)* and *CDH1* genes, as well as the fusion of the *claudin 18* (*CLDN18)* and *Rho GTPase Activating Protein 26* (*ARHGAP26)* genes.

The *RHOA* gene encodes the RhoA GTPase that is involved in various signaling pathways including the cell cycle, cytoskeleton organization and cell motility. Mutations in this gene lead to tumor progression and metastasis due to increased motility and degradation of the cytoskeleton. The *CDH1* gene encodes the E-cadherin protein involved in cell adhesion. The loss of its expression is a genetic marker of the diffuse type leading initially to neoplastic formation due to the loss of adhesion and then early metastatic progression [39].

Chromosomally instable subtype (CIN)

The CIN subtype accounts for nearly 50% of GC worldwide. This subtype is characterized by a high rate of aneuploidy. In addition to these chromosomal aberrations, 71% of the CIN-positive subtype is characterized by the presence of mutations in the *Tumor Protein P53 (TP53)* gene. Many signaling pathways are deregulated in this subtype, including the human epidermal growth factor receptor-2 (HER-2) pathway, which is currently the only theranostic biomarker validated by the scientific community in GC [40, 41].

Microsatellite instabilities subtype (MSI)

GC with MSI are found in about 20% of patients. In this subtype, major genetic alterations lead to the inactivation of genes involved in DNA mismatch repair (MMR). The most frequent somatic anomaly is the hyper-methylation of the *MLH1* gene promoter, whose inactivation induces a high rate of somatic mutations in the genome at the origin of tumorigenesis [39].

An additional classification from the Asian Cancer Research Group (ACRG) divided GC into MSI and MSS (microsatellite stable) subtypes [42]. TCGA and ACRG molecular classifications are not yet consensual in the clinical context. In order to improve the effectiveness of GC treatments, it would be important to associate the TNM classification with the histopathology and the molecular classifications.

I.3. Current Management of Gastric Cancer Patients

The goal of treatment approaches is to accomplish the proper post-operative action, guarantying acceptable quality of life and long-term oncological outcomes [43]. Currently, the prognosis of GC is closely related to the TNM stage [44, 45] (Figure I.6). Once the patient's tumor staging has been determined, treatment options are selected by a multidisciplinary team. Endoscopic resection is applicable to early-stage GAC, when the tumor is confined to the mucosa and there is virtually no risk of lymph nodes metastases [46]. If tumors do not have the requirements for endoscopic resection, surgery is the replacement modality.

Surgery

Surgery is the primary curative modality for GC. Depending on the location of the tumor, full gastrectomy is preferred for distal tumors and partial gastrectomy for proximal tumors. In addition to gastrectomy, lymph node resection is usually performed to remove all lymph nodes in the vicinity of the stomach lymph node area [47, 48]. The survival benefit of gastrectomy to reduce tumor volume in presence of distant metastases has not been documented [49].

Studies have shown that surgery alone results in a high rate of tumor recurrence [50]. Therefore, GC patients are usually treated with both modalities: surgery plus pre- and post-operative radiotherapy / chemotherapy.

Radiotherapy

Radiation techniques have improved over the years, with the exposure of healthy tissues being reduced [51]. Studies have confirmed that concurrent chemotherapy / radiotherapy was superior to chemotherapy or radiotherapy alone for tumor down-staging and pathological reduction rate [52].

Chemotherapy

Conventional chemotherapies that include platinum (cisplatin and oxaliplatin), fluoropyrimidine (5-fluorouracil, S-1 and capecitabine), irinotecan and taxanes (docetaxel and paclitaxel) are used to treat GC patients (Table I.2). In general, a combination of

chemotherapies is more effective for overall survival compared to a sole chemotherapeutic agent [53–55].

Table I.2. Active chemotherapeutic agents for gastric cancer.
Classified into Antimetabolite, Platinum Preparation, Topoisomerase Inhibitor, Taxane.
Adapted from: Yamashita, 2021 [56].

Antimetabolite	Fluorouracil (5-FU)	1st line chemotherapy
	Levofolinate Calcium (Leucovorin-LV)	1st-line chemotherapy
	Tegafur / Gimeracil / Oteracil potassium (S1)	1st-line chemotherapy (currently available for oral medicines)
	Capecitabine (Xeloda)	1st-line chemotherapy (currently available for oral medicines)
	Trifluridine / Tipiracil hydrochloride (Lonsarf)	2sd-line chemotherapy (currently available for oral medicines)
DNA Alkylant	Cisplatin (CDDP)	1st line chemotherapy
	Oxaliplatin (OHP)	1st line chemotherapy
Topoisomerase inhibitor	Irinotecan (CPT-11)	2sd-line chemotherapy
Microtubule Poison	Docetaxel (DTX)	2sd-line chemotherapy
	Paclitaxel (PTX)	3rd-line chemotherapy

Targeted therapies

Selected patients may be eligible to targeted therapies. So far, the only approved targeted therapies are the monoclonal anti-HER-2 antibody “trastuzumab” (first line setting) [41] and the monoclonal anti-vascular endothelial growth factor receptor-2 (VEGFR-2) antibody “ramucirumab” (second line setting) [57]. Other trials to target the HER-2 receptor have failed: the LOGiC and TyTAN trials of lapatinib and the GATSBY trial of a trastuzumab–emtansine antibody–drug conjugate [58–60].

Immune checkpoint inhibitors

The recent encouraging results from use of the immune checkpoint inhibitors (ICI) have paved the way to a new era of cancer immunotherapy. It has emerged as a promising strategy in several malignancies [61–63]. ICI such as programmed cell death-1 (PD-1) or programmed cell death-ligand1 (PD-L1) monoclonal antibodies have improved the overall survival of GC: the phase III ATTRACTION-2 trial of “nivolumab” (human immunoglobulin four monoclonal antibody against PD-1) demonstrated a survival benefit in Asian patients, which led to the approval of “nivolumab” as a treatment for GC in Japan [64]. Another anti-PD-1 monoclonal antibody, “pembrolizumab”, received accelerated approval for treatment of PD-L1-positive GC in third or later-line treatment by the US Food and Drug Administration (FDA) on the basis of results of a large phase II trial [65]. Other clinical trials of anti-PD-1/PD-L1 therapies for GC are summarized in Table I.3.

Ipilimumab as anti-cytotoxic T lymphocyte antigen-4 (CTLA-4) monoclonal antibody could be another strategy of ICI to treat GC [67, 68]. ICI are ongoing as a new treatment tool for GC patients. Multiple trials are in progress investigating the role of ICI in combination regimens [66].

Table I.3. Pivotal clinical trials of anti-PD-1/PD-L1 therapies for gastric cancer.
PBO: placebo; BSC: best supportive care; XP: capecitabine + cisplatin; FP: 5-fluorouracil and cisplatin; capeOX: capecitabine + oxaliplatin; FOLFOX: oxaliplatin + 5-fluorouracil + tetrahydrofolic acid; SOX: S-1 + oxaliplatin; FLOT: 5-FU+ leucovorin + oxaliplatin + docetaxel. Adapted from: Kawazoe, 2021 [66].

Target	Phase	Trial	Line	Agents (experimental)	Control	Result
PD-1	III	ATTRACTION-2 (NCT02267343)	3rd or later	Nivolumab	PBO	Positive
PD-1	II	KEYNOTE-059 (NCT02335411)	3rd or later	Pembrolizumab	–	Positive
PD-L1	III	JAVELIN300 (NCT02625623)	3rd	Avelumab	Irinotecan/taxanes/BSC	Negative
PD-1	III	KEYNOTE-061 (NCT02370498)	2nd	Pembrolizumab	Paclitaxel	Negative
PD-1	III	KEYNOTE-063 (NCT03019588)	2nd	Pembrolizumab	Paclitaxel	Terminated
PD-1	III	KEYNOTE-062 (NCT02494583)	1st	Pembrolizumab or Pembrolizumab+CTx	XP/FP	Negative
PD-L1	III	JAVELIN100 (NCT02625610)	1st maintenance	Avelumab	CapeOX/FOLFOX	Negative
PD-1	III	ATTRACTION-4 (NCT02746796)	1st	+Nivolumab	SOX/CapeOX	positive for PFS/negative for OS
PD-1	III	KEYNOTE-811 (NCT03615326)	1st	+Pembrolizumab	FP/CapeOX/SOX +Tmab	Ongoing
PD-1	III	KEYNOTE-859 (NCT03675737)	1st	+Pembrolizumab	FP/CapeOX	Ongoing
PD-1	III	KEYNOTE-585 (NCT03221426)	Neoadjuvant	+Pembrolizumab	XP/FP/FLOT	Ongoing
PD-1	III	ATTRACTION-5 (NCT03006705)	Adjuvant	+Nivolumab	S-1/CapeOX	Ongoing
PD-1	III	CheckMate-577 (NCT02743494)	Adjuvant	Nivolumab	PBO	Ongoing

Much progress has been made in understanding the pathogenesis of GC. The optimization of the available treatments should go further. Then, the focus should be oriented towards fine-tuning treatment strategies and developing new drugs. However, such strategies may come at an important price. As a consequence, the development of a novel system that reduces the price and time of drug discovery is ongoing in cancer research. Such is the case of using three-dimensional (3D) cell culture models in drug discovery research. This will be further detailed in chapter III.

I.4. References

[1] E. Van Cutsem, X. Sagaert, B. Topal, K. Haustermans, and H. Prenen, "Gastric cancer," *Lancet*, vol. 388, no. 10060, pp. 2654–2664, Nov. 2016, doi: 10.1016/S0140-6736(16)30354-3.

[2] P. Karimi, F. Islami, S. Anandasabapathy, N. D. Freedman, and F. Kamangar, "Gastric Cancer: Descriptive Epidemiology, Risk Factors, Screening, and Prevention," *Cancer Epidemiol. Prev. Biomarkers*, vol. 23, no. 5, pp. 700–713, May 2014, doi: 10.1158/1055-9965.EPI-13-1057.

[3] H. Sung *et al.*, "Global Cancer Statistics 2020: GLOBOCAN Estimates of Incidence and Mortality Worldwide for 36 Cancers in 185 Countries," *CA. Cancer J. Clin.*, vol. 71, no. 3, pp. 209–249, May 2021, doi: 10.3322/caac.21660.

[4] V. Herrera and J. Parsonnet, "Helicobacter pylori and gastric adenocarcinoma," *Clin. Microbiol. Infect.*, vol. 15, no. 11, pp. 971–976, Nov. 2009, doi: 10.1111/J.1469-0691.2009.03031.X.

[5] M. Balakrishnan, R. George, A. Sharma, and D. Y. Graham, "Changing Trends in Stomach Cancer Throughout the World," *Curr. Gastroenterol. Rep.*, vol. 19, no. 8, p. 36, Aug. 2017, doi: 10.1007/S11894-017-0575-8.

[6] WHO, "International Agency for Research on Cancer," 2020. https://gco.iarc.fr/today/data/factsheets/cancers/7-Stomach-fact-sheet.pdf (accessed Oct. 06, 2021).

[7] "Cancer Statistics Review, 1975-2016 - SEER Statistics." https://seer.cancer.gov/archive/csr/1975_2016/ (accessed Oct. 06, 2021).

[8] C. Mattiuzzi and G. Lippi, "Current Cancer Epidemiology," *J. Epidemiol. Glob. Health*, vol. 9, no. 4, p. 217, Dec. 2019, doi: 10.2991/JEGH.K.191008.001.

[9] S. Pincock, "Nobel Prize winners Robin Warren and Barry Marshall," *Lancet*, vol. 366, no. 9495, p. 1429, Oct. 2005, doi: 10.1016/S0140-6736(05)67587-3.

[10] P. Rawla and A. Barsouk, "Epidemiology of gastric cancer: global trends, risk factors and prevention," *Przegląd Gastroenterol.*, vol. 14, no. 1, p. 26, 2019, doi: 10.5114/PG.2018.80001.

[11] P. Moayyedi *et al.*, "Relation of adult lifestyle and socioeconomic factors to the prevalence of Helicobacter pylori infection," *Int. J. Epidemiol.*, vol. 31, no. 3, pp. 624–631, Jun. 2002, doi: 10.1093/IJE/31.3.624.

[12] Z. Kadar *et al.*, "Geographic particularities in incidence and etiopathogenesis of sporadic gastric cancer," *Polish J. Pathol.*, vol. 66, no. 3, pp. 254–259, 2015, doi: 10.5114/PJP.2015.54959.

[13] J. Watari et al., "Helicobacter pylori associated chronic gastritis, clinical syndromes, precancerous lesions, and pathogenesis of gastric cancer development," *World J. Gastroenterol.,* vol. 20, no. 18, pp. 5461–5473, May 2014, doi: 10.3748/wjg.v20.i18.5461.

[14] S. Tsugane and S. Sasazuki, "Diet and the risk of gastric cancer: review of

epidemiological evidence," *Gastric Cancer*, vol. 10, no. 2, pp. 75–83, Jun. 2007, doi: 10.1007/S10120-007-0420-0.

[15] S. T. Mayne, M. C. Playdon, and C. L. Rock, "Diet, nutrition, and cancer: past, present and future," *Nat. Rev. Clin. Oncol.*, vol. 13, no. 8, pp. 504–515, Mar. 2016, doi: 10.1038/nrclinonc.2016.24.

[16] T. Boysen *et al.*, "EBV-associated gastric carcinoma in high- and low-incidence areas for nasopharyngeal carcinoma," *Br. J. Cancer*, vol. 101, no. 3, pp. 530–533, Jul. 2009, doi: 10.1038/SJ.BJC.6605168.

[17] G. Murphy, R. Pfeiffer, M. C. Camargo, and C. S. Rabkin, "Meta-analysis Shows That Prevalence of Epstein–Barr Virus-Positive Gastric Cancer Differs Based on Sex and Anatomic Location," *Gastroenterology*, vol. 137, no. 3, pp. 824–833, Sep. 2009, doi: 10.1053/J.GASTRO.2009.05.001.

[18] R. S. van der Post, C. Oliveira, P. Guilford, and F. Carneiro, "Hereditary gastric cancer: what's new? Update 2013–2018," *Fam. Cancer*, vol. 18, no. 3, pp. 363–367, Apr. 2019, doi: 10.1007/S10689-019-00127-7.

[19] R. C. Fitzgerald and C. Caldas, "Clinical implications of E-cadherin associated hereditary diffuse gastric cancer," *Gut*, vol. 53, no. 6, pp. 775–778, Jun. 2004, doi: 10.1136/GUT.2003.022061.

[20] N. Nicole McMillian *et al.*, "NCCN Guidelines Version 5.2021 Gastric Cancer Continue NCCN Guidelines Panel Disclosures," 2021. https://www.nccn.org/guidelines/guidelines-detail?category=1&id=1434 (accessed Oct. 08, 2021).

[21] H. T. Lynch, W. Grady, G. Suriano, and D. Huntsman, "Gastric cancer: New genetic developments," *J. Surg. Oncol.*, vol. 90, no. 3, pp. 114–133, Jun. 2005, doi: 10.1002/JSO.20214.

[22] L. G. Capelle *et al.*, "Risk and Epidemiological Time Trends of Gastric Cancer in Lynch Syndrome Carriers in The Netherlands," *Gastroenterology*, vol. 138, no. 2, pp. 487–492, Feb. 2010, doi: 10.1053/J.GASTRO.2009.10.051.

[23] J. Groden *et al.*, "Identification and characterization of the familial adenomatous polyposis coli gene," *Cell*, vol. 66, no. 3, pp. 589–600, Aug. 1991, doi: 10.1016/0092-8674(81)90021-0.

[24] P. Dinarvand *et al.*, "Familial Adenomatous Polyposis Syndrome: An Update and Review of Extraintestinal Manifestations," *Arch. Pathol. Lab. Med.*, vol. 143, no. 11, pp. 1382–1398, Nov. 2019, doi: 10.5858/ARPA.2018-0570-RA.

[25] M. C. Gallagher, R. K. S. Phillips, and S. Bulow, "Surveillance and management of upper gastrointestinal disease in Familial Adenomatous Polyposis," *Fam. Cancer*, vol. 5, no. 3, pp. 263–273, Sep. 2006, doi: 10.1007/S10689-005-5668-0.

[26] C. Oliveira *et al.*, "E-Cadherin (CDH1) and p53 rather than SMAD4 and Caspase-10 germline mutations contribute to genetic predisposition in Portuguese gastric cancer patients," *Eur. J. Cancer*, vol. 40, no. 12, pp. 1897–1903, Aug. 2004, doi: 10.1016/J.EJCA.2004.04.027.

[27] J. A. Ajani, J. Lee, T. Sano, Y. Y. Janjigian, D. Fan, and S. Song, "Gastric adenocarcinoma," *Nat. Rev. Dis. Prim.*, vol. 3, no. 1, pp. 1–19, Jun. 2017, doi: 10.1038/NRDP.2017.36.

[28] S. JR, H. AH, B. K, and G. W, "Cardia cancer: attempt at a therapeutically relevant classification," *Chirurg.*, vol. 58, no. 1, pp. 25–32, Jan. 1987. Available: https://europepmc.org/article/med/3829805.

[29] P. LAUREN, "The two histological main types of gastric carcinoma: diffuse and so-called intestinal-type carcinoma. an attempt at a histo-clinical classification," *Acta Pathol. Microbiol. Scand.*, vol. 64, pp. 31–49, 1965, doi: 10.1111/apm.1965.64.1.31.

[30] P. P. Assumpção *et al.*, "The diffuse-type gastric cancer epidemiology enigma," *BMC Gastroenterol.*, vol. 20, no. 1, pp. 1–7, Jul. 2020, doi: 10.1186/S12876-020-01354-4.

[31] M. Pompaiah and S. Bartfeld, "Gastric organoids: an emerging model system to study *Helicobacter pylori* pathogenesis," *Curr. Top. Microbiol. Immunol.*, vol. 400, pp. 149–168, Jan. 2017, doi: 10.1007/978-3-319-50520-6_7.

[32] T. Seidlitz *et al.*, "Mouse models of human gastric cancer subtypes with stomach-specific CreERT2-mediated pathway alterations," *Gastroenterology*, vol. 157, no. 6, pp. 1599-1614.e2, Dec. 2019, doi: 10.1053/J.GASTRO.2019.09.026.

[33] K. Liu *et al.*, "Comparison between gastric and esophageal classification system among adenocarcinomas of esophagogastric junction according to AJCC 8th edition: a retrospective observational study from two high-volume institutions in China," *Gastric Cancer*, vol. 22, no. 3, pp. 506–517, Nov. 2018, doi: 10.1007/S10120-018-0890-2.

[34] Arocena M. G. et al., "MRI and endoscopic ultrasonography in the staging of gastric cancer ," *Rev. Esp. Enferm Dig.,* vol. 98, no. 8, pp. 582-590, Aug. 2006, doi: 10.4321/s1130-01082006000800003.

[35] "TNM staging for stomach cancer | Cancer Research UK." https://www.cancerresearchuk.org/about-cancer/stomach-cancer/stages/tnm-staging.

[36] A. J. Bass *et al.*, "Comprehensive molecular characterization of gastric adenocarcinoma," *Nature*, vol. 513, no. 7517, pp. 202–209, Sep. 2014, doi: 10.1038/nature13480.

[37] J. Kim *et al.*, "Integrated genomic characterization of oesophageal carcinoma," *Nature*, vol. 541, no. 7636, pp. 169–174, Jan. 2017, doi: 10.1038/nature20805.

[38] Y. Sunakawa and H.-J. Lenz, "Molecular classification of gastric adenocarcinoma: translating new insights from the cancer genome atlas research network," *Curr. Treat. Options Oncol.*, vol. 16, no. 4, pp. 1–18, Mar. 2015, doi: 10.1007/S11864-015-0331-Y.

[39] I. Riquelme *et al.*, "Molecular classification of gastric cancer: Towards a pathway-driven targeted therapy," *Oncotarget*, vol. 6, no. 28, p. 24750, 2015, doi: 10.18632/ONCOTARGET.4990.

[40] Y. Matsui, M. Inomata, M. Tojigamori, K. Sonoda, N. Shiraishi, and S. Kitano, "Suppression of tumor growth in human gastric cancer with HER2 overexpression by an anti-HER2 antibody in a murine model," *Int. J. Oncol.*, vol. 27, no. 3, pp. 681–685, Sep.

2005, doi: 10.3892/IJO.27.3.681.

[41] Y. J. Bang *et al.*, "Trastuzumab in combination with chemotherapy versus chemotherapy alone for treatment of HER2-positive advanced gastric or gastro-oesophageal junction cancer (ToGA): a phase 3, open-label, randomised controlled trial," *Lancet*, vol. 376, no. 9742, pp. 687–697, Aug. 2010, doi: 10.1016/S0140-6736(10)61121-X.

[42] R. Cristescu *et al.*, "Molecular analysis of gastric cancer identifies subtypes associated with distinct clinical outcomes," *Nat. Med.*, vol. 21, no. 5, pp. 449–456, Apr. 2015, doi: 10.1038/NM.3850.

[43] E. C. Smyth *et al.*, "Gastric cancer: ESMO clinical practice guidelines for diagnosis, treatment and follow-up," *Ann. Oncol.*, vol. 27, pp. v38–v49, Sep. 2016, doi: 10.1093/ANNONC/MDW350.

[44] T. Sano *et al.*, "Proposal of a new stage grouping of gastric cancer for TNM classification: International Gastric Cancer Association staging project," *Gastric Cancer*, vol. 20, no. 2, pp. 217–225, Feb. 2016, doi: 10.1007/S10120-016-0601-9.

[45] M. B. Amin *et al.*, "The Eighth Edition AJCC Cancer Staging Manual: Continuing to build a bridge from a population-based to a more 'personalized' approach to cancer staging," *CA. Cancer J. Clin.*, vol. 67, no. 2, pp. 93–99, Mar. 2017, doi: 10.3322/CAAC.21388.

[46] T. Gotoda, "Endoscopic resection of early gastric cancer," *Gastric Cancer*, vol. 10, no. 1, pp. 1–11, Feb. 2007, doi: 10.1007/S10120-006-0408-1.

[47] S. S. Lee, H. Y. Chung, O. K. Kwon, and W. Yu, "Long-term quality of life after distal subtotal and total gastrectomy symptom-and behavior-o riented con sequences," *Ann. Surg.*, vol. 263, no. 4, pp. 738–744, 2016, doi: 10.1097/SLA.0000000000001481.

[48] J. J. Bonenkamp *et al.*, "Extended lymph-node dissection for gastric cancer," *N. Engl. J. Med.,* vol. 340, no. 12, pp. 908–914, Oct. 2008, doi: 10.1056/NEJM199903253401202.

[49] K. Fujitani *et al.*, "Gastrectomy plus chemotherapy versus chemotherapy alone for advanced gastric cancer with a single non-curable factor (REGATTA): a phase 3, randomised controlled trial," *Lancet Oncol.*, vol. 17, no. 3, pp. 309–318, Mar. 2016, doi: 10.1016/S1470-2045(15)00553-7.

[50] D. Liu *et al.*, "The patterns and timing of recurrence after curative resection for gastric cancer in China," *World J. Surg. Oncol.*, vol. 14, no. 1, pp. 1–11, Dec. 2016, doi: 10.1186/S12957-016-1042-Y.

[51] J. A. Ajani *et al.*, "Gastric cancer, version 3.2016, NCCN clinical practice guidelines in oncology," *J. Natl. Compr. Cancer Netw.*, vol. 14, no. 10, pp. 1286–1312, Oct. 2016, doi: 10.6004/JNCCN.2016.0137.

[52] L. L. Gunderson, R. Bruce Hoskins, A. C. Cohen, S. Kaufman, W. C. Wood, and R. W. Carey, "Combined modality treatment of gastric cancer," *Int. J. Radiat. Oncol.*, vol. 9, no. 7, pp. 965–975, Jul. 1983, doi: 10.1016/0360-3016(83)90383-8.

[53] D. Cunningham *et al.*, "Perioperative chemotherapy versus surgery alone for resectable gastroesophageal cancer," *N. Engl. J. Med.*, vol. 355, no. 1, pp. 11–20, Jul. 2006, doi: 10.1056/NEJMoa055531.

[54] S. E. Al-Batran *et al.*, "Histopathological regression after neoadjuvant docetaxel, oxaliplatin, fluorouracil, and leucovorin versus epirubicin, cisplatin, and fluorouracil or capecitabine in patients with resectable gastric or gastro-oesophageal junction adenocarcinoma (FLOT4-AIO): results from the phase 2 part of a multicentre, open-label, randomised phase 2/3 trial," *Lancet Oncol.*, vol. 17, no. 12, pp. 1697–1708, Dec. 2016, doi: 10.1016/S1470-2045(16)30531-9.

[55] U. Vanhoefer *et al.*, "Final results of a randomized phase iii trial of sequential high-dose methotrexate, fluorouracil, and doxorubicin versus etoposide, leucovorin, and fluorouracil versus infusional fluorouracil and cisplatin in advanced gastric cancer: a trial of the european organization for research and treatment of cancer gastrointestinal tract cancer cooperative group," *J. Clin. Oncol.*, vol. 18, no. 14, pp. 2648–2657, Jul. 2000, doi: 10.1200/JCO.2000.18.14.2648.

[56] K. Yamashita, K. Hosoda, M. Niihara, and N. Hiki, "History and emerging trends in chemotherapy for gastric cancer," *Ann. Gastroenterol. Surg.*, vol. 5, no. 4, pp. 446–456, Jul. 2021, doi: 10.1002/AGS3.12439.

[57] C. S. Fuchs *et al.*, "Ramucirumab monotherapy for previously treated advanced gastric or gastro-oesophageal junction adenocarcinoma (REGARD): An international, randomised, multicentre, placebo-controlled, phase 3 trial," *Lancet*, vol. 383, no. 9911, pp. 31–39, 2014, doi: 10.1016/S0140-6736(13)61719-5.

[58] M. F. Press *et al.*, "HER2 status in advanced or metastatic gastric, esophageal, or gastroesophageal adenocarcinoma for entry to the TRIO-013/LOGiC Trial of Lapatinib," *Mol. Cancer Ther.*, vol. 16, no. 1, pp. 228–238, Jan. 2017, doi: 10.1158/1535-7163.MCT-15-0887.

[59] P. C. Thuss-Patience *et al.*, "Trastuzumab emtansine versus taxane use for previously treated HER2-positive locally advanced or metastatic gastric or gastro-oesophageal junction adenocarcinoma (GATSBY): an international randomised, open-label, adaptive, phase 2/3 study," *Lancet Oncol.*, vol. 18, no. 5, pp. 640–653, May 2017, doi: 10.1016/S1470-2045(17)30111-0.

[60] M. Wheelden and N. S. Yee, "Clinical evaluation of the safety and efficacy of trifluridine/tipiracil in the treatment of advanced gastric/gastroesophageal junction adenocarcinoma: evidence to date," *Onco. Targets. Ther.*, vol. 13, pp. 7459–7465, Jul. 2020, doi: 10.2147/OTT.S216598.

[61] D. M. Pardoll, "The blockade of immune checkpoints in cancer immunotherapy," *Nat. Rev. Cancer*, vol. 12, no. 4, p. 252, Apr. 2012, doi: 10.1038/NRC3239.

[62] R. J. Motzer *et al.*, "Nivolumab versus Everolimus in Advanced Renal-Cell Carcinoma," *N. Engl. J. Med.*, vol. 373, no. 19, pp. 1803–1813, Nov. 2015, doi: 10.1056/NEJMOA1510665.

[63] R. S. Herbst *et al.*, "Pembrolizumab versus docetaxel for previously treated, PD-L1-positive, advanced non-small-cell lung cancer (KEYNOTE-010): a randomised controlled trial," *Lancet*, vol. 387, no. 10027, pp. 1540–1550, Apr. 2016, doi: 10.1016/S0140-6736(15)01281-7.

[64] Y. K. Kang *et al.*, "Nivolumab in patients with advanced gastric or gastro-oesophageal

junction cancer refractory to, or intolerant of, at least two previous chemotherapy regimens (ONO-4538-12, ATTRACTION-2): a randomised, double-blind, placebo-controlled, phase 3 trial," *Lancet*, vol. 390, no. 10111, pp. 2461–2471, Dec. 2017, doi: 10.1016/S0140-6736(17)31827-5.

[65] C. S. Fuchs *et al.*, "Safety and efficacy of pembrolizumab monotherapy in patients with previously treated advanced gastric and gastroesophageal junction cancer: phase 2 clinical KEYNOTE-059 Trial," *JAMA Oncol.*, vol. 4, no. 5, pp. e180013–e180013, May 2018, doi: 10.1001/JAMAONCOL.2018.0013.

[66] A. Kawazoe, K. Shitara, N. Boku, T. Yoshikawa, and M. Terashima, "Current status of immunotherapy for advanced gastric cancer," *Jpn. J. Clin. Oncol.*, vol. 51, no. 1, pp. 20–27, Jan. 2021, doi: 10.1093/JJCO/HYAA202.

[67] A. Högner and P. Thuss-Patience, "Immune checkpoint inhibition in oesophago-gastric carcinoma," *Pharmaceuticals*, vol. 14, no. 2, pp. 1–18, Feb. 2021, doi: 10.3390/PH14020151.

[68] J. Tintelnot *et al.*, "Ipilimumab or FOLFOX with Nivolumab and Trastuzumab in previously untreated HER2-positive locally advanced or metastatic EsophagoGastric Adenocarcinoma - the randomized phase 2 INTEGA trial (AIO STO 0217)," *BMC Cancer*, vol. 20, no. 1, pp. 1–10, Jun. 2020, doi: 10.1186/S12885-020-06958-3.

Chapter II
Tumor Microenvironment in Gastric Cancer

II.1. Introduction

The tumor microenvironment (TME) favors the growth and the expansion of cancer cells. It is complex and different from healthy tissue microenvironment. Inflammation appears to be an initial step in creating TME, the activation of epithelial stem progenitors and the recruitment of various immune cells are also associated to the process. TME is largely considered as the origin of the initiation and the development of malignant tumors [1]. Generally, the TME modifies the proliferative and invasive capacity of cancer cells, and it increases the aggressiveness and the progression of primary tumors [2]. It is getting clear that the biology of cancer can no longer be studied by the sole analysis of tumor cells, but it must also include the contributions of the TME [3]. The TME contains many cellular and stroma components. These include immune and inflammatory cells (T and B lymphocytes; natural killer cells (NK), dendritic cells (DC), tumor-associated macrophages (TAM), myeloid-derived suppressor cells (MDSC), neutrophils), stromal cells (fibroblasts, cancer-associated fibroblasts (CAF), mesenchymal stem cells (MSC), adipocytes, pericytes), blood and lymph vessels, extracellular matrix (ECM) and secreted proteins [4–6] (Figure II.1).

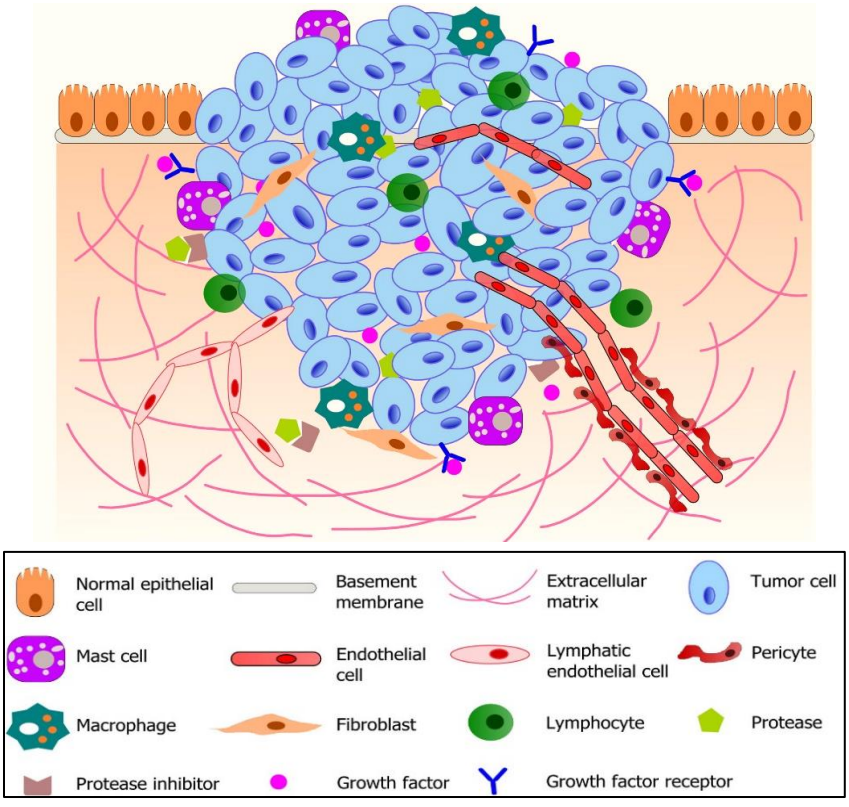

Figure II.1. Illustration of tumor microenvironment (TME).
Cancer cells surrounded by TME. Adapted from: Joyce, 2009 [7]; Koontongkaew, 2013 [8]; Xu, 2014 [9].

Multiple studies in GC have established the association of TME content with the theranostic status [10, 11]. For example, the poor prognosis of the diffuse GC subtype could be explained by the high stromal infiltration and close interaction between cancer cells and CAF [12, 13].

In the following section, we will develop the characterization of CAF, the stromal cells that we were interested to use in our model during this thesis.

II.2. Cancer-Associated Fibroblasts

CAF are a dominant stromal component, they contribute in many ways to tumor progression. They can also have an antitumorigenic activity [14]. The definitive origin of CAF and the conversion mechanisms are not yet known [15–17]. The origin of these cells can include infiltrating fibroblasts, MSC, endothelial cells, etc. [18, 19]. Many activation mechanisms of CAF have been proposed; they are summarized in Figure II.2. Markers were described to distinguish CAF from normal fibroblasts such as alpha smooth muscle actin (αSMA) and fibroblast activation protein (FAP) [20]. It is not possible to use a single nomenclature to define CAF, hence the specific markers and origin remain controversial. A distinction must be made between CAF derived from patient's own tumor and fibroblasts present at the metastatic site for advanced tumors. This second situation is not easily exploitable because it is less common to perform surgery on metastases than on primary tumors [21, 22].

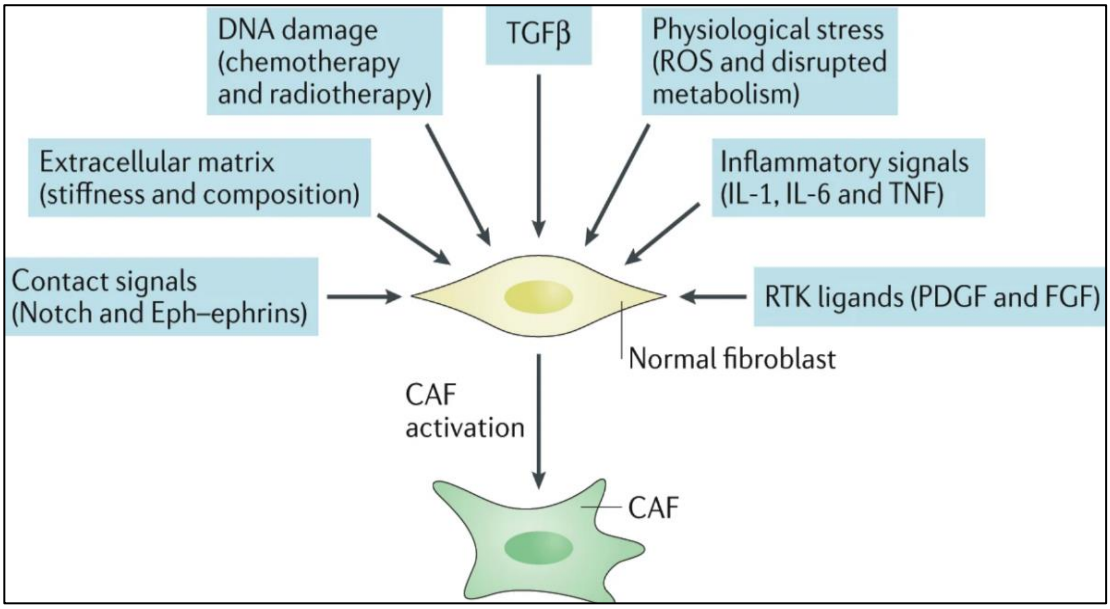

Figure II.2. Multiple mechanisms of cancer-associated fibroblasts (CAF) activation. TGFβ: transforming growth factor-β; ROS: reactive oxygen species; IL: interleukin; TNF: tumor necrosis factor; RTK: receptor tyrosine kinase; PDGF: platelet-derived growth factor; FGF: fibroblast growth factor. From: Sahai, 2020 [22].

CAF can regulate tumorigenesis by producing soluble molecules, including vascular endothelial growth factor (VEGF), fibroblast growth factor (FGF), platelet-derived growth factor (PDGF), epidermal growth factor (EGF), interleukins (IL) and transforming growth factor-beta (TGF-β). They can also produce molecules that can suppress cancer growth [23] (Figure II.3). Tumor-inhibiting CAF could be present in the TME as a host defense mechanism to restrain cancer progression [24, 25].

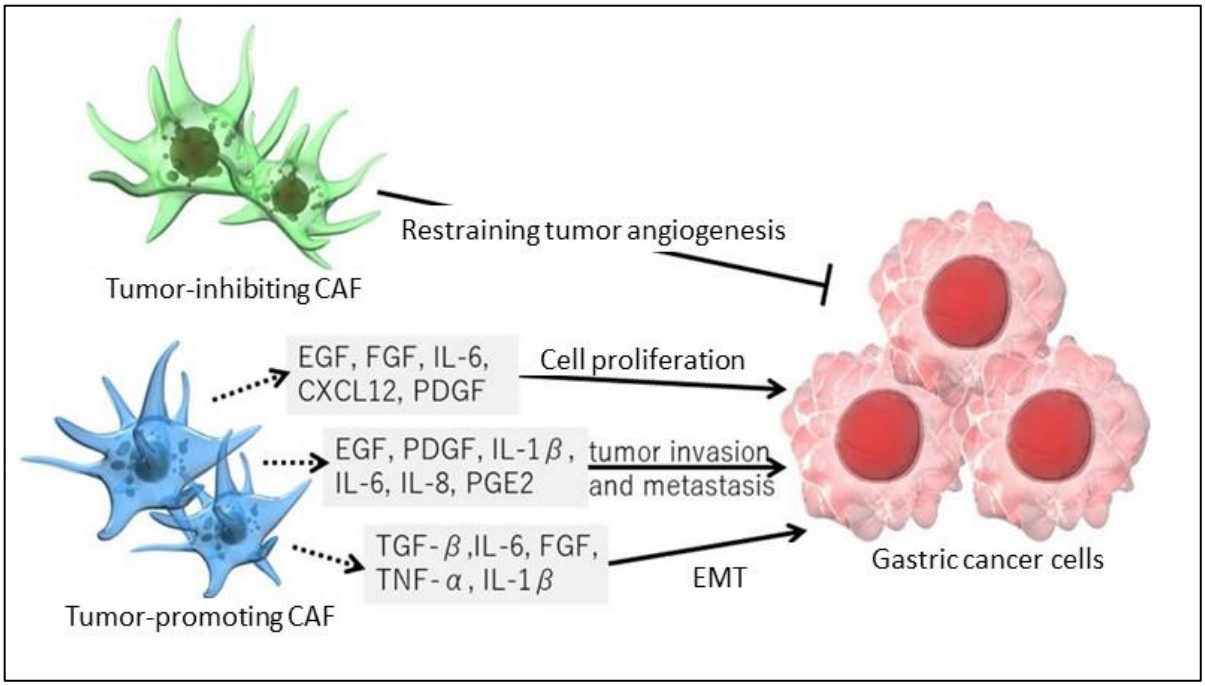

Figure II.3. The interplay between cancer-associated fibroblasts (CAF) and gastric cancer (GC) cells.
CAF regulate tumor growth by secreting various molecules. EGF: epidermal growth factor; FGF: fibroblast growth factor; IL: interleukin; CXCL12: C-X-C motif chemokine ligand 12; PDGF: platelet-derived growth factor; PGE2: prostaglandin E2; TGFβ: transforming growth factor-β; TNF: tumor necrosis factor; EMT: epithelial-mesenchymal transition. Adapted from: Oya, 2020 [26].

Altogether, it seems like CAF are widely heterogeneous and their subtypes have to be considered as “states” rather than fixed cell types [27]. They can be classified into 4 broad categories: immune, desmoplastic, contractile and aggressive [28] (Figure II.4). Such a classification can clarify differences between existing CAF until a more comprehensive report, which will help cluster CAF across different cancers to identify other subpopulations and their characteristic markers.

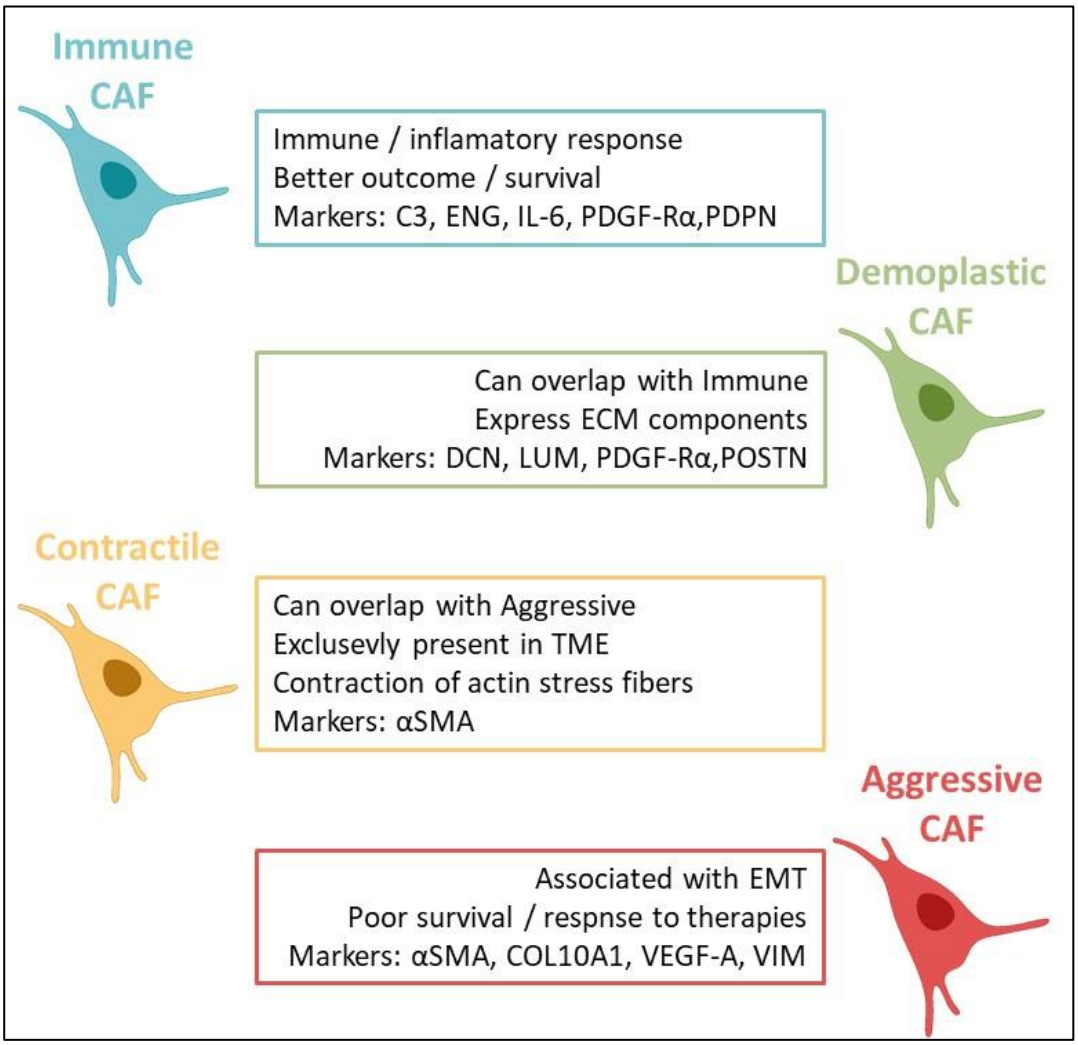

Figure II.4. Proposed categories of cancer-associated fibroblasts (CAF).
The immune subpopulation is associated with C3: complement system components; ENG: endoglin; IL-6: interleukin-6; PDGF-Rα: platelet-derived growth factor-receptor alpha and PDPN: podoplanin expression. The desmoplastic subpopulation is specifically characterized by a high expression of DCN: decorin; LUM: lumican and POSTN: periostin. The contractile subpopulation is defined by a high expression of factors involved in contraction of actin stress fibers. Aggressive CAF highly express COL10A1: collagen; VEGF-A: vascular endothelial growth factor and VIM: vimentin. Both contractile and aggressive subtypes show the highest expression of αSMA: alpha smooth muscle actin and are linked to poor patient survival / outcome. Adapted from: Simon, 2021 [28].

Based on previous studies, the histology of CAF accumulated in colon, esophagus, breast, and liver cancer could reflect a poor prognosis [29–31]. GC is highly infiltrated by CAF, especially undifferentiated GC, where the presence of CAF support tumor growth and metastasis by direct cell-to-cell contact or in a paracrine manner [32, 33]. IL-6 secreted by CAF has an important role by promoting GC cells growth, since the knockout of IL-6 inhibits GC [34]. Therefore, exploring the function of CAF in GC through experimental models is highly recommended. For this purpose, several methods to isolate CAF from GC tissues have been established. CAF are not immortalized but can be used at low passage numbers.

CAF implication in GC metastasis

The main cause of GC low survival rate is metastasis [35]. Although, like cancer cells, CAF are sensitive to chemotherapeutic agents, they are implicated in GC metastasis, because of their known role in enhancing epithelial-mesenchymal transition (EMT), a phenomenon by which cancer cells lose polarity and adhesion, and gain migratory and invasive capacity [36, 37]. Many secreted factors are involved, including IL-6 [38], FGF-9 [39] and C-X-C motif chemokine ligand 12 (CXCL12) [40], in addition to CD9-positive exosomes from CAF [41]. In CAF treated by chemotherapy, the glycoprotein 130 (gp130) was identified as a candidate factor contributing to the increased migration of GC cells [42].

CAF and GC chemotherapy resistance

As developed earlier, chemotherapies are one of the main options of GC therapy. Nonetheless, patients often show resistance to chemotherapy. The TME has been studied as one of the important underlying mechanism of drug resistance in GC [43]. CAF are able to cooperate with GC cells and provide them a protective niche allowing the escape from the cytotoxic effects of chemotherapy [44]. Several mechanisms have been confirmed such as the secretion of the IL-6 or the IL-7, in addition to the decrease of drugs intake [45, 46].

Targeting CAF for clinical benefit

From the characteristics presented above, targeting CAF would be beneficial in the treatment of GC. Several therapeutic approaches targeting CAF have been proposed as novel agents, such as PT630, a fibroblasts activation protein (FAP) inhibitor [47] or sibrotuzumab, an anti-FAP [48], or other options [49, 50]. However, the survival benefit of targeting CAF remains

uncertain, as several studies have reported controversial results [51–53]. Recent advanced technologies in single-cell transcriptome profiling in several cancers revealed that CAF have molecular and functional inter- and intra-cancer heterogeneity. Additional studies should evaluate CAF specific markers in GC environment to best select CAF-targeting drugs against GC [54, 55].

Altogether, the TME shows a very important role in the development of tumor cells and deserves to be studied more. The main challenge is to overcome the difficulties of modeling the TME and the capacity to control such models. TME represents a complex system, starting from the ECM to the different types of cells that can be present to support tumor. Classic cancer models, such as two-dimensional (2D) cultures, failed to mimic such complex environment. Patient-derived xenograft (PDX) are a better system, getting cancer cells into live mice, yet it is limited by standardizing difficulties and high associated costs. Development of *in vitro* models and the use of three-dimensional (3D) culture technologies can be suitable to better mimic the *in vivo* TME and help further understanding of the impact of each component of the TME [56].

II.3. References

[1] L. A. Liotta and E. C. Kohn, “The microenvironment of the tumour–host interface,” *Nat.*, vol. 411, no. 6835, pp. 375–379, May 2001, doi: 10.1038/35077241.

[2] S. S. McAllister and R. A. Weinberg, “Tumor-host interactions: a far-reaching relationship,” *J. Clin. Oncol.,* vol. 28, no. 26, pp. 4022–4028, Jul. 2010, doi: 10.1200/JCO.2010.28.4257.

[3] D. Hanahan and R. A. Weinberg, “Hallmarks of cancer: the next generation,” *Cell*, vol. 144, no. 5, pp. 646–674, Mar. 2011, doi: 10.1016/J.CELL.2011.02.013.

[4] H. Wiig, O. Tenstad, P. O. Iversen, R. Kalluri, and R. Bjerkvig, “Interstitial fluid: the overlooked component of the tumor microenvironment?,” *Fibrogenes. Tissue Repair*, vol. 3, no. 1, pp. 1–11, Jul. 2010, doi: 10.1186/1755-1536-3-12.

[5] P. I. Ribeiro Franco, A. P. Rodrigues, L. B. de Menezes, and M. Pacheco Miguel, “Tumor microenvironment components: Allies of cancer progression,” *Pathol. - Res. Pract.*, vol. 216, no. 1, p. 152729, Jan. 2020, doi: 10.1016/J.PRP.2019.152729.

[6] T. Kovács, E. Mikó, G. Ujlaki, Z. Sári, and P. Bai, “The microbiome as a component of the tumor microenvironment,” *Adv. Exp. Med. Biol.*, vol. 1225, pp. 137–153, 2020, doi: 10.1007/978-3-030-35727-6_10.

[7] J. A. Joyce and J. W. Pollard, “Microenvironmental regulation of metastasis,” *Nat. Rev. Cancer*, vol. 9, no. 4, pp. 239–252, Mar. 2008, doi: 10.1038/NRC2618.

[8] S. Koontongkaew, “The tumor microenvironment contribution to development, growth, invasion and metastasis of head and neck squamous cell carcinomas,” *J. Cancer*, vol. 4, no. 1, p. 66, 2013, doi: 10.7150/JCA.5112.

[9] X. Xu, M. C. Farach-Carson, and X. Jia, “Three-dimensional in vitro tumor models for cancer research and drug evaluation,” *Biotechnol. Adv.*, vol. 32, no. 7, pp. 1256–1268, Nov. 2014, doi: 10.1016/J.BIOTECHADV.2014.07.009.

[10] Y. Wu *et al.*, “Comprehensive genomic meta-analysis identifies intra-tumoural stroma as a predictor of survival in patients with gastric cancer,” *Gut*, vol. 62, no. 8, pp. 1100–1111, Aug. 2013, doi: 10.1136/GUTJNL-2011-301373.

[11] M. T. Uhlik *et al.*, “Stromal-based signatures for the classification of gastric cancer,” *Cancer Res.*, vol. 76, no. 9, pp. 2573–2586, May 2016, doi: 10.1158/0008-5472.CAN-16-0022.

[12] D. Izumi *et al.*, “CXCL12/CXCR4 activation by cancer-associated fibroblasts promotes integrin β1 clustering and invasiveness in gastric cancer,” *Int. J. Cancer*, vol. 138, no. 5, pp. 1207–1219, Mar. 2016, doi: 10.1002/IJC.29864.

[13] L. Bu *et al.*, “Biological heterogeneity and versatility of cancer-associated fibroblasts in the tumor microenvironment,” *Oncogene*, vol. 38, no. 25, pp. 4887–4901, Feb. 2019, doi: 10.1038/S41388-019-0765-Y.

[14] R. Kalluri, “The biology and function of fibroblasts in cancer,” *Nat. Rev. Cancer*, vol. 16, no. 9, pp. 582–598, Aug. 2016, doi: 10.1038/NRC.2016.73.

[15] F. Calvo *et al.*, "Mechanotransduction and YAP-dependent matrix remodelling is required for the generation and maintenance of cancer-associated fibroblasts," *Nat. Cell Biol.*, vol. 15, no. 6, pp. 637–646, May 2013, doi: 10.1038/NCB2756.

[16] J. Paulsson and P. Micke, "Prognostic relevance of cancer-associated fibroblasts in human cancer," *Semin. Cancer Biol.*, vol. 25, pp. 61–68, Apr. 2014, doi: 10.1016/J.SEMCANCER.2014.02.006.

[17] C. T. Foster, F. Gualdrini, and R. Treisman, "Mutual dependence of the MRTF–SRF and YAP–TEAD pathways in cancer-associated fibroblasts is indirect and mediated by cytoskeletal dynamics," *Genes Dev.*, vol. 31, no. 23–24, pp. 2361–2375, Dec. 2017, doi: 10.1101/GAD.304501.117.

[18] H. Sugimoto, T. M. Mundel, M. W. Kieran, and R. Kalluri, "Identification of fibroblast heterogeneity in the tumor microenvironment," *Cancer Biol. Ther.,* vol. 5, no. 12, pp. 1640–1646, 2006, doi: 10.4161/CBT.5.12.3354.

[19] A. Arina *et al.*, "Tumor-associated fibroblasts predominantly come from local and not circulating precursors," *Proc. Natl. Acad. Sci.*, vol. 113, no. 27, pp. 7551–7556, Jul. 2016, doi: 10.1073/PNAS.1600363113.

[20] K. Räsänen and A. Vaheri, "Activation of fibroblasts in cancer stroma," *Experimental Cell Research*, vol. 316, no. 17. Academic Press Inc., pp. 2713–2722, Oct. 15, 2010, doi: 10.1016/j.yexcr.2010.04.032.

[21] M. V. Plikus *et al.*, "Fibroblasts: Origins, definitions, and functions in health and disease," *Cell*, vol. 184, no. 15, pp. 3852–3872, Jul. 2021, doi: 10.1016/J.CELL.2021.06.024.

[22] E. Sahai *et al.*, "A framework for advancing our understanding of cancer-associated fibroblasts," *Nat. Rev. Cancer*, vol. 20, no. 3, pp. 174–186, Jan. 2020, doi: 10.1038/S41568-019-0238-1.

[23] Y. Mizutani *et al.*, "Meflin-positive cancer-associated fibroblasts inhibit pancreatic carcinogenesis," *Cancer Res.*, vol. 79, no. 20, pp. 5367–5381, Oct. 2019, doi: 10.1158/0008-5472.CAN-19-0454.

[24] Z. Wang *et al.*, "Cancer-associated fibroblasts suppress cancer development: the other side of the coin," *Front. Cell Dev. Biol.*, vol. 0, p. 146, Feb. 2021, doi: 10.3389/FCELL.2021.613534.

[25] L. Zhou, K. Yang, R. R. Wickett, and Y. Zhang, "Dermal fibroblasts induce cell cycle arrest and block epithelial–mesenchymal transition to inhibit the early stage melanoma development," *Cancer Med.*, vol. 5, no. 7, pp. 1566–1579, Jul. 2016, doi: 10.1002/CAM4.707.

[26] Y. Oya, Y. Hayakawa, and K. Koike, "Tumor microenvironment in gastric cancers," *Cancer Sci.*, vol. 111, no. 8, pp. 2696–2707, Aug. 2020, doi: 10.1111/CAS.14521.

[27] C. Zeltz, I. Primac, P. Erusappan, J. Alam, A. Noel, and D. Gullberg, "Cancer-associated fibroblasts in desmoplastic tumors: emerging role of integrins," *Semin. Cancer Biol.*, vol. 62, pp. 166–181, May 2020, doi: 10.1016/J.SEMCANCER.2019.08.004.

[28] T. Simon and B. Salhia, “Cancer associated fibroblast subpopulations with diverse and dynamic roles in the tumor microenvironment,” *Mol. Cancer Res.*, p. molcanres.0282.2021, Oct. 2021, doi: 10.1158/1541-7786.MCR-21-0282.

[29] E. M. de Kruijf *et al.*, “Tumor–stroma ratio in the primary tumor is a prognostic factor in early breast cancer patients, especially in triple-negative carcinoma patients,” *Breast Cancer Res. Treat.*, vol. 125, no. 3, pp. 687–696, Apr. 2010, doi: 10.1007/S10549-010-0855-6.

[30] Z. Lv *et al.*, “Tumor–stroma ratio is a prognostic factor for survival in hepatocellular carcinoma patients after liver resection or transplantation,” *Surgery*, vol. 158, no. 1, pp. 142–150, Jul. 2015, doi: 10.1016/J.SURG.2015.02.013.

[31] W. E. Mesker *et al.*, “The carcinoma–stromal ratio of colon carcinoma is an independent factor for survival compared to lymph node status and tumor stage,” *Anal. Cell. Pathol.*, vol. 29, no. 5, pp. 387–398, Jan. 2007.

[32] T. Hasegawa *et al.*, “Cancer-associated fibroblasts might sustain the stemness of scirrhous gastric cancer cells via transforming growth factor-β signaling,” *Int. J. Cancer*, vol. 134, no. 8, pp. 1785–1795, Apr. 2014, doi: 10.1002/IJC.28520.

[33] X. Liu *et al.*, “Cancer-associated fibroblast infiltration in gastric cancer: the discrepancy in subtypes pathways and immunosuppression,” *J. Transl. Med.*, vol. 19, no. 1, pp. 1–16, Jul. 2021, doi: 10.1186/S12967-021-03012-Z.

[34] H. Kinoshita *et al.*, “Interleukin-6 mediates epithelial–stromal interactions and promotes gastric tumorigenesis,” *PLoS One*, vol. 8, no. 4, p. e60914, Apr. 2013, doi: 10.1371/JOURNAL.PONE.0060914.

[35] Y. Yonemura *et al.*, “Effects of neoadjuvant laparoscopic hyperthermic intraperitoneal chemotherapy and neoadjuvant intraperitoneal/systemic chemotherapy on peritoneal metastases from gastric cancer,” *Ann. Surg. Oncol.*, vol. 24, no. 2, pp. 478–485, Aug. 2016, doi: 10.1245/S10434-016-5487-6.

[36] R. Cristescu *et al.*, “Molecular analysis of gastric cancer identifies subtypes associated with distinct clinical outcomes,” *Nat. Med.*, vol. 21, no. 5, pp. 449–456, Apr. 2015, doi: 10.1038/nm.3850.

[37] G. Krzysiek-Maczka *et al.*, “Role of Helicobacter pylori infection in cancer-associated fibroblast-induced epithelial-mesenchymal transition in vitro,” *Helicobacter*, vol. 23, no. 6, p. e12538, Dec. 2018, doi: 10.1111/HEL.12538.

[38] X. Wu *et al.*, “IL-6 secreted by cancer-associated fibroblasts promotes epithelial-mesenchymal transition and metastasis of gastric cancer via JAK2/STAT3 signaling pathway,” *Oncotarget*, vol. 8, no. 13, p. 20741, 2017, doi: 10.18632/ONCOTARGET.15119.

[39] R. Wang *et al.*, “Downregulation of miRNA-214 in cancer-associated fibroblasts contributes to migration and invasion of gastric cancer cells through targeting FGF9 and inducing EMT,” *J. Exp. Clin. Cancer Res.*, vol. 38, no. 1, pp. 1–15, Jan. 2019, doi: 10.1186/S13046-018-0995-9.

[40] D. Izumi *et al.*, “CXCL12/CXCR4 activation by cancer-associated fibroblasts promotes

integrin β1 clustering and invasiveness in gastric cancer," *Int. J. Cancer*, vol. 138, no. 5, pp. 1207–1219, Mar. 2016, doi: 10.1002/IJC.29864.

[41] Y. Miki *et al.*, "CD9-positive exosomes from cancer-associated fibroblasts stimulate the migration ability of scirrhous-type gastric cancer cells," *Br. J. Cancer*, vol. 118, no. 6, pp. 867–877, Feb. 2018, doi: 10.1038/bjc.2017.487.

[42] T. Ishii et al., "Drug-exposed cancer-associated fibroblasts facilitate gastric cancer cell progression following chemotherapy," Gastric Cancer, vol. 24, no. 4, pp. 810–822, Apr. 2021, doi: 10.1007/S10120-021-01174-9.

[43] M. B. Meads, R. A. Gatenby, and W. S. Dalton, "Environment-mediated drug resistance: a major contributor to minimal residual disease," *Nat. Rev. Cancer*, vol. 9, no. 9, pp. 665–674, Aug. 2009, doi: 10.1038/NRC2714.

[44] K. H. T. Paraiso and K. S. M. Smalley, "Fibroblast-mediated drug resistance in cancer," *Biochem. Pharmacol.*, vol. 85, no. 8, pp. 1033–1041, Apr. 2013, doi: 10.1016/J.BCP.2013.01.018.

[45] C.-H. Heldin, K. Rubin, K. Pietras, and A. Östman, "High interstitial fluid pressure — an obstacle in cancer therapy," *Nat. Rev. Cancer*, vol. 4, no. 10, pp. 806–813, Oct. 2004, doi: 10.1038/nrc1456.

[46] F. Lotti *et al.*, "Chemotherapy activates cancer-associated fibroblasts to maintain colorectal cancer-initiating cells by IL-17A," *J. Exp. Med.*, vol. 210, no. 13, pp. 2851–2872, Dec. 2013, doi: 10.1084/JEM.20131195.

[47] A. M. Santos, J. Jung, N. Aziz, J. L. Kissil, and E. Puré, "Targeting fibroblast activation protein inhibits tumor stromagenesis and growth in mice," *J. Clin. Invest.*, vol. 119, no. 12, p. 3613, Dec. 2009, doi: 10.1172/JCI38988.

[48] A. M. Scott *et al.*, "A phase i dose-escalation study of sibrotuzumab in patients with advanced or metastatic fibroblast activation protein-positive cancer," *Clin. Cancer Res.*, vol. 9, no. 5, 2003.

[49] X. Chen and E. Song, "Turning foes to friends: targeting cancer-associated fibroblasts," *Nat. Rev. Drug Discov.*, vol. 18, no. 2, pp. 99–115, Nov. 2018, doi: 10.1038/S41573-018-0004-1.

[50] K. C. Valkenburg, A. E. de Groot, and K. J. Pienta, "Targeting the tumour stroma to improve cancer therapy," *Nat. Rev. Clin. Oncol.*, vol. 15, no. 6, pp. 366–381, Apr. 2018, doi: 10.1038/S41571-018-0007-1.

[51] K. Narra *et al.*, "Phase II trial of single agent Val-boroPro (talabostat) inhibiting fibroblast activation protein in patients with metastatic colorectal cancer," *Cancer Biol. Ther.*, vol. 6, no. 11, pp. 1691–1699, 2007, doi: 10.4161/CBT.6.11.4874.

[52] H. Park *et al.*, "The prognostic significance of cancer-associated fibroblasts in pancreatic ductal adenocarcinoma," *Tumor Biol.*, vol. 39, no. 10, pp. 1–9, Oct. 2017, doi: 10.1177/1010428317718403.

[53] A. D. Rhim *et al.*, "Stromal elements act to restrain, rather than support, pancreatic ductal adenocarcinoma," *Cancer Cell*, vol. 25, no. 6, pp. 735–747, Jun. 2014, doi:

10.1016/J.CCR.2014.04.021.

[54] H. Li *et al.*, “Reference component analysis of single-cell transcriptomes elucidates cellular heterogeneity in human colorectal tumors,” *Nat. Genet. 2017*, vol. 49, no. 5, pp. 708–718, Mar. 2017, doi: 10.1038/ng.3818.

[55] C. Neuzillet *et al.*, “Inter- and intra-tumoural heterogeneity in cancer-associated fibroblasts of human pancreatic ductal adenocarcinoma,” *J. Pathol.*, vol. 248, no. 1, pp. 51–65, May 2019, doi: 10.1002/PATH.5224.

[56] J. Hoarau-Véchot, A. Rafii, C. Touboul, and J. Pasquier, “Halfway between 2d and animal models: are 3d cultures the ideal tool to study cancer-microenvironment interactions?,” *Int. J. Mol. Sci., Vol. 19, Page 181*, vol. 19, no. 1, p. 181, Jan. 2018, doi: 10.3390/IJMS19010181.

Chapter III
Three-Dimensional Cancer Models

III.1. General Introduction

Cancer research and the development of anti-cancer drugs rely on preclinical cancer models. A variety of cancer models have been developed as means to understand cancer mechanisms, identify novel targets and select efficient cytotoxic drugs.

The historical *in vitro* cancer model used for analyzing the cytotoxic potential of novel therapies is based, in solid cancers, on monolayers of adherent cells in two-dimensional (2D) cultures (so called flat biology). Despite undeniable effectiveness, several limitations characterize these approaches, including reduced cell-cell and cell-matrix interactions or exposure to diffusible metabolites originating from other compartments, such as blood vessels.

Animal models were widely used to bypass the limits of 2D cancer models, especially using patients-derived xenografts (PDX). Although mouse-based systems may not offer the best experimental set up, due to differences between humans and animals, syngeneic mouse models or humanized mice can indeed be used to study tumor *vs.* stroma interactions. Nevertheless, ethical, cost and regulatory issues limit the use of animal models.

To bridge the gap between *in vitro* and *in vivo*, three-dimensional (3D) culture systems have been elaborated to present a more realistic approach to biological responses. Several 3D culture models have been reported, predominantly multicellular tumor spheroids (MCTS / spheroids) and patient-derived tumor organoids (PDTO / organoids).

In this chapter, the current status of *in vitro* and *ex vivo* 3D models of cancers will be developed in 2 scientific reviews that were written during the thesis preparation.

The first review (in press in "*Bulletin de Cancer*" in *November 2021*) was prepared in response to an invitation by the editor of the "*Bulletin du Cancer*" journal, the official journal of 'Société Française du Cancer'. This review inspects the use of spheroids and organoids as solid cancer models by highlighting their differences and discussing their impact on drug development *(section III.2. Review 1)*.

The second review (published in the journal "*Cancers*" in *September 2020*) presents an overview of the important findings from analyses of spheroids and organoids, especially in the

areas of molecular profiling, drug discovery, pathogen infection and personalized medicine focusing on gastric cancer *(section III.3. Review 2)*.

Version en Français

La recherche sur le cancer et le développement de médicaments anticancéreux reposent sur des modèles précliniques. Divers modèles de cancer ont été développés pour comprendre les mécanismes du cancer, identifier de nouvelles cibles et sélectionner des médicaments cytotoxiques efficaces.

Le modèle historique de cancer *in vitro* utilisé pour analyser le potentiel cytotoxique de nouvelles thérapies est basé, dans les cancers solides, sur des monocouches de cellules adhérentes en cultures bidimensionnelles (2D). Malgré une efficacité indéniable, plusieurs limites caractérisent ces approches, notamment la réduction des interactions cellule-cellule et cellule-matrice ou l'exposition à des métabolites diffusibles provenant d'autres compartiments comme les vaisseaux sanguins.

Les modèles animaux ont été largement utilisés pour contourner les limites des modèles de cancer 2D, en particulier en utilisant des xénogreffes dérivées de patients (PDX). Bien que les systèmes basés sur la souris n'offrent peut-être pas la meilleure configuration expérimentale, en raison des différences entre les humains et les animaux, des modèles de souris syngéniques ou des souris humanisées peuvent en effet être utilisés pour étudier les interactions tumeur vs stroma. Néanmoins, des problèmes éthiques, de coûts et de réglementation limitent l'utilisation de modèles animaux.

Pour combler le fossé entre l'*in vitro* et l'*in vivo*, des systèmes de culture tridimensionnels (3D) ont été élaborés qui présentent une approche plus réaliste des réponses biologiques. Plusieurs modèles de culture 3D ont été rapportés, principalement des sphéroïdes tumoraux multicellulaires (MCTS / sphéroïdes) et des organoïdes tumoraux dérivés de patients (PDTO / organoïdes).

Dans ce chapitre, l'état actuel des modèles 3D *in vitro* et *ex vivo* de cancers sera développé dans les 2 revues écrites pendant la préparation de la thèse.

La première revue (en presse dans le journal "*Bulletin de Cancer*" en *Novembre 2021*) a été préparée en français pour le "*Bulletin du Cancer*", le journal officiel de la Société Française du Cancer. Cette revue examine l'utilisation des sphéroïdes et des organoïdes comme modèles

de cancer solides en soulignant leurs différences et en discutant de leur impact sur le développement de médicaments *(section III.2. Review 1)*.

La deuxième revue (publiée dans le journal "*Cancers*" en *Septembre 2020*) présente une vue d'ensemble des résultats importants des analyses de sphéroïdes et d'organoïdes, en particulier dans les domaines du profilage moléculaire, de la découverte de médicaments, de l'infection par des agents pathogènes et de la médecine personnalisée, en se concentrant sur le cancer gastrique *(section III.3. Review 2)*.

III.2. Review 1: Spheroids to Organoids: Solid Cancer Models for Anticancer Drug Discovery

Authors: George Alzeeb[#], Laurent Corcos[#], Catherine Le Jossic-Corcos[#]*

[#]*INSERM U1078, Université de Brest, 22 avenue Camille Desmoulins, 29200 BREST FRANCE*

**Correspondance:* catherine.corcos@univ-brest.fr

Bulletin de Cancer 2021, in press; doi: 10.1016/j.bulcan.2021.09.019

Accepted: October 2021

Abstract: Cell culture is an important and necessary technology in oncology research. Currently, two-dimensional (2D) cell culture models are the most widely used, but they cannot reproduce the complexity and pathophysiology of tumors *in vivo*. This may be a major cause of the high rate of attrition of anticancer drugs entering clinical trials, the rate of new anticancer drugs entering the market being less than 5%. One way to improve the success of new cancer drugs in the clinic is based on the use of three-dimensional (3D) cell culture models, more able to represent the complex environment and architecture of tumors. These 3D culture systems are also a powerful research tool for modeling the evolution of cancer from early stages to metastasis. Spheroids and organoids, the most adaptable models among 3D culture systems, are beginning to be used in pharmaceutical research and personalized medicine. In this article, we review the use of spheroids and organoids by highlighting their differences, discussing their impact on drug development, and looking at future challenges.

This review will be presented in this thesis as its published format in "Bulletin du Cancer".

Titre : Des sphéroïdes aux organoïdes : modèles de cancers solides pour la découverte de molécules anticancéreuses

Résumé : La culture cellulaire est une technologie importante et nécessaire dans la recherche en oncologie. Actuellement, les modèles de culture cellulaire en deux dimensions (2D) sont les plus utilisés, mais ils ne peuvent pas reproduire la complexité et la pathophysiologie des tumeurs *in vivo*. Ceci peut contribuer au fort taux d'attrition des candidats médicaments entrant dans les essais cliniques, le taux de nouveaux médicaments anticancéreux entrant dans le marché étant ≤ 5 %. Une voie d'amélioration repose sur l'utilisation de modèles de culture cellulaire tridimensionnels (3D), plus à même de représenter l'environnement et l'architecture complexes des tumeurs. Ces systèmes de culture en 3D constituent également un puissant outil de recherche permettant de modéliser l'évolution du cancer depuis les premiers stades jusqu'aux métastases. Les sphéroïdes et les organoïdes, les modèles les plus adaptables parmi les systèmes de culture en 3D, commencent à être utilisés dans la recherche pharmaceutique et dans la médecine personnalisée. Dans cette revue, nous faisons le point sur l'utilisation des sphéroïdes et des organoïdes en soulignant leurs différences, en discutant leur impact sur le développement des médicaments et en examinant les défis futurs.

Mots clés : cancer ; culture cellulaire ; sphéroïdes ; organoïdes ; criblage de molécules ; médecine personnalisée.

Abréviations

2D	Deux Dimensions
3D	Trois Dimensions
CAF	Cancer-Associated Fibroblasts (Fibroblastes Associés au Cancer)
CG	Cancer Gastrique
FDA	Food and Drug Administration
HIF	Facteurs Inductibles d'Hypoxie
HUVEC	Human Umbilical Vein Endothelial Cells
KIF	Famille de Kinésine
LRP	Lipoprotéines
MEC	Matrice Extracellulaire
MET	Microenvironnement Tumoral
NK	Natural Killer
PDX	Patient-Derived Xenograft
PRMT5	Protéine Arginine Méthyl-Transférase 5
TEM	Transition Epithélio-Mésenchymateuse

Bull Cancer 2020; xx: xxx

en ligne sur / *on line on*
www.em-consulte.com/revue/bulcan
www.sciencedirect.com

Synthèse

Des sphéroïdes aux organoïdes : modèles de cancers solides pour la découverte de molécules anticancéreuses

George Alzeeb, Laurent Corcos, Catherine Le Jossic-Corcos

Reçu le 6 septembre 2021
Accepté le 26 septembre 2021
Disponible sur internet le :

Université de Brest, Inserm U1078, 22, avenue Camille-Desmoulins, 29200 Brest, France

Correspondance :
Catherine Le Jossic-Corcos, Université de Brest, Inserm U1078, 22, avenue Camille-Desmoulins, 29200 Brest, France.
catherine.corcos@univ-brest.fr

Mots clés
Cancer
Culture cellulaire
Sphéroïdes
Organoïdes
Criblage de molécules
Médecine personnalisée

Résumé

La culture cellulaire est une technologie importante et nécessaire dans la recherche en oncologie. Actuellement, les modèles de culture cellulaire en deux dimensions (2D) sont les plus utilisés, mais ils ne peuvent pas reproduire la complexité et la pathophysiologie des tumeurs in vivo. Ceci peut contribuer au fort taux d'attrition des candidats médicaments entrant dans les essais cliniques, le taux de nouveaux médicaments anticancéreux entrant dans le marché étant $\leq$ 5 %. Une voie d'amélioration repose sur l'utilisation de modèles de culture cellulaire tridimensionnels (3D), plus à même de représenter l'environnement et l'architecture complexes des tumeurs. Ces systèmes de culture en 3D constituent également un puissant outil de recherche permettant de modéliser l'évolution du cancer depuis les premiers stades jusqu'aux métastases. Les sphéroïdes et les organoïdes, les modèles les plus adaptables parmi les systèmes de culture en 3D, commencent à être utilisés dans la recherche pharmaceutique et dans la médecine personnalisée. Dans cette revue, nous faisons le point sur l'utilisation des sphéroïdes et des organoïdes en soulignant leurs différences, en discutant leur impact sur le développement des médicaments et en examinant les défis futurs.

Keywords
Cancer
Cell culture
Spheroids
Organoids
Drug screening
Precision medicine

Summary

Spheroids to organoids: Solid cancer models for anticancer drug discovery

Cell culture is an important and necessary technology in oncology research. Currently, two-dimensional (2D) cell culture models are the most widely used, but they cannot reproduce the complexity and pathophysiology of tumors in vivo. *This may be a major cause of the high rate of attrition of anticancer drugs entering clinical trials, the rate of new anticancer drugs entering the market being less than 5 %. One way to improve the success of new cancer drugs in the clinic is based on the use of three-dimensional (3D) cell culture models, more able to represent the complex environment and architecture of tumors. These 3D culture systems are also a powerful*

Pour citer cet article : Alzeeb G, et al. Des sphéroïdes aux organoïdes : modèles de cancers solides pour la découverte de molécules anticancéreuses. Bull Cancer (2021), https://doi.org/10.1016/j.bulcan.2021.09.019

research tool for modeling the evolution of cancer from early stages to metastasis. Spheroids and organoids, the most adaptable models among 3D culture systems, are beginning to be used in pharmaceutical research and personalized medicine. In this article, we review the use of spheroids and organoids by highlighting their differences, discussing their impact on drug development, and looking at future challenges.

Abréviations

2D	**Deux Dimensions**
3D	**Trois Dimensions**
AKR1C3	**Aldo-Keto Reductase**
CAF	**Cancer-associated fibroblast**
FDA	**Food and Drug Administration**
FZD	**Frizzled**
HIF	**Facteurs Inductibles par l'Hypoxie**
HUVEC	**Human Umbilical Vein Endothelial Cells**
KIF	**Famille de Kinésine**
LRP	**Lipoprotéines**
MCTS	**Multicellular Tumor Spheroids**
MEC	**Matrice Extracellulaire**
MET	**Microenvironnement Tumoral**
NK	**Natural Killer**
PDTO	**Patient-Derived Tumor Organoids**
PDX	**Patient-Derived Xenograft**
PRMT5	**Protéine Arginine Méthyl-Transférase 5**
TEM	**Transition Epithélio-Mésenchymateuse**

Introduction

Avec environ 19,3 millions de nouveaux cas diagnostiqués et presque dix millions de décès en 2020 dans le monde, le cancer reste une maladie particulièrement mortelle [1]. Malgré les progrès dans le domaine de la prévention, du diagnostic et du traitement au cours des dernières décennies, de nombreux obstacles restent à surmonter pour améliorer la survie des patients atteints de cancer [2]. Actuellement, un seul agent anticancéreux potentiel sur 5000 à 10 000 est approuvé par la FDA (*Food and Drug Administration*), et seul cinq pour cent des molécules à visée thérapeutique, toutes pathologies confondues, entrant dans la phase I des essais cliniques, sont finalement approuvées [3]. L'un des principaux défis du développement de nouveaux traitements anticancéreux est le transfert des importants progrès de la recherche vers la clinique [4]. Il est généralement admis que les modèles expérimentaux, *in vitro* et *in vivo*, sont des outils essentiels dans le domaine de la recherche en oncologie. Cependant, les modèles utilisés, dans les phases précoces, en particulier, reproduisent mal la complexité et l'hétérogénéité des tumeurs, auxquelles contribuent des facteurs génétiques intrinsèques et le microenvironnement, et sont incapables de stopper la progression de la maladie et de prédire la réponse au traitement [5].

Le modèle de culture cellulaire traditionnel en cancérologie des tumeurs solides est celui de la culture de lignées cellulaires cancéreuses en monocouche à deux dimensions (2D) (le cas des cellules de cancers hématologiques, qui se cultivent en suspension, ne sera pas traité dans cette revue). Ce modèle continue de jouer un rôle important pour la compréhension des mécanismes fondamentaux de la tumorigenèse grâce à sa grande disponibilité, sa facilité de manipulation, sa reproductibilité et son faible coût [6]. Toutefois, la culture en 2D impose des contraintes géométriques et mécaniques non physiologiques en raison de la nécessaire adhésion des cellules à un support solide artificiel (généralement en polystyrène). Une telle culture affecte la polarité des cellules et, donc, potentiellement, les phénotypes tumoraux caractéristiques des tumeurs d'origine [7]. Par conséquent, l'utilisation des modèles animaux, plus physiologiques, s'est intensifiée, augmentant ainsi la durée et le coût global du processus de découverte et de développement des médicaments. La xénogreffe de fragments de tumeur, appelée « *patient-derived xenograft* » (PDX), chez la souris immunodéprimée, est la plus utilisée pour étudier le développement des cancers humains et leurs réponses aux traitements [8].

Au cours des dernières décennies, de nouvelles techniques de modélisation des tumeurs solides ont été développées. Celles-ci reposent sur la culture de cellules maintenues dans un environnement tridimensionnel (3D), grâce à l'utilisation de substrats (boîtes/flacons de culture) à faible adhésivité cellulaire. Ainsi, la culture en 3D permet d'utiliser, *in vitro*, des échantillons complexes ou des mini-organes dans un environnement contrôlé. Ces modèles ont également l'avantage de mimer le comportement tumoral, qui dépend de signaux environnementaux, et des interactions cellule-cellule et cellule-matrice extracellulaire (MEC) [9]. Il est rapporté que les agents cytotoxiques sont généralement plus actifs dans les cultures en 2D qu'en 3D, conduisant, sans doute, à surévaluer leur activité par l'utilisation de la 2D uniquement. En revanche, la culture en 3D permettrait de mieux anticiper les phénomènes de résistance [10]. Outre la résistance aux agents anticancéreux, les modèles de culture en 3D peuvent également aider à prévoir la pénétration des médicaments dans les tumeurs, une limite importante, et souvent négligée, à l'origine d'échappement thérapeutique [11]. Deux modèles de culture cellulaire en 3D sont principalement utilisés : les sphéroïdes et les organoïdes [12]. La différence entre sphéroïde et organoïde est encore floue et l'utilisation d'un terme ou de l'autre relève essentiellement de la préférence des auteurs. Généralement, le terme de sphéroïde désigne les structures 3D simples préparées à partir des lignées cellulaires cancéreuses immortalisées, tandis que le terme d'organoïde est utilisé pour

Pour citer cet article : Alzeeb G, et al. Des sphéroïdes aux organoïdes : modèles de cancers solides pour la découverte de molécules anticancéreuses. Bull Cancer (2021), https://doi.org/10.1016/j.bulcan.2021.09.019

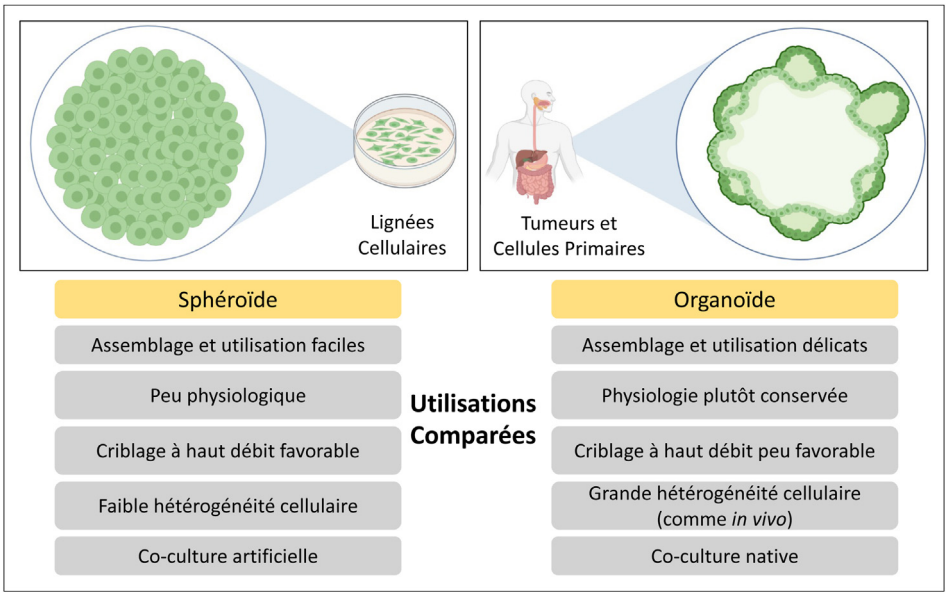

FIGURE 1

Comparaison sphéroïdes/organoïdes

Représentations schématiques d'un sphéroïde et d'un organoïde et tableau comparatif de leurs caractéristiques principales

les structures complexes et est souvent appliqué aux cellules cancéreuses primaires et aux cultures de biopsies tissulaires. Les progrès techniques permettent d'enrichir ces modèles, en particulier par la co-culture de cellules épithéliales cancéreuses avec des cellules stromales, ce qui permet de mieux représenter la MEC et mimer la physiologie tumorale.

Dans cette revue, nous décrivons l'état actuel de l'utilisation de la technologie de culture cellulaire en 3D pour modéliser certains aspects du cancer. Nous traitons deux des modèles les plus couramment utilisés pour la recherche en oncologie, les sphéroïdes et les organoïdes, en particulier pour le criblage de molécules anticancéreuses (*figure 1*). Nous soulignons également les différences entre ces deux modèles et relevons certaines de leurs limites.

Les sphéroïdes tumoraux multicellulaires

Les sphéroïdes tumoraux multicellulaires (« *multicellular tumor spheroids* », MCTS) sont des agrégats de cellules cultivées en 3D dans une matrice (e.g. matrigel ou agarose) ou en suspension, et développant des interactions complexes cellule-cellule et cellule-MEC [13]. Dans les approches utilisant des matrices, les sphéroïdes sont obtenus en favorisant la croissance cellulaire dans des structures tridimensionnelles naturelles (collagène, fibronectine, agarose, laminine, gélatine) ou synthétiques (oxyde de polyéthylène ou polyéthylène glycol) pour ressembler aux interactions tumeur-MEC *in vivo* [14]. Dans les méthodes de culture en suspension, aucun support artificiel n'est utilisé pour favoriser la croissance cellulaire. Ces méthodes ont pour effet d'empêcher la fixation des cellules sur le support, les forçant ainsi à s'agréger (ou à mourir par anoïkis) et à former des sphéroïdes [15] (*tableau I*). Bien que plusieurs méthodes permettent de générer des sphéroïdes (sur une surface non adhérente, par lévitation magnétique, en culture par gouttes ou « *hanging drop* »), toutes les lignées cellulaires ne sont pas capables de former des sphéroïdes [16]. En effet, chaque lignée cellulaire et chaque méthode choisie nécessitent une optimisation spécifique. La durée de la culture et la densité cellulaire sont les deux paramètres les plus importants.

De nombreuses études font état de différences dans l'expression des gènes et des protéines entre les sphéroïdes et les cultures en 2D, résultant en des modifications du métabolisme, de la communication cellulaire et de l'efficacité des médicaments [17]. Les sphéroïdes bien développés ressemblent à des microtumeurs ou à des régions micrométastatiques avasculaires observées *in vivo* [16]. Les tumeurs solides, qui présentent souvent des régions ayant des taux de prolifération différents, et des régions déficientes en oxygène – en raison du manque d'approvisionnement en sang dans les nodules tumoraux en croissance – reproduisent une hypoxie, un centre nécrotique, un gradient de nutriments (glucose, etc.) et une distribution hétérogène de lactate et d'ATP, ce que la culture 2D ne peut pas reproduire [15] (*figure 2*).

Les sphéroïdes et le microenvironnement tumoral

Le développement et la progression des tumeurs reposent, en grande partie, sur le dialogue entre les cellules tumorales, les cellules stromales et immunitaires voisines et la MEC. Une meilleure compréhension de la manière dont les interactions

Pour citer cet article : Alzeeb G, et al. Des sphéroïdes aux organoïdes : modèles de cancers solides pour la découverte de molécules anticancéreuses. Bull Cancer (2021), https://doi.org/10.1016/j.bulcan.2021.09.019

Tableau I
Avantages et inconvénients des techniques de culture des sphéroïdes couramment utilisées

Les types de cultures des sphéroïdes	Avantages	Inconvénients
Dans une matrice	Les propriétés physicochimiques et biologiques sont personnalisables Une grande variété de matériaux naturels et synthétiques peut être utilisée Des interactions forcées cellule-cellule et cellule-MEC sont établies	La MEC est artificielle et des matériaux externes sont nécessaires Certains biomatériaux peuvent interférer avec la réponse thérapeutique Faible reproductibilité, taille difficile à contrôler Le gradient d'oxygène, de nutriments et de pH n'est pas toujours reproduit Inclus dans une matrice, les cellules sont difficilement accessibles Peu compatibles avec les techniques de criblage à haut débit
En suspension	La MEC est produite par les cellules et aucun biomatériau externe n'est nécessaire Des interactions naturelles cellule-cellule et cellule-MEC sont établies Les co-cultures sont possibles Le gradient d'oxygène, de nutriments et de pH est reproduit Les sphéroïdes sont facilement accessibles La majorité des techniques sont peu coûteuses Compatibles avec les techniques de criblage à haut débit	Des optimisations peuvent être nécessaires pour la formation des sphéroïdes uniformes Les sphéroïdes peuvent se désagréger facilement Peu de protocoles et d'essais sont normalisés

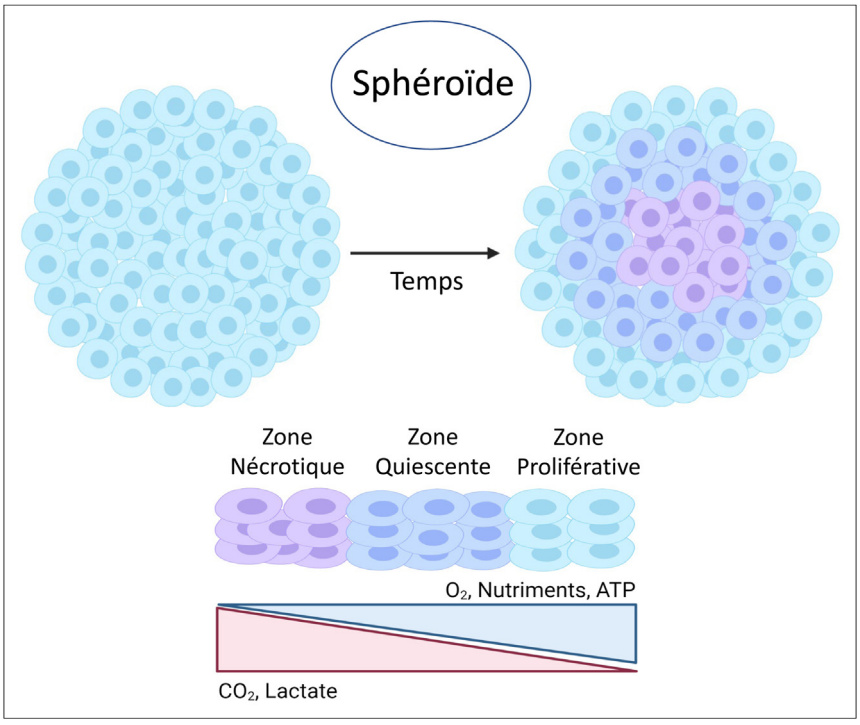

Figure 2
Représentation simplifiée d'un sphéroïde et de la formation des différentes couches cellulaires : couche externe proliférative, couche intermédiaire quiescente et un centre nécrotique. Les gradients d'oxygène, de nutriments, d'ATP, de CO2 et de lactate sont représentés

Pour citer cet article : Alzeeb G, et al. Des sphéroïdes aux organoïdes : modèles de cancers solides pour la découverte de molécules anticancéreuses. Bull Cancer (2021), https://doi.org/10.1016/j.bulcan.2021.09.019

cellulaires et moléculaires, au sein du microenvironnement tumoral (MET), façonnent la biologie tumorale et, par conséquent, le résultat clinique, est nécessaire [18]. Afin de reproduire l'hétérogénéité cellulaire des tumeurs solides et de mieux prendre en compte les phénomènes de résistance aux traitements, dont ceux qui pourraient être majorés, voire causés, par les interactions cellules cancéreuses-cellules stromales, des sphéroïdes pluricellulaires peuvent être assemblés. Ils associent des cellules épithéliales cancéreuses et des cellules stromales, comme les fibroblastes associés au cancer, dénommés *« cancer-associated fibroblasts »* (CAF), les cellules endothéliales ou les cellules immunitaires [19]. Les interactions cellules-cellules au sein des sphéroïdes affectent leur prolifération, leur survie et les réponses aux traitements en renforçant la formation des jonctions, l'activation de récepteurs d'adhésion (E-cadhérine) et la sécrétion des protéines de la MEC [20]. Ces interactions, couplées à la production de plusieurs protéines de la MEC (collagène, fibronectine, laminine, élastine), augmentent la densité des sphéroïdes et forment une barrière physique qui limite le transport des médicaments au sein de la masse cellulaire [21]. Les sphéroïdes constitués de cellules tumorales et de CAF, le type cellulaire le plus abondant dans la Transition Épithélio-Mésenchymateuse (TEM), sont largement utilisés pour tester des candidats médicaments. À titre d'exemple, des sphéroïdes bicellulaires, associant cellules cancéreuses et CAF, ont développé une résistance au paclitaxel liée à une modification d'expression de la protéine CD26 impliquée dans le contrôle de la transduction du signal d'apoptose et de la régulation immunitaire [22]. Plusieurs autres études ont démontré le potentiel thérapeutique de molécules anticancéreuses, ciblant les interactions entre CAF et cellules tumorales [23]. Dans un modèle de sphéroïdes, formés à partir des cellules cancéreuses de la prostate et de CAF, il a été montré que les CAF induisaient l'expression des gènes de régulation de la biosynthèse du cholestérol et des stéroïdes dans les cellules cancéreuses. Le blocage de ces deux voies par la simvastatine et un inhibiteur de l'aldo-keto-reductase (AKR1C3) ont eu un fort effet d'inhibition de croissance [24]. Dans un autre exemple, l'acriflavine, un composé connu pour inhiber des facteurs inductibles d'hypoxie (HIF) et la TEM, conduisant à l'activation de p53 et à l'induction de l'apoptose, a été identifié comme un inhibiteur de CAF dans un modèle de sphéroïdes associant des cellules de cancer colorectal et des CAF. Les auteurs suggèrent l'association, à l'avenir, de l'acriflavine aux chimiothérapies du cancer colorectal [25]. En outre, les sphéroïdes fournissent un modèle *in vitro* qui peut permettre de détecter la transformation de l'architecture d'une tumeur pré-invasive en une tumeur maligne, qui présente une perte progressive de l'architecture tissulaire [26]. Actuellement, il n'est pas possible d'utiliser une nomenclature unique, basée sur des marqueurs partagés et des fonctions similaires, pour définir les CAF. On doit distinguer deux cas de figure : d'une part, l'utilisation des CAF dérivés de la tumeur du patient et, d'autre part, les fibroblastes présents au site métastatique pour les tumeurs avancées, mais cette seconde situation n'est pas aisément exploitable, car il est moins fréquent d'opérer les métastases par rapport aux tumeurs primaires. Dans le cas d'une médecine personnalisée, il serait particulièrement approprié de pouvoir disposer des CAF de la tumeur et des fibroblastes – dont potentiellement des CAF – du site métastatique. Deux excellentes revues font le point des connaissances et des usages, d'une part, des fibroblastes [27] et, d'autre part, des CAF [28]. Le principe de réalité fait que les expériences sont réalisées avec des populations de CAF plus ou moins bien caractérisées.

En outre, le développement d'un modèle pertinent de sphéroïdes multicellulaires nécessiterait de connaître les différents types de cellules constituant la tumeur étudiée (cellules endothéliales, immunitaires en particulier) et leurs proportions. Ainsi, une triple co-culture, associant cellules cancéreuses pancréatiques, fibroblastes et cellules endothéliales (*« Human umbilical vein endothelial cells »*, HUVEC), a permis de mettre en évidence une diminution de la sensibilité des cellules cancéreuses à la chimiothérapie, mimant ainsi la résistance aux traitements observée *in vivo* [29]. La présence de cellules immunitaires T et NK a pu être associée à la mortalité de cellules du cancer colorectal dans des sphéroïdes multicellulaires [30].

Les sphéroïdes et la découverte des molécules anticancéreuses

Les modèles de culture cellulaire 3D permettent le criblage, à moyen débit, de candidats médicaments et l'identification des cibles cellulaires, deux étapes qui sont souvent les plus limitantes pour la découverte de molécules au potentiel thérapeutique [31]. Les modèles 3D montrent, cependant, leur supériorité, par rapport aux cultures 2D, du fait d'une plus grande proximité de leur profil d'expression génique avec celui des tumeurs. Par exemple, *KIFC1* et *KIF11*, deux membres de la famille de la kinésine-14 dont l'altération, généralement une surexpression, a été rapportée dans plusieurs cancers (poumons, ovaires, pancréas, seins, colon/rectum…) [32], sont surexprimés dans les sphéroïdes par rapport aux cellules cancéreuses gastriques parentales en 2D ; l'inhibition de l'expression de ces deux gènes perturbe la formation des sphéroïdes [33,34]. De plus, l'exploration des mécanismes d'échappement immunitaire des tumeurs et le criblage d'agents, ou de combinaisons d'agents d'immunothérapie, ont permis de montrer que le blocage de PD-1, par des anticorps spécifiques, renforce la cytotoxicité des cellules T contre les sphéroïdes gastriques exprimant PD-L1 [35].

Cependant, l'intégration des sphéroïdes aux processus de criblage à haut débit, pour prometteuse qu'elle soit, n'en est qu'à ses débuts, mais la relative simplicité des protocoles et la bonne reproductibilité des résultats plaident largement en leur faveur [36]. Les systèmes d'imagerie à haut débit, tels que l'Incucyte™

(Essen BioSciences) ou W8™ (CellDynamics), permettant un suivi et une analyse à long terme de la culture 3D, sont bien adaptés à cette fin [37].

Bien que des approches non spécifiques de patient, comme le modèle des sphéroïdes associant des lignées cellulaires établies, aient contribué à améliorer la recherche de candidats médicaments, les taux des molécules anticancéreuses approuvées, après l'ensemble des phases de développement, restent très bas. La possibilité de caractériser, au cas par cas, les composantes génétique et cellulaire individualisées de la tumeur permettrait de sélectionner rapidement la meilleure option thérapeutique.

Les organoïdes tumoraux dérivés de patients

Les organoïdes tumoraux, parfois appelés tumoroïdes, par opposition aux organoïdes non tumoraux, dérivés des patients (« *patient-derived tumor organoids* », PDTO) ou organoïdes, sont des mini-organes reconstitués *in vitro* et inclus dans une MEC. Ils sont préparés à partir de : i) tumeurs primaires dissociées mécaniquement ou enzymatiquement ; ou de ii) cellules souches primaires [38]. La structure et la fonctionnalité des organoïdes reflètent les caractéristiques spécifiques des tissus d'origine, par leur architecture globale, la distribution de différents types de cellules différenciées et leurs fonctions tissulaires et cellulaires spécifiques [39]. Les protocoles de préparation des organoïdes à partir de tissus normaux ont été adaptés pour produire des organoïdes dérivés de plusieurs cancers humains. En règle générale, ces protocoles consistent à dissocier les tissus tumoraux en petits fragments (10 mm^3 environ). Les cellules tumorales libérées des tissus sont reprises dans une matrice de membrane basale extraite d'une tumeur de souris (Englebreth-Holm Swarm) et contenant les principaux composants de la MEC, comme la laminine et le collagène de type IV [40]. Cependant, la variabilité de composition de cette matrice rend le contrôle de l'environnement de la culture plus difficile et peut réduire la reproductibilité. Pour ces raisons, des hydrogels synthétiques ont été récemment introduits [41].

De nombreuses caractéristiques ont encouragé l'utilisation des organoïdes comme modèles du cancer, puisqu'ils sont issus directement des patients et ne sont donc pas limités par les différences entre espèces, ce qui est le principal inconvénient des modèles animaux. En outre, les organoïdes peuvent également être produits en quantité et cryo-conservés, ce qui permet de créer des bibliothèques d'organoïdes représentatives de différents types et sous-types de cancers, en faisant un outil extrêmement utile pour les études précliniques [42,43].

Les organoïdes comme modèles pour étudier la sensibilité aux traitements et favoriser une médecine personnalisée

Les différences interindividuelles de sensibilité aux médicaments anticancéreux sont souvent mal prises en compte, dans la plupart des études utilisant des lignées cellulaires établies en 2D, en raison du manque de cellules suffisamment représentatives de profils génétiques différents. Le modèle d'organoïdes, élaboré à partir de tissu sain et de tissu cancéreux du même patient, permet d'identifier de possibles effets toxiques sur la contrepartie saine des tumeurs. Ainsi, une bibliothèque, composée de vingt cultures d'organoïdes de cancers colorectaux génétiquement différents et d'organoïdes dérivés de tissus normaux, a été utilisée pour cribler des molécules permettant d'identifier des traitements dépendant de la présence de mutations. L'intégration des données génomiques et des réponses aux traitements ont montré qu'un seul des organoïdes était sensible au LGK974, un inhibiteur de la protéine WNT secrétée, la porcupine [44]. Un autre avantage de la culture d'organoïdes pour modéliser des maladies réside dans leur capacité à mimer les pathologies observées au sein même des organes. Par exemple, les organoïdes de cancers gastriques humains, infectés par la bactérie *Helicobacter pylori*, reproduisent les signes typiques de cette infection bactérienne chez l'Homme [45]. Le compartiment immunitaire a également été caractérisé dans ces modèles où des lymphocytes T $CD3^+$, $CD8^+$ et $CD3^+/CD4^+$ ont été observés, ainsi que des cellules B, des cellules *natural killer* (NK) et des macrophages [46]. Enfin, les organoïdes ont été utilisés pour modéliser des métastases, et, en particulier, pour étudier les différents processus d'invasion [47], (*figure 3*). Au total, un grand nombre de données ont démontré la pertinence de l'utilisation d'organoïdes tumoraux dans la thérapie personnalisée du cancer [48] (*tableau II*). Récemment, un panel de 76 molécules thérapeutiques potentielles, testées sur 30 organoïdes de cancer du pancréas, a permis d'identifier un inhibiteur de PRMT5 (protéine arginine méthyl-transférase 5), l'EZP015556, comme un potentiel médicament pour inhiber les tumeurs MTAP (un gène généralement non exprimé dans le cancer du pancréas) – négatives [49]. En réalisant un criblage de médicaments sur des organoïdes de cancer primaire du foie humain, l'inhibition de ERK a été identifiée comme une approche thérapeutique potentielle [50].

Contrairement aux modèles classiques en cancérologie, qui nécessitent une grande quantité de matériel biologique (comme les souris PDX), les organoïdes peuvent être cultivés à partir d'un petit échantillon, dérivé d'une biopsie, avec un taux de réussite élevé pour la modélisation personnalisée des tumeurs [51]. De plus, différents organoïdes peuvent être générés à partir de plusieurs zones de la tumeur pour être plus représentatifs de l'hétérogénéité tumorale. Les organoïdes présentent ainsi un excellent système pour modéliser des sous-types de cancers présentant des mutations génomiques uniques [52]. Au total, ce nouveau modèle a un grand potentiel pour la personnalisation des traitements du cancer, en particulier pour les études de corrélation gène-médicament, le criblage préclinique de molécules anticancéreuses et la prédiction des réponses au traitement. Néanmoins, ce modèle présente aussi des

Pour citer cet article : Alzeeb G, et al. Des sphéroïdes aux organoïdes : modèles de cancers solides pour la découverte de molécules anticancéreuses. Bull Cancer (2021), https://doi.org/10.1016/j.bulcan.2021.09.019

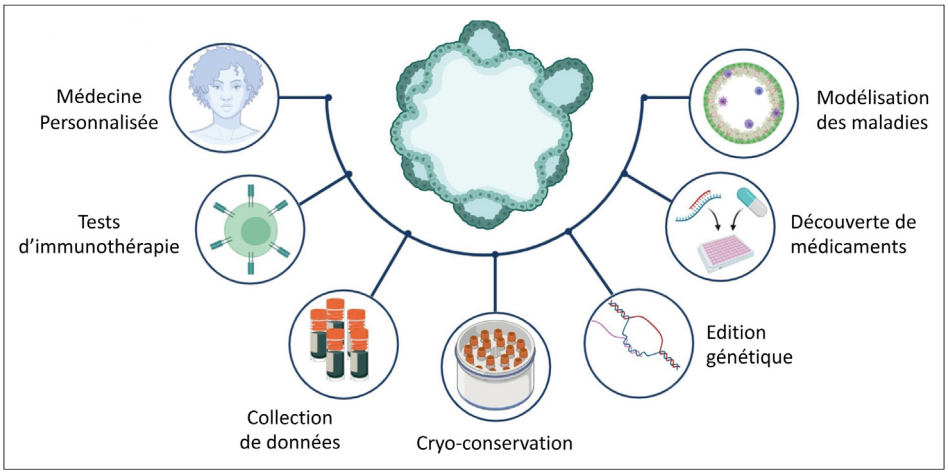

FIGURE 3
Principales applications des organoïdes

TABLEAU II
Approches et essais possibles sur les organoïdes pour étudier les caractéristiques d'un cancer

Signes distinctifs du cancer	Essais possibles en utilisant les organoïdes
Résistance à la mort cellulaire	Tests de viabilité : PI, MTT*
Suppression de croissance	Tests de prolifération et mesure de la taille
Immunothérapie	Co-culture avec des cellules immunitaires
Angiogenèse	Co-culture avec des cellules endothéliales
Organisation spatiale	Imagerie : confocale, bi-photonique
Instabilité et mutations du génome	Séquençage du génome entier et/ou séquençage ciblé

* PI: propidium iodide; MTT: 3-(4,5-dimethylthiazol-2-yl)-2,5-diphenyltetrazolium bromide.

limites pratiques avant de pouvoir en généraliser l'utilisation. Premièrement, la culture des organoïdes peut être coûteuse par le nécessaire ajout de facteurs de croissance spécialisés qui sont nécessaires pour différencier et maintenir les cultures. Ce problème devrait s'atténuer avec le temps, à mesure que de nouvelles méthodes plus efficaces seront mises au point. Par exemple, l'hydro-solution, contenant des hétérodimères des récepteurs de la famille Frizzled (FZD) et des lipoprotéines de basse densité (LRP5/6), favorise la croissance des organoïdes, constituant une alternative qui ne contient pas de sérum [53]. De plus, la stabilisation des protéines WNT, par l'intermédiaire des lipides, peut être considérée comme un autre moyen de culture des organoïdes dans un milieu sans sérum [54]. Deuxièmement, des développements des techniques d'imagerie et de détection sont nécessaires pour suivre le comportement (croissance) et les réponses (toxicité) des organoïdes, en particulier pour les cellules situées au centre de la structure. Enfin, l'absence de composants du stroma, la rareté des vaisseaux sanguins et de cellules immunitaires dans ces cultures constituent une autre limitation. Les études futures viseront à lever ces restrictions, avec des co-cultures incorporant des éléments cellulaires (et microbiens) supplémentaires [55]. L'utilisation de cellules souches pluripotentes, pour développer des organoïdes dotés d'un système nerveux fonctionnel [56] ou de vaisseaux sanguins [57], pourrait compléter avantageusement l'intérêt des organoïdes, en particulier pour évaluer la résistance aux traitements.

Les méthodes courantes de culture des organoïdes se font dans un environnement relativement statique où s'accumulent des déchets biologiques produits par le catabolisme cellulaire [58]. Les technologies des « organes sur puces » ou « *organ-on-chip* » permettent de contourner certaines limitations, en apposant un courant fluidique, créant ainsi un microenvironnement dynamique à même d'assurer les fonctions nécessaires pour

reproduire des pathologies complexes [59,60]. Bien que les développements de cette méthodologie en fassent une approche prometteuse pour l'évaluation préclinique des médicaments, il est encore prématuré de la proposer en remplacement des cultures de sphéroïdes ou d'organoïdes [61].

Conclusion

Les progrès des techniques de culture cellulaire en 3D offrent la possibilité à la fois de mieux identifier des candidats médicaments et de mieux comprendre et prédire la survenue de résistance tumorale aux anticancéreux. Cependant, l'harmonisation des techniques est nécessaire pour assurer une meilleure reproductibilité des données, avant que les modèles 3D puissent être considérés comme la référence pour le développement des stratégies thérapeutiques anticancéreuses. Il sera, notamment, important de mieux caractériser les éléments de structuration des sphéroïdes et des organoïdes, comme la manière dont les populations cellulaires s'assemblent et comment l'expression des gènes ou les profils métabolomiques, par exemple, sont modifiés par les traitements expérimentaux. L'ensemble de cette caractérisation biophysique et biochimique pourra conduire à développer des modèles mathématiques capables de prédire la croissance *in vitro* et la réponse aux traitements. Tout en reconnaissant le caractère très prometteur des organoïdes pour tendre vers une médecine personnalisée au lit du malade, on peut se remémorer un point d'histoire, datant des années 1960, bien avant l'avènement des techniques standardisées de culture cellulaire, à savoir l'utilisation d'explants d'organes pour l'analyse de réponses cellulaires aux traitements médicamenteux… À l'époque, cependant, les développements technologiques, loin de s'inscrire dans l'ère « -omique », n'auraient pas permis de « pousser » aussi loin les investigations dans ces modèles !

Remerciements : La préparation de cette synthèse a été soutenue par l'INSERM et l'Université de Brest. George Alzeeb a bénéficié d'une allocation doctorale du Ministère de l'enseignement supérieur et de la recherche.

Déclaration de liens d'intérêts : les auteurs déclarent ne pas avoir de liens d'intérêts.

Références

[1] Sung H, et al. Global cancer statistics 2020: GLOBOCAN estimates of incidence and mortality worldwide for 36 cancers in 185 countries. CA Cancer J Clin 2021;71(3):209–49. http://dx.doi.org/10.3322/caac.21660.

[2] Cox S, et al. La médecine de précision en oncologie : challenges, enjeux et nouveaux paradigmes. Bull Cancer 2019;106(2):97–104. http://dx.doi.org/10.1016/J.BULCAN.2019.01.007.

[3] Zhang Z, et al. Overcoming cancer therapeutic bottleneck by drug repurposing. Signal Transduct Target Ther 2020;5(1):1–25. http://dx.doi.org/10.1038/s41392-020-00213-8.

[4] Ocana A, Pandiella A, Siu LL, Tannock IF. Preclinical development of molecular-targeted agents for cancer. Nat Rev Clin Oncol 2011;8(4):200–9. http://dx.doi.org/10.1038/nrclinonc.2010.194.

[5] Kamb A. What's wrong with our cancer models? Nat Rev Drug Discov 2005;4(2):161–5. http://dx.doi.org/10.1038/nrd1635.

[6] Gillet J-P, Varma S, Gottesman MM. The clinical relevance of cancer cell lines. J Natl Cancer Inst 2013;105:452–8. http://dx.doi.org/10.1093/jnci/djt007.

[7] McCaffrey LM, Macara IG. Epithelial organization, cell polarity and tumorigenesis. Trends Cell Biol 2011;21(12):727–35. http://dx.doi.org/10.1016/J.TCB.2011.06.005.

[8] Jung J, Seol HS, Chang S. The generation and application of patient-derived xenograft model for cancer research. Cancer Res Treat 2018;50(1):1–10. http://dx.doi.org/10.4143/crt.2017.307.

[9] Sensi F, D'Angelo E, D'Aronco S, Molinaro R, Agostini M. Preclinical three-dimensional colorectal cancer model: the next generation of in vitro drug efficacy evaluation. J Cell Physiol 2018;234(1):181–91. http://dx.doi.org/10.1002/jcp.26812.

[10] Longati P, et al. 3D pancreatic carcinoma spheroids induce a matrix-rich, chemoresistant phenotype offering a better model for drug testing. BMC Cancer 2013;13. http://dx.doi.org/10.1186/1471-2407-13-95.

[11] Minchinton AI, Tannock IF. Drug penetration in solid tumours. Nat Rev Cancer 2006;6(8):583–92. http://dx.doi.org/10.1038/nrc1893.

[12] Alzeeb G, Metges JP, Corcos L, Le C, Jossic-Corcos. Three-dimensional culture systems in gastric cancer research. Cancers 2020;12(10. MDPI AG):1–20. http://dx.doi.org/10.3390/cancers12102800.

[13] Larsen CJ. Sphéroïdes : le modèle de référence pour la culture in vitro des tumeurs solides ? Bull Cancer 2018;105(1):25–34. http://dx.doi.org/10.1016/J.BULCAN.2017.09.008.

[14] Knight E, Przyborski S. Advances in 3D cell culture technologies enabling tissue-like structures to be created in vitro. J Anat Dec 2015;227(6):746–56. http://dx.doi.org/10.1111/JOA.12257.

[15] Mehta G, Hsiao AY, Ingram M, Luker GD, Takayama S. Opportunities and challenges for use of tumor spheroids as models to test drug delivery and efficacy. J Control Release 2012;164(2):192–204. http://dx.doi.org/10.1016/j.jconrel.2012.04.045.

[16] Friedrich J, Seidel C, Ebner R, Kunz-Schughart LA. Spheroid-based drug screen: considerations and practical approach. Nat Protoc 2009;4(3):309–24. http://dx.doi.org/10.1038/nprot.2008.226.

[17] Koroknai V, Patel V, Szász I, Ádány R, Balazs M. Gene expression signature of BRAF inhibitor resistant melanoma spheroids. Pathol Oncol Res 2020;26(4):2557. http://dx.doi.org/10.1007/S12253-020-00837-9.

[18] Bissell MJ, Radisky D. Putting tumours in context. Nat Rev Cancer 2001;1(1):46–54. http://dx.doi.org/10.1038/35094059.

[19] Lao Z, et al. Improved methods to generate spheroid cultures from tumor cells, tumor cells & fibroblasts or tumor-fragments: microenvironment, microvesicles and MiRNA. PLoS One 2015;10(7):e0133895. http://dx.doi.org/10.1371/JOURNAL.PONE.0133895.

[20] Nederman T, Glimelius B, Norling B, Carlsson J, Brunk U. Demonstration of an extracellular matrix in multicellular tumor spheroids. Cancer Res 1984;44(7):3090–7.

[21] Trédan O, Galmarini CM, Patel K, Tannock IF. Drug resistance and the solid tumor microenvironment. JNCI J Natl Cancer Inst 2007;99(19):1441–54. http://dx.doi.org/10.1093/JNCI/DJM135.

[22] Jeong S-Y, Lee J-H, Shin Y, Chung S, Kuh H-J. Co-culture of tumor spheroids and fibroblasts

in a collagen matrix-incorporated microfluidic chip mimics reciprocal activation in solid tumor microenvironment. PLoS One Jul 2016;11(7):e0159013. http://dx.doi.org/10.1371/JOURNAL.PONE.0159013.

[23] Togo S, Polanska U, Horimoto Y, Orimo A. Carcinoma-associated fibroblasts are a promising therapeutic target. Cancers (Basel) 2013;5(4):149–69. http://dx.doi.org/10.3390/cancers5010149.

[24] Neuwirt H, et al. Cancer-associated fibroblasts promote prostate tumor growth and progression through upregulation of cholesterol and steroid biosynthesis. Cell Commun Signal 2020;18(1):1–18. http://dx.doi.org/10.1186/S12964-019-0505-5.

[25] Fourniols T, Bastien E, Canevat A, Feron O, Préat V. Inhibition of colorectal cancer-associated fibroblasts by lipid nanocapsules loaded with acriflavine or paclitaxel. Int J Pharm 2020;584:119337. http://dx.doi.org/10.1016/J.IJPHARM.2020.119337.

[26] Rizki A, et al. A human breast cell model of preinvasive to invasive transition. Cancer Res Mar 2008;68(5):1378–87. http://dx.doi.org/10.1158/0008-5472.CAN-07-2225.

[27] Plikus MV, et al. Fibroblasts: origins, definitions, functions in health and disease. Cell 2021;184(15):3852–72. http://dx.doi.org/10.1016/J.CELL.2021.06.024.

[28] Sahai E, et al. A framework for advancing our understanding of cancer-associated fibroblasts. Nat Rev Cancer 2020;20(3):174–86. http://dx.doi.org/10.1038/S41568-019-0238-1.

[29] Lazzari G, Nicolas V, Matsusaki M, Akashi M, Couvreur P, Mura S. Multicellular spheroid based on a triple co-culture: a novel 3D model to mimic pancreatic tumor complexity. Acta Biomater 2018;78:296–307. http://dx.doi.org/10.1016/j.actbio.2018.08.008.

[30] Courau T, et al. Cocultures of human colorectal tumor spheroids with immune cells reveal the therapeutic potential of MICA/B and NKG2A targeting for cancer treatment. J Immunother Cancer 2019;7(1). http://dx.doi.org/10.1186/S40425-019-0553-9.

[31] Simon GM, Niphakis MJ, Cravatt BF. Determining target engagement in living systems. Nat Chem Biol 2013;9(4):200–5. http://dx.doi.org/10.1038/nchembio.1211.

[32] Rath O, Kozielski F. Kinesins and cancer. Nat Rev Cancer 2012;12(8):527–39. http://dx.doi.org/10.1038/NRC3310.

[33] Oue N, et al. Induction of KIFC1 expression in gastric cancer spheroids. Oncol Rep 2016;36(1):349–55. http://dx.doi.org/10.3892/or.2016.4781.

[34] Imai T, et al. Overexpression of KIF11 in gastric cancer with intestinal mucin phenotype. Pathobiology 2017;84(1):16–24. http://dx.doi.org/10.1159/000447303.

[35] Zhou S, et al. Evaluation of PD-1 blockade using a multicellular tumor spheroid model. Am J Transl Res 2019;11(12):7471–8 [Accessed: Apr. 23, 2020. (Online). Disponible sur : http://www.ncbi.nlm.nih.gov/pubmed/31934294].

[36] Yuhas JM, Li AP, Martinez AO, Ladman AJ. A simplified method for production and growth of multicellular tumor spheroids. Cancer Res 1977;37(10):3639–43.

[37] Aftab O, Fryknäs M, Hammerling U, Larsson R, Gustafsson MG. Detection of cell aggregation and altered cell viability by automated label-free video microscopy: a promising alternative to endpoint viability assays in high-throughput screening. J Biomol Screen 2015;20(3):372–81. http://dx.doi.org/10.1177/1087057114562158.

[38] Sato T, et al. Long-term expansion of epithelial organoids from human colon, adenoma, adenocarcinoma, Barrett's epithelium. Gastroenterology 2011;141(5):1762–72. http://dx.doi.org/10.1053/j.gastro.2011.07.050.

[39] Werner K, Weitz J, Stange DE. Organoids as model systems for gastrointestinal diseases: tissue engineering meets genetic engineering. Curr Pathobiol Rep 2016;4(1. Springer):1–9. http://dx.doi.org/10.1007/s40139-016-0100-z.

[40] Kretzschmar K, Clevers H. Organoids: modeling development and the stem cell niche in a dish. Dev Cell 2016;38(6):590–600. http://dx.doi.org/10.1016/J.DEVCEL.2016.08.014.

[41] Gjorevski N, et al. Designer matrices for intestinal stem cell and organoid culture. Nat 2016;539(7630):560–4. http://dx.doi.org/10.1038/nature20168.

[42] Yan HHN, et al. A comprehensive human gastric cancer organoid biobank captures tumor subtype heterogeneity and enables therapeutic screening. Cell Stem Cell 2018;23(6):882e11–97e11. http://dx.doi.org/10.1016/J.STEM.2018.09.016.

[43] Phan N, et al. A simple high-throughput approach identifies actionable drug sensitivities in patient-derived tumor organoids. Commun Biol 2019;2(1):1–11. http://dx.doi.org/10.1038/s42003-019-0305-x.

[44] Van De Wetering M, et al. Prospective derivation of a living organoid biobank of colorectal cancer patients. Cell 2015;161(4):933–45. http://dx.doi.org/10.1016/j.cell.2015.03.053.

[45] Bartfeld S, et al. In vitro expansion of human gastric epithelial stem cells and their responses to bacterial infection. Gastroenterology 2015;148(1):126e6–36e6. http://dx.doi.org/10.1053/j.gastro.2014.09.042.

[46] Neal JT, et al. Organoid modeling of the tumor immune microenvironment. Cell 2018;175(7):1972e16–88e16. http://dx.doi.org/10.1016/j.cell.2018.11.021.

[47] Cheung KJ, Gabrielson E, Werb Z, Ewald AJ. Collective invasion in breast cancer requires a conserved basal epithelial program. Cell 2013;155(7):1639–51. http://dx.doi.org/10.1016/J.CELL.2013.11.029.

[48] Pauli C, et al. Personalized in vitro and in vivo cancer models to guide precision medicine. Cancer Discov 2017;7(5):462–77. http://dx.doi.org/10.1158/2159-8290.CD-16-1154.

[49] Driehuis E, et al. Pancreatic cancer organoids recapitulate disease and allow personalized drug screening. Proc Natl Acad Sci 2019;116(52):26580–90. http://dx.doi.org/10.1073/PNAS.1911273116.

[50] Broutier L, et al. Human primary liver cancer–derived organoid cultures for disease modeling and drug screening. Nat Med 2017;23(12):1424–35. http://dx.doi.org/10.1038/nm.4438.

[51] Boj SF, et al. Organoid models of human and mouse ductal pancreatic cancer. Cell 2015;160(1–2):324s–38s. http://dx.doi.org/10.1016/j.cell.2014.12.021.

[52] Nanki K, et al. Divergent routes toward Wnt and R-spondin niche independency during human gastric carcinogenesis. Cell 2018;174(4):856e17–69e17. http://dx.doi.org/10.1016/j.cell.2018.07.027.

[53] Janda CY, et al. Surrogate Wnt agonists that phenocopy canonical Wnt and β-catenin signalling. Nat 2017;545(7653):234–7. http://dx.doi.org/10.1038/nature22306.

[54] Tüysüz N, et al. Lipid-mediated Wnt protein stabilization enables serum-free culture of human organ stem cells. Nat Commun 2017;8(1):1–11. http://dx.doi.org/10.1038/ncomms14578.

[55] Yin X, Mead BE, Safaee H, Langer R, Karp JM, Levy O. Engineering stem cell organoids. Cell Stem Cell 2016;18(1):25–38. http://dx.doi.org/10.1016/J.STEM.2015.12.005.

[56] Workman MJ, et al. Engineered human pluripotent-stem-cell-derived intestinal tissues with a functional enteric nervous system. Nat Med 2016;23(1):49–59. http://dx.doi.org/10.1038/nm.4233.

[57] Holloway EM, et al. Differentiation of human intestinal organoids with endogenous vascular endothelial cells. Dev Cell 2020;54(4):516e7–28e7. http://dx.doi.org/10.1016/J.DEVCEL.2020.07.023.

[58] Park SE, Georgescu A, Huh D. Organoids-on-a-chip. Science 2019;364(6444):960. http://dx.doi.org/10.1126/SCIENCE.AAW7894.

[59] Sung JH, et al. Recent advances in body-on-a-chip systems. Anal Chem 2019;91(1):330. http://dx.doi.org/10.1021/ACS.ANALCHEM.8B05293.

[60] Shirure VS, et al. Tumor-on-a-chip platform to investigate progression and drug sensitivity in cell lines and patient-derived organoids. Lab Chip 2018;18(23):3687–702. http://dx.doi.org/10.1039/C8LC00596F.

[61] Vidi P-A, et al. Disease-on-a-chip: mimicry of tumor growth in mammary ducts. Lab Chip 2014;14(1):172–7. http://dx.doi.org/10.1039/C3LC50819F.

III.3. Review 2: Three-Dimensional Culture Systems in Gastric Cancer Research

Authors: George Alzeeb[1], Jean-Philippe Metges[2], Laurent Corcos[1,2] and Catherine Le Jossic-Corcos[1,*]

1 *Inserm, University Brest, EFS, UMR 1078, GGB, F-29200 Brest, France;*

2 *CHU de Brest, Inserm, University Brest, EFS, UMR 1078, GGB, F-29200 Brest, France;*

******* *Correspondence: catherine.corcos@univ-brest.fr Received: 21 August 2020;*

Cancers 2020, 12, 2800; doi:10.3390/cancers12102800

Accepted: 27 September 2020; Published: 29 September 2020

Abstract: Gastric cancer (GC), which includes cancer of the esophagus, the oesophagogastric junction, and the stomach fundus, is highly deadly with strong regional influence, Asia being the most affected. GC is often detected at late stages, with 30% of metastatic cases at diagnosis. Many authors have devised models to both unravel the mechanisms of GC development and to evaluate candidate therapeutics. Among these models, 2D-cell cultures are progressively replaced by 3D-cell cultures that recapitulate, much more comprehensively, tumor cellular and genetic heterogeneity, as well as responsiveness to environmental changes, such as exposure to drugs or irradiation. With respect to the specifics of GC, there are high hopes from such model systems, especially with the aim of identifying prognostic markers and novel drug targets.

This review will be presented in this thesis as its published format in Cancers

cancers

MDPI

Review

Three-Dimensional Culture Systems in Gastric Cancer Research

George Alzeeb [1], Jean-Philippe Metges [2], Laurent Corcos [1,2] and Catherine Le Jossic-Corcos [1,*]

1 Inserm, University Brest, EFS, UMR 1078, GGB, F-29200 Brest, France; george.alzeeb@univ-brest.fr (G.A.); laurent.corcos@univ-brest.fr (L.C.)
2 CHU de Brest, Inserm, University Brest, EFS, UMR 1078, GGB, F-29200 Brest, France; jean-philippe.metges@univ-brest.fr
* Correspondence: catherine.corcos@univ-brest.fr

Received: 21 August 2020; Accepted: 27 September 2020; Published: 29 September 2020

Simple Summary: It is getting more and more clear that cancer cell culture models are switching from two-dimension to three-dimensional, in order to better reflect in vivo situations where tumor cells have to cope with a highly interactive three-dimensional microenvironment. Several such culture models have been reported, predominantly multicellular tumor spheroids (MCTS) and patient-derived tumor organoids (PDTO). These are used both to investigate fundamental aspects of cancer development and as test systems for innovative therapies against gastric cancer, the fifth most common cancer and the third leading cause of cancer-related deaths worldwide. The authors review the actual state of research in this field to provide an overview of the contribution of MCTS and PDTO, especially in the areas of molecular profiling, drug discovery, pathogen infection, and personalized medicine.

Abstract: Gastric cancer (GC), which includes cancer of the esophagus, the oesophagogastric junction, and the stomach fundus, is highly deadly with strong regional influence, Asia being the most affected. GC is often detected at late stages, with 30% of metastatic cases at diagnosis. Many authors have devised models to both unravel the mechanisms of GC development and to evaluate candidate therapeutics. Among these models, 2D-cell cultures are progressively replaced by 3D-cell cultures that recapitulate, much more comprehensively, tumor cellular and genetic heterogeneity, as well as responsiveness to environmental changes, such as exposure to drugs or irradiation. With respect to the specifics of GC, there are high hopes from such model systems, especially with the aim of identifying prognostic markers and novel drug targets.

Keywords: gastric cancer; spheroids; organoids; personalized medicine

1. Introduction

Gastric cancer (GC) is the fifth most common cancer and the third leading cause of cancer-related deaths worldwide, according to data from Global Cancer Statistics 2018 [1]. Adenocarcinomas of the esophagogastric junction (AEG) overlap histologically with GC and constitute an entity with rising incidence rates [2,3]. Lauren's criteria are the most widely used to classify gastric adenocarcinomas, differentiating them histologically into intestinal and diffuse types [4]. Environmental factors such as *Helicobacter pylori* (*H. pylori*) infections, the greatest risk factor for GC [5], diet, and lifestyle are often associated with the intestinal type, while the diffuse type is more often associated with genetic abnormalities [6]. The Cancer Genome Atlas (TCGA) research network separated gastric adenocarcinomas into four different molecular subgroups: (i) positive for the Epstein–Barr virus (EBV) with frequent PIK3CA mutations and CDKN2A silencing, (ii) a microsatellite instable (MSI)

subtype with a hyper-mutation phenotype, (iii) a genomically stable (GS) subtype displaying diffuse histology and frequent CDH1 and RHOA mutations, and iv) a chromosomal instable (CIN) subtype displaying aneuploidy and frequent mutations of TP53 as well as activation of the receptor tyrosine kinase (RTK)-RAS pathway [7]. The molecular characterization of AEG revealed their high similarity to the CIN subtype of GC [8]. The prognosis of GC is poor and most advanced forms of the disease still remain incurable [9]. Hence, GC treatment remains a major challenge and relies on surgical resection as the primary curative modality, i.e., for localized forms. Nonetheless, complementary approaches, such as neo-adjuvant and adjuvant chemotherapy (5-fluoruracil, oxaliplatin, docetaxel and epirubicin), have shown improved survival rates [10–12]. In addition, genetic alterations represent molecular targets for novel treatment options. So far, the only approved targeted therapies are: (i) anti-human epidermal growth factor receptor-2 monoclonal antibody "trastuzumab" and (ii) anti-vascular endothelial growth factor receptor-2 monoclonal antibody "ramucirumab" [13,14], while other therapeutic targets like Programmed cell Death protein 1 (PD-1) inhibition are under clinical investigation [15]. Although treatment effectiveness has improved during the past decade, GC survival rates remain poor [16]. This calls for an urgent need to develop innovative therapies available to GC patients.

The conventional in vitro cancer model used to screen novel therapies is the monolayer two-dimension (2D) cancer cell line (CCL) culture [17]. 2D culture models impose unnatural geometric and mechanical constraints by adhering cells to an artificial substrate (plastic or glass). Such a culture affects cell polarity and therefore, potentially, tumor phenotypes. Three-dimensional (3D) culture systems have been developed to better mimic the functional aspects of tissues [18]. This results from (i) the organization of cells in layers with different proliferation rates, (ii) the formation of diffusion gradients of nutrients, oxygen and metabolic wastes, (iii) the specifics of cell-cell interactions, (iv) the expression of specific genes and (v) induction of chemoresistance [19–21]. Several 3D culture models have been reported [22], predominantly multicellular tumor spheroids (MCTS) [23] and patient-derived tumor organoids (PDTO) [24,25]. The main characteristics of these 3D models are presented in Table 1.

Table 1. Comparison between spheroids and organoids. (++ favorable, + possible), See references [26–30] for examples of studies that used either spheroids or organoids methodologies.

3D Culture Models	Spheroids	Organoids
Origin	Cancer cell lines	Patient tumor
Protocol	Easy to use	Delicate
Architecture	Simplified	Closer to organ
Reproducibility	High	Medium-high
Cellularity	Defined cell type	Different cell types
Cancer subtype modeling	+	++
Biological material produced	Abundant	Abundant
Genetic manipulation	++	++
Co-culture	++	+
High-throughput drug screening	++	+
Prediction of clinical drug response in vitro	+	++
Cost	Low	Medium
Biobanks	Unavailable	Available

MCTS models promote the formation of well-developed spheroids that resemble avascular tumor sites or micrometastatic regions in vivo [31]. Different co-culture approaches have been developed, including mixed populations of tumor cells and cancer associated fibroblasts (CAF), which showed increased ability to form spheroids [32]. Several studies validated the anticancer therapeutic potential of targeting the interactions between CAF and carcinoma cells [33]. However, using CCL to produce MCTS renders this approach hardly patient specific because most tumors contain highly heterogeneous subsets of cancer cells [34]. In vivo animal testing research is often employed for observing the effects on a living subject. The gold standard in vivo model for tumor development and analysis is patient-derived xenograft (PDX) [35]. Such a model conserves the clinical tumor architecture, the genotypic and

phenotypic characteristics of the primary tumor as well as interactions with the microenvironment and the characteristics of patient's tumor, recapitulating the inter-tumor heterogeneity [36]. However this still does not provide immediate clinically actionable data [37]. In addition, their use is quite expensive and time consuming, and raises ethical issues, at times where alternative in vitro/ex vivo models are gaining momentum. These reasons make in vivo models unsuitable for routine testing purposes and encourage the application of 3D cultures that permit recapitulating several mechanisms of drug resistance found in tumors in vivo.

Huge efforts in preclinical personalized therapy testing were explored by the recent development of PDTO as ex vivo models of human cancers, including GC [38]. Organoids are 3D cultures of multiple organ-specific cells of different types that can retain the morphologies and gene expression profiles of their organs of origin [39]. Organoids enable drug screening for personalized therapies as they provide genotypic stability and constitute a valuable tool to study pathogen infections [40,41]. A comparison of the main specificities of 2D, 3D, and PDX animal models is presented in Table 2.

Table 2. Comparison between 2D, 3D cell culture and PDX animal models [42–45].

Test System Main Features	2D Cell Culture [42,43]	3D Cell Culture [44]	PDX Animal Model [45]
Physiological relevance	Limited	Better than 2D standard culture	Most physiological environment
Model complexity	Limited	Complex	Very complex
Gene expression	Stable at early passages	Close to in vivo tumors	Close to in vivo tumors
Immune system	No but co-cultures of cancer cells and immune cells possible	No but co-cultures of cancer cells and immune cells possible	No
Efficient drug screening	Yes	Yes	No
Disease modeling	Naive	Feasible	Sophisticated methods
Data provider	Easily exploitable	Easily exploitable	Hardly exploitable
Controlled microenvironment	Yes	Yes	No
Reproducibility	Favorable	Not so favorable	Unsuited
Cost	Low	Some expensive materials and special equipment required	High
Ethical and regulatory issues	No	No	No

In this review, we present the current status of in vitro / ex vivo 3D models of human GC as a surrogate to in vivo tumors. We describe established MCTS and PDTO methods in GC models and present an overview of important findings from different spheroids- and organoids-based studies, especially in the fields of molecular profiling, drug discovery, pathogen infection and personalized medicine. Lastly, we also attempt to propose ways for improving the relevance of next-generation 3D models.

2. Three D Multicellular Tumor Spheroid Model

Since Sutherland et al. established MCTS in the 1970s [46], this model has been one of the most commonly explored and characterized among the currently available 3D in vitro tumor models [47]. MCTS are aggregates of CCL grown with or without scaffolds representing avascular tumor nodules or micro-metastases [48]. Spheroids with diameters larger than 400–500 µm sustain oxygen and nutrient gradients associated with specific functional domains (proliferative outer layer, quiescent intermediate

layer, and the necrotic center) [49] (Figure 1). As a result, protein and gene expression profiles of MCTS are closer to those of tumors than 2D tumor cell cultures [50]. In addition, MCTS can be constructed from tumor cells alone or combined to other cell types that can produce an extracellular matrix (ECM). They can be used to analyze the influence of 3D-specific cell-cell interactions on tumor progression, cell invasion or angiogenesis. As such, they are well suited to recapitulate the complexity and the cellular heterogeneity of tumors, a hallmark of cancer that may explain resistance to chemotherapy and participate in metastatic invasion. Hence, different 3D-co-culture approaches have been developed to analyze the interaction of tumor cells, fibroblasts, stem cells, adipocytes, or other cells present in the tumor microenvironment and to study the influence of these interactions on tumor progression or cell invasion [51–53].

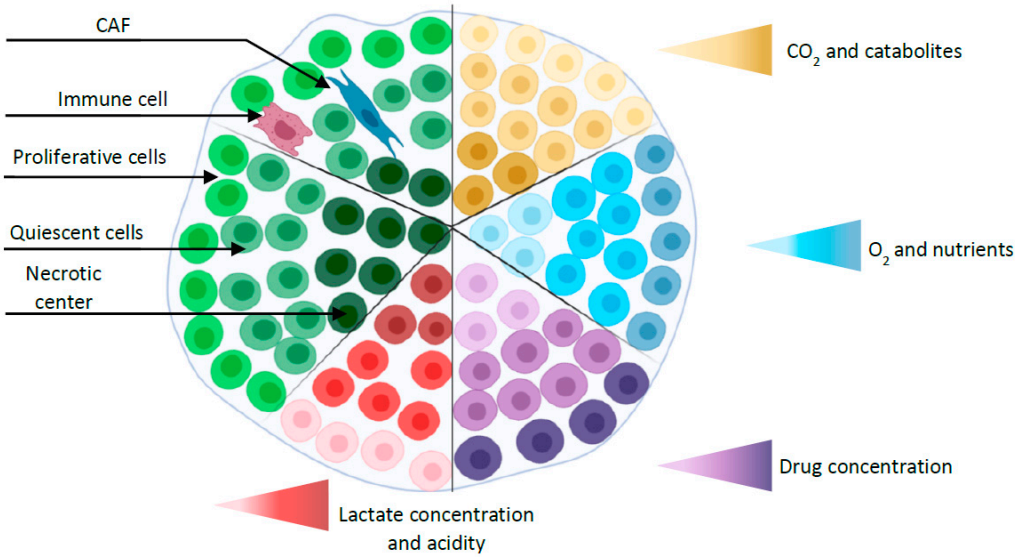

Figure 1. Simplified representation of a spheroid with different layers (proliferative outer layer, a quiescent intermediate layer, and the necrotic center) and gradients (oxygen, nutrients, CO_2, catabolites, and drug concentration). Co-culture spheroid is represented by the addition of cancer-associated fibroblast (CAF) and immune cell.

2.1. MCTS Production Methodologies

Spheroid formation methodologies can be divided into two major categories: (i) scaffold-based models that take advantage of diverse natural (collagen, fibronectin, agarose, laminin, gelatin) [54], or synthetic (polyethylene oxide or polyethylene glycol) [55] materials to mimic in vivo tumor–ECM interactions [56] and (ii) scaffold-free models, which include mainly non-adherent, suspension, and hanging drop cultures, result in preventing cells attachment to the support, thereby forcing them to aggregate and form spheroids [49]. The plates used for this method are made non-adherent by coating them with an inert, non-cytotoxic and non-degradable substrate: agarose or poly-2-hydroxyethyl methacrylate (poly-HEMA) [57]. The principle of suspension culture methods is to keep the cells in suspension, either by agitation or by increasing medium viscosity (by addition of carboxy-methyl-cellulose) [58], but the spheroid size cannot be controlled, which can pose a problem when used in drug testing [59]. Finally, the hanging drop method involves cell suspension drops deposited on the underside of an adherent tissue culture lid. Cells aggregate at the bottom of the drop by gravity and form spheroids of uniform sizes [60]. However, the drops cannot exceed a volume of 50 µL in order to resist gravity [61]. The non-adherent surface method has been widely used for GC studies [62] (Table 3).

Table 3. Description, advantages and disadvantages of commonly used MCTS culture techniques. (* Refers to studies on colorectal cancer).

Spheroids Production Methods	Description	Advantages	Disadvantages	References
Scaffold-based models	3D construction that provides an ECM capable of supporting cells	Simple Mimic in vivo microenvironment Cell-ECM interactions Long-term culture Directly visualize and analyze	Difficulty of cell recovery Scaffold consistency can be variable across lots Nonuniform control (composition, size) Co-culture delicate Not suitable for drug testing	[27,63]
Non-adherent surfaces	Prevent attachment to the support	Simple Available pre-coated plates Uniform spheroid size control Ease of cell recovery Long-term culture Co-culture feasible Useful for drug screening Directly visualize and analyze	Low throughput production Defined co-culture cellular ratio Requires transfer of spheroids for analysis	[64–67]
Suspension culture	Keeps the cells in suspension to avoid sedimentation	High throughput production Homogeneous media composition Long-term culture	High shear force Nonuniform control (composition, size) Not easily suitable for drug testing Requires special equipment Requires a centrifugation step	[23] *
Hanging drop technique	Gravity based spheroid formation	Simple Uniform spheroid size control Co-culture feasible	Small size of spheroids Low throughput production Tedious spheroid handling and transfer Difficulty of long-term culture Defined co-culture cellular ratio Not suitable for drug testing	[68–70] *

2.2. Applications of MCTS in Gastric Cancer

2.2.1. Gene Expression Profiling

Genetic and epigenetic alterations contribute to the development and progression of multifactorial diseases such as GC [71]. Investigating the gene expression profiles of GC paves the way towards identifying novel diagnostic or prognostic biomarkers and developing future individualized medicine strategies. In vitro 3D experiments have gone a long way in understanding the molecular aspects of complex diseases [72]. CD44, a cell surface adhesion marker expressed by cancer stem cells (CSC) [73] has been reported as overexpressed in GC spheroids [64]. Oue et al. showed that KIFC1 and KIF11, two members of the kinesin-14 family, were overexpressed in spheroids compared to parental cells [74,75], while their knockdown inhibited spheroid formation [74,76]. In a similar context, this group also reported the under-expression of the claspin (CLSPN) gene, which codes for a nuclear protein involved in DNA replication and S-phase regulation, in spheroids [77]. Recently, Lee et al. demonstrated, using a limiting dilution protocol in a microwell-based culture chip, that gene expression of spheroid-forming cells was closely related to histological diffuse and intestinal type [78]. They observed an increase in expression levels of SOX2, a transcription factor expressed in stem cells), CD44 and E-cadherin in the diffuse type spheroid cell lines (SNU-638 and SNU-484) [79]. In addition, the expression of ERBB3 increased in spheroids made from intestinal type cell lines (MKN-28 and NCI-N87) [79]. miRNA expression was also investigated in GC MCTS models. Magalhães et al observed that the expression of has-miR-29c-5p, which regulated the expression of DNMT3A, CDC42, RCC2, and CDK6, was lower in the 3D model compared to 2D [26]. Changes in the microenvironment of the in vitro cells by 3D cultures can also impact on gene expression by modifying alternative splicing [80]. Indeed, a study by Branco da Cunha et al. showed an alternative splicing product of CD44 in GC spheroids, where the standard CD44 isoform (CD44s) was substituted by CD44 variant 6 (CD44v6) [81]. This increased progressively with the advancement of GC stages, from gastric pre-neoplastic lesions to advanced carcinoma [82]. Consequently, targeting the genes that distinguish MCTS from monolayer cell cultures introduces promising anticancer therapies. However, current studies on gene expression profiles of GC spheroids only scratch the surface and further studies need to be conducted to further clarify this process.

2.2.2. Gastric Cancer Stem Cells: Biomarkers Identification

Cancer stem cells (CSC) are defined as a subpopulation of cancer cells that have a high capacity of self-renewal and differentiation into mature tumor cells, where multiple pathways are involved such as Notch, Wnt, Hedgehog and PI3K [83,84]. CSC constitute less than 5% of total tumor cells but they may play a crucial role as initiators of the heterogeneous lineage of cancer cells that constitute the tumor [85,86]. Because of their intrinsic resistance to anticancer drugs, CSC remains after chemotherapy or radiation therapy could be responsible for relapse after treatment. In addition, a poor prognosis of GC was associated with the expression of stem cell markers and related proteins, including CD44, SOX2 and OCT4/3 [87]. Nonetheless, gCSC markers have not been unambiguously identified [87]. For example, Rocco et al. reported that $CD44^+/CD133^+$ cells, detectable in primary GC, did not exhibit stem-like properties [88]. In this section, we will focus on studies that apply MCTS models to provide additional and better evidence of specific cell markers to identify gCSC.

Takaishi et al. identified gCSC for the first time, using CD44 as a marker from a panel of human gastric CCLs. $CD44^+$ cells could self-renew and form MCTS in a serum-free medium. CD44 knockdown reduced spheroid colony formation [89]. Han et al. reported that $CD44^+/EpCAM^+$ (Epithelial Cell Adhesion Molecule) cells grew exponentially in vitro as cancer spheres and had greater resistance to anticancer drugs than other subpopulations of cells. These results suggested that $CD44^+/EpCAM^+$ cells could be used as a model system for gCSC research [90], although these markers are not specific of gCSC. It resulted that spheroid body formation has been increasingly used as a functional approach for enriching in stem cell markers. Liu et al. were the first to develop spheroid body cells from

human gastric CCL 'MKN-45'. They demonstrated that these cells could generate greater numbers of new spheroid bodies than the parental cells and that spheroid body-forming cells were capable of self-renewal and proliferation, which are important CSC characteristics [91]. In addition, when cultured in stem cell conditioned media, these spheroid body-forming cells showed a significant overexpression of CD44 and ABCG2 (adenosine triphosphate binding cassette transporter G2) compared to the parental cells [92]. Furthermore, Zhang et al. found that spheroid cells from gastric CCL could self-renew and may also play roles in tumor initiation, chemo-resistance, and migration [87]. As already mentioned [79], using a limiting dilution protocol and a microwell-based culture chip to produce spheroids, Lee et al. demonstrated that these spheroids had larger populations of cells with stem cell-like properties, compared to spheroids formed by conventional tumor spheroid culture methods [78]. It is worth noting that these methods are hindered by poor single-cell seeding and low throughput. Other molecules have been reported as CSC-associated markers in GC. While Jiang et al. suggested that CD90 could be used to identify and isolate gCSC [93], Tian et al. documented a high expression of SOX2 in gastric MCTS and demonstrated the important role of SOX2 in sustaining stem cell properties [94]. In addition, using the MCTS method to isolate gCSC, Ptch and Gli1 (Sonic hedgehog (SHH) pathway target genes) were shown to be more expressed in MCTS cells than in adherent cells, suggesting that the SHH pathway was essential for the maintenance of CSC in human GC [95]. Ohkuma et al. demonstrated, using 3D invasion assays, that gastric $CD71^{-}$ cell subpopulations had higher migratory and a more invasive potential compared to $CD71^{+}$ cells, suggesting that low expression of CD71 could mark subpopulations of gCSC [96]. In addition, Yoon et al. found increased activity of RhoA in diffuse gCSC and a decreased spheroid formation after RhoA inhibition [97]. Despite this evidence, more studies are needed to further identify and characterize common gCSC biomarkers, especially as a means to better discriminate between CSC subpopulations, which will help to introduce better GC therapies [28,98].

2.2.3. Drug Discovery

Standard 2D cell cultures have largely contributed to the development of many cancer therapies. However, the limitations of this model in reproducing in vivo tumor complexity and pathophysiology [99] may be one cause of the high attrition rate for cancer drugs entering early clinical trials [100]. Admittedly, culturing cells in 3D differentially impacts on their sensitivity to cytotoxic agents, as compared to 2D cultures, and usually makes them more resistant to treatment [101]. In this section, we will provide an overview of the implications of MCTS models in the development of anticancer drugs as well as in the discovery of novel treatment targets in GC.

As discussed earlier in this review, gCSC are involved in tumor maintenance, resistance to treatments and tumor progression. Novel treatment modalities targeting gCSC have been developed using 3D models. Courtois et al. analyzed MCTS spheroid formation revealing CSC-presence and showed that metformin, an anti-diabetic drug with anti-proliferative effects, targeted gCSC, indicating that use of metformin could be a promising strategy to inhibit tumor growth [102]. Akrami et al. showed that ibuprofen, a nonsteroidal anti-inflammatory drug, prevented the initiation and the progression of GC [103]. They suggested that the anticancer effect of ibuprofen on gCSC was linked to inhibition of the Wnt/β-catenin signaling pathway [104]. After demonstrating its importance in sustaining CSC properties, Tian et al. proposed SOX2 as a potential target for GC therapy [94]. Similarly, Nishikawa et al. suggested that ALDH in gCSC may turn into a novel treatment target [105]. In addition, Koh et al. found that pantoprazole downregulated JAK2/STAT3 signaling, while inhibiting cellular migration or invasion in GC at the same time [106]. Because the efficacy of anticancer drugs relies on their ability to penetrate tumors efficiently, MCTS models are an ideal platform in view of their capacity to generate an ECM that obstructs drug penetration [107]. From that perspective, Sha et al. have constructed a recombinant protein named anti-EGFR-iRGD consisting of an anti-EGFR VHH (the variable domain from the heavy chain of the antibody to epidermal growth factor receptors) fused to iRGD, a tumor-specific binding peptide with high permeability. Anticancer activity and penetration of anti-EGFR-iRGD were evaluated with the MCTS model. Results from this study showed

improvements in MCTS penetration as well as anti-GC efficacy when the anti-EGFR was fused with iRGD [27]. In addition, anti-EGFR-iRGD could enhance the efficacy of chemotherapeutic drugs, such as doxorubicin, bevacizumab, and placitaxel, in the inhibition of GC [27,108]. Furthermore, sTRAIL-iRGD, a recombinant protein with a high permeability index, displayed an anti-tumor effect in MCTS, with limited systemic toxicity [63,109]. Immunotherapy has had its fair share of applications using MCTS. Examples include exploring tumor immune escape mechanisms and screening immunotherapy agents or combinations pre-clinically. MCTS were also used for the evaluation of penetration and cytotoxicity of immune cells [110]. Zhou et al. established MCTS from a human gastric CCL to evaluate the cytotoxicity resulting from PD-1 blockade [111], a strategy to improve cancer therapy in the immuno-oncology field [112]. MCTS were formed in a medium containing IFN-γ and TNF-α to obtain PD-L1-expressing spheroids. The spheroids were then incubated with T cells in the absence or presence of PD-1 blockade. PD-1 blockade enhanced T-cell cytotoxicity against gastric spheroids expressing PD-L1 [111]. The potential of 3D culture models for the development of new anticancer strategies has evolved lately [113], demonstrating that CSC are more resistant to drugs than other malignant cells in the tumor aggregate [114]. Nonetheless, the heterogeneity of MCTS models could lead to reproducibility problems, leading to disputable biological information not well suited to test and select appropriate potential anticancer drugs [115].

3. Gastric Organoids

Although generic approaches, such as MCTS models, have participated in improving GC treatment, patient survival rates remain poor and there is still an urgent need to develop novel effective therapies with a model that would allow taking into account the genetic make-up of the individual tumor and provide immediate treatment selection. So-called organoids are one relevant option, although there is still no consensus on the definition of 'organoid' [39]. In general, organoids are in vitro 3D culture models grown from stem cells of primary tissues [116]. They can recapitulate key features and functions of their organs of origins such as architecture and gene expression profiles [117]. The many potential applications of this novel technology are beginning to be explored and used in many research areas, particularly in cancer research. The organoids co-culture approach can mimic the tumor immune microenvironment preserving T cell receptor and immune check point [118]. The first PDTO was established in 2011 when Sato et al. developed a long-term in vitro culture protocol for primary human epithelial cells isolated from small intestinal adenomas, metaplastic Barret epithelium and colon cancer tissues [119]. This innovation goes back to the identification of a particular intestinal stem cell marker, the leucine-rich repeat-containing G protein-coupled receptor 5 (Lgr5) by Barker et al. in 2007 [120]. Sato et al. next reported the first protocol that allowed establishing adult stem cells-derived organoids using $Lgr5^+$ stem cells from intestinal crypts [121]. Since then, this protocol was applied to develop organoids from different organs including the pancreas [122], liver [123], esophagus [124], prostate [125], lung [126], breast [127], brain [116], and others [128]. Gastric organoids development was based on the localization of highly proliferative $Lgr5^+$ gastric stem cells at the base of pyloric glands [129], shortly after the identification of Lgr5 as an intestinal stem cell marker [120]. This identification was facilitated by the fact that the gastric epithelium, like the intestinal epithelium, is constantly renewed and filled with rapidly proliferating stem cells. Stange et al. found, at the gland base of the gastric corpus, specialized chief cells marked by 'Troy'. They demonstrated that a single $Troy^+$ chief cell could generate gastric organoids [130]. In the following, we describe briefly the culture of patient-derived gastric cancer organoids (PDTO) and review important findings from organoids applications in GC studies.

Gastric organoids can be established from normal and cancerous gastric tissues. They are embedded into an ECM (matrigel) in a manner that recapitulates 3D in vivo conditions [129,131]. Methods used for culturing organoids from normal tissues have been adapted to successfully produce organoids from several human cancers [132]. PDTO can be propagated from surgical tumor specimens or endoscopic biopsies [133] (Figure 2). In general, protocols used to culture gastric organoids start from rinsing

and mincing tumor tissues into small pieces (2–5 mm^3). Released tumor cells from bulk tissues are then resuspended in matrigel [134] and overlaid with culture medium supplemented with essential components such as epidermal growth factor (EGF), noggin, R-spondin1, Wnt, fibroblast growth factor (FGF), gastrin, transforming growth factor (TGF), nicotinamide, insulin-like growth factor (IGF), and p38 inhibitor glycogen synthase kinase (GSK) [135]. These supplements make organoids culture environments very complex and different from conventional 2D culture media, which may limit strict comparisons in cell behavior. Gastric organoids tend to have a conserved architecture, with gastric glands budding around a central lumen [39]. However, contamination by epithelial and stromal cells, as well as the scarcity of cancer cells, represent a major challenge in culturing PDTO [130,136]. Primary PDTO appear like a mosaic of normal and cancer cells. Mechanical or enzymatic disruption allows passing organoids to maintain the culture for many months and even be cryo-preserved. In addition, PDTO biobanks were created either from primary [131,137] or metastatic tumors [138]. These biobanks offer a biological access to human GC, facilitate drug screening, validate biomarkers, and enable personalized medicine. However, statistical issues are raised, since too small a repertoire of banked cells might not be representative enough of the genetic heterogeneity of GC.

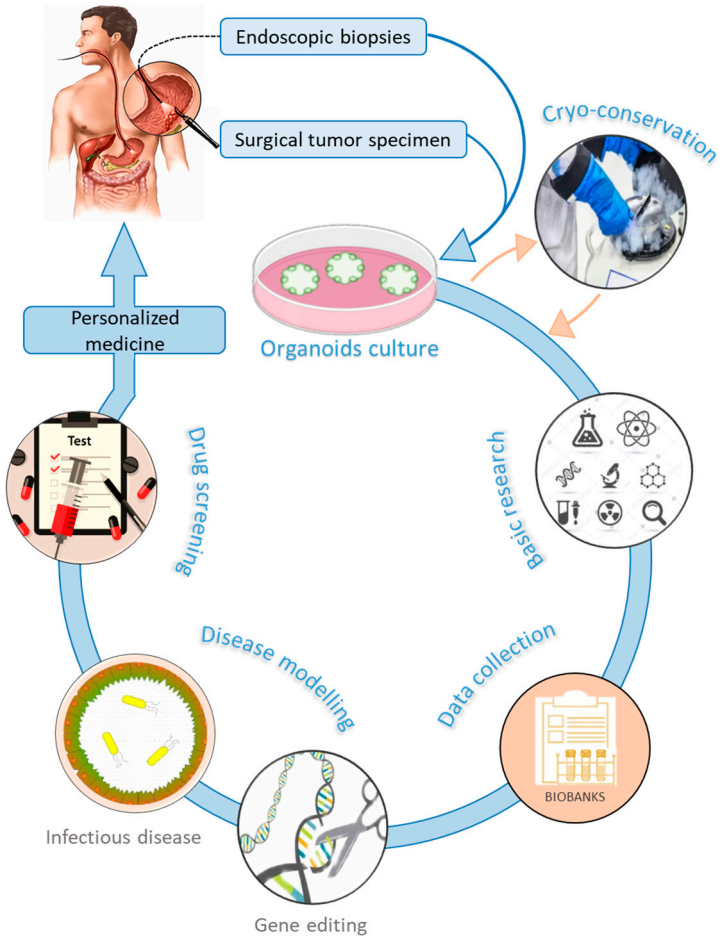

Figure 2. Graphical representation of gastric organoids applications and implication in personalized medicine.

3.1. Applications of Organoids in Gastric Cancer

3.1.1. Helicobacter Pylori Infection

H. pylori is a highly harmful human pathogen that infects approximately 60% of the world's population [139]. *H. pylori* infection causes chronic gastritis, the major risk factor for GC

development [140,141]. Injection of the cytotoxicity-associated gene A (CagA) by *H. pylori* into gastric epithelial cells induces pathogenesis [142]. Additionally, CagA upregulates Sonic Hedgehog (Shh), the regulator of gastric epithelial differentiation and function [143,144]. The majority of data generated on *H. pylori* pathogenesis was obtained from gastric CCL or in vivo animal models. However, the mechanisms of *H. pylori* infection that trigger GC initiation are poorly described. Bartfeld et al. developed a system to culture human gastric organoids from adult stem cells (aSCs) that can be productively infected by *H. pylori* [135]. Similarly, McCracken et al. reported the de novo generation of human gastric organoids through the direct differentiation of human pluripotent stem cells (hPSCs), to be used to model the pathophysiological response of the gastric epithelium to *H. pylori* [30]. Two hallmarks of *H. pylori* infection, the enhancement of gastric epithelial cells proliferation and the activation of nuclear factor-κB signaling, were discovered in 2D cell culture and were then validated in H. pylori-infected gastric organoids [135,145]. In addition, Wroblewski et al. showed that β-catenin was involved in the proliferation mechanism in H. pylori-infected organoids [146]. The activation of β-catenin and snail altered the expression and the localization of claudin-7, a protein implicated in the formation of tight junctions between epithelial cells [146]. In addition, Bertaux-Skeirik et al. have explored a new role of CD44 in *H. pylori*-induced proliferation, based on the fact that CD44 acts as a co-receptor for c-Met [147]. *H. pylori*-induced gastric pathology was contributed by the pathogen's ability to colonize, alter and manipulate $Lgr5^{+}$ progenitor-stem cells [148]. Moreover, Holokai et al. developed a human gastric organoid–immune cell co-culture system that allowed studying PD-L1 and PD-1 interactions, located on the gastric epithelial cells and the host's immune cells, respectively, during *H.* pylori infection. They suggested that *H. pylori* infections modulate the PD-L1 immune checkpoint which may protect gastric epithelial cells against an immune response [149].

3.1.2. Gastric Cancer Tumorigenesis

To date, the links between genotypes and phenotypes in the development of GC are poorly understood. Several transgenic animal models of GC tumorigenesis have been developed [150]. However, these models have all shown limitations linked to genetic background irrelevance, animal resistance and the inability to allow questioning the mechanisms that characterize the aggressive metastatic tumors. Recently however, organoids proved helpful for understanding the functional roles of driver gene mutations in the initiation and progression of cancers including colorectal [151] and gastric cancers. Knocking out CDH1, a tumor suppressor gene, Nanki et al. enhanced the transformation potential of normal gastric organoids to a diffuse GC morphology, indicating the implication of CDH1 in morphological and migratory features of GC. They showed occurrence of divergent genetic and epigenetic routes for developing WNT and R-spondin niche independency. In addition, they suggested that the loss of CDH1 and TP53 induced R-spondin independency uniquely during gastric tumorigenesis [137]. Another study by Sethi et al. showed that knocking out both CDKN2A and TP53 in dysplastic gastric organoids promoted cancer phenotypes [29]. Chen et al. investigated the role of epithelium–stroma interaction in the progression and the maintenance of gastric organoids. They demonstrated that $Trp53^{-/-}$ macrophages present in the early stroma affected wound healing and tumor promotion. Additionally, they identified R-spondin 3 as an endogenous source supplied by fibroblasts that could sustain the growth niche in gastric tissue homeostasis and early cancer development [152]. Wang et al. demonstrated that silencing C8orf76 (chromosome 8 open reading frame 76), a booster of GC cell proliferation, suppressed tumor growth in PDTO [153]. Hence, the organoid model proved highly pertinent to identify several human molecular pathways associated with disease progression.

3.1.3. Drug Sensitivity and Personalized Medicine

Intratumor heterogeneity [154] accounts for a large part of the limited benefits of current treatments. PDTO is a powerful ex vivo tool to take into account the genetic heterogeneity of primary tumors [155]. Drug exposure of organoids established from tumors obtained from seven patients treated with

epirubicin, oxaliplatin, and 5-fluorouracil was correlated with the response of the primary tumor in each patient [156]. In a similar study, Li et al. demonstrated that malignant ascites-derived organoids preserved the histological architecture and the genomic landscape of the corresponding malignant ascite tumor cells, a common manifestation in advanced GC [157]. Vlachogiannis et al. showed the clinical potential of PDTO for selecting the best treatment option in cancers using a compound library of drugs. They also showed their capacity to recapitulate patient responses. Treatment with lapatinib, a tyrosine kinase inhibitor that targets the EGFR and HER2 tyrosine kinases, was effective against ErbB2-amplified PDTO compared to wild-type PDTO [138]. The evolution of translational research, through its applications with PDTO models, makes it emerge as a crucial strategy in personalized medicine programs [131,158]. New clinical trials are required to further validate the benefits of GC PDTO in personalized medicine, i.e., assessing the correlation between the in vivo primary tumor response and the ex vivo drug-mediated cytotoxicity. The OPPOSITE trial [159] is aimed at filling this gap.

4. Concluding Remarks

In this article, we attempted to provide an overview of the development of the major 3D cell culture models of human GC. This rapidly evolving field, which comprises mainly spheroid and organoid structures, aims at providing an ex-vivo alternative to the quite demanding and expensive PDX in vivo system. Hence, MCTS systems are well suited to analyze the interactions between the cells that compose the tumor, including CSC, CAF, immune and endothelial cells. As such, they are also convenient to analyze the effects of cytotoxic drugs, as well as to identify novel biomarkers. Alternatively, organoids have proven quite useful to address issues such as the contribution of PD-L1/PD1 from immune cells to the susceptibility to infection by helicobacter pylori or the specific roles of genes and gene pathways in gastric tumorigenesis and the response of cancer cells to chemotherapeutic drugs. Hence, these ex-vivo cell culture systems already represent plausible alternatives to PDX or to other animal models. Still, harmonization of techniques is needed to ensure better data reproducibility from the use of 3D models, before these can be seen as the gold standard for the preclinical screening of therapeutic strategies for GC.

Author Contributions: C.L.J.-C. and L.C. selected the subject of the review. J.-P.M. input medical data relative to GC. G.A. prepared the Tables and Figures. All authors analyzed the bibliography and drafted the manuscript. All authors have read and agreed to the published version of the manuscript.

Funding: This work was supported by grants from the INSERM, from Brest University and from the Ligue Contre le Cancer, Comité du Finistère (n° RAB18153NNA and n° RAB19101NNA to Catherine Le Jossic-Corcos and Laurent Corcos, respectively).

Acknowledgments: George Alzeeb received a fellowship from Brest University ("Contrat Doctoral d'Etablissement"). Laurent Corcos was partially apointed by Brest University Hospital.

Conflicts of Interest: The authors declare no conflict of interest. The sponsors had no role in the design, execution, interpretation, or writing of the study.

References

1. Bray, F.; Ferlay, J.; Soerjomataram, I.; Siegel, R.L.; Torre, L.A.; Jemal, A. Global cancer statistics 2018: GLOBOCAN estimates of incidence and mortality worldwide for 36 cancers in 185 countries. *CA Cancer J. Clin.* **2018**, *68*, 394–424. [CrossRef] [PubMed]
2. McColl, K.E.L.; Going, J.J. Aetiology and classification of adenocarcinoma of the gastrooesophageal junction/cardia. *Gut* **2010**, *59*, 282–284. [CrossRef] [PubMed]
3. Arnold, M.; Soerjomataram, I.; Ferlay, J.; Forman, D. Global incidence of oesophageal cancer by histological subtype in 2012. *Gut* **2015**, *64*, 381–387. [CrossRef] [PubMed]
4. Lauren, P. The Two Histological Main Types of Gastric Carcinoma: Diffuse and So-Called Intestinal-Type Carcinoma. an Attempt At a Histo-Clinical Classification. *Acta Pathol. Microbiol. Scand.* **1965**, *64*, 31–49. [CrossRef] [PubMed]

5. Venerito, M.; Vasapolli, R.; Rokkas, T.; Malfertheiner, P. Gastric cancer: Epidemiology, prevention, and therapy. *Helicobacter* **2018**, *23*, e12518. [CrossRef]
6. Hu, B.; Hajj, N.E.; Sittler, S.; Lammert, N.; Barnes, R.; Meloni-Ehrig, A. Gastric cancer: Classification, histology and application of molecular pathology. *J. Gastrointest. Oncol.* **2012**, *3*, 251–261.
7. Bass, A.J.; Thorsson, V.; Shmulevich, I.; Reynolds, S.M.; Miller, M.; Bernard, B.; Hinoue, T.; Laird, P.W.; Curtis, C.; Shen, H.; et al. Comprehensive molecular characterization of gastric adenocarcinoma. *Nature* **2014**, *513*, 202–209.
8. Kim, J.; Bowlby, R.; Mungall, A.J.; Robertson, A.G.; Odze, R.D.; Cherniack, A.D.; Shih, J.; Pedamallu, C.S.; Cibulskis, C.; Dunford, A.; et al. Integrated genomic characterization of oesophageal carcinoma. *Nature* **2017**, *541*, 169–174.
9. Hohenberger, P.; Gretschel, S. Gastric cancer. *Lancet* **2003**, *362*, 305–315. [CrossRef]
10. Cunningham, D.; Allum, W.H.; Stenning, S.P.; Thompson, J.N.; Van De Velde, C.J.H.; Nicolson, M.; Scarffe, J.H.; Lofts, F.J.; Falk, S.J.; Iveson, T.J.; et al. Perioperative chemotherapy versus surgery alone for resectable gastroesophageal cancer. *N. Engl. J. Med.* **2006**, *355*, 11–20. [CrossRef]
11. Al-Batran, S.E.; Hofheinz, R.D.; Pauligk, C.; Kopp, H.G.; Haag, G.M.; Luley, K.B.; Meiler, J.; Homann, N.; Lorenzen, S.; Schmalenberg, H.; et al. Histopathological regression after neoadjuvant docetaxel, oxaliplatin, fluorouracil, and leucovorin versus epirubicin, cisplatin, and fluorouracil or capecitabine in patients with resectable gastric or gastro-oesophageal junction adenocarcinoma (FLOT4-AIO): Results from the phase 2 part of a multicentre, open-label, randomised phase 2/3 trial. *Lancet Oncol.* **2016**, *17*, 1697–1708.
12. Vanhoefer, U.; Rougier, P.; Wilke, H.; Ducreux, M.P.; Lacave, A.J.; Van Cutsem, E.; Planker, M.; Dos Santos, J.G.; Piedbois, P.; Paillot, B.; et al. Final Results of a Randomized Phase III Trial of Sequential High-Dose Methotrexate, Fluorouracil, and Doxorubicin Versus Etoposide, Leucovorin, and Fluorouracil Versus Infusional Fluorouracil and Cisplatin in Advanced Gastric Cancer: A Trial of the European Organization for Research and Treatment of Cancer Gastrointestinal Tract Cancer Cooperative Group. *J. Clin. Oncol.* **2000**, *18*, 2648–2657. [PubMed]
13. Bang, Y.J.; Van Cutsem, E.; Feyereislova, A.; Chung, H.C.; Shen, L.; Sawaki, A.; Lordick, F.; Ohtsu, A.; Omuro, Y.; Satoh, T.; et al. Trastuzumab in combination with chemotherapy versus chemotherapy alone for treatment of HER2-positive advanced gastric or gastro-oesophageal junction cancer (ToGA): A phase 3, open-label, randomised controlled trial. *Lancet* **2010**, *376*, 687–697. [CrossRef]
14. Fuchs, C.S.; Tomasek, J.; Yong, C.J.; Dumitru, F.; Passalacqua, R.; Goswami, C.; Safran, H.; Dos Santos, L.V.; Aprile, G.; Ferry, D.R.; et al. Ramucirumab monotherapy for previously treated advanced gastric or gastro-oesophageal junction adenocarcinoma (REGARD): An international, randomised, multicentre, placebo-controlled, phase 3 trial. *Lancet* **2014**, *383*, 31–39. [CrossRef]
15. Kim, S.T.; Cristescu, R.; Bass, A.J.; Kim, K.M.; Odegaard, J.I.; Kim, K.; Liu, X.Q.; Sher, X.; Jung, H.; Lee, M.; et al. Comprehensive molecular characterization of clinical responses to PD-1 inhibition in metastatic gastric cancer. *Nat. Med.* **2018**, *24*, 1449–1458. [CrossRef]
16. Thrift, A.P.; El-Serag, H.B. Burden of Gastric Cancer. *Clin. Gastroenterol. Hepatol.* **2020**, *18*, 534–542. [CrossRef]
17. Gillet, J.-P.; Varma, S.; Gottesman, M.M. the Clinical relevance of Cancer Cell Lines. *J. Natl. Cancer Inst.* **2013**, *105*, 452–458. [CrossRef]
18. Sensi, F.; D'Angelo, E.; D'Aronco, S.; Molinaro, R.; Agostini, M. Preclinical three-dimensional colorectal cancer model: The next generation of in vitro drug efficacy evaluation. *J. Cell. Physiol.* **2018**, *234*, 181–191. [CrossRef]
19. Anton, D.; Burckel, H.; Josset, E.; Noel, G. Three-dimensional cell culture: A breakthrough in vivo. *Int. J. Mol. Sci.* **2015**, *16*, 5517–5527. [CrossRef]
20. Fayad, W.; Brnjic, S.; Berglind, D.; Blixt, S.; Shoshan, M.C.; Berndtsson, M.; Olofsson, M.H.; Linder, S. Restriction of cisplatin induction of acute apoptosis to a subpopulation of cells in a three-dimensional carcinoma culture model. *Int. J. Cancer* **2009**, *125*, 2450–2455. [CrossRef]
21. D'angelo, E.; Natarajan, D.; Sensi, F.; Ajayi, O.; Fassan, M.; Mammano, E.; Pilati, P.; Pavan, P.; Bresolin, S.; Preziosi, M.; et al. Patient-derived scaffolds of colorectal cancer metastases as an organotypic 3D model of the liver metastatic microenvironment. *Cancers* **2020**, *12*, 364. [CrossRef] [PubMed]
22. Katt, M.E.; Placone, A.L.; Wong, A.D.; Xu, Z.S.; Searson, P.C. In vitro tumor models: Advantages, disadvantages, variables, and selecting the right platform. *Front. Bioeng. Biotechnol.* **2016**, *4*, 12. [CrossRef] [PubMed]

23. Sutherland, R.M.; Sordat, B.; Bamat, J.; Gabbert, H.; Bourrat, B.; Mueller-Klieser, W. Oxygenation and Differentiation in Multicellular Spheroids of Human Colon Carcinoma. *Cancer Res.* **1986**, *46*, 5320–5329. [PubMed]
24. Drost, J.; Clevers, H. Organoids in cancer research. *Nat. Rev. Cancer* **2018**, *18*, 407–418. [CrossRef] [PubMed]
25. Zanoni, M.; Cortesi, M.; Zamagni, A.; Arienti, C.; Pignatta, S.; Tesei, A. Modeling neoplastic disease with spheroids and organoids. *J. Hematol. Oncol.* **2020**, *13*, 1–15. [CrossRef] [PubMed]
26. Magalhães, L.; Quintana, L.G.; Lopes, D.C.F.; Vidal, A.F.; Pereira, A.L.; D'Araujo Pinto, L.C.; De Jesus Viana Pinheiro, J.; Khayat, A.S.; Goulart, L.R.; Burbano, R.; et al. APC gene is modulated by hsa-miR-135b-5p in both diffuse and intestinal gastric cancer subtypes. *BMC Cancer* **2018**, *18*, 1055. [CrossRef] [PubMed]
27. Sha, H.; Zou, Z.; Xin, K.; Bian, X.; Cai, X.; Lu, W.; Chen, J.; Chen, G.; Huang, L.; Blair, A.M.; et al. Tumor-penetrating peptide fused EGFR single-domain antibody enhances cancer drug penetration into 3D multicellular spheroids and facilitates effective gastric cancer therapy. *J. Control. Release* **2014**, *200*, 188–200. [CrossRef]
28. Bekaii-Saab, T.; El-Rayes, B. Identifying and targeting cancer stem cells in the treatment of gastric cancer. *Cancer* **2017**, *123*, 1303–1312. [CrossRef]
29. Sethi, N.S.; Kikuchi, O.; Duronio, G.N.; Stachler, M.D.; McFarland, J.M.; Ferrer-Luna, R.; Zhang, Y.; Bao, C.; Bronson, R.; Patil, D.; et al. Early TP53 alterations engage environmental exposures to promote gastric premalignancy in an integrative mouse model. *Nat. Genet.* **2020**, *52*, 219–230. [CrossRef]
30. McCracken, K.W.; Catá, E.M.; Crawford, C.M.; Sinagoga, K.L.; Schumacher, M.; Rockich, B.E.; Tsai, Y.-H.; Mayhew, C.N.; Spence, J.R.; Zavros, Y.; et al. Modelling human development and disease in pluripotent stem-cell-derived gastric organoids. *Nature* **2014**, *516*, 400–404. [CrossRef]
31. Friedrich, J.; Seidel, C.; Ebner, R.; Kunz-Schughart, L.A. Spheroid-based drug screen: Considerations and practical approach. *Nat. Protoc.* **2009**, *4*, 309–324. [CrossRef]
32. Liao, C.P.; Adisetiyo, H.; Liang, M.; Roy-Burman, P. Cancer-associated fibroblasts enhance the gland-forming capability of prostate cancer stem cells. *Cancer Res.* **2010**, *70*, 7294–7303. [CrossRef] [PubMed]
33. Togo, S.; Polanska, U.; Horimoto, Y.; Orimo, A. Carcinoma-Associated Fibroblasts Are a Promising Therapeutic Target. *Cancers* **2013**, *5*, 149–169. [CrossRef] [PubMed]
34. Cho, S.Y.; Kang, W.; Han, J.Y.; Min, S.; Kang, J.; Lee, A.; Kwon, J.Y.; Lee, C.; Park, H. An integrative approach to precision cancer medicine using patient-derived xenografts. *Mol. Cells* **2016**, *39*, 77–86. [PubMed]
35. Jung, J.; Seol, H.S.; Chang, S. The generation and application of patient-derived xenograft model for cancer research. *Cancer Res. Treat.* **2018**, *50*, 1–10. [CrossRef]
36. Byrne, A.T.; Alférez, D.G.; Amant, F.; Annibali, D.; Arribas, J.; Biankin, A.V.; Bruna, A.; Budinská, E.; Caldas, C.; Chang, D.K.; et al. Interrogating open issues in cancer precision medicine with patient-derived xenografts. *Nat. Rev. Cancer* **2017**, *17*, 254–268. [CrossRef]
37. Lin, M.; Gao, M.; Cavnar, M.J.; Kim, J. Utilizing gastric cancer organoids to assess tumor biology and personalize medicine. *World J. Gastrointest. Oncol.* **2019**, *11*, 509–517. [CrossRef]
38. Aberle, M.R.; Burkhart, R.A.; Tiriac, H.; Olde Damink, S.W.M.; Dejong, C.H.C.; Tuveson, D.A.; van Dam, R.M. Patient-derived organoid models help define personalized management of gastrointestinal cancer. *Br. J. Surg.* **2018**, *105*, e48–e60. [CrossRef]
39. Lau, H.C.H.; Kranenburg, O.; Xiao, H.; Yu, J. Organoid models of gastrointestinal cancers in basic and translational research. *Nat. Rev. Gastroenterol. Hepatol.* **2020**, *17*, 203–222. [CrossRef]
40. Van De Wetering, M.; Francies, H.E.; Francis, J.M.; Bounova, G.; Iorio, F.; Pronk, A.; Van Houdt, W.; Van Gorp, J.; Taylor-Weiner, A.; Kester, L.; et al. Prospective derivation of a living organoid biobank of colorectal cancer patients. *Cell* **2015**, *161*, 933–945. [CrossRef]
41. Schlaermann, P.; Toelle, B.; Berger, H.; Schmidt, S.C.; Glanemann, M.; Ordemann, J.; Bartfeld, S.; Mollenkopf, H.J.; Meyer, T.F. A novel human gastric primary cell culture system for modelling Helicobacter pylori infection in vitro. *Gut* **2016**, *65*, 202–213. [CrossRef] [PubMed]
42. Breslin, S.; O'Driscoll, L. Three-dimensional cell culture: The missing link in drug discovery. *Drug Discov. Today* **2013**, *18*, 240–249. [CrossRef] [PubMed]
43. Cancer Tissue Engineering—New Perspectives in Understand Google Scholar. Available online: https://scholar.google.com/scholar?hl=en&as_sdt=0%2C5&q=Cancer+tissue+engineering—New+perspectives+in+understanding+the+biology+of+solid+tumours—A+critical+review&btnG= (accessed on 11 September 2020).

44. Fischbach, C.; Chen, R.; Matsumoto, T.; Schmelzle, T.; Brugge, J.S.; Polverini, P.J.; Mooney, D.J. Engineering tumors with 3D scaffolds. *Nat. Methods* **2007**, *4*, 855–860. [CrossRef]
45. De-Souza, A.S.C.; Costa-Casagrande, T.A. Animal models for colorectal cancer. *ABCD. Arq. Bras. Cir. Dig.* **2018**, *31*. [CrossRef] [PubMed]
46. Inch, W.; Credie, J.; Sutherland, R. Growth of nodular carcinomas in rodents compared with multi-cell spheroids in tissue culture. *Subj. Strain Bibliogr.* **1970**, *34*, 271–282.
47. Hickman, J.A.; Graeser, R.; de Hoogt, R.; Vidic, S.; Brito, C.; Gutekunst, M.; van der Kuip, H. Imi Predect consortium Three-dimensional models of cancer for pharmacology and cancer cell biology: Capturing tumor complexity in vitro/ex vivo. *Biotechnol. J.* **2014**, *9*, 1115–1128. [CrossRef] [PubMed]
48. Hirschhaeuser, F.; Menne, H.; Dittfeld, C.; West, J.; Mueller-Klieser, W.; Kunz-Schughart, L.A. Multicellular tumor spheroids: An underestimated tool is catching up again. *J. Biotechnol.* **2010**, *148*, 3–15. [CrossRef]
49. Mehta, G.; Hsiao, A.Y.; Ingram, M.; Luker, G.D.; Takayama, S. Opportunities and challenges for use of tumor spheroids as models to test drug delivery and efficacy. *J. Control. Release* **2012**, *164*, 192–204. [CrossRef]
50. Ghosh, S.; Spagnoli, G.C.; Martin, I.; Ploegert, S.; Demougin, P.; Heberer, M.; Reschner, A. Three-dimensional culture of melanoma cells profoundly affects gene expression profile: A high density oligonucleotide array study. *J. Cell. Physiol.* **2005**, *204*, 522–531. [CrossRef]
51. Krueger, S.; Kalinski, T.; Wolf, H.; Kellner, U.; Roessner, A. Interactions between human colon carcinoma cells, fibroblasts and monocytic cells in coculture Regulation of cathepsin B expression and invasiveness. *Cancer Lett.* **2005**, *223*, 313–322. [CrossRef]
52. Lamichhane, S.P.; Arya, N.; Kohler, E.; Xiang, S.; Christensen, J.; Shastri, V.P. Recapitulating epithelial tumor microenvironment in vitro using three dimensional tri-culture of human epithelial, endothelial, and mesenchymal cells. *BMC Cancer* **2016**, *16*, 1–12. [CrossRef] [PubMed]
53. Sebrell, T.A.; Hashimi, M.; Sidar, B.; Wilkinson, R.A.; Kirpotina, L.; Quinn, M.T.; Malkoç, Z.; Taylor, P.J.; Wilking, J.N.; Bimczok, D. A Novel Gastric Spheroid Co-culture Model Reveals Chemokine-Dependent Recruitment of Human Dendritic Cells to the Gastric Epithelium. *Cell. Mol. Gastroenterol. Hepatol.* **2019**, *8*, 157–171.e3. [CrossRef]
54. Ravi, M.; Paramesh, V.; Kaviya, S.R.; Anuradha, E.; Paul Solomon, F.D. 3D cell culture systems: Advantages and applications. *J. Cell. Physiol.* **2015**, *230*, 16–26. [CrossRef] [PubMed]
55. Place, E.S.; George, J.H.; Williams, C.K.; Stevens, M.M. Synthetic polymer scaffolds for tissue engineering. *Chem. Soc. Rev.* **2009**, *38*, 1139–1151. [CrossRef] [PubMed]
56. Estrada, M.F.; Rebelo, S.P.; Davies, E.J.; Pinto, M.T.; Pereira, H.; Santo, V.E.; Smalley, M.J.; Barry, S.T.; Gualda, E.J.; Alves, P.M.; et al. Modelling the tumour microenvironment in long-term microencapsulated 3D co-cultures recapitulates phenotypic features of disease progression. *Biomaterials* **2016**, *78*, 50–61. [CrossRef] [PubMed]
57. Yuhas, J.M.; Li, A.P.; Martinez, A.O.; Ladman, A.J. A Simplified Method for Production and Growth of Multicellular Tumor Spheroids. *Cancer Res.* **1977**, *37*, 3639–3643.
58. Yamada, K.M.; Cukierman, E. Modeling Tissue Morphogenesis and Cancer in 3D. *Cell* **2007**, *130*, 601–610. [CrossRef]
59. Lin, R.-Z.; Chang, H.-Y. Recent advances in three-dimensional multicellular spheroid culture for biomedical research. *Biotechnol. J.* **2008**, *3*, 1172–1184. [CrossRef]
60. Jørgensen, A.; Young, J.; Nielsen, J.E.; Joensen, U.N.; Toft, B.G.; Rajpert-De Meyts, E.; Loveland, K.L. Hanging drop cultures of human testis and testis cancer samples: A model used to investigate activin treatment effects in a preserved niche. *Br. J. Cancer* **2014**, *110*, 2604–2614. [CrossRef]
61. Kurosawa, H. Methods for inducing embryoid body formation: In vitro differentiation system of embryonic stem cells. *J. Biosci. Bioeng.* **2007**, *103*, 389–398. [CrossRef]
62. Fennema, E.; Rivron, N.; Rouwkema, J.; van Blitterswijk, C.; De Boer, J. Spheroid culture as a tool for creating 3D complex tissues. *Trends Biotechnol.* **2013**, *31*, 108–115. [CrossRef] [PubMed]
63. Huang, Y.; Li, X.; Sha, H.; Zhang, L.; Bian, X.; Han, X.; Liu, B. STRAIL-iRGD is a promising therapeutic agent for gastric cancer treatment. *Sci. Rep.* **2017**, *7*, 1–13. [CrossRef] [PubMed]
64. Mayer, B.; Klement, G.; Kaneko, M.; Man, S.; Jothy, S.; Rak, J.; Kerbel, R.S. Multicellular Gastric Cancer Spheroids Recapitulate Growth Pattern and Differentiation Phenotype of Human Gastric Carcinomas. *Gastroenterology* **2001**, *121*, 839–852. [CrossRef] [PubMed]

65. Xiao, Y.; Pan, J.; Geng, Q.; Wang, G. Lnc RNA MALAT 1 increases the stemness of gastric cancer cells via enhancing SOX 2 mRNA stability. *FEBS Open Bio* **2019**, *9*, 1212–1222. [CrossRef]
66. Song, H.; Shi, L.; Xu, Y.; Xu, T.; Fan, R.; Cao, M.; Xu, W.; Song, J. BRD4 promotes the stemness of gastric cancer cells via attenuating miR-216a-3p-mediated inhibition of Wnt/β-catenin signaling. *Eur. J. Pharmacol.* **2019**, *852*, 189–197. [CrossRef]
67. Liu, J.; Ma, L.; Wang, Z.; Wang, L.; Liu, C.; Chen, R.; Zhang, J. MicroRNA Expression Profile of Gastric Cancer Stem Cells in the MKN-45 Cancer Cell Line. *Acta Biochim. Biophys. Sin.* **2014**, *46*, 92–99. [CrossRef]
68. Kelm, J.M.; Timmins, N.E.; Brown, C.J.; Fussenegger, M.; Nielsen, L.K. Method for generation of homogeneous multicellular tumor spheroids applicable to a wide variety of cell types. *Biotechnol. Bioeng.* **2003**, *83*, 173–180. [CrossRef]
69. Yang, Z.; Wang, Z.; Fan, Y.; Zheng, Q. Expression of CD133 in SW620 colorectal cancer cells is modulated by the microenvironment. *Oncol. Lett.* **2012**, *4*, 75–79. [CrossRef]
70. Al-Husaini, K.; Elkamel, E.; Han, X.; Chen, P. Therapeutic potential of a cell penetrating peptide (CPP, NP1) mediated siRNA delivery: Evidence in 3D spheroids of colon cancer cells. *Can. J. Chem. Eng.* **2020**, *98*, 1240–1254. [CrossRef]
71. McLean, M.H.; El-Omar, E.M. Genetics of gastric cancer. *Nat. Rev. Gastroenterol. Hepatol.* **2014**, *11*, 664–674. [CrossRef]
72. Baker, B.M.; Chen, C.S. Deconstructing the third dimension-how 3D culture microenvironments alter cellular cues. *J. Cell Sci.* **2012**, *125*, 3015–3024. [CrossRef] [PubMed]
73. Ishimoto, T.; Nagano, O.; Yae, T.; Tamada, M.; Motohara, T.; Oshima, H.; Oshima, M.; Ikeda, T.; Asaba, R.; Yagi, H.; et al. CD44 Variant Regulates Redox Status in Cancer Cells by Stabilizing the xCT Subunit of System xc- and Thereby Promotes Tumor Growth. *Cancer Cell* **2011**, *19*, 387–400. [CrossRef] [PubMed]
74. Oue, N.; Mukai, S.; Imai, T.; Pham, T.T.B.; Oshima, T.; Sentani, K.; Sakamoto, N.; Yoshida, K.; Yasui, W. Induction of KIFC1 expression in gastric cancer spheroids. *Oncol. Rep.* **2016**, *36*, 349–355. [CrossRef] [PubMed]
75. Oue, N.; Sentani, K.; Sakamoto, N.; Uraoka, N.; Yasui, W. Molecular carcinogenesis of gastric cancer: Lauren classification, mucin phenotype expression, and cancer stem cells. *Int. J. Clin. Oncol.* **2019**, *24*, 771–778. [CrossRef] [PubMed]
76. Imai, T.; Oue, N.; Nishioka, M.; Mukai, S.; Oshima, T.; Sakamoto, N.; Sentani, K.; Matsusaki, K.; Yoshida, K.; Yasui, W. Overexpression of KIF11 in Gastric Cancer with Intestinal Mucin Phenotype. *Pathobiology* **2017**, *84*, 16–24. [CrossRef]
77. Kobayashi, G.; Sentani, K.; Hattori, T.; Yamamoto, Y.; Imai, T.; Sakamoto, N.; Kuraoka, K.; Oue, N.; Sasaki, N.; Taniyama, K.; et al. Clinicopathological significance of claspin overexpression and its association with spheroid formation in gastric cancer. *Hum. Pathol.* **2019**, *84*, 8–17. [CrossRef]
78. Lee, J.W.; Sung, J.S.; Park, Y.S.; Chung, S.; Kim, Y.H. Isolation of spheroid-forming single cells from gastric cancer cell lines: Enrichment of cancer stem-like cells. *Biotechniques* **2018**, *65*, 197–203. [CrossRef]
79. Lee, J.W.; Sung, J.S.; Park, Y.S.; Chung, S.; Kim, Y.H. Identification of different gene expressions between diffuse- and intestinal-type spheroid-forming gastric cancer cells. *Gastric Cancer* **2019**, *22*, 967–979. [CrossRef]
80. Birgersdotter, A.; Sandberg, R.; Ernberg, I. Gene expression perturbation in vitro A growing case for three-dimensional (3D) culture systems. *Semin. Cancer Biol.* **2005**, *15*, 405–412. [CrossRef]
81. Branco da Cunha, C.; Klumpers, D.D.; Koshy, S.T.; Weaver, J.C.; Chaudhuri, O.; Seruca, R.; Carneiro, F.; Granja, P.L.; Mooney, D.J. CD44 alternative splicing in gastric cancer cells is regulated by culture dimensionality and matrix stiffness. *Biomaterials* **2016**, *98*, 152–162. [CrossRef]
82. Da Cunha, C.B.; Oliveira, C.; Wen, X.; Gomes, B.; Sousa, S.; Suriano, G.; Grellier, M.; Huntsman, D.G.; Carneiro, F.; Granja, P.L.; et al. De novo expression of CD44 variants in sporadic and hereditary gastric cancer. *Lab. Investig.* **2010**, *90*, 1604–1614. [CrossRef] [PubMed]
83. Farnie, G.; Clarke, R.B. Mammary stem cells and breast cancer Role of notch signalling. *Stem Cell Rev.* **2007**, *3*, 169–175. [CrossRef] [PubMed]
84. Dubrovska, A.; Kim, S.; Salamone, R.J.; Walker, J.R.; Maira, S.M.; García-Echeverría, C.; Schultz, P.G.; Reddy, V.A. The role of PTEN/Akt/PI3K signaling in the maintenance and viability of prostate cancer stem-like cell populations. *Proc. Natl. Acad. Sci. USA* **2009**, *106*, 268–273. [CrossRef] [PubMed]
85. Wu, C.; Alman, B.A. Side population cells in human cancers. *Cancer Lett.* **2008**, *268*, 1–9. [CrossRef] [PubMed]

86. Clarke, M.F.; Dick, J.E.; Dirks, P.B.; Eaves, C.J.; Jamieson, C.H.M.; Jones, D.L.; Visvader, J.; Weissman, I.L.; Wahl, G.M. Cancer stem cells Perspectives on current status and future directions: AACR workshop on cancer stem cells. *Cancer Res.* **2006**, *66*, 9339–9344. [CrossRef]
87. Zhang, X.; Hua, R.; Wang, X.; Huang, M.; Gan, L.; Wu, Z.; Zhang, J.; Wang, H.; Cheng, Y.; Li, J.; et al. Identification of stem-like cells and clinical significance of candidate stem cell markers in gastric cancer. *Oncotarget* **2016**, *7*, 9815–9831. [CrossRef] [PubMed]
88. Rocco, A.; Liguori, E.; Pirozzi, G.; Tirino, V.; Compare, D.; Franco, R.; Tatangelo, F.; Palaia, R.; D'Armiento, F.P.; Pollastrone, G.; et al. CD133 and CD44 Cell surface markers do not identify cancer stem cells in primary human gastric tumors. *J. Cell. Physiol.* **2012**, *227*, 2686–2693. [CrossRef]
89. Takaishi, S.; Okumura, T.; Tu, S.; Wang, S.S.W.; Shibata, W.; Vigneshwaran, R.; Gordon, S.A.K.; Shimada, Y.; Wang, T.C. Identification of Gastric Cancer Stem Cells Using the Cell Surface Marker CD44. *Stem Cells* **2009**, *27*, 1006–1020. [CrossRef]
90. Han, M.E.; Jeon, T.Y.; Hwang, S.H.; Lee, Y.S.; Kim, H.J.; Shim, H.E.; Yoon, S.; Baek, S.Y.; Kim, B.S.; Kang, C.D.; et al. Cancer spheres from gastric cancer patients provide an ideal model system for cancer stem cell research. *Cell. Mol. Life Sci.* **2011**, *68*, 3589–3605. [CrossRef]
91. Liu, J.; Ma, L.; Xu, J.; Liu, C.; Zhang, J.; Liu, J.; Chen, R.; Zhou, Y. Spheroid body-forming cells in the human gastric cancer cell line MKN-45 possess cancer stem cell properties. *Int. J. Oncol.* **2013**, *42*, 453–459. [CrossRef]
92. Liu, J.; Zhou, Y.; Ma, L.; Xu, J.; Liu, C.; Zhang, J.; Liu, J.; Chen, R.; Qian, H. Co-expression of CD44 and ABCG2 in spheroid body-forming cells of gastric cancer cell line MKN45. *Hepatogastroenterology* **2013**, *60*, 975–980. [PubMed]
93. Jiang, J.; Zhang, Y.; Chuai, S.; Wang, Z.; Zheng, D.; Xu, F.; Zhang, Y.; Li, C.; Liang, Y.; Chen, Z. Trastuzumab (herceptin) targets gastric cancer stem cells characterized by CD90 phenotype. *Oncogene* **2012**, *31*, 671–682. [CrossRef] [PubMed]
94. Tian, T.; Zhang, Y.; Wang, S.; Zhou, J.; Xu, S. Sox2 enhances the tumorigenicity and chemoresistance of cancer stem-like cells derived from gastric cancer. *J. Biomed. Res.* **2012**, *26*, 336–345. [CrossRef] [PubMed]
95. Song, Z.; Yue, W.; Wei, B.; Wang, N.; Li, T.; Guan, L.; Shi, S.; Zeng, Q.; Pei, X.; Chen, L. Sonic hedgehog pathway is essential for maintenance of cancer stem-like cells in human gastric cancer. *PLoS ONE* **2011**, *6*, e17687. [CrossRef] [PubMed]
96. Ohkuma, M.; Haraguchi, N.; Ishii, H.; Mimori, K.; Tanaka, F.; Kim, H.M.; Shimomura, M.; Hirose, H.; Yanaga, K.; Mori, M. Absence of CD71 transferrin receptor characterizes human gastric adenosquamous carcinoma stem cells. *Ann. Surg. Oncol.* **2012**, *19*, 1357–1364. [CrossRef]
97. Yoon, C.; Cho, S.J.; Aksoy, B.A.; Park, D.J.; Schultz, N.; Ryeom, S.W.; Yoon, S.S. Chemotherapy resistance in diffuse-type gastric adenocarcinoma is mediated by RhoA activation in cancer stem-like cells. *Clin. Cancer Res.* **2016**, *22*, 971–983. [CrossRef]
98. Atashzar, M.R.; Baharlou, R.; Karami, J.; Abdollahi, H.; Rezaei, R.; Pourramezan, F.; Zoljalali Moghaddam, S.H. Cancer stem cells: A review from origin to therapeutic implications. *J. Cell. Physiol.* **2020**, *235*, 790–803. [CrossRef]
99. Costa, E.C.; Moreira, A.F.; de Melo-Diogo, D.; Gaspar, V.M.; Carvalho, M.P.; Correia, I.J. 3D tumor spheroids: An overview on the tools and techniques used for their analysis. *Biotechnol. Adv.* **2016**, *34*, 1427–1441. [CrossRef]
100. Ocana, A.; Pandiella, A.; Siu, L.L.; Tannock, I.F. Preclinical development of molecular-targeted agents for cancer. *Nat. Rev. Clin. Oncol.* **2011**, *8*, 200–209. [CrossRef]
101. Longati, P.; Jia, X.; Eimer, J.; Wagman, A.; Witt, M.R.; Rehnmark, S.; Verbeke, C.; Toftgård, R.; Löhr, M.; Heuchel, R.L. 3D pancreatic carcinoma spheroids induce a matrix-rich, chemoresistant phenotype offering a better model for drug testing. *BMC Cancer* **2013**, *13*, 1–13. [CrossRef]
102. Courtois, S.; Durán, R.V.; Giraud, J.; Sifré, E.; Izotte, J.; Mégraud, F.; Lehours, P.; Varon, C.; Bessède, E. Metformin targets gastric cancer stem cells. *Eur. J. Cancer* **2017**, *84*, 193–201. [CrossRef] [PubMed]
103. Akrami, H.; Aminzadeh, S.; Fallahi, H. Inhibitory effect of ibuprofen on tumor survival and angiogenesis in gastric cancer cell. *Tumor Biol.* **2015**, *36*, 3237–3243. [CrossRef] [PubMed]
104. Akrami, H.; Moradi, B.; Borzabadi Farahani, D.; Mehdizadeh, K. Ibuprofen reduces cell proliferation through inhibiting Wnt/β catenin signaling pathway in gastric cancer stem cells. *Cell Biol. Int.* **2018**, *42*, 949–958. [CrossRef]

105. Nishikawa, S.; Konno, M.; Hamabe, A.; Hasegawa, S.; Kano, Y.; Ohta, K.; Fukusumi, T.; Sakai, D.; Kudo, T.; Haraguchi, N.; et al. Aldehyde dehydrogenasehigh gastric cancer stem cells are resistant to chemotherapy. *Int. J. Oncol.* **2013**, *42*, 1437–1442. [CrossRef] [PubMed]
106. Koh, J.S.; Joo, M.K.; Park, J.J.; Yoo, H.S.; Choi, B.I.; Lee, B.J.; Chun, H.J.; Lee, S.W. Inhibition of STAT3 in gastric cancer: Role of pantoprazole as SHP-1 inducer. *Cell Biosci.* **2018**, *8*, 50. [CrossRef]
107. Minchinton, A.I.; Tannock, I.F. Drug penetration in solid tumours. *Nat. Rev. Cancer* **2006**, *6*, 583–592. [CrossRef] [PubMed]
108. Sha, H.; Li, R.; Bian, X.; Liu, Q.; Xie, C.; Xin, X.; Kong, W.; Qian, X.; Jiang, X.; Hu, W.; et al. A tumor-penetrating recombinant protein anti-EGFR-iRGD enhance efficacy of paclitaxel in 3D multicellular spheroids and gastric cancer in vivo. *Eur. J. Pharm. Sci.* **2015**, *77*, 60–72. [CrossRef] [PubMed]
109. Liu, R.; Ma, X.; Wang, H.; Xi, Y.; Qian, M.; Yang, W.; Luo, D.; Fan, L.; Xia, X.; Zhou, J.; et al. The novel fusion protein sTRAIL-TMTP1 exhibits a targeted inhibition of primary tumors and metastases. *J. Mol. Med.* **2014**, *92*, 165–175. [CrossRef]
110. Sherman, H.; Gitschier, H.J.; Rossi, A.E. A novel three-dimensional immune oncology model for high-throughput testing of tumoricidal activity. *Front. Immunol.* **2018**, *9*, 857. [CrossRef]
111. Zhou, S.; Zhu, M.; Meng, F.; Shao, J.; Xu, Q.; Wei, J.; Liu, B. Evaluation of PD-1 blockade using a multicellular tumor spheroid model. *Am. J. Transl. Res.* **2019**, *11*, 7471–7478.
112. Salmaninejad, A.; Valilou, S.F.; Shabgah, A.G.; Aslani, S.; Alimardani, M.; Pasdar, A.; Sahebkar, A. PD-1/PD-L1 pathway: Basic biology and role in cancer immunotherapy. *J. Cell. Physiol.* **2019**, *234*, 16824–16837. [CrossRef] [PubMed]
113. Langhans, S.A. Three-dimensional in vitro cell culture models in drug discovery and drug repositioning. *Front. Pharmacol.* **2018**, *9*, 6. [CrossRef] [PubMed]
114. Pattabiraman, D.R.; Weinberg, R.A. Tackling the cancer stem cells-what challenges do they pose? *Nat. Rev. Drug Discov.* **2014**, *13*, 497–512. [CrossRef] [PubMed]
115. Das, V.; Fürst, T.; Gurská, S.; Džubák, P.; Hajdúch, M. Reproducibility of uniform spheroid formation in 384-well plates: The effect of medium evaporation. *J. Biomol. Screen.* **2016**, *21*, 923–930. [CrossRef] [PubMed]
116. Eiraku, M.; Sasai, Y. Self-formation of layered neural structures in three-dimensional culture of ES cells. *Curr. Opin. Neurobiol.* **2012**, *22*, 768–777. [CrossRef] [PubMed]
117. Werner, K.; Weitz, J.; Stange, D.E. Organoids as Model Systems for Gastrointestinal Diseases: Tissue Engineering Meets Genetic Engineering. *Curr. Pathobiol. Rep.* **2016**, *4*, 1–9. [CrossRef]
118. Neal, J.T.; Li, X.; Zhu, J.; Giangarra, V.; Grzeskowiak, C.L.; Ju, J.; Liu, I.H.; Chiou, S.H.; Salahudeen, A.A.; Smith, A.R.; et al. Organoid Modeling of the Tumor Immune Microenvironment. *Cell* **2018**, *175*, 1972–1988.e16. [CrossRef]
119. Sato, T.; Stange, D.E.; Ferrante, M.; Vries, R.G.J.; Van Es, J.H.; Van Den Brink, S.; Van Houdt, W.J.; Pronk, A.; Van Gorp, J.; Siersema, P.D.; et al. Long-term expansion of epithelial organoids from human colon, adenoma, adenocarcinoma, and Barrett's epithelium. *Gastroenterology* **2011**, *141*, 1762–1772. [CrossRef]
120. Barker, N.; Van Es, J.H.; Kuipers, J.; Kujala, P.; Van Den Born, M.; Cozijnsen, M.; Haegebarth, A.; Korving, J.; Begthel, H.; Peters, P.J.; et al. Identification of stem cells in small intestine and colon by marker gene Lgr5. *Nature* **2007**, *449*, 1003–1007. [CrossRef]
121. Sato, T.; Vries, R.G.; Snippert, H.J.; Van De Wetering, M.; Barker, N.; Stange, D.E.; Van Es, J.H.; Abo, A.; Kujala, P.; Peters, P.J.; et al. Single Lgr5 stem cells build crypt-villus structures in vitro without a mesenchymal niche. *Nature* **2009**, *459*, 262–265. [CrossRef]
122. Boj, S.F.; Hwang, C.I.; Baker, L.A.; Chio, I.I.C.; Engle, D.D.; Corbo, V.; Jager, M.; Ponz-Sarvise, M.; Tiriac, H.; Spector, M.S.; et al. Organoid models of human and mouse ductal pancreatic cancer. *Cell* **2015**, *160*, 324–338. [CrossRef]
123. Huch, M.; Gehart, H.; Van Boxtel, R.; Hamer, K.; Blokzijl, F.; Verstegen, M.M.A.; Ellis, E.; Van Wenum, M.; Fuchs, S.A.; De Ligt, J.; et al. Long-term culture of genome-stable bipotent stem cells from adult human liver. *Cell* **2015**, *160*, 299–312. [CrossRef]
124. DeWard, A.D.; Cramer, J.; Lagasse, E. Cellular heterogeneity in the mouse esophagus implicates the presence of a nonquiescent epithelial stem cell population. *Cell Rep.* **2014**, *9*, 701–711. [CrossRef]
125. Chua, C.W.; Shibata, M.; Lei, M.; Toivanen, R.; Barlow, L.J.; Bergren, S.K.; Badani, K.K.; McKiernan, J.M.; Benson, M.C.; Hibshoosh, H.; et al. Single luminal epithelial progenitors can generate prostate organoids in culture. *Nat. Cell Biol.* **2014**, *16*, 951–961. [CrossRef]

126. Wong, A.P.; Bear, C.E.; Chin, S.; Pasceri, P.; Thompson, T.O.; Huan, L.J.; Ratjen, F.; Ellis, J.; Rossant, J. Directed differentiation of human pluripotent stem cells into mature airway epithelia expressing functional CFTR protein. *Nat. Biotechnol.* **2012**, *30*, 876–882. [CrossRef]
127. Sachs, N.; de Ligt, J.; Kopper, O.; Gogola, E.; Bounova, G.; Weeber, F.; Balgobind, A.V.; Wind, K.; Gracanin, A.; Begthel, H.; et al. A Living Biobank of Breast Cancer Organoids Captures Disease Heterogeneity. *Cell* **2018**, *172*, 373–386.e10. [CrossRef]
128. Clevers, H. Modeling Development and Disease with Organoids. *Cell* **2016**, *165*, 1586–1597. [CrossRef] [PubMed]
129. Barker, N.; Huch, M.; Kujala, P.; van de Wetering, M.; Snippert, H.J.; van Es, J.H.; Sato, T.; Stange, D.E.; Begthel, H.; van den Born, M.; et al. Lgr5+ve Stem Cells Drive Self-Renewal in the Stomach and Build Long-Lived Gastric Units In Vitro. *Cell Stem Cell* **2010**, *6*, 25–36. [CrossRef] [PubMed]
130. Stange, D.E.; Koo, B.K.; Huch, M.; Sibbel, G.; Basak, O.; Lyubimova, A.; Kujala, P.; Bartfeld, S.; Koster, J.; Geahlen, J.H.; et al. XDifferentiated Troy+ chief cells act as reserve stem cells to generate all lineages of the stomach epithelium. *Cell* **2013**, *155*, 357. [CrossRef] [PubMed]
131. Seidlitz, T.; Merker, S.R.; Rothe, A.; Zakrzewski, F.; Von Neubeck, C.; Grützmann, K.; Sommer, U.; Schweitzer, C.; Schölch, S.; Uhlemann, H.; et al. Human gastric cancer modelling using organoids. *Gut* **2019**, *68*, 207–217. [CrossRef]
132. Gao, D.; Vela, I.; Sboner, A.; Iaquinta, P.J.; Karthaus, W.R.; Gopalan, A.; Dowling, C.; Wanjala, J.N.; Undvall, E.A.; Arora, V.K.; et al. Organoid cultures derived from patients with advanced prostate cancer. *Cell* **2014**, *159*, 176–187. [CrossRef] [PubMed]
133. Gao, M.; Lin, M.; Rao, M.; Thompson, H.; Hirai, K.; Choi, M.; Georgakis, G.V.; Sasson, A.R.; Bucobo, J.C.; Tzimas, D.; et al. Development of Patient-Derived Gastric Cancer Organoids from Endoscopic Biopsies and Surgical Tissues. *Ann. Surg. Oncol.* **2018**, *25*, 2767–2775. [CrossRef] [PubMed]
134. Hughes, C.S.; Postovit, L.M.; Lajoie, G.A. Matrigel: A complex protein mixture required for optimal growth of cell culture. *Proteomics* **2010**, *10*, 1886–1890. [CrossRef] [PubMed]
135. Bartfeld, S.; Bayram, T.; Van De Wetering, M.; Huch, M.; Begthel, H.; Kujala, P.; Vries, R.; Peters, P.J.; Clevers, H. In vitro expansion of human gastric epithelial stem cells and their responses to bacterial infection. *Gastroenterology* **2015**, *148*, 126–136.e6. [CrossRef]
136. Yan, H.H.N.; Siu, H.C.; Law, S.; Ho, S.L.; Yue, S.S.K.; Tsui, W.Y.; Chan, D.; Chan, A.S.; Ma, S.; Lam, K.O.; et al. A Comprehensive Human Gastric Cancer Organoid Biobank Captures Tumor Subtype Heterogeneity and Enables Therapeutic Screening. *Cell Stem. Cell* **2018**, *23*, 882–897.e11. [CrossRef]
137. Nanki, K.; Toshimitsu, K.; Takano, A.; Fujii, M.; Shimokawa, M.; Ohta, Y.; Matano, M.; Seino, T.; Nishikori, S.; Ishikawa, K.; et al. Divergent Routes toward Wnt and R-spondin Niche Independency during Human Gastric Carcinogenesis. *Cell* **2018**, *174*, 856–869.e17. [CrossRef]
138. Vlachogiannis, G.; Hedayat, S.; Vatsiou, A.; Jamin, Y.; Fernández-Mateos, J.; Khan, K.; Lampis, A.; Eason, K.; Huntingford, I.; Burke, R.; et al. Patient-derived organoids model treatment response of metastatic gastrointestinal cancers. *Science* **2018**, *359*, 920–926. [CrossRef]
139. Hooi, J.K.Y.; Lai, W.Y.; Ng, W.K.; Suen, M.M.Y.; Underwood, F.E.; Tanyingoh, D.; Malfertheiner, P.; Graham, D.Y.; Wong, V.W.S.; Wu, J.C.Y.; et al. Global Prevalence of Helicobacter pylori Infection: Systematic Review and Meta-Analysis. *Gastroenterology* **2017**, *153*, 420–429. [CrossRef]
140. Salama, N.R.; Hartung, M.L.; Müller, A. Life in the human stomach: Persistence strategies of the bacterial pathogen Helicobacter pylori. *Nat. Rev. Microbiol.* **2013**, *11*, 385–399. [CrossRef]
141. Camilo, V.; Sugiyama, T.; Touati, E. Pathogenesis of *Helicobacter pylori* infection. *Helicobacter* **2017**, *22*, e12405. [CrossRef]
142. Odenbreit, S.; Püls, J.; Sedlmaier, B.; Gerland, E.; Fischer, W.; Haas, R. Translocation of Helicobacter pylori CagA into gastric epithelial cells by type IV secretion. *Science* **2000**, *287*, 1497–1500. [CrossRef] [PubMed]
143. Xiao, C.; Ogle, S.A.; Schumacher, M.A.; Orr-Asman, M.A.; Miller, M.L.; Lertkowit, N.; Varro, A.; Hollande, F.; Zavros, Y. Loss of Parietal Cell Expression of Sonic Hedgehog Induces Hypergastrinemia and Hyperproliferation of Surface Mucous Cells. *Gastroenterology* **2010**, *138*, 550–561. [CrossRef] [PubMed]
144. Schumacher, M.A.; Donnelly, J.M.; Engevik, A.C.; Xiao, C.; Yang, L.; Kenny, S.; Varro, A.; Hollande, F.; Samuelson, L.C.; Zavros, Y. Gastric sonic hedgehog acts as a macrophage chemoattractant during the immune response to Helicobacter pylori. *Gastroenterology* **2012**, *142*, 1150–1159.e6. [CrossRef]

145. Schumacher, M.A.; Feng, R.; Aihara, E.; Engevik, A.C.; Montrose, M.H.; Ottemann, K.M.; Zavros, Y. Helicobacter pylori-induced sonic hedgehog expression is regulated by NFκB pathway activation: The use of a novel in vitro model to study epithelial response to infection. *Helicobacter* **2015**, *20*, 19–28. [CrossRef] [PubMed]
146. Wroblewski, L.E.; Piazuelo, M.B.; Chaturvedi, R.; Schumacher, M.; Aihara, E.; Feng, R.; Noto, J.M.; Delgado, A.; Israel, D.A.; Zavros, Y.; et al. Helicobacter pylori targets cancer-associated apical-junctional constituents in gastroids and gastric epithelial cells. *Gut* **2015**, *64*, 720–730. [CrossRef] [PubMed]
147. Bertaux-Skeirik, N.; Feng, R.; Schumacher, M.A.; Li, J.; Mahe, M.M.; Engevik, A.C.; Javier, J.E.; Peek, R.M., Jr.; Ottemann, K.; Orian-Rousseau, V.; et al. CD44 Plays a Functional Role in Helicobacter pylori-induced Epithelial Cell Proliferation. *PLoS Pathog.* **2015**, *11*, e1004663. [CrossRef]
148. Sigal, M.; Rothenberg, M.E.; Logan, C.Y.; Lee, J.Y.; Honaker, R.W.; Cooper, R.L.; Passarelli, B.; Camorlinga, M.; Bouley, D.M.; Alvarez, G.; et al. Helicobacter pylori activates and expands Lgr5+ stem cells through direct colonization of the gastric glands. *Gastroenterology* **2015**, *148*, 1392–1404.e21. [CrossRef]
149. Holokai, L.; Chakrabarti, J.; Broda, T.; Chang, J.; Hawkins, J.A.; Sundaram, N.; Wroblewski, L.E.; Peek, R.M.; Wang, J.; Helmrath, M.; et al. Increased Programmed Death-Ligand 1 is an Early Epithelial Cell Response to Helicobacter pylori Infection. *PLoS Pathog.* **2019**, *15*, e1007468. [CrossRef]
150. Hayakawa, Y.; Fox, J.G.; Gonda, T.; Worthley, D.L.; Muthupalani, S.; Wang, T.C. Mouse models of gastric cancer. *Cancers* **2013**, *5*, 92–130. [CrossRef]
151. Matano, M.; Date, S.; Shimokawa, M.; Takano, A.; Fujii, M.; Ohta, Y.; Watanabe, T.; Kanai, T.; Sato, T. Modeling colorectal cancer using CRISPR-Cas9-mediated engineering of human intestinal organoids. *Nat. Med.* **2015**, *21*, 256–262. [CrossRef]
152. Chen, J.; Lau, B.T.; Andor, N.; Grimes, S.M.; Handy, C.; Wood-Bouwens, C.; Ji, H.P. Single-cell transcriptome analysis identifies distinct cell types and niche signaling in a primary gastric organoid model. *Sci. Rep.* **2019**, *9*, 1–12. [CrossRef] [PubMed]
153. Wang, X.; Liang, Q.; Zhang, L.; Gou, H.; Li, Z.; Chen, H.; Dong, Y.; Ji, J.; Yu, J. C8orf76 promotes gastric tumorigenicity and metastasis by directly inducing lncRNA DUSP5P1 and associates with patient outcomes. *Clin. Cancer Res.* **2019**, *25*, 3128–3140. [CrossRef]
154. Roerink, S.F.; Sasaki, N.; Lee-Six, H.; Young, M.D.; Alexandrov, L.B.; Behjati, S.; Mitchell, T.J.; Grossmann, S.; Lightfoot, H.; Egan, D.A.; et al. Intra-tumour diversification in colorectal cancer at the single-cell level. *Nature* **2018**, *556*, 437–462. [CrossRef] [PubMed]
155. Xue, X.; Shah, Y.M. In vitro organoid culture of primary mouse colon tumors. *J. Vis. Exp.* **2013**, *17*, e50210. [CrossRef] [PubMed]
156. Steele, N.G.; Chakrabarti, J.; Wang, J.; Biesiada, J.; Holokai, L.; Chang, J.; Nowacki, L.M.; Hawkins, J.; Mahe, M.; Sundaram, N.; et al. An Organoid-Based Preclinical Model of Human Gastric Cancer. *CMGH* **2019**, *7*, 161–184. [CrossRef]
157. Li, J.; Xu, H.; Zhang, L.; Song, L.; Feng, D.; Peng, X.; Wu, M.; Zou, Y.; Wang, B.; Zhan, L.; et al. Malignant ascites-derived organoid (MADO) cultures for gastric cancer in vitro modelling and drug screening. *J. Cancer Res. Clin. Oncol.* **2019**, *145*, 2637–2647. [CrossRef]
158. Gambardella, V.; Tarazona, N.; Cejalvo, J.M.; Lombardi, P.; Huerta, M.; Roselló, S.; Fleitas, T.; Roda, D.; Cervantes, A. Personalized Medicine: Recent Progress in Cancer Therapy. *Cancers* **2020**, *12*, 1009. [CrossRef]
159. OPPOSITE: Outcome Prediction Of Systemic Treatment in Esophagogastric Carcinoma Full Text View ClinicalTrials.gov. Available online: https://clinicaltrials.gov/ct2/show/NCT03429816 (accessed on 16 May 2020).

III.4. General Conclusions

Well-established and characterized 2D culture models were and remain an essential tool in cancer research. They permit understanding the mechanisms that operate in live cells. The limitations of such models have encouraged researchers to develop 3D culture models to better mimic the complex physiopathological features of the tumor *in vitro* avoiding animal experimentation in fundamental research in early preclinical studies.

In the last 10 years, such novel models have drawn much attention. Moving from 2D to 3D culture models demonstrated strong improvements in molecular profiling, drug discovery, and pathogen infection. Still, the harmonization of techniques is needed to ensure better reproducibility in using 3D models, before these can be seen as the future gold standard in the preclinical screening of therapeutic strategies for GC. Additional applications could also be developed in order to provide spheroid structural information, to determine the way cell populations get assembled, to characterize gene expression and metabolomics of MCTS and PDTO. This could be in part approached by laser microscopy, flow cytometry and colorimetric techniques. Such heterogeneous data could be used to develop mathematical models capable of predicting *in vitro* growth and treatment response. Finally, organoids appear to be the key model that will allow the implementation of personalized medicine in clinics. Although initial promising studies of immunocompetent organoids were reported, further development and optimization of protocols are needed. A major challenge of 3D culture models remains the establishment of an intact TME and optimal culture conditions for all co-cultured cell types including immune cells.

It remains, despite the wealth of data generated by these models, that users face important limitations. More tuning studies have to be conducted to entirely characterize 3D models, in particular the most complex models such as organoids or microfluidic 3D cultures.

Should we start assuming a major transition from 2D to 3D cell culture in GC research? The work performed in this thesis was mainly focused on developing a flexible 3D model of spheroids cultured in suspension focusing on GC, choosing the most suitable technique of culture that allowed controlling different culture parameters. This model will be used to test the toxicity of a drug combination (statin and taxane) (See Chapter IV). Additionally, the

spheroids will serve to study the interaction and the organization between cancer cells and TME components (CAF in our first approach) (See Chapter V)

Version en Français

Des modèles de culture en 2D bien établis et caractérisés ont été et restent un outil essentiel dans la recherche sur le cancer. Ils permettent de comprendre les mécanismes opérant dans les cellules *in vivo*. Les limites de ces modèles ont encouragé les chercheurs à développer des modèles de culture 3D pour mieux imiter les caractéristiques physiopathologiques complexes de la tumeur *in vitro* en évitant l'expérimentation animale dans la recherche fondamentale lors des premières études précliniques.

Au cours des dix dernières années, ces nouveaux modèles ont suscité beaucoup d'intérêt. Le passage de modèles de culture en 2D à des modèles en 3D a permis d'améliorer considérablement le profilage moléculaire, la découverte de médicaments et l'infection par des agents pathogènes. Cependant, l'harmonisation des techniques est nécessaire pour assurer une meilleure reproductibilité dans l'utilisation des modèles 3D, avant que ceux-ci puissent être considérés comme le futur model standard dans le criblage préclinique des stratégies thérapeutiques pour le cancer gastrique. D'autres applications pourraient également être développées afin de fournir des informations sur la structure des sphéroïdes, de déterminer la manière dont les populations cellulaires s'assemblent, de caractériser l'expression des gènes et la métabolomique des sphéroïdes et des organoïdes. Ceci pourrait être abordé en partie par la microscopie en 3D, la cytométrie de flux et les techniques colorimétriques. Ces données hétérogènes pourraient être utilisées pour développer des modèles mathématiques capables de prédire la croissance *in vitro* et la réponse au traitement. Enfin, les organoïdes semblent être le modèle clé qui permettra la mise en œuvre de la médecine personnalisée en clinique. Bien que des études prometteuses initiales sur les organoïdes immunocompétents aient été rapportées, un développement et une optimisation supplémentaires des protocoles sont nécessaires. Un défi majeur des modèles de culture 3D reste l'établissement d'un microenvironnement tumoral intact et des conditions de culture optimales pour tous les types cellulaires co-cultivés, y compris les cellules immunitaires.

Malgré la richesse des données générées par ces modèles, des limitations importantes se posent encore aux utilisateurs. Des études plus pointues doivent être menées pour caractériser entièrement les modèles 3D, en particulier les modèles les plus complexes comme les organoïdes ou les cultures 3D en systèmes microfluidiques.

Devons-nous proposer une transition majeure de la culture cellulaire 2D vers la culture 3D dans la recherche sur le cancer gastrique ? Le travail effectué dans cette thèse a été principalement axé sur le développement d'un modèle 3D flexible de sphéroïdes cultivés sans adhésion au support en se concentrant sur le cancer gastrique, et en choisissant la technique de culture la plus appropriée qui permet de contrôler différents paramètres de culture. Ce modèle sera utilisé pour évaluer la toxicité d'une combinaison thérapeutique (statine et taxane) (voir chapitre IV). En outre, les sphéroïdes serviront à étudier l'interaction et l'organisation entre les cellules cancéreuses et les composants de la matrice extracellulaire (CAF dans notre première approche) (voir chapitre V).

Chapter IV
Gastric Cancer Cell Death Analyzed by Live Cell Imaging of Spheroids

IV.1. General Introduction

This chapter presents part of the research work that I have been doing during the preparation of this thesis. This work analyses drug-induced cytotoxicity using a medium-throughput technique to determine the effectiveness of a drug combination to treat gastric cancer (GC) cell lines cultured in 3D. The obtained results have been included in a research article in press in "*Scientific Reports*" in *January 2022*.

These results will be shown under their submission form to the journal, including different sections of the article: introduction, discussion, materials and method, supplementary data and references in the section below*: IV.2. Research Article 1.*

Aim of this work

Although treatment efficacy has improved during the past decade, GC survival rates remain poor. This calls for an urgent need to develop novel therapies to treat patients with GC. Drug repurposing has become a powerful and efficient alternative strategy for the discovery of novel therapeutic options, especially in an adjuvant context.

Statins are competitive inhibitors of the 3-hydroxy-3-methyl-glutaryl-coenzyme A reductase (HMG-CoA Red) enzyme, hence reduce circulating cholesterol levels and the incidence of cardiovascular diseases [1]. They block protein prenylation by depletion of intermediate metabolites like farnesyl pyrophosphate (FPP) and geranyl geranyl pyrophosphate (GGP). These are critical factors required for the post-translational modification and activation of various small monomeric GTPases onco-proteins, including from the Ras and Rho families, which regulate cellular mechanisms such as cytoskeletal reorganization, transformation, migration and proliferation [2]. The inhibition of Ras / Rho-prenylation may suppress downstream pro-oncogenic signaling pathways, such as the PI3K / Akt / mTOR and MAPK / ERK pathways, that are overactive in many types of cancers [3]. A large amount of *in vitro* and *in vivo* data have suggested that micromolar concentrations of statins bear anti-tumor activity potential, since they decreased cellular proliferation, inhibited metastasis and induced apoptosis [4, 5].

The synergism between lovastatin and chemotherapeutic agents has also been reported in different cancers showing increased cell death, reduced tumor growth or metastases [6]. In a previous study, our team reported that the association of lovastatin and docetaxel, an anti-cancer taxane compound used to treat GC and other solid tumors, provided a more than additive apoptotic response of the human HGT-1 GC cell line grown in standard 2D cultures [7].

As mentioned in Chapter III, 3D culture systems have been demonstrated to efficiently predict the *in vivo* efficacy of therapeutic agents. In this part of the thesis research work, our goal was to ask if the previous observations made in 2D-grown cells, would still hold for HGT-1 and AGS (another human GC cell line) cells grown in 3D.

To this end, we established a 3D cell culture model of spheroids, either as a single cell type, or combined with cancer-associated fibroblasts (CAF). We made use of the IncuCyte™ live imaging and analysis system to determine the growth and the cytotoxicity or apoptosis inducing potential of lovastatin and docetaxel. The results showed that the combination of docetaxel and lovastatin was an efficient strategy to engage human GC cells grown as 3D-spheroids into apoptosis.

IncuCyte™: a simple microscope for long-term imaging inside an incubator

While multiple culture methods were developed for 3D cell culture (Chapter III), tools for analysis of these structures are still very limited. Most current assays are designed as endpoint tests, where cells have to be fixed or lysed for analysis. Thus, only one single data point is obtained, whereas one needs to follow dynamic changes in the culture over time. Since human cells typically divide once per day (or less in 3D models), growth monitoring requires imaging over several days or weeks under optimal physiological conditions [8]. Imaging of living samples remains challenging because of several technical difficulties, such as the phototoxicity linked to fluorescence emission and the necessity to execute imaging in environmental conditions that are as close to the physiological ones (carbon dioxide, oxygen, temperature and humidity). These limitations are critical when samples are mammalian cells that are affected by the surrounding atmosphere. To overcome these limitations, a microscope (developed by Essen BioScience, IncuCyte™ microscope) was introduced into the

cell culture incubator. In contrast to histopathology or scanning electron microscopy, this approach is non-destructive. The IncuCyte™ spheroid module, an integrated system for real-time visualization and automated analysis of spheroid growth was used in our work, with spheroids grown in 96-well ultra-low attachment (ULA) microplates [9].

The IncuCyte™ system allows automated data acquisition of brightfield, phase contrast and two types of fluorescence (red and green), with objectives that can be changed automatically (4×, 10×, 20×). Time-lapse images can be acquired from two filters simultaneously and combined with brightfield / phase contrast images, which allows the study of spheroid morphology and growth. Hence, a comprehensive visualization of spheroid morphology, intercellular compaction (loose aggregates or compact spheroids) and size characteristic for each cell type can be obtained. These are parameters of interest to characterize cell viability and 3D structure [10]. Beside difficulties associated with imaging, another issue arises with 3D microscopy, *i.e.* the difficulty to analyze and compare quantitative data. For this purpose, computer programs were developed in combination with image acquisition hardware. By proposing a direct analysis of the generated data, a tool like the IncuCyte™ is very robust and it should prove well suited to high-throughput screening of drugs [11]. Nevertheless, incubator microscopes are not designed to obtain z-stack images, which would help determine the actual 3D organization of spheroids. This bears importance, in particular for multicellular spheroids whose intimate cellular arrangement may be specific for a given type of cancer cell put to interact with support cells like fibroblasts. For this reason, we turned to another image acquiring 3D modality, two-photon laser microscopy (Chapter V) [12].

References

[1] L. Corcos and C. Le Jossic-Corcos, “Statins: Perspectives in cancer therapeutics,” Dig. Liver Dis., vol. 45, no. 10, pp. 795–802, Oct. 2013, doi: 10.1016/J.DLD.2013.02.002.

[2] M. Thurnher, O. Nussbaumer, and G. Gruenbacher, “Novel aspects of mevalonate pathway inhibitors as antitumor agents,” Clin Cancer Res, vol. 18, no. 13., pp. 3524–3531, Jul. 2012, doi: 10.1158/1078-0432.CCR-12-0489.

[3] T. Wang *et al.*, “Simvastatin-induced breast cancer cell death and deactivation of PI3K/Akt and MAPK/ERK signalling are reversed by metabolic products of the mevalonate pathway,” *Oncotarget*, vol. 7, no. 3, pp. 2532–2544, Jan. 2016, doi: 10.18632/oncotarget.6304.

[4] P. J. Mullen, R. Yu, J. Longo, M. C. Archer, and L. Z. Penn, “The interplay between cell signalling and the mevalonate pathway in cancer,” *Nat Rev Cancer*, vol. 16, no. 11, pp. 718–731, Oct. 2016, doi: 10.1038/nrc.2016.76.

[5] M. Ahmadi *et al.*, “Pleiotropic effects of statins: A focus on cancer,” *Biochim Biophys Acta Molecul Basis Dis*, vol. 1866, no. 12, p. 165968, Dec. 2020, doi: 10.1016/j.bbadis.2020.165968.

[6] L. X. Vásquez-Bochm *et al.*, “Transcriptome-based identification of lovastatin as a breast cancer stem cell-targeting drug,” *Pharmacol. Reports*, vol. 71, no. 3, pp. 535–544, Jun. 2019, doi: 10.1016/j.pharep.2019.02.011.

[7] J. Follet et al., “The association of statins and taxanes: an efficient combination trigger of cancer cell apoptosis,” Br. J. Cancer, vol. 106, no. 4, pp. 685–692, Feb. 2012, doi: 10.1038/bjc.2012.6.

[8] M. Lal-Nag *et al.*, “Exploring drug dosing regimens in vitro using real-time 3d spheroid tumor growth assays,” *SLAS Discov.*, vol. 22, no. 5, pp. 537–546, Jun. 2017, doi: 10.1177/2472555217698818.

[9] B. Isherwood *et al.*, “Live cell in vitro and in vivo imaging applications: accelerating drug discovery,” *Pharm., Vol. 3, Pages 141-170*, vol. 3, no. 2, pp. 141–170, Apr. 2011, doi: 10.3390/PHARMACEUTICS3020141.

[10] O. Aftab, M. Fryknäs, U. Hammerling, R. Larsson, and M. G. Gustafsson, “Detection of cell aggregation and altered cell viability by automated label-free video microscopy: A promising alternative to endpoint viability assays in high-throughput screening,” *J. Biomol. Screen.*, vol. 20, no. 3, pp. 372–381, Mar. 2015, doi: 10.1177/1087057114562158.

[11] H. Karlsson, M. Fryknäs, R. Larsson, and P. Nygren, “Loss of cancer drug activity in colon cancer HCT-116 cells during spheroid formation in a new 3-D spheroid cell culture system,” *Exp. Cell Res.*, vol. 318, no. 13, pp. 1577–1585, Aug. 2012, doi: 10.1016/J.YEXCR.2012.03.026.

[12] T. Nemoto, R. Kawakami, T. Hibi, K. Iijima, and K. Otomo, “Two-photon excitation fluorescence microscopy and its application in functional connectomics,” *Microscopy*, vol. 64, no. 1, pp. 9–15, Feb. 2015, doi: 10.1093/JMICRO/DFU110.

Version en français

Ce chapitre présente une partie des travaux de recherche que j'ai menés lors de la préparation de cette thèse. Ce travail analyse la cytotoxicité d'une combinaison de médicaments vis-à-vis de lignées cellulaires de cancers gastriques (CG) cultivées en 3D, selon une technique à moyen débit (plaques 96 puits). Les résultats obtenus ont été inclus dans un article de recherche en presse dans le journal "*Scientific Reports*" en *Janvier 2022*.

Ces résultats seront présentés sous leur format de soumission à la revue, comprenant différentes sections de l'article : introduction, discussion, matériel et méthodes, données supplémentaires et références dans la section ci-dessous : *IV.2. Research Article 1*.

But de ce travail

Bien que l'efficacité des traitements se soit améliorée au cours de la dernière décennie, les taux de survie au CG restent faibles. Cela pointe l'urgence de développer de nouvelles thérapies. Le repositionnement des médicaments est devenu une stratégie alternative puissante et efficace pour la découverte de nouvelles options thérapeutiques, en particulier dans un contexte adjuvant.

Les statines sont des inhibiteurs compétitifs de l'enzyme 3-hydroxy-3-méthyl-glutaryl-coenzyme A réductase (HMG-CoA Red), réduisant ainsi le taux de cholestérol circulant et l'incidence des maladies cardiovasculaires. Ils bloquent la prénylation des protéines par réduction des taux de métabolites intermédiaires comme le farnésyl pyrophosphate (FPP) et le géranyl géranyl pyrophosphate (GGP). Ce sont des composés requis pour la modification post-traductionnelle et l'activation de GTPases monomériques, y compris des familles Ras et Rho, qui régulent les mécanismes cellulaires tels que la réorganisation du cytosquelette, la transformation, la migration et la prolifération cellulaires. L'inhibition de la prénylation de Ras / Rho peut bloquer les voies de signalisation pro-oncogèniques en aval, telles que les voies PI3K / Akt / mTOR et MAPK / ERK, qui sont hyperactives dans de nombreux types de cancers. Un grand nombre de données *in vitro* et *in vivo* ont suggéré que des concentrations micromolaires de statines avaient une activité anti-tumorale, en raison de leur capacité à diminuer la prolifération cellulaire, inhiber les métastases et induire l'apoptose.

La synergie entre la lovastatine et les agents chimiothérapeutiques a également été rapportée dans différents cancers montrant une mort cellulaire accrue, une croissance tumorale réduite ou l'incidence de métastases diminuée. Dans une étude précédente, notre équipe a démontré que l'association de lovastatine et de docétaxel, un composé taxane anticancéreux utilisé pour traiter les cancers gastriques et d'autres tumeurs solides, a induit une réponse apoptotique plus qu'additive de la lignée cellulaire gastrique humaine HGT-1 cultivée en conditions 2D standard.

Comme mentionné au chapitre III, il a été démontré que les systèmes de culture 3D prédisent efficacement l'efficacité *in vivo* des agents thérapeutiques. Dans cette partie du travail, notre objectif était de tester si les observations précédentes faites dans des cellules cultivées en 2D, seraient toujours valables pour les cellules HGT-1 et AGS (une autre lignée cellulaire humaine CG) cultivées en 3D.

À cette fin, nous avons établi un modèle de culture cellulaire 3D de sphéroïdes, soit en tant que type cellulaire unique, soit en combinaison avec des fibroblastes associés au cancer (CAF). Nous avons utilisé le système d'imagerie et d'analyse en direct IncuCyte^{TM} pour déterminer la croissance et la cytotoxicité de la lovastatine et du docétaxel. Les résultats ont montré que la combinaison docétaxel + lovastatine était une stratégie efficace pour engager les cellules CG humaines, cultivées sous forme de sphéroïdes 3D, dans l'apoptose.

IncuCyte^{TM}: un microscope simple pour l'imagerie en temps réel à l'intérieur d'un incubateur

Alors que de multiples méthodes de culture sont développées pour la culture des cellules en 3D (chapitre III), les outils d'analyse de ces structures sont encore limités. La plupart des tests actuels sont conçus comme des tests en point final, où les cellules doivent être fixées ou lysées pour être analysées. Ainsi, on n'obtient qu'un seul point de données au lieu de suivre les changements dynamiques de la culture dans le temps. En se divisant généralement une fois par jour (ou moins dans un modèle 3D), le suivi de la croissance des cellules humaines nécessite une acquisition des images sur plusieurs jours ou semaines dans des conditions physiologiques optimales. L'imagerie des échantillons vivants reste un défi à cause de plusieurs difficultés techniques, telles que la phototoxicité liée à l'émission de fluorescence ainsi que la nécessité d'exécuter l'imagerie dans des conditions environnementales aussi

proches que possible des conditions physiologiques (dioxyde de carbone, oxygène, température et humidité). Ces limitations sont critiques lorsque les échantillons sont des cellules de mammifères qui sont affectées par l'atmosphère environnante. Pour surmonter ces limitations, un microscope (développé par Essen BioScience, le microscope IncuCyte™) est introduit dans l'incubateur de la culture cellulaire. Contrairement à l'histopathologie ou à la microscopie électronique à balayage, cette approche est non-destructive. Le module sphéroïde de l'IncuCyte™, un système qui permet pour la visualisation en temps réel et l'analyse automatisée de la croissance des sphéroïdes, a été utilisé dans nos travaux, avec des sphéroïdes cultivés dans des microplaques-96 puits à faible adhésion.

Le système IncuCyte™ permet l'acquisition automatisée des images en lumière blanche, contraste de phase et deux couleurs de fluorescence (rouge et vert), avec des objectifs qui peuvent être changés automatiquement (4×, 10×, 20×). Des images prises à intervalles réguliers peuvent être acquises à partir de deux filtres simultanément et combinées avec des images en contraste de phase, ce qui permet d'étudier la morphologie et la croissance des sphéroïdes. Ainsi, une visualisation complète de la morphologie des sphéroïdes, de la compaction intercellulaire (agrégats fragiles ou sphéroïdes compacts) et de la taille caractéristique de chaque type de cellule peut être obtenue. Ce sont des paramètres d'intérêt pour caractériser la viabilité des cellules formant la structure 3D. Une des difficultés liées à l'imagerie est d'analyser et de comparer les données quantitatives. À cette fin, des logiciels d'analyse ont été développés en combinaison avec les appareils d'acquisition d'images. En proposant une analyse directe des données générées, un outil comme l'IncuCyte™ est robuste et bien adapté au criblage à haut débit des médicaments. Néanmoins, les microscopes d'incubation ne sont pas conçus pour obtenir des images en profondeur, qui permettraient de déterminer l'organisation 3D réelle des sphéroïdes. Ceci est important, en particulier pour les sphéroïdes pluricellulaires dont l'arrangement cellulaire peut être spécifique d'un type donné de cellule cancéreuse mise en interaction avec des cellules de soutien comme les fibroblastes. Pour cette raison, nous nous sommes tournés vers une autre modalité d'acquisition d'images 3D, la microscopie à deux photons (chapitre V).

IV.2. Research Article 1: Gastric Cancer Cell Death Analyzed by Live Cell Imaging of Spheroids

Authors: George Alzeeb [1], Danielle Arzur [1], Valérie Trichet [2], Matthieu Talagas[3,4], Laurent Corcos [5,6], Catherine Le Jossic-Corcos [1,*]

[1] *Univ Brest, Inserm, EFS, UMR 1078, GGB, F-29200 Brest, France*
[2] *Inserm, Univ Nantes, UMR 1238 Phy-Os "Bone Sarcomas and Remodeling of Calcified Tissues", F-44035 Nantes, France*
[3] *Univ Brest, Laboratoire Interactions Epithéliums-Neurones, F-29200 Brest, France.*
[4] *Department of Dermatology, University Hospital of Brest, F-29200 Brest, France.*
[5] *Inserm, Univ Brest, EFS, UMR 1078, GGB, F-29200 Brest, France*
[6] *CHU de Brest, Inserm, Univ Brest, EFS, UMR 1078, GGB, F-29200 Brest, France*
* *Correspondence: catherine.corcos@univ-brest.fr; phone 33 2 98 01 79 02*

Accepted to be published in the journal 'Scientific Reports': 06 January 2022

Abstract: Gastric cancer (GC) is the third cause of cancer-related mortality worldwide and is often diagnosed at advanced stages of the disease. This makes the development of more comprehensive models and efficient treatments crucial. One option is based on repurposing already marketed drugs as adjuvants to chemotherapy. Accordingly, we have previously developed the combination of docetaxel and the cholesterol-lowering drug, lovastatin, as a powerful trigger of HGT-1 human GC cells' apoptosis using 2D cultures. Because 3D models, known as spheroids, are getting recognized as possibly better suited than 2Ds in toxicological research, we aimed to investigate the efficacy of this drug combination with such a model. We established monocellular spheroids from two human (GC) cell lines, HGT-1 and AGS, and bicellular spheroids from these cells mixed with cancer-associated fibroblasts. With these, we surveyed drug-induced cytotoxicity with MTT assays. In addition, we used the IncuCyte™ live imaging and analysis system to follow spheroid growth and apoptosis. Taken together, our results showed that the lovastatin+docetaxel combination was an efficient strategy to eliminate GC cells grown in 2D or 3D cultures, lending further support in favor of repurposing lovastatin as an adjuvant to taxane-based anticancer treatment.

This article will be presented in this thesis as its submitted format to Scientific Reports.

1. Introduction

With over one million new cases annually, gastric cancer (GC) is the fifth most diagnosed malignancy. The high mortality rate makes it the fourth most common cause of cancer-related deaths, with 768 793 deaths worldwide in 2018 [1]. There are marked geographical differences in the incidence of GC. It is highest in Central and East Asia (71% of cases) followed by Eastern Europe (10%) and Latin America (6%) [2].

GC is difficult to detect at an early stage, in absence of highly specific warning signs, and roughly 30% of patients have metastases at diagnosis, which results in poor prognosis [3]. Surgical resection is the main treatment for localized forms. Nonetheless, complementary approaches, such as adjuvant chemotherapy, have shown better survival rates [4, 5]. However, for advanced GC, improving treatment efficacy remains a major challenge and calls for an urgent need to develop innovative therapies [6]. Inhibition of programmed death-1 (PD-1) / programmed death-ligand 1 (PD-L1) axis with immune checkpoint inhibitors (ICI) has recently been emerging as a novel treatment strategy for advanced GC [7]. Combined treatment is often the basis of current chemotherapy regimen, by which anti-tumor agents show stronger effects [8]. This may extend to drug repurposing as an alternative strategy [9].

Statins are widely used for the treatment of hypercholesterolemia [10]. Lovastatin, like other statins, reduces serum cholesterol levels through inhibition of the 3-hydroxy-3-methyl-glutaryl-coenzyme A reductase (HMG-CoA Red), a rate-limiting enzyme in the mevalonate pathway [11]. In addition, a large amount of *in vitro* and *in vivo* data have suggested that statins bear anti-tumor activity potential, since they decreased cellular proliferation, inhibited metastasis and induced apoptosis [12–16] including in human breast cancer [17], esophageal carcinoma [18], melanoma [19] cells, or breast cancer stem cells [20]. The synergism between lovastatin and chemotherapeutic agents, such as doxorubicin and idarubicin, has also been reported in different cancers [21–23].

Two-dimensional (2D) cell cultures have largely contributed to the development of many cancer therapies. However, the types of cell-cell and cell-matrix interactions generally dictated, for epithelial cells, by the necessity to adhere to a solid support, may make 2D models sub-optimal in absence of micro-environmental constraints and dynamic interactions as they occur in tumors [24]. To better mimic the functional aspects of tissues and present a more realistic model of biological responses, three-dimensional (3D) culture systems have been increasingly recognized as more reliable *in vitro* test models [25]. Multicellular tumor

spheroids (MCTS), which associate one or more cell types, are one of the most extensively explored models in preclinical oncology research [26]. The potential of MCTS in predicting the *in vivo* efficacy of different chemotherapeutic agents has been clearly evidenced, and the responses to treatment in the MCTS model could be closer to the *in vivo* situation [27, 28]. Indeed, various factors such as cell-cell interactions, metabolic status and expression of drug-resistance genes may be different between 2D and 3D cultures and could affect evaluation of drug activity [29]. An important characteristic of solid tumor microenvironments is their heterogeneous cellular composition [30]. The cross-talk between cancer cells and stroma components, such as fibroblasts, endothelial and immune cells, influences various features related to tumor progression or cell invasion [31, 32]. The model of hetero-type MCTS overcomes some of the limitations of 2D co-cultures and provides a closer resemblance to tumors [33].

Several spheroid engineering methodologies have been developed, following the pioneering studies by Sutherland et al. who established MCTS in the 1970s [34]. Novel technologies combining round-bottom geometry with ultra-low attachment (ULA) surface chemistry allowed standardizing 3D cultures and generated reproducible MCTS, which qualifies this model for medium-high throughput screening of anticancer drugs [35]. Recently, assays that measure the effects of drugs in real-time have been designed to mimic *in vivo* drug responses [36, 37]. Medium-high throughput imaging systems, such as IncuCyte™ (Essen BioSciences), are well-suited for this purpose, as they enable the long term follow-up of growth or death of 3D cultures [38].

In a previous study, our team reported that the association of lovastatin and docetaxel, an anticancer taxane compound, which affects microtubule dynamics [39, 40] and is used to treat GC and other solid tumors [41], provided an over-additive apoptotic response of the human HGT-1 GC cell line grown in standard 2D conditions [42]. Since the 3D model has been recognized as often more resistant to cytotoxic drugs than the 2D model [43, 44], we decided to ask if our previous observations that demonstrated the potential benefit of associating lovastatin + docetaxel as a strong trigger of cancer cell death, would still hold for two human GC cell lines, HGT-1 and AGS, grown in 3D. To this end, we established a spheroid model, either as a single cell type, or combined with cancer-associated fibroblasts (CAF). We made use of the IncuCyte™ live imaging and analysis system to determine the growth and the cytotoxicity or apoptosis inducing potential of lovastatin and docetaxel.

2. Results

Docetaxel and lovastatin are cytotoxic to human gastric cancer HGT-1 and AGS cells in 2D model

We have shown previously that lovastatin enhanced the apoptosis induction brought about by docetaxel in HGT-1 human gastric cancer (GC) cells in 2D [42]. In the present study, we selected, for further *in vitro* experiments, the same concentrations of 5nM docetaxel (D 5nM), 12.5µM lovastatin (L 12.5µM) or a combination of 5nM docetaxel + 12.5µM lovastatin (D+L). To evaluate the cytotoxicity of the drugs, 2D cultured HGT-1 cells were treated with D 5nM, L 12.5µM and D+L for 36 h (Figure IV.1(a)) and 48 h (Figure IV.1(b)), and cytotoxicity was determined using MTT assays. The results showed a significant reduction of cell viability down to 57% ($p<0.001$) and 65% ($p<0.01$), respectively, by D 5nM and L 12.5µM treatments at 36 h, and down to 47% ($p<0.001$) and 28% ($p<0.001$) after 48 h of treatment. The exposure to both drugs had a cumulative effect on cell viability that was reduced down to 39% ($p<0.001$) for 36 h of treatment and to 20% ($p<0.001$) for 48 h. We have also evaluated the cytotoxicity effect of D 5nM and / or L 12.5µM of AGS cells after 48 h of treatment. Similar results were obtained for AGS cells (Supplementary Figure IV.1).

Figure IV.1.

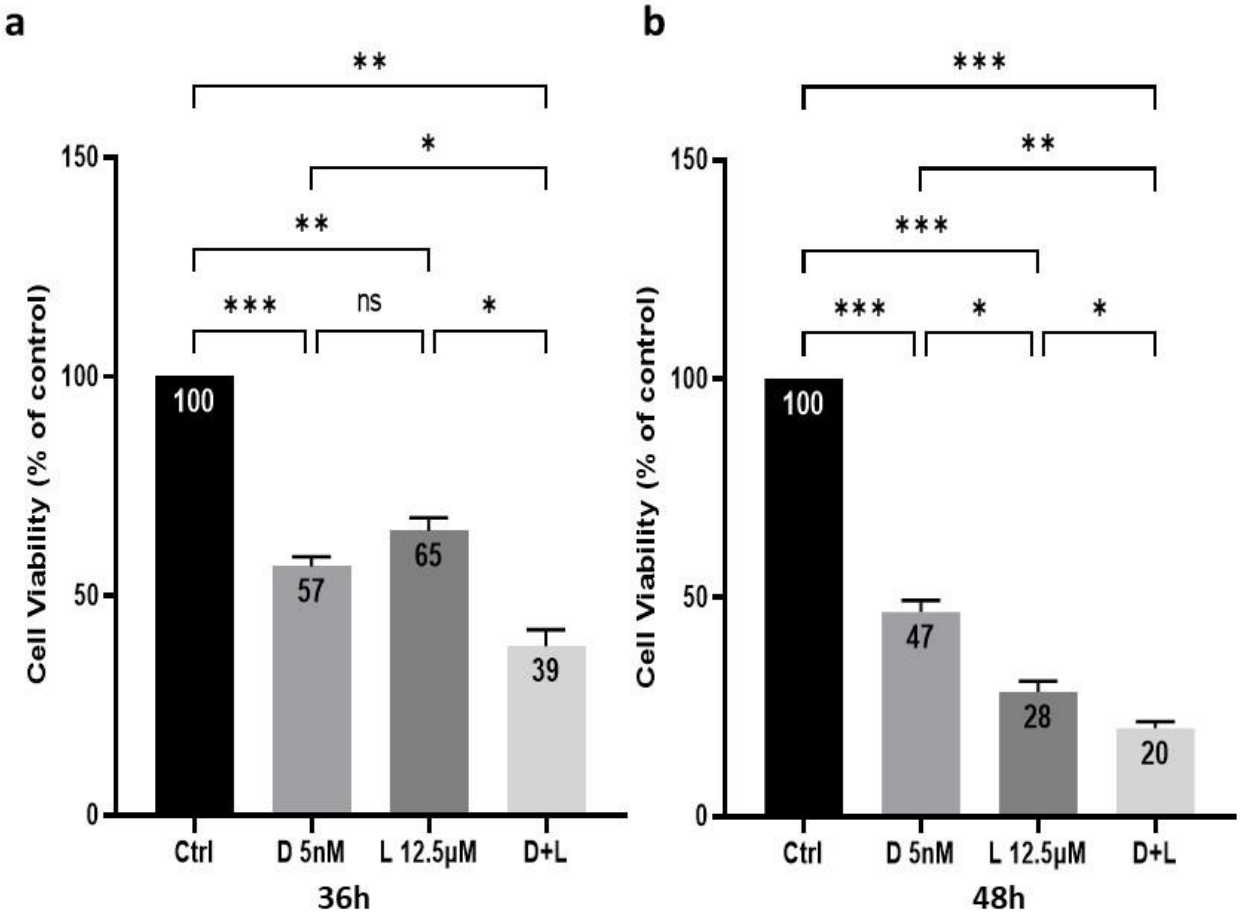

Figure IV.1. Toxicity of docetaxel and lovastatin in human gastric cancer HGT-1 cells in 2D culture.
The cells were incubated at 37 °C for 36 (a) and 48 (b) h of treatment with 5nM docetaxel (D 5nM), 12.5µM lovastatin (L 12.5µM) and 5nM docetaxel + 12.5µM lovastatin (D+L). Cell viability was determined by the MTT assay. The results are shown as the mean ± SD of n=3 independent experiments with four technical replicates in each. ns, $p > 0.05$; *$p \leq 0.05$; **$p \leq 0.01$; ***$p \leq 0.001$, one-way ANOVA followed by Tukey analysis.

HGT-1 and AGS gastric cancer cells efficiently develop as MCTS

The non-adherent surface method has been widely used in GC studies for its advantage to allow production of spheroids of uniform sizes, an essential requirement for cytotoxicity screening. HGT-1 cells were seeded (500 cells / well) into 96-well ultra-low attachment plates and cultured under standard conditions to develop into spheroids. MCTS formation was rapid and highly reproducible using the HGT-1 cell line as well as with AGS cells (Figure IV.2) grown

in ultra-low attachment dishes. AGS spheroids were more compact than HGT-1 spheroids. AGS spheroids, but not HGT-1 spheroids showed a few necrotic cells in the central areas as expected from compact spheroid structures. A few mitotic figures were visible on spheroid sections (Supplementary Figure IV.2). To get equal sizes of 6 days-old spheroids, we generated AGS spheroids by seeding 1000 cells / well, instead of 500 for HGT-1 cells. Incubation for 6 days alone and without matrix was sufficient to form tightly packed spheroids. Six days-old HGT-1 spheroids were uniform with a diameter of about 540 ± 45 µm and about 6.5 ± 0.2 × 10^3 cells each. Six days-old AGS spheroids were in the same size range with about 14 ± 0.3 × 10^3 cells each.

Figure IV.2.

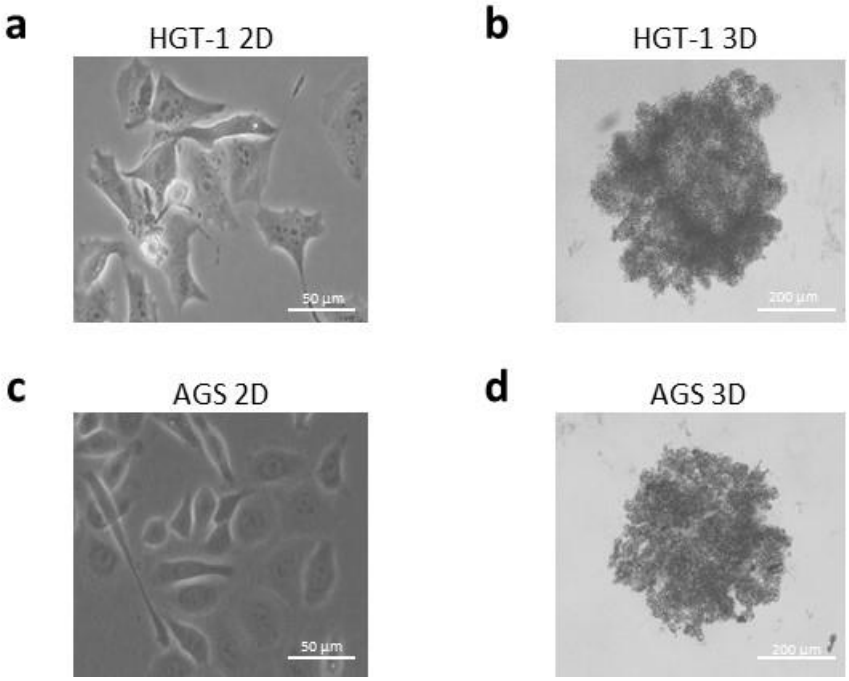

Figure IV.2. Phase contrast and bright field photographs of HGT-1 and AGS cells in 2D or 3D cultures.
Bright field photographs of HGT-1 (a: 2D, b: 3D-after 6 days of culture) and AGS (c: 2D, d: 3D-after 6 days of culture) human GC cell lines.

Docetaxel and lovastatin strongly reduce HGT-1 MCTS growth

To characterize the effects of the drugs on the growth of HGT-1 MCTS, we assessed their effects in real-time. Six days-old HGT-1 spheroids were treated with D 5nM, L 12.5µM and D+L. Spheroid sizes, recorded using the IncuCyte™ live imaging and analysis system, showed that D 5nM, L 12.5µM and D+L induced reduction in spheroid growth after 48 h, as shown by bright field photographs of spheroids in Figure IV.3(a). The effects of the drugs on growth reduction of HGT-1 spheroids, were analyzed in real-time after up to 144 h. The most effective inhibition of growth was achieved using both drugs (Figure IV.3(b)). Hence, real-time area monitoring showed that docetaxel reduced the size of GC MCTS, and this effect was strongly enhanced by lovastatin.

Figure IV.3.

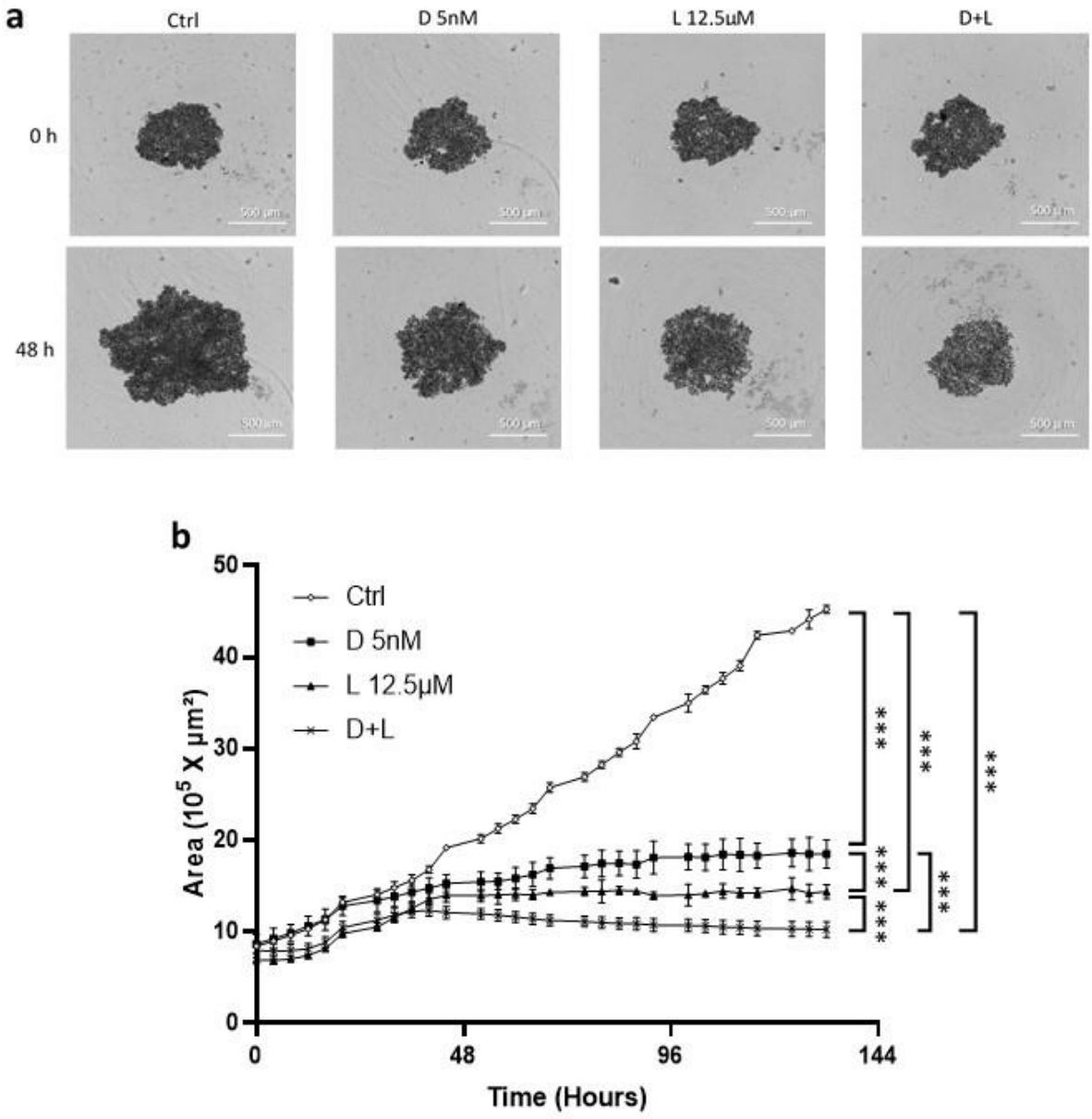

Figure IV.3. Effects of docetaxel and lovastatin treatments on the growth of HGT-1 spheroids.

(a) Bright field photographs of 6 days-old HGT-1 MCTS at 0 h and 48 h of treatment with 5nM docetaxel (D 5nM), 12.5µM lovastatin (L 12.5µM) and 5nM docetaxel + 12.5µM lovastatin (D+L), captured with the IncuCyte™ live imaging. (b) Real-time growth monitoring (Area 10^5 x µm²) of HGT-1 MCTS was performed using the IncuCyteTM live imaging and analysis system. Six days-old spheroids (starting as 0 on the graph) were treated with 5nM docetaxel (D 5nM) (black squares), 12.5µM lovastatin (L 12.5µM) (black triangles) or 5nM docetaxel + 12.5µM lovastatin (D+L) (black X) for up to 144 h. Control (Ctrl) MCTS are shown as white lozenges. The results are shown as the mean ± SD of n=3 independent experiments with four technical replicates in each. ***p ≤ 0.001, one-way ANOVA followed by Tukey analysis.

Docetaxel and lovastatin trigger strong cytotoxicity in HGT-1 and AGS MCTS

To examine the cell killing effects of docetaxel and lovastatin in a 3D culture system of GC cells, we performed MTT assays, with some modifications compared to the standard assay (see the Materials and Methods section). Six days-old HGT-1 spheroids were treated for 48 h by D 5nM, L 12.5µM and D+L before adding the MTT reagent. As compared to control, treatment with D 5nM or L 12.5µM resulted in reduction of MCTS viability down to 62% (p<0.01) and 43% (p<0.01) of control, respectively. The association of D 5nM and L 12.5µM showed the strongest cytotoxicity against HGT-1 MCTS and reduced cells viability down to 30% (p<0.01) (Figure IV.4(a)). Dynamic recording of the effect of drugs shows that control, untreated spheroids kept growing over time, whereas treated spheroids stopped growing and eventually regressed (Supplementary Videos, cytotoxicity files). These results indicated that docetaxel and lovastatin possessed strong cell killing activity in 3D spheroids of HGT-1 cells, similarly to 2D-grown cells (Figure IV.1). These results were correlated with MCTS HGT-1 growth, where all treatments reduced spheroid sizes as shown in Figure IV.3. We have also examined the cell killing effects of D 5nM, L 12.5µM and D+L on 6 days-old AGS MCTS using the same MTT assay. Similar results were obtained 48 h after treatment for 3D-grown AGS cells (Supplementary Figure IV.3).

In order to appreciate the effects of the drugs by other means, we generated an HGT-1 sub-population labeled with a RedTomato tag. Such cells should allow for a simplified measurement of cytotoxicity since dead cells are expected to lose RedTomato expression, allowing direct reading of the drop in RedTomato fluorescence intensity by IncuCyte™ as an indicator of decreased cell viability, as reported in the case of GFP protein drop in cells dying in response to drugs [45]. HGT-1 and HGT-1-RedTomato cells were equally sensitive to the 2 cytotoxic drugs in monolayer cultures (Supplementary Figure IV.4). Red fluorescence photographs of 6 days-old spheroids treated by D 5nM, L 12.5µM and D+L at 0 and 48 h are shown in Figure IV.4(b). Direct measurement of RedTomato mean intensity of 6 days-old spheroids after exposure to D 5nM and L 12.5µM for 48 h produced results that overlapped well with those obtained in the MTT assay. While D 5nM and L 12.5µM reduced fluorescence intensity down to 53% (p<0.001) and 39% (p<0.001), respectively, the strongest effects were obtained upon addition of both compounds (20%, p<0.001) (Figure IV.4 (c)).

Figure IV.4.

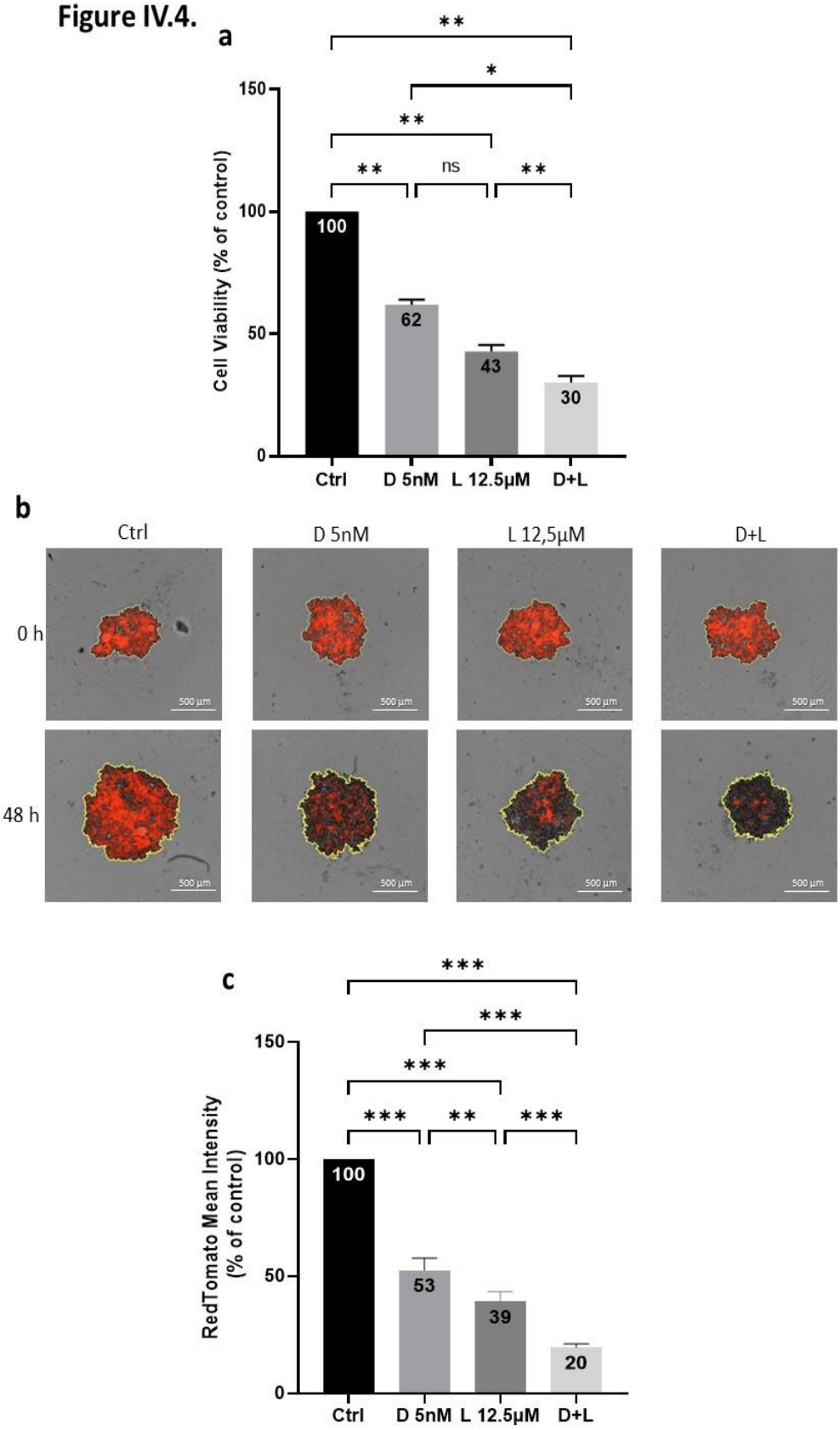

Figure IV.4. Cytotoxicity of docetaxel and lovastatin for HGT-1 MCTS.
(a) Cell viability was determined by the MTT assay after 48 h of treatment with 5nM docetaxel (D 5nM), 12.5µM lovastatin (L 12.5µM) and 5nM docetaxel+12.5µM lovastatin (D+L) of six days-old HGT-1 spheroids. The results are shown as the mean ± SD of n=3

independent experiments with four technical replicates in each. ns, $p > 0.05$; *$p \leq 0.05$; **$p \leq 0.01$, one-way ANOVA followed by Tukey analysis. (b) Red fluorescence photographs of 6 days-old spheroids formed by HGT-1cells expressing RedTomato at 0 h and 48 h of treatment with D 5nM, L 12.5µM and D+L captured with the IncuCyte™ live imaging. (c) Fluorescence signal generation by 6 days-old HGT-1-RedTomato MCTS exposed to 5nM docetaxel (D 5nM), 12.5µM lovastatin (L 12.5µM) and 5nM docetaxel + 12.5µM lovastatin (D+L) for 48 h. The results are shown as the mean ± SD of n=3 independent experiments with four technical replicates in each. **$p \leq 0.01$; ***$p \leq 0.001$, one-way ANOVA followed by Tukey analysis.

Docetaxel and lovastatin trigger HGT-1 and AGS spheroid cells apoptosis

To further examine if docetaxel and lovastatin-induced cell viability reduction was related to apoptosis, we performed Annexin V staining followed by fluorescence-activated cell intensity measurement using IncuCyte™. Red fluorescence photographs of 6 days-old HGT-1 spheroids showing binding of Annexin V at 0 and 72 hours of treatment with D 5nM, L 12.5µM, and D+L are shown in Figure IV.5(a). Concurrently with the reduced cell viability, apoptosis increased dramatically in response to the drugs. As shown in Figure IV.5(b), Annexin V fluorescence intensity was increased in response to D 5nM (by 192%, $p<0.01$) and L 12.5µM (by 184%, $p<0.01$) after 72 h. In addition, the highest apoptosis level (233%, $p<0.001$) was obtained after exposure to both drugs (D+L). To characterize, in more details the effects of the drugs on apoptosis induction of HGT-1 MCTS, we assessed their effects in real-time (Supplementary Figure IV.5) and we determined the level of nuclei fragmentation by Hoechst 33342 staining of the cells (Supplementary Figure IV.6(a)). Comparable results were obtained for AGS cells (Supplementary Figure IV.6(b)). In addition, caspases 3 and 7 activity was increased by two-fold in both HGT-1 and AGS spheroids (Supplementary Figure IV.6(c) and (d)). Altogether, these results showed that combined treatment promoted high levels of apoptosis in human HGT-1 GC spheroids, similarly to 2D monolayers [42], as well as in AGS cells.

Figure IV.5.

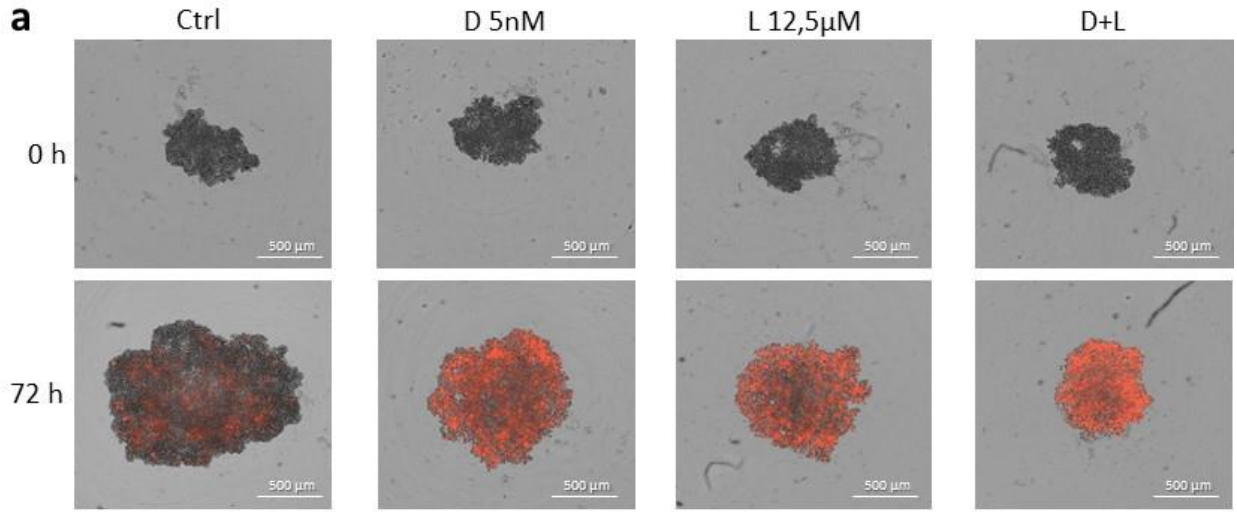

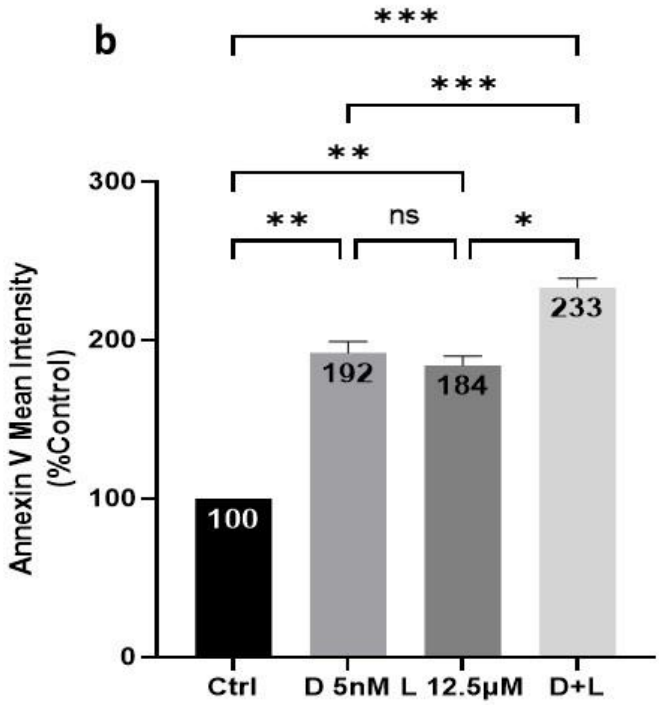

Figure IV.5. Apoptosis induction by docetaxel and lovastatin in HGT-1 spheroids.
(a) Red fluorescence photographs of HGT-1 spheroids at 0 h and 72 h of treatment with 5nM docetaxel (D 5nM), 12.5µM lovastatin (L 12.5µM) and 5nM docetaxel + 12.5µM lovastatin (D+L) in presence of Annexin V fluorescent reagent (IncuCyte™) captured with the IncuCyte™ live imaging. (b) Annexin V binding on 6 days-old HGT-1 MCTS after 72 h of treatment with 5nM docetaxel (D 5nM), 12.5µM lovastatin (L 12.5µM) and 5nM docetaxel + 12.5µM lovastatin (D+L). The Annexin V reagent was added at the same time as the drugs. The results are shown as the mean ± SD of n=3 independent experiments with four technical replicates in each. ns, $p > 0.05$; *$p \leq 0.05$; **$p \leq 0.01$; ***$p \leq 0.001$, one-way ANOVA followed by Tukey analysis.

Bicellular MCTS show sensitivity to docetaxel and lovastatin

In order to better mimic tumors, we established hetero-type MCTS from human HGT-1 or AGS GC cells and human CAF in primary culture. We explored the effects of different ratio of GC cells to CAF: 1:1; 1:2; 1:5; 1:9 on growth. In addition, we followed drug response, as determined by spheroid growth for the 1:1; 1:2 and 1:5 ratios. We observed that the effect of drugs was similar between all ratio conditions. We may hypothesize that CAF did not strongly influence the response of the spheroids to lovastatin and / or docetaxel under our conditions. Therefore, we fixed the ratio at 1:1. Gene expression analysis showed that the CAF grown in 2D confirmed their stromal nature, as shown for αSMA, FAP, VIM, FGF-2, IL-6 and SDF-1 markers [46], while these genes were essentially not expressed in HGT-1 or AGS cells (Supplementary Figure IV.7). Bright field photographs of 6 days-old monocellular HGT-1 spheroids (500 and 250 cells) and 250 HGT-1 + 250 CAF bicellular spheroids are shown in Figure IV.6(a). MCTS growth and shape were analyzed over time (Figure IV.6 (b)). Bicellular (250 CAF + 250 HGT-1) spheroids were more compact compared to HGT-1 spheroids; they reached respectively ~1,6 x 10^5 μm^2 and ~5 x 10^5 μm^2 after 6 days of culture. It has to be stated that this analysis shows the evolution of spheroid sizes but not the actual number of cells that compose the spheroids. In addition, the count of HGT-1 cells, recovered from mono- or bicellular spheroids, showed no significant differences at the same age of spheroids (Supplementary Figure IV.8). In this mixed model, cells were firmly attached to each other and were hard to dissociate by mechanical force. These data indicated that the presence of fibroblasts, in 1:1 ratio with cancer cells, promoted assembly of highly compact 3D cell structures (Supplementary Videos, bicellular spheroids formation until day 8). In addition, AGS + CAF spheroids, assembled from 500 AGS + 500 CAF were smaller and more compact than monocellular 500 AGS spheroids, similarly to HGT-1 + CAF bicellular spheroids (data not shown).

Figure IV.6.

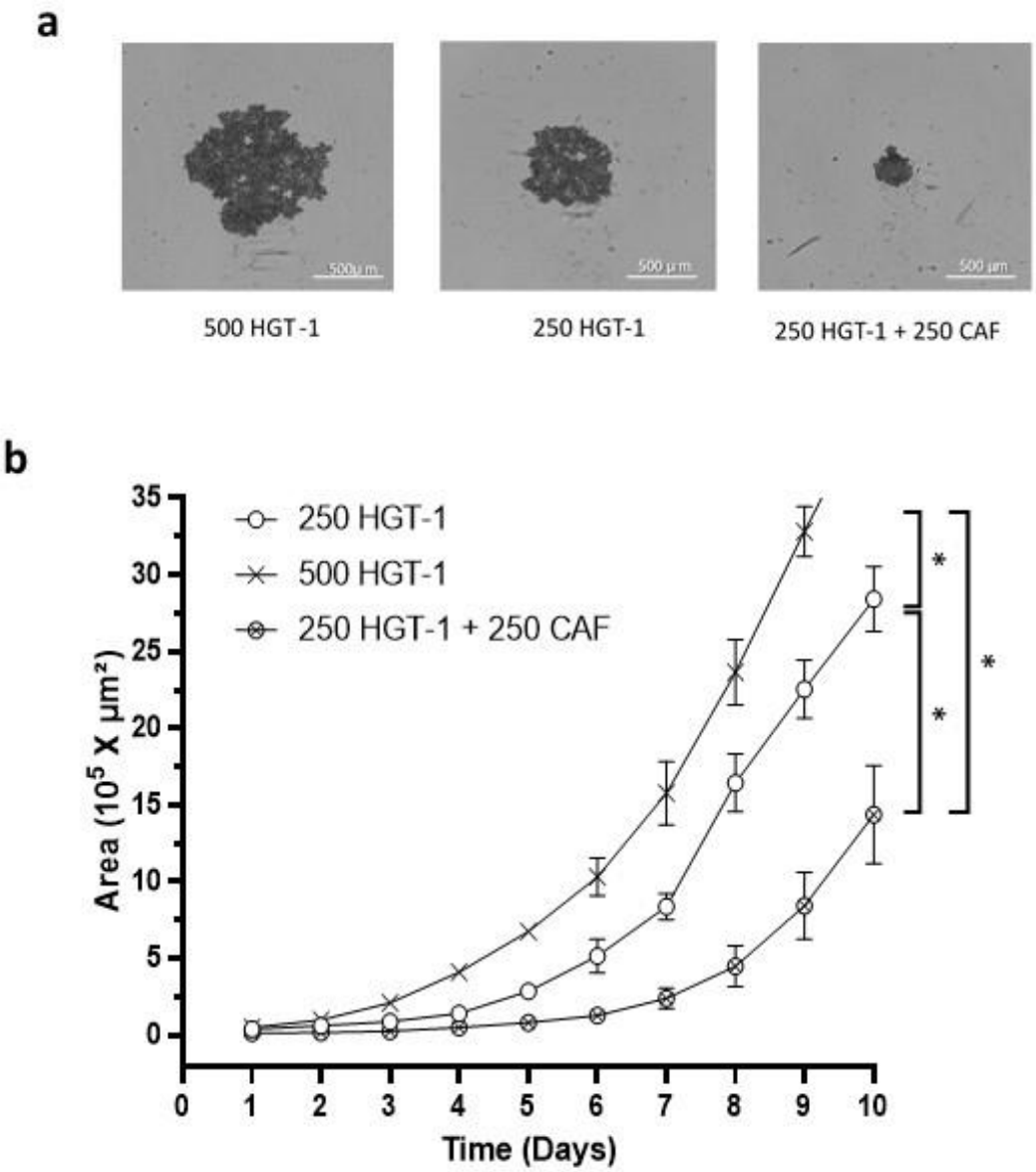

Figure IV.6. Growth of bicellular MCTS.
(a) Bright field photographs of 6 days-old monocellular spheroids formed from 500 or 250 HGT-1 cells and bicellular (250 CAF + 250 HGT-1) spheroids captured with the IncuCyte™ live imaging. (b) Real-time growth monitoring (Area 10^5 x μm^2) was performed using the IncuCyte™ live imaging. Monocellular MCTS generated from: i) 250 HGT-1 cells is represented by white circles, ii) 500 HGT-1 cells is represented by black X symbol and iii) bicellular MCTS generated from 250 HGT-1 + 250 CAF is represented by X inside circles. The results are shown as the mean ± SD of n=3 independent experiments with four technical replicates in each. *p≤0.05; one-way ANOVA followed by Tukey analysis.

Then, we treated 6 days-old HGT-1 + CAF bicellular MCTS by D 5nM, L 12.5µM and D+L. Reduction of spheroids size was shown upon treatments. As shown by bright field photographs of spheroids in Figure IV.7(a), the association of docetaxel and lovastatin triggered a stronger size reduction of MCTS compared to single docetaxel treatment after 48 h. This was also reflected over time up to 144h (Figure IV.7(b)). To determine if this size reduction of MCTS was link to cell death, we performed MTT assays from 6 days-old bicellular spheroids after 48 h of treatment. D 5nM showed a stronger cell killing activity (viability reduced by 44%, $p<0.001$) than L 12.5µM (viability reduced by 33%, $p<0.01$). The association of D+L had the largest effect on cell viability reduction (up to 64%, $p<0.001$) (Figure IV.7(c)). We have also examined cell death inducing effects of D 5nM, L 12.5µM and D+L on 6 days-old AGS + CAF bicellular spheroids using an MTT assay (Supplementary Figure IV.9). Combined treatment had a cumulative effect on cell viability, similarly to HGT-1 MCTS.

Figure IV.7.

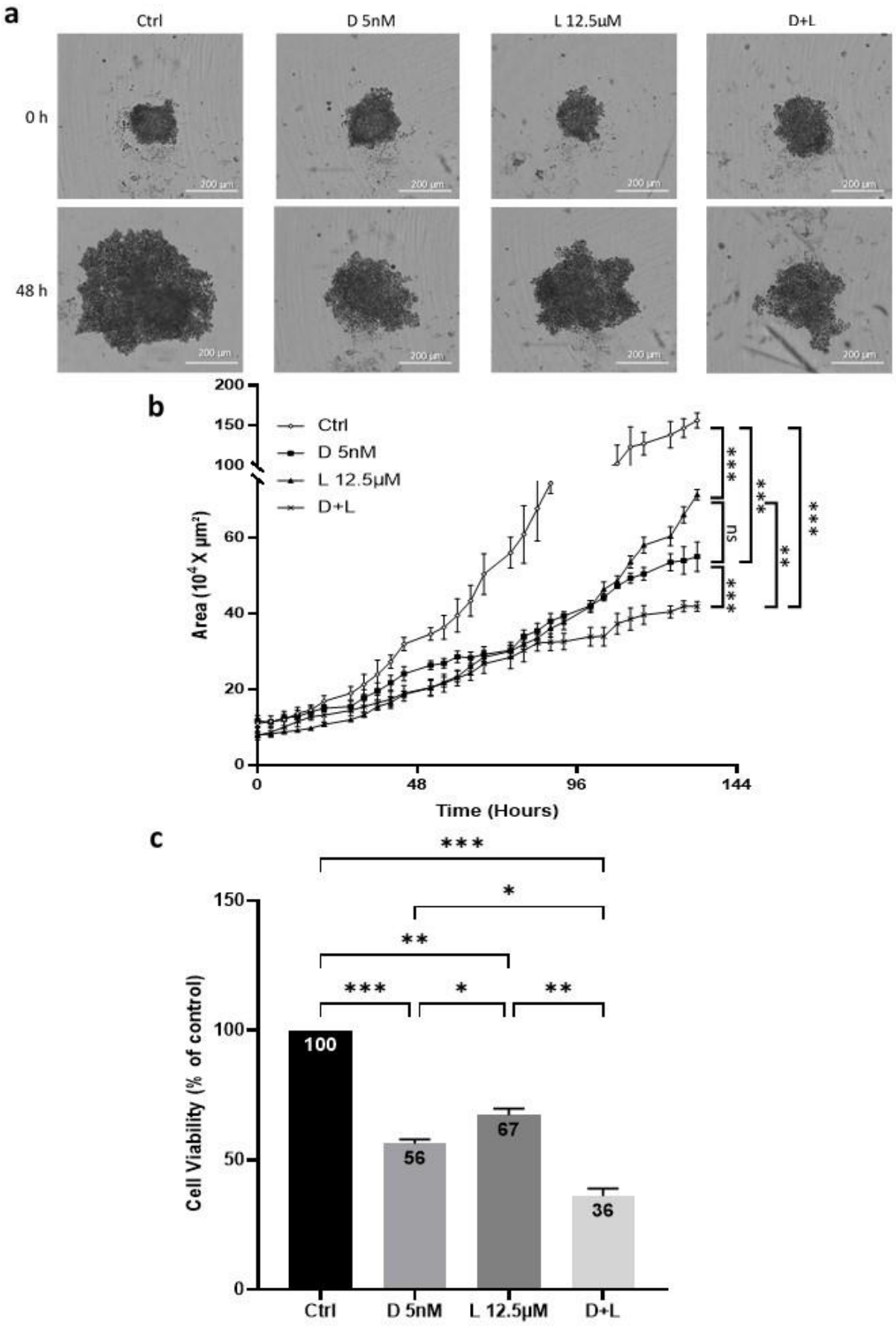
a
Ctrl
D 5nM
L 12.5uM
D+L
0 h
48 h
200 µm
b
Ctrl
D 5nM
L 12.5µM
D+L
Area (10⁴ X µm²)
Time (Hours)
ns
c
Cell Viability (% of control)
100
56
67
36
Ctrl
D 5nM
L 12.5µM
D+L

Figure IV.7. Effects of drug treatments on bicellular MCTS.
(a) Bright field photographs of 6 days-old HGT-1 + CAF spheroids at 0 h and 48 h of treatment with 5nM docetaxel (D 5nM), 12.5µM lovastatin (L 12.5µM) and 5nM docetaxel + 12.5µM lovastatin (D+L), captured with the IncuCyte™ live imaging. (b) Real-time growth monitoring (Area 10^4 x μm^2) of mixed spheroids formed from 250 HGT-1 + 250 CAF was performed using the IncuCyte™ live imaging and analysis system. Single treatments with 5nM docetaxel (D 5nM) (black squares), 12.5µM lovastatin (L 12.5µM) (black triangles) and combined treatment with 5nM docetaxel + 12.5µM lovastatin (D+L) (black X) were applied on 6 days-old MCTS and compared to control (white lozenges). The results are shown as the mean ± SD of n=3 independent experiments with four technical replicates in each. ns, $p > 0.05$; **$p \leq 0.01$; ***$p \leq 0.001$, one-way ANOVA followed by Tukey analysis. (c) The variation of bicellular MCTS viability was determined by the MTT assay after 48 h of treatment by 5nM docetaxel (D 5nM), 12.5µM lovastatin (L 12.5µM) and combined treatment with 5nM docetaxel + 12.5µM lovastatin (D+L). The results are shown as the mean ± SD of n=3 independent experiments with four technical replicates in each. *$p \leq 0.05$; **$p \leq 0.01$; ***$p \leq 0.001$, one-way ANOVA followed by Tukey analysis.

3. Discussion

Although treatment efficacy has improved during the past decade, survival rates of GC patients remain low [47]. The limitations of 2D cell culture model that lacks tumor complexity and direct pathophysiology relevance may be one of the main causes of the poor rate of cancer drugs entering early clinical trials, and even more so, become marketed drugs [48]. Novel preclinical models such as 3D cultures may be more predictive than 2D cultures for cancer therapy research [49]. Several distinct factors between 2D and 3D cultures, such as metabolic state and expression of drug resistance transporters could affect the activity of anti-cancer drugs [29].

Following on our previous studies showing that blunting the mevalonate pathway with lovastatin amplified the apoptotic response brought about by docetaxel [42], we asked whether such results might also apply to cells grown in 3D as spheroids. This was motivated by the fact that cell-cell interactions might be different between 2D and 3D culture conditions. Although this may sometimes be the case [44, 50], the present results showed that in both culture conditions, the lovastatin + docetaxel combination proved to be similarly able to trigger efficient apoptosis, to a larger extent than single drug treatments.

Here, HGT-1 and AGS cells were found to spontaneously form spheroids in ULA round-bottom microplates with high reproducibility. These spheroids were used for drug toxicity evaluation. We made use of high-throughput image microscopy (IncuCyte^{TM}) to analyze several growth-impairing conditions of spheroids, as reported [51]. Protein and gene expression profiles of MCTS are reportedly more similar to those of tumors than 2D cancer cells [52, 53]. In addition, 3D cell models are usually more resistant to cytotoxic treatments compared to cells in 2D cultures [54, 55]. This may have applied also here, as cells derived from 6 days-old spheroids were slightly less sensitive to the drugs than 2D-cultured cells after 48 h of treatment (Supplementary Figure IV.10). However, it is important to consider spheroid sizes when comparing therapeutic responses [56]. The spheroids generated here were homogenous and reached sizes in this range after 6 days. Although AGS spheroids were more compact than HGT-1 spheroids, both showed comparable sensitivities to the drugs or their combinations. Following drug treatments, we obtained quite overlapping results, by both the MTT assay and the live microscopy analysis system (Figures IV.3,4).

Cancer cells are strongly influenced by their microenvironment, which modulates local tumor progression and has a significant impact on therapy [57]. The co-culture of tumor cells with

CAF in MCTS permits to reproduce, at least in part, the interactions between different cell types, which are known to affect disease progression and the efficacy of anticancer therapies [58, 59]. Several studies showed that distinct signaling pathways may be activated in 2D *vs* 3D culture, in the presence or absence of stromal cells upon treatment with RAF inhibitors [60], anti-androgens [61], cetuximab, trastuzumab, vorinostat or everolimus [62] and doxorubicin [63]. Here, we developed an *in vitro* GC 3D direct co-culture model using human GC cells and GC-associated CAF. From day 2 of co-culture, spheroids assumed a tight shape, as compared to pure HGT-1 spheroids. This had no detrimental impact on drug response, as the combination of docetaxel and lovastatin showed strong cytotoxicity in this setup also (Figure IV.7).

Overall, the cytotoxic responses observed here in 2D or 3D models were presumably mostly due to some of the many changes induced by lovastatin at the transcriptomic and metabolomics levels, rather than to docetaxel that had very limited effects [42, 64]. Because the two drugs share no common mechanism of action, we believe, that they acted independently to trigger cell death, rather than activating the same death pathway.

Our results showed, by 3 analytical methods, from 2D cell cultures to 3D, that the combination of a *bona fide* anticancer agent, like docetaxel, and lovastatin deserved much interest. Real-time monitoring of drug response of 3D tumor spheroids proved to be a quite sensitive and reliable approach to determine the overall cell toxicity, both in mono- and bicellular spheroids. This toxicity resulted in apoptosis, as shown by enhanced nuclear fragmentation (revealed by Hoechst 33342 nuclear staining) and increased Caspases 3/7 activities. As an extension to this study, it could be envisioned to look at the response of GC organoids, *i.e.,* tumor fragments recovered right after surgery of human patients, to *in vitro* treatments with lovastatin and / or docetaxel. This might allow an even better application of 3D model screening assays to improve further the efficiency of drug screening. Transposed to a clinical setup, these results may lead to propose the association of lovastatin with docetaxel for the treatment of patients with GC. One evident advantage of this combination therapy would be to use lower drug doses than usually implemented, thereby reducing potential toxic side-effects, like those that have been reported for patients regularly taking statins or for cancer patients undergoing taxane anticancer therapy.

4. Methods

Cell culture

HGT-1 human gastric cancer cells (a gift of Pr. C. Laboisse, Nantes University hospital, France) were grown at 37°C under a humidified atmosphere with 5% CO_2 in Dulbecco's modified Eagle's medium (DMEM) (Corning, MA, USA), containing 4.5 g/L glucose and supplemented with 5% fetal bovine serum (FBS) (Gibco-Invitrogen, Cergy-Pontoise, France) without antibiotics (complete medium). AGS human gastric cancer cells (from the American Tissue Type Collection, ref. ATCC® CRL-1739™) were grown in the same medium supplemented with 10% FBS.

Lentiviral infection

The self-inactivating HIV-1-based lentiviral vector, pRRL-sin-MND-Tomato-IRES-Puro was purchased from VectUB (vectorology platform, University of Bordeaux, France). The vector expresses RedTomato and co-expresses the puromycin resistance gene. 40 000 HGT-1 cells were infected with lentiviruses (at a multiplicity of Infection of 2) and selected with puromycin (1 µg/mL). We obtained RedTomato fluorescent HGT-1 populations.

Preparation of mono- and bicellular tumor cells spheroids

Two-Dimension cultured HGT-1 or AGS cells were collected and used to generate spheroids by seeding 500 or 1000 cells/well (in 200 µL of complete medium), respectively, in ultra-low attachment 96-well round bottom microplates (Corning, Amsterdam, Netherlands). Following cell aggregation, ~550 µm diameter spheroids were obtained after 6 days of incubation under standard culture conditions.

To obtain bicellular spheroids, cells of each type were added together in 1:1 ratio (250 HGT-1 + 250 CAF or 500 AGS + 500 CAF).

Isolation, characterization and maintenance of fibroblast cultures

A written informed consent form was elaborated together with the Ethics Committee of Brest University Hospital (headed by Pr. J.M. Boles). Patients signed the form, which was returned to the Anatomy and Pathology department of Brest University Hospital that provided us with

tissue samples. From these, we isolated CAF following growth in primary tissue culture. We confirm that all methods were carried out in accordance with relevant guidelines and regulations and that all experimental protocols were approved by Brest University Hospital in respect with French regulations.

Cancer Associated Fibroblasts were obtained from a GC patient-ablated tumor after tissue dissociation with collagenase and growth in culture in DMEM (Corning, MA, USA) containing 4.5 g/L glucose supplemented with 10% FBS (Gibco-Invitrogen, Cergy-Pontoise, France). After about 10 days in culture, no more epithelial cells adhered to the dish and fibroblasts cells emerged and kept growing. Cells were then passaged every 2 weeks. They were used for RNA preparation to analyze their expression of fibroblast-specific transcripts at early (<7) passages and 70–90% confluence, so as to maintain their *in vivo* characteristics [65].

Drugs

Lovastatin and Docetaxel were from TCI Europe (Belgium) and Sanofi Aventis (France), respectively. Appropriate ranges of concentrations were chosen from previous dose-response studies in 2D [42]. Lovastatin was dissolved and diluted in dimethyl-sulfoxide (DMSO). The final concentration of DMSO used in culture did not exceed 0.4%, a concentration that had no overt cytotoxic effect *per se*. Docetaxel was used after dilution in 0.9% sodium chloride.

MTT assay

To evaluate 2D-cell viability, cells were seeded into 96-well culture plates at a density of 5000 cells/well and grown in 100 µL of medium. After 24h, the medium was replaced by 100 µL of fresh medium containing the drugs. After 36 or 48 hours of treatment, 10 µL of MTT labeling reagent (Millipore) dissolved in Phosphate Buffered Saline were added to each well (MTT reagent final concentration was 0.5 mg/ml). Plates were incubated for 2h at 37 °C. Then, formazan crystals were dissolved by adding 100 µL of solubilization solution (Isopropanol, Triton X-100 10%, 0.1M HCl) into each well. MTT reduction was quantified by measuring the light absorbance at 570 nm using an absorbance microplate reader (Multiskan Spectrum microplate spectrophotometer, ThermoFisher).

MTT assay for the MCTS cultures was carried out with slight modifications of the standard protocol. After 48 h of treatment, 100 µL (1/2 of total) of medium were carefully removed.

The spheroids were then dissociated mechanically before the addition of 10 µL MTT reagent into each well. The plates were incubated for 2h at 37 °C. After incubation, formazan crystals were dissolved by adding 100 µL of solubilization solution into each well. Then 150 µL of medium from each well containing the MCTS culture were transferred to a new, flat-bottom 96-well plate. Absorbance was recorded as described for 2D cells.

Multicellular tumor spheroids size measurement

An IncuCyte™ S1 live-cell analysis system (Sartorius, Essen Bioscience), placed inside a conventional tissue culture incubator at 37°C with 5% CO_2, was used for real-time imaging of spheroids. Images of each spheroid were taken using a 4x phase contrast lens, every 4h for 11 days, and each condition was run in quadruplicate. Each well contained a single spheroid settled at the center. Images were analyzed and data were generated using the spheroid automated software algorithm functions from IncuCyte 2019B Rev2 software (Sartorius, Essen Bioscience) where virtual masks were created to surround spheroids. The size of spheroids was calculated as the largest object area in each image.

Evaluation of the RedTomato fluorescence intensity in spheroids

The fluorescence signal generated from HGT-1 RedTomato-labeled cells, cultured as spheroids, was analyzed in the IncuCyte™ system. MCTS were imaged every 4h with 1 image/well in phase contrast and Red fluorescence channels (400 ms exposure) using a 4x lens, each condition being run in quadruplicate. Automated real-time assessment by live-cell analysis was measured as red area generated by viable HGT-1 RedTomato-labeled cells. The fluorescence is proportional to the number of intact viable cells in the well for all RedTomato cells with normalization on contrast phase areas. Data were analyzed using the spheroid software functions from IncuCyte 2019B Rev2 software.

IncuCyte™ Annexin V apoptosis assay

The IncuCyte™ S1 live-cell analysis system was used to determine apoptosis levels of 3D cultured HGT-1 cells treated with the drugs. HGT-1 spheroids were cultured for 6 days and Annexin V Red reagent (Sartorius) was added at the same time as drugs. Throughout the assay, both phase and fluorescent images were collected using phase contrast and Red fluorescence

channels (400 ms exposure) with a 4x lens. One image was taken every 4h for 5 days, and each condition was run in quadruplicate. Automated real-time assessment by live-cell analysis was measured as red area for all cells stained red with Annexin V Reagent normalized to contrast phase area. Images were analyzed and data were generated using the spheroid automated software algorithm functions from IncuCyte 2019B Rev2 software.

Statistics

Statistical analysis was performed using GraphPad Prism. Data are presented as the mean ± S.D and experiments were repeated at least three times. *p*-values were calculated using one-way ANOVA with Tukey analysis. The results were considered significant for $*p<0.05$, $**p<0.01$ and $***p<0.001$.

5. Supplementary Materials and Methods

Determination of apoptotic nuclear fragmentation and caspase activation

After 48 h of treatment, the spheroids were dissociated mechanically before they were stained with Hoechst 33342 (Sigma) at 10 µg/ml in complete medium for 10 min at 37°C. Nuclei of apoptotic cells with fragmented chromatin were brightly stained. At least 400 cells were counted for each sample, and the percentage of total apoptotic cells was calculated.
The activity of caspase-3 and caspase-7 was determined with the luminescent Caspase-Glo™ 3/7 Assay kit (Promega, France) according to the manufacturer's instructions. Briefly, after treatment of 6 days-old spheroids, an equal volume of Caspase-Glo™ 3/7 reagent was added to the sample in the assay well. Samples were incubated at room temperature for 1 hour and the enzyme activity was measured with a luminometer (Fluoroskan ascent FL, Thermo electron corporation).

Histological analysis of HGT-1 and AGS spheroids

Spheroids were fixed with buffered formalin for 1 hour at room temperature, embedded in a gel matrix (7401151, Cytoblock Replacement Reagents, Thermo Scientific, Waltham, USA) according to the manufacturer's instructions, prior to dehydration and paraffin-embedding. Five µm thick sections were stained with haematoxylin, eosin and saffron. Images acquisition was performed with AxioVision 4.8 software (Zeiss, Oberkochen, Germany).

Drug resistance assays

Sensitivity to drugs was assessed using the MTT assay. Sixty 6 days-old spheroids were dissociated mechanically and 5000 healthy MCTS-dissociated cells or parental cells per well were plated in 96-well plates in 100 µL of DMEM supplemented with 5% FBS with or without drugs (docetaxel, lovastatin). To analyze drug sensitivity of MCTS-dissociated cells, as compared to 2D-only grown cells, we treated both cell populations with 5nM docetaxel +/- 12.5µM lovastatin. Forty-eight hours after treatment, 10 µL of the MTT labeling reagent dissolved in Phosphate Buffered Saline were added to each well (final concentration 0.5 mg/ml). The plates were incubated for 2h at 37 °C. After incubation, formazan crystals were dissolved by adding 100 µL of the solubilization solution (Isopropanol, Triton X-100 10%, 0.1M

HCl) into each well. MTT reduction was quantified by measuring the light absorbance at 570 nm using an absorbance microplate reader (Multiskan Spectrum microplate spectrophotometer, ThermoFisher). Each test was repeated three times in quadruplicate determinations.

RNA extraction and RT-PCR analysis

Total RNA was isolated using TRIzol (Invitrogen) according to the manufacturer's protocol. Samples of 2 µg of total RNA were reverse-transcribed using random hexamers and MMLV (Moloney-murine-leukaemia virus) reverse transcriptase (New England Biolabs). RT reactions (1 µL out of a 25 µL reaction volume) were used as templates for PCR experiments.

The characteristics of primers and amplicons size are in the table below:

Name of gene	primers	sequence	amplicon length (bp)	T°m (°C)	Cycles (number)
α SMA : alpha smooth muscle actin	forward	AGGAAGGACCTCTATGCTAACAAT	378	54	29
	reverse	AACACATAGGTAACGAGTCAGAGC			
FAP : Fibroblast activated protein	forward	CAAGTGGCAAGTGGGAGGCCA	245	59	27
	reverse	TGGGGATGCCTGGGCCGTAG			
FGF-2 : Fibroblast growth factor 2	forward	CGCCCGGCCACTTCAAGGAC	120	56	27
	reverse	AGCTTGATGTGAGGGTCGCTCTTC			
IL-6 : Interleukin-6	forward	TCGAGCCCACCGGGAACGAAA	84	54	29
	reverse	GACCGAAGGCGCTTGTGGAGA			
SDF-1 : Stroma-derived factor-1	forward	TGAGCTACAGATGCCCATGC	177	56	27
	reverse	TTCTCCAGGTACTCCTGAATCC			
VIM : Vimentin	forward	GAAGGCGAGGAGAGCAGGATTTC	99	54	24
	reverse	AGTGGGTATCAACCAGAGGGAGTG			
GAPDH : Glyceraldehyde 3-phosphate dehydrogenase	forward	GAGTCAACGGATTTGGTCGT	238	54	24
	reverse	TTGATTTTGGAGGGATCTCG			

6. Supplementary Figures

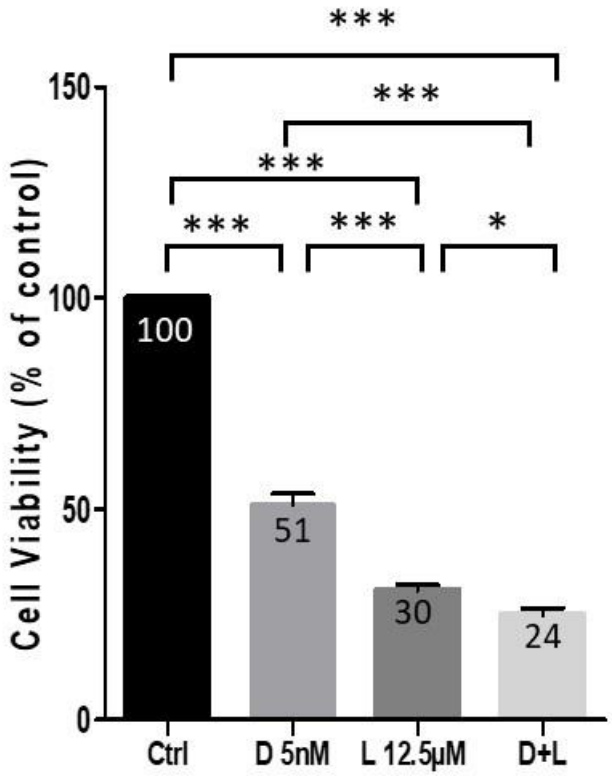

Supplementary Figure IV.1. Toxicity of docetaxel and lovastatin in human gastric cancer AGS cells in 2D culture.

The cells were incubated at 37 °C for 48 h upon treatment with 5nM docetaxel (D 5nM), 12.5µM lovastatin (L 12.5µM) or 5nM docetaxel + 12.5µM lovastatin (D+L). Cell viability was measured by the MTT assay. The results are shown as the mean ± SD of n=3 independent replicates with four technical replicates in each. *$p \leq 0.05$; ***$p \leq 0.001$, one-way ANOVA followed by Tukey analysis.

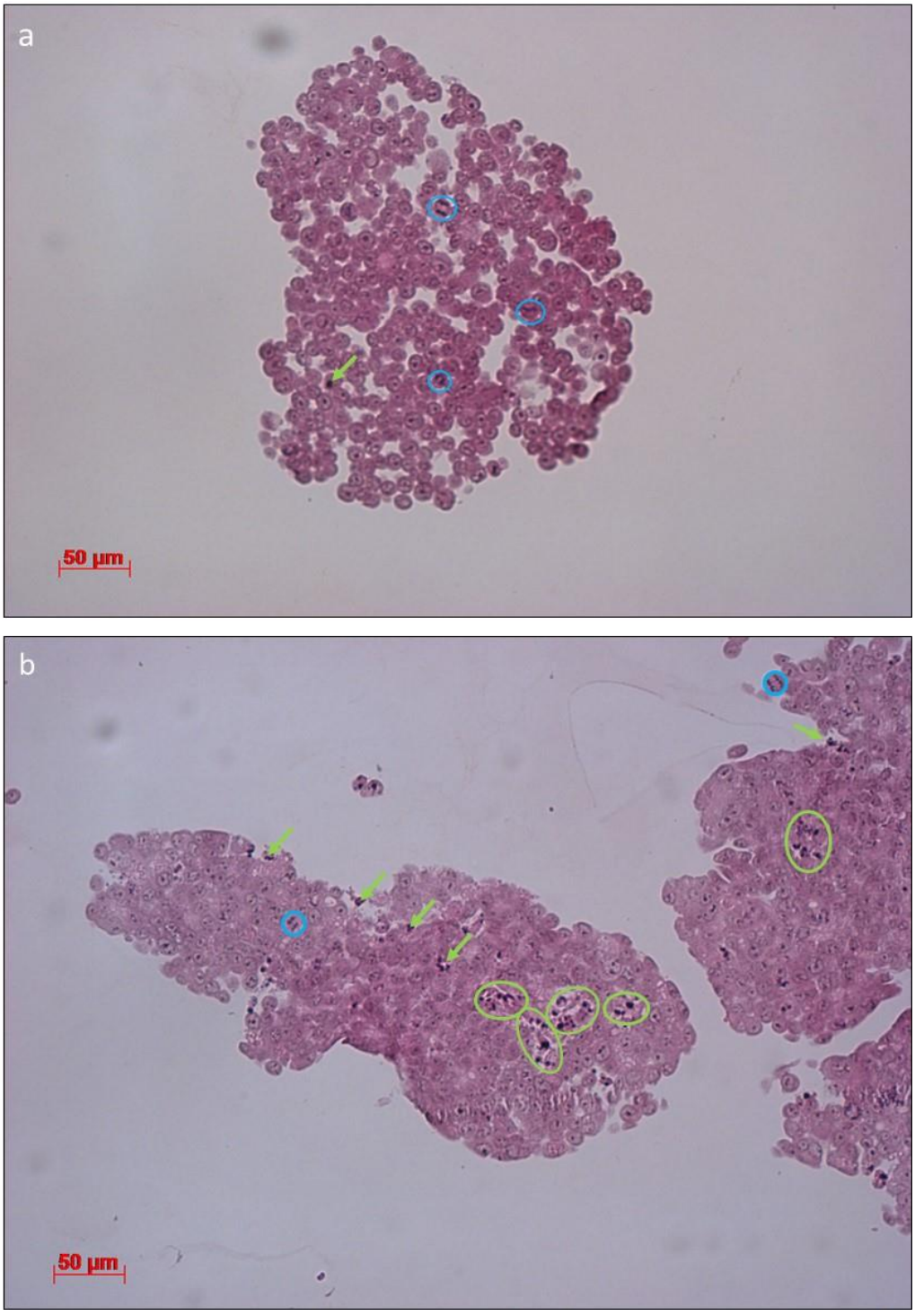

Supplementary Figure IV.2. Histological sections of HGT-1 and AGS spheroids.
HGT-1 cells (a) are grouped into loosely cohesive clusters. Mitotic figures are visible (blue circles). A few isolated necrotic cells are present (green arrow).
AGS cells (b) are grouped into cohesive clusters. Necrotic areas are present in the center of the clusters (green arrows and circles). A few mitotic figures are visible (blue circle).

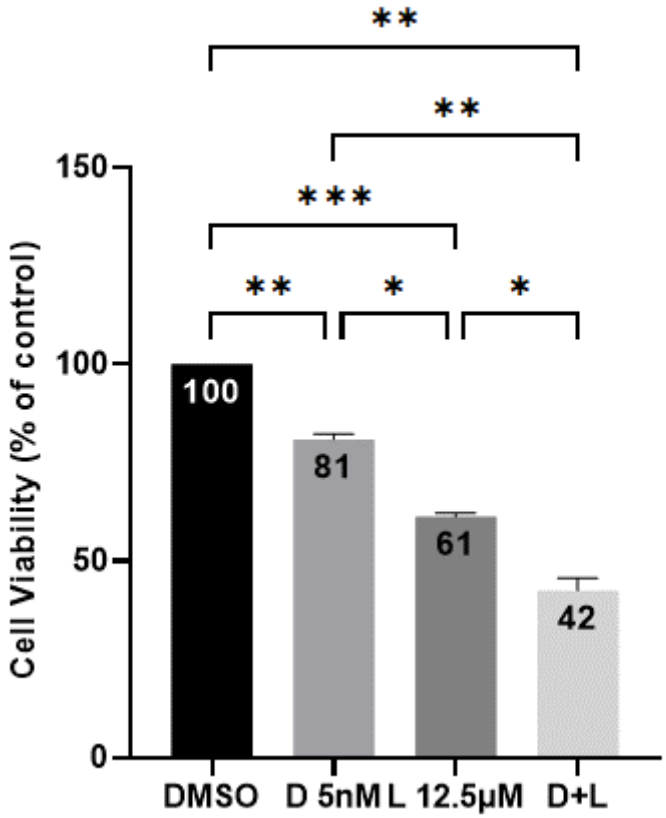

Supplementary Figure IV.3. Cytotoxicity of docetaxel and lovastatin for AGS spheroids. Cell viability was determined by the MTT assay after 48h of treatment with 5nM docetaxel (D 5nM), 12.5µM lovastatin (L 12.5µM) or 5nM docetaxel + 12.5µM lovastatin (D+L) of six days-old AGS spheroids. The results are shown as the mean ± SD of n=3 independent replicates with four technical replicates in each. *p ≤ 0.05; **p ≤ 0.01; ***p ≤ 0.001, one-way ANOVA followed by Tukey analysis.

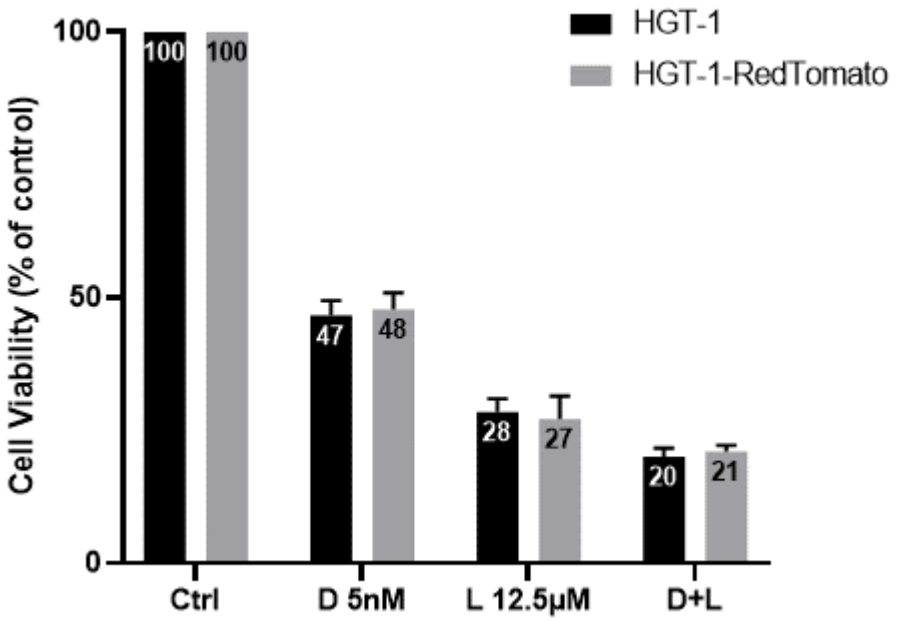

Supplementary Figure IV.4. Cell toxicity of drugs on RedTomato-labelled HGT-1 cells. The cells were incubated at 37 °C for 48h upon treatment by 5nM docetaxel (D 5nM), 12.5µM lovastatin (L 12.5µM) or 5nM docetaxel + 12.5µM lovastatin (D+L). Cell viability was measured by the MTT assay. The results are shown as the mean ± SD of n=3 independent replicates with four technical replicates in each.

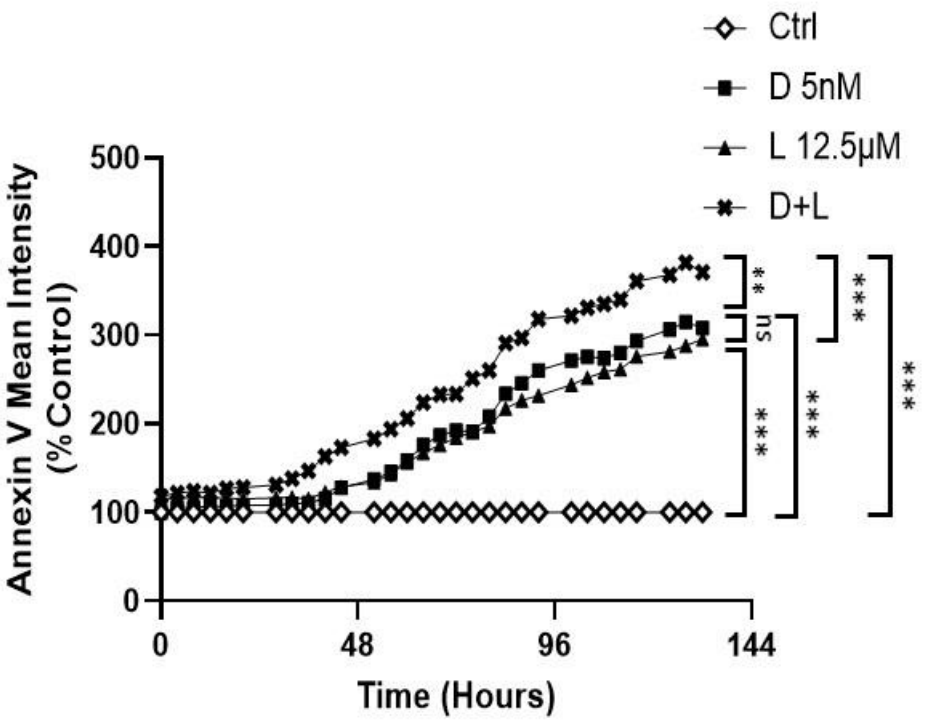

Supplementary Figure IV.5. Real-time apoptosis induction by docetaxel and lovastatin in HGT-1 spheroids.

Real-time Annexin V fluorescent reagent (IncuCyte^{TM}) measurements are shown. Six days-old MCTS were treated with 5nM docetaxel (D 5nM) (black squares), 12.5µM lovastatin (L 12.5µM) (black triangles) and the combined treatment 5nM docetaxel + 12.5µM lovastatin (D+L) (black X). The control condition is shown as white lozenges. The Annexin V reagent was added at the same time as the drugs. The results are shown as the mean of n=3 independent replicates with four technical replicates in each. ns $p > 0.05$; **$p \leq 0.01$; ***$p \leq 0.001$, one-way ANOVA followed by Tukey analysis.

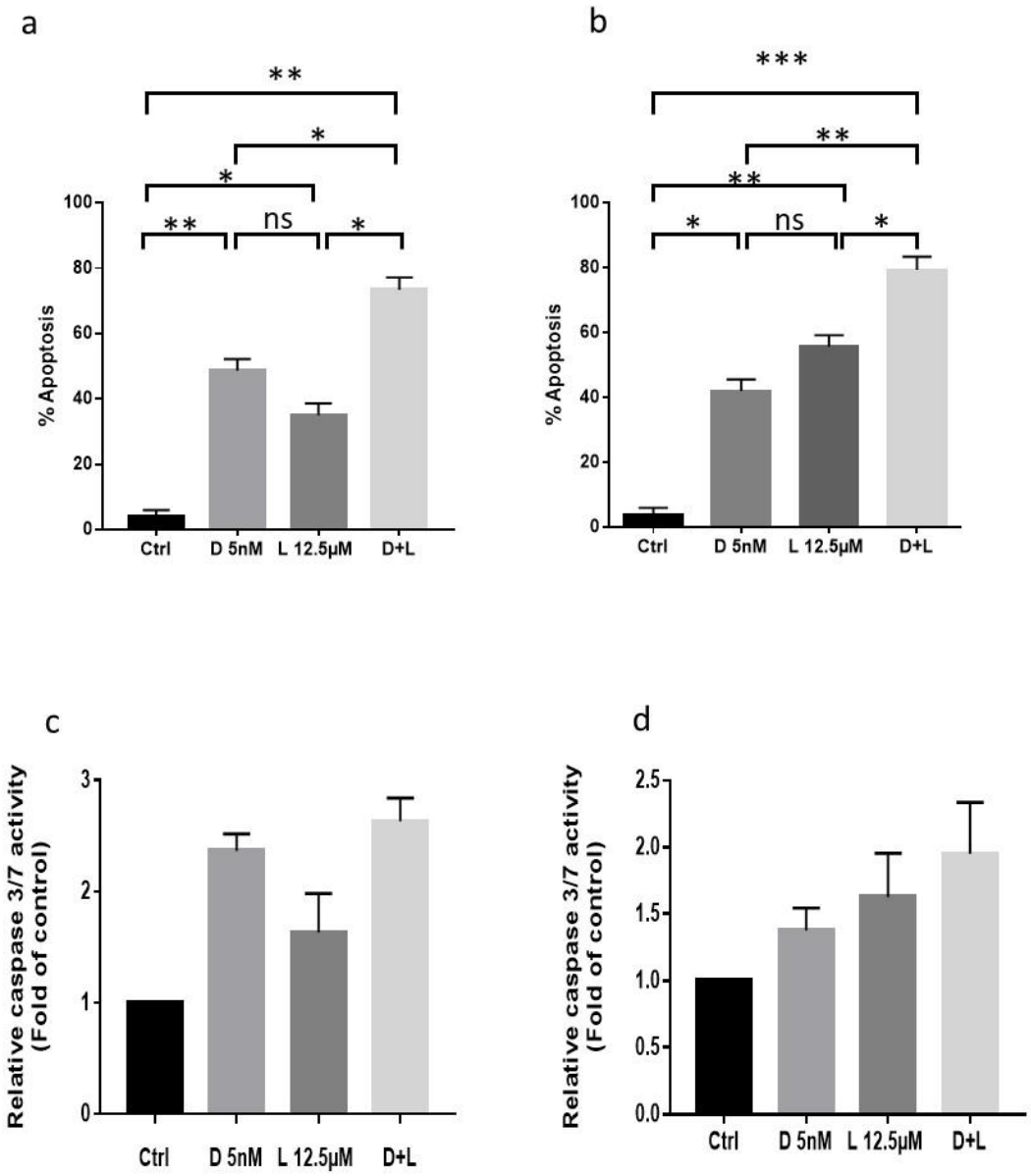

Supplementary Figure IV.6. Apoptosis induction by docetaxel and lovastatin in HGT-1 and AGS spheroids

After 48 h of treatment by 5nM docetaxel (D 5nM), 12.5µM lovastatin (L 12.5µM) or 5nM docetaxel + 12.5µM lovastatin (D+L), apoptosis of 6 days-old HGT-1 (a) or AGS (b) spheroids was evaluated by Hoechst 33342 staining of fragmented nuclei. The results are shown as the mean ± SD of n=3 independent replicates with four technical replicates in each. ns $p > 0.05$; *$p \leq 0.05$; **$p \leq 0.01$; ***$p \leq 0.001$, one-way ANOVA followed by Tukey analysis.

Caspase 3/7 activity (caspase-GloTM 3/7 assay, Promega) was determined after 24h of treatment by 5nM docetaxel (D 5nM), 12.5µM lovastatin (L 12.5µM) or 5nM docetaxel + 12.5µM lovastatin (D+L), in 6 days-old HGT-1 (c) or AGS (d) spheroids. The results are mean ± SD of three wells; they should be considered as indicative since they are from a single experiment.

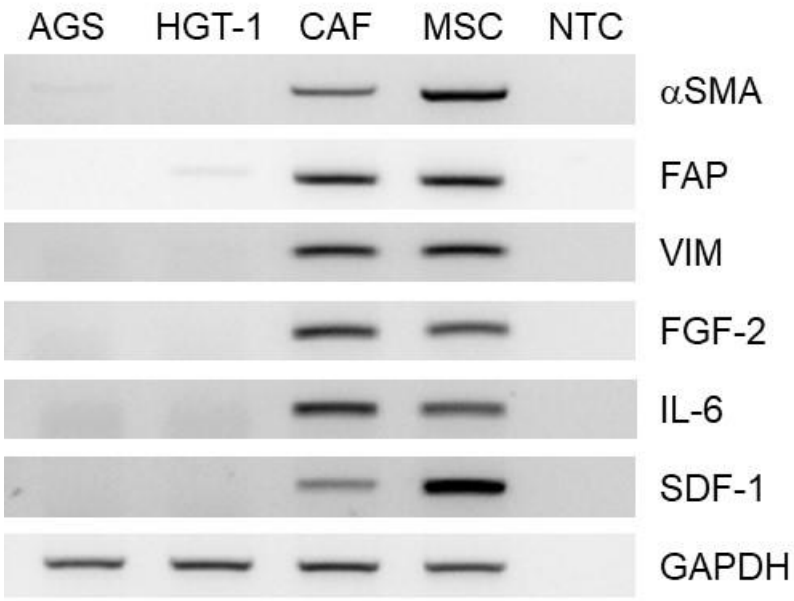

Supplementary Figure IV.7. Gene expression levels in HGT-1, AGS, CAF and MSC.
RNA levels of fibroblast markers were analyzed by RT-PCR (see materials and methods) in HGT-1 cells, AGS cells, in CAF and in mesenchymal stem cells (MSC). NTC: no template control, negative control for PCR. Alpha-smooth muscle actin (α-SMA), fibroblast activation protein (FAP), vimentin (VIM), fibroblast growth factor-2 (FGF-2), interleukin-6 (IL-6), stromal-derived factor-1 (SDF-1), glyceraldehyde-3-phosphate dehydrogenase (GAPDH). MWM: 100pb DNA ladder molecular weight marker (Promega).

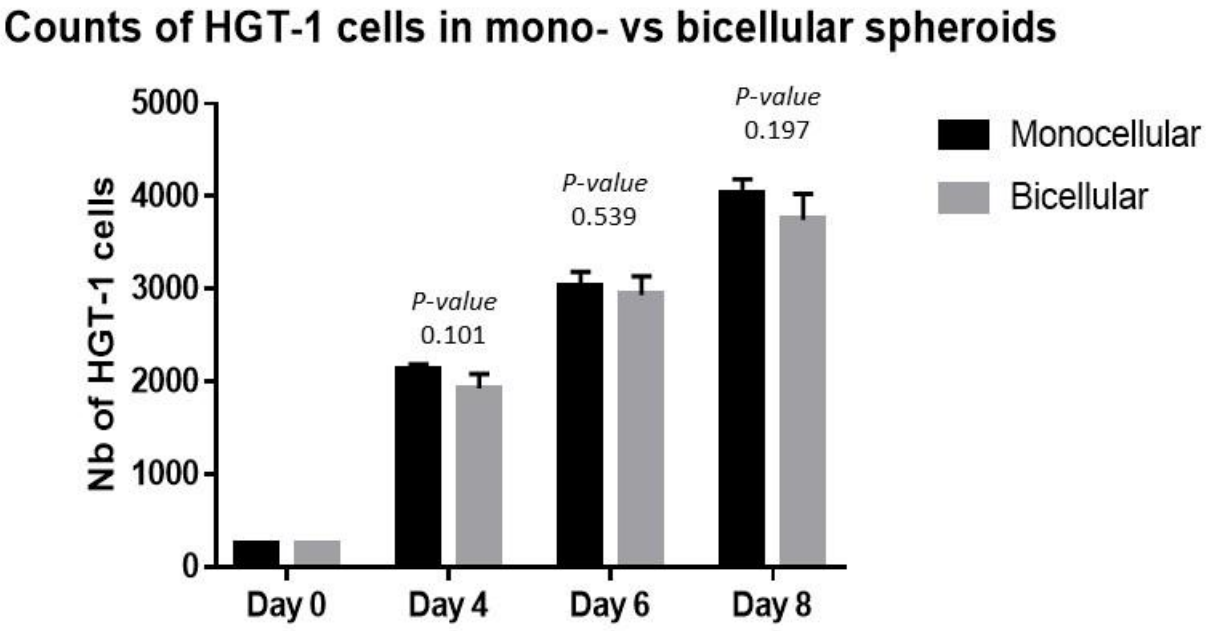

Supplementary Figure IV.8. Counts of HGT-1 cells in mono- vs bicellular spheroids.
GFP-labelled HGT-1 cells were counted following dissociation of mono- or bicellular spheroids up to 8 days. The results are shown as the mean ± SD of n=3 independent replicates. P-value were issued from Student's t-test.

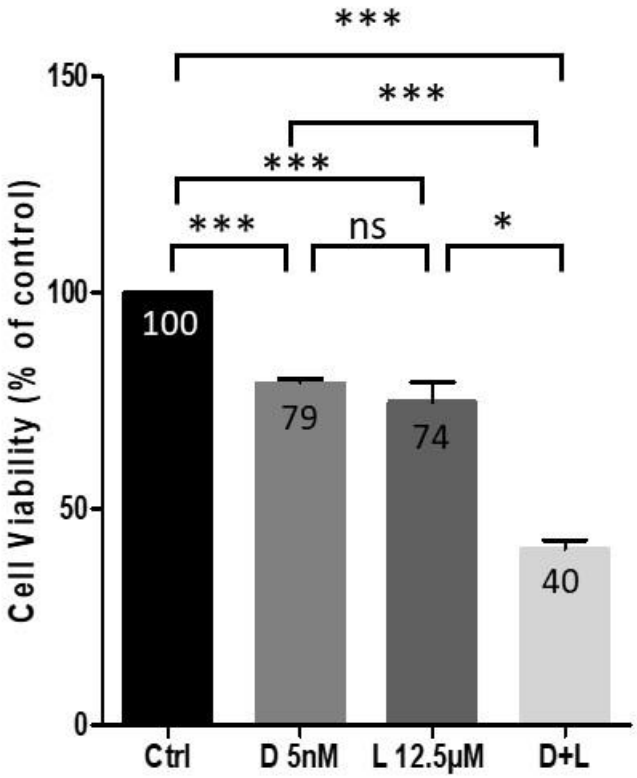

Supplementary Figure IV.9. Effects of drug treatments on bicellular MCTS (AGS+CAF). The variation of mixed spheroids (500 AGS + 500 CAF) viability was determined by the MTT assay after 48 h of treatment by 5nM docetaxel (D 5nM), 12.5µM lovastatin (L 12.5µM) and combined treatment with 5nM docetaxel + 12.5µM lovastatin (D+L). The results are shown as the mean ± SD of n=3 independent replicates with four technical replicates in each. ns $p > 0.05$; *$p \leq 0.05$; ***$p \leq 0.001$, one-way ANOVA followed by Tukey analysis.

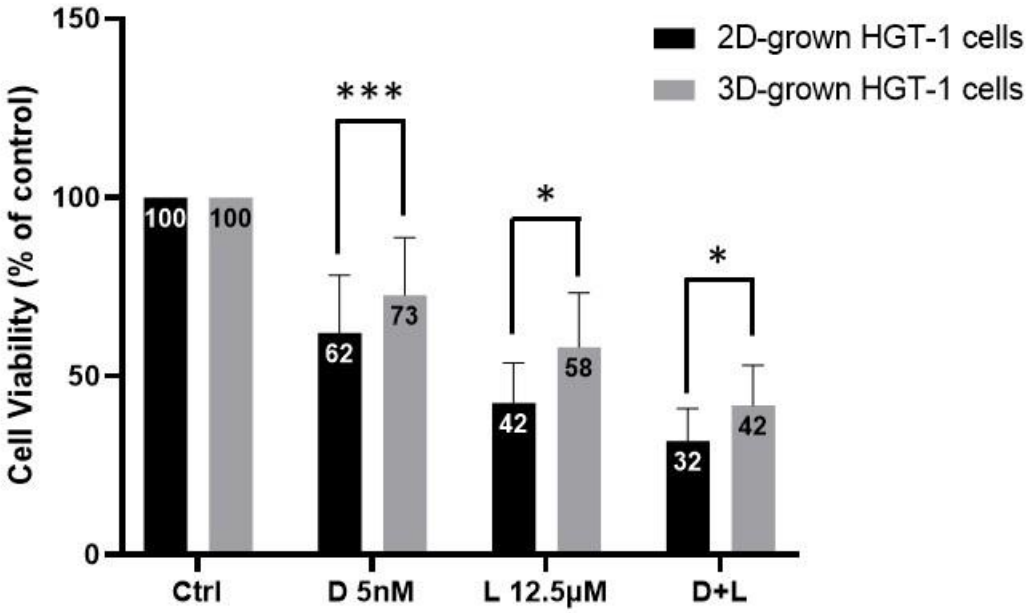

Supplementary Figure IV.10. Effects of drugs in HGT-1 2D cells compared to HGT-1 cells recovered from MCTS and re-grown in 2D.

MTT assay was used to analyze drug toxicity for 48h in HGT-1 2D cells and in HGT-1 cells recovered from six days-old HGT-1 MCTS. The results are shown as the mean ± SD of n=3 independent replicates with four technical replicates in each. *$p \leq 0.05$; ***$p \leq 0.001$, Student's t-test.

7. Supplementary Movies

Supplementary movies files will be available with the thesis manuscript

Effects of docetaxel and lovastatin treatments on the growth of HGT-1 spheroids. Movies show real-time HGT-1 spheroid growth after treatment with 5nM docetaxel, 12.5µM lovastatin and 5nM docetaxel + 12.5µM lovastatin (D+L), captured with the IncuCyte™ live imaging microscope. Day 0 correspond to 5 days-old spheroids. Drugs were added at day 1: on 6 days-old spheroids.

Bicellular HGT-1 + CAF spheroids formation. Movies show real-time 250 HGT-1, 500 HGT-1 and 250 HGT-1 + 250 CAF spheroids formation going from 0 to 8 days of culture, captured with the IncuCyte™ live imaging microscope.

8. References

[1] H. Sung *et al.*, "Global Cancer Statistics 2020: GLOBOCAN Estimates of Incidence and Mortality Worldwide for 36 Cancers in 185 countries," *CA. Cancer J. Clin.*, vol. 71, no. 3, pp. 209–249, May 2021, doi: 10.3322/caac.21660.

[2] M. Balakrishnan, R. George, A. Sharma, and D. Y. Graham, "Changing trends in stomach cancer throughout the world," *Current Gastroenterology Reports*, vol. 19, no. 8. Current Medicine Group LLC 1, Aug. 2017, doi: 10.1007/s11894-017-0575-8.

[3] E. C. Smyth, M. Nilsson, H. I. Grabsch, N. C. van Grieken, and F. Lordick, "Gastric cancer," *The Lancet*, vol. 396, no. 10251. Lancet Publishing Group, pp. 635–648, Aug. 29, 2020, doi: 10.1016/S0140-6736(20)31288-5.

[4] D. Cunningham *et al.*, "Perioperative chemotherapy versus surgery alone for resectable gastroesophageal cancer," *N. Engl. J. Med.*, vol. 355, no. 1, pp. 11–20, Jul. 2006, doi: 10.1056/NEJMoa055531.

[5] S. E. Al-Batran *et al.*, "Histopathological regression after neoadjuvant docetaxel, oxaliplatin, fluorouracil, and leucovorin versus epirubicin, cisplatin, and fluorouracil or capecitabine in patients with resectable gastric or gastro-oesophageal junction adenocarcinoma (FLOT4-AIO): results from the phase 2 part of a multicentre, open-label, randomised phase 2/3 trial," *Lancet Oncol.*, vol. 17, no. 12, pp. 1697–1708, Dec. 2016, doi: 10.1016/S1470-2045(16)30531-9.

[6] E. Niccolai, A. Taddei, D. Prisco, and A. Amedei, "Gastric cancer and the epoch of immunotherapy approaches," *World J. Gastroenterol.*, vol. 21, no. 19, pp. 5778–5793, May 2015, doi: 10.3748/wjg.v21.i19.5778.

[7] K. Kono, S. Nakajima, and K. Mimura, "Current status of immune checkpoint inhibitors for gastric cancer," *Gastric Cancer*, vol. 23, no. 4, pp. 565–578, May 2020, doi: 10.1007/S10120-020-01090-4.

[8] S. Vahed, R. Salehi, S. Davaran, and S. Sharifi, "Liposome-based drug co-delivery systems in cancer cells," *Mater. Sci. Eng. C,* vol. 71, pp. 1327-1341, Feb. 2016, doi: 10.1016/j.msec.2016.11.073.

[9] N. C. Baker, S. Ekins, A. J. Williams, and A. Tropsha, "A bibliometric review of drug repurposing," Drug Discov. *Today*, vol. 23, no. 3, pp. 661–672, Mar. 2018, doi: 10.1016/J.DRUDIS.2018.01.018.

[10] C. R. Sirtori, "The pharmacology of statins," *Pharmacological Research*, vol. 88. pp. 3–11, Aug. 19, 2014, doi: 10.1016/j.phrs.2014.03.002.

[11] S. Karr, "Epidemiology and management of hyperlipidemia.," *Am. J. Manag. Care*, vol. 23, no. 9, pp. 139-148, Jun. 2017, PMID. 28978219.

[12] C. Vaklavas, Y. S. Chatzizisis, and A. M. Tsimberidou, "Common cardiovascular medications in cancer therapeutics.," *Pharmacol. Ther.*, vol. 130, no. 2, pp. 177–190, Jan. 2011, doi: 10.1016/J.PHARMTHERA.2011.01.009.

[13] N. Berndt, A. D. Hamilton, and S. M. Sebti, "Targeting protein prenylation for cancer therapy," *Nature Reviews Cancer*, vol. 11, no. 11, pp. 775–791, Nov. 24, 2011, doi:

10.1038/nrc3151.

[14] T. Wang *et al.*, "Simvastatin-induced breast cancer cell death and deactivation of PI3K/Akt and MAPK/ERK signalling are reversed by metabolic products of the mevalonate pathway," *Oncotarget*, vol. 7, no. 3, pp. 2532–2544, 2016, doi: 10.18632/oncotarget.6304.

[15] P. J. Mullen, R. Yu, J. Longo, M. C. Archer, and L. Z. Penn, "The interplay between cell signalling and the mevalonate pathway in cancer," *Nature Reviews Cancer*, vol. 16, no. 11, pp. 718–731, Oct. 24, 2016, doi: 10.1038/nrc.2016.76.

[16] W.-B. Zhong *et al.*, "A synergistic anti-cancer effect of troglitazone and lovastatin in a human anaplastic thyroid cancer cell line and in a mouse xenograft model," *Int. J. Mol. Sci.*, vol. 19, no. 7, p. 1834, Jun. 2018, doi: 10.3390/ijms19071834.

[17] T. Yang *et al.*, "Effects of lovastatin on MDA-MB-231 breast cancer cells: An antibody microarray analysis," *J. Cancer*, vol. 7, no. 2, pp. 192–199, 2016, doi: 10.7150/jca.13414.

[18] O. O. Ogunwobi and I. L. P. Beales, "Statins inhibit proliferation and induce apoptosis in Barrett's esophageal adenocarcinoma cells," *Am. J. Gastroenterol.*, vol. 103, no. 4, pp. 825–837, Apr. 2008, doi: 10.1111/j.1572-0241.2007.01773.x.

[19] S. A. Glynn, D. O'Sullivan, A. J. Eustace, M. Clynes, and N. O'Donovan, "The 3-hydroxy-3-methylglutaryl-coenzyme A reductase inhibitor, simvastatin, lovastatin and mevastatin inhibit proliferation and invasion of melanoma cells," *BMC Cancer*, vol. 8, Jan. 2008, doi: 10.1186/1471-2407-8-9.

[20] L. X. Vásquez-Bochm *et al.*, "Transcriptome-based identification of lovastatin as a breast cancer stem cell-targeting drug," *Pharmacol. Reports*, vol. 71, no. 3, pp. 535–544, Jun. 2019, doi: 10.1016/j.pharep.2019.02.011.

[21] S. M. Kornblau *et al.*, "Blockade of adaptive defensive changes in cholesterol uptake and synthesis in AML by the addition of pravastatin to idarubicin + high-dose Ara-C: A phase 1 study," *Blood*, vol. 109, no. 7, pp. 2999–3006, Apr. 2007, doi: 10.1182/blood-2006-08-044446.

[22] A. Martirosyan, J. W. Clendening, C. A. Goard, and L. Z. Penn, "Lovastatin induces apoptosis of ovarian cancer cells and synergizes with doxorubicin: Potential therapeutic relevance," *BMC Cancer*, vol. 10, Mar. 2010, doi: 10.1186/1471-2407-10-103.

[23] T. Wang, Y. Jiang, H. Chu, X. Liu, Y. Dai, and D. Wang, "Doxorubicin and Lovastatin co-delivery liposomes for synergistic therapy of liver cancer," *J. Drug Deliv. Sci. Technol.*, vol. 52, pp. 452–459, Aug. 2019, doi: 10.1016/j.jddst.2019.04.045.

[24] C. Jensen and Y. Teng, "Is it time to start transitioning from 2D to 3D cell culture?," *Frontiers in Molecular Biosciences*, vol. 7. Frontiers Media S.A., Mar. 06, 2020, doi: 10.3389/fmolb.2020.00033.

[25] G. Alzeeb, J. P. Metges, L. Corcos, and C. Le Jossic-Corcos, "Three-dimensional culture systems in gastric cancer research," *Cancers*, vol. 12, no. 10, pp. 1–20, Oct. 01, 2020, doi: 10.3390/cancers12102800.

[26] D. V. LaBarbera, B. G. Reid, and B. H. Yoo, "The multicellular tumor spheroid model for

high-throughput cancer drug discovery," *Expert Opinion on Drug Discovery*, vol. 7, no. 9, pp. 819–830, Sep. 2012, doi: 10.1517/17460441.2012.708334.

[27] S. Thippabhotla, C. Zhong, and M. He, "3D cell culture stimulates the secretion of in vivo like extracellular vesicles," *Sci. Rep.*, vol. 9, no. 1, Dec. 2019, doi: 10.1038/s41598-019-49671-3.

[28] G. Lazzari, P. Couvreur, and S. Mura, "Multicellular tumor spheroids: a relevant 3D model for the in vitro preclinical investigation of polymer nanomedicines," *Polym. Chem.*, vol. 8, no. 34, pp. 4947–4969, Aug. 2017, doi: 10.1039/C7PY00559H.

[29] V. S. Nirmalanandhan, A. Duren, P. Hendricks, G. Vielhauer, and G. S. Sittampalam, "Activity of anticancer agents in a three-dimensional cell culture model," *Assay Drug Dev. Technol.*, vol. 8, no. 5, pp. 581–590, Oct. 2010, doi: 10.1089/adt.2010.0276.

[30] M. J. Bissell and W. C. Hines, "Why don't we get more cancer? A proposed role of the microenvironment in restraining cancer progression," *Nat. Med.*, vol. 17, no. 3., pp. 320–329, Mar. 2011, doi: 10.1038/nm.2328.

[31] D. C. Lazăr, M. F. Avram, I. Romoşan, M. Cornianu, S. Tăban, and A. Goldiş, "Prognostic significance of tumor immune microenvironment and immunotherapy: Novel insights and future perspectives in gastric cancer," *World J. Gastroenterol.*, vol. 24, no. 32., pp. 3583–3616, Aug. 28, 2018, doi: 10.3748/wjg.v24.i32.3583.

[32] I. H. Ham, D. Lee, and H. Hur, "Role of cancer-associated fibroblast in gastric cancer progression and resistance to treatments," *Journal of Oncology*, vol. 2019., 2019, doi: 10.1155/2019/6270784.

[33] T. A. Sebrell *et al.*, "A novel gastric spheroid co-culture model reveals chemokine-dependent recruitment of human dendritic cells to the gastric epithelium," *CMGH*, vol. 8, no. 1, pp. 157-171.e3, Jan. 2019, doi: 10.1016/j.jcmgh.2019.02.010.

[34] W. Inch, J. Credie, and R. Sutherland, "Growth of nodular carcinomas in rodents compared with multi-cell spheroids in tissue culture.," *Subj. Strain Bibliogr.*, vol. 34, pp. 271-282, Jan. 1970, Available: https://mouseion.jax.org/ssbb1970/265. PMID. 5471822.

[35] M. Vinci *et al.*, "Advances in establishment and analysis of three-dimensional tumor spheroid-based functional assays for target validation and drug evaluation," BMC Biol., vol. 10, no. 29, Mar. 2012. doi: 10.1186/1741-7007-10-29.

[36] L. Li, Q. Zhou, T. C. Voss, K. L. Quick, and D. V. LaBarbera, "High-throughput imaging: Focusing in on drug discovery in 3D," *Methods*, vol. 96, pp. 97–102, Mar. 2016, doi: 10.1016/j.ymeth.2015.11.013.

[37] J. Wang *et al.*, "Anti-gastric cancer activity in three-dimensional tumor spheroids of bufadienolides OPEN," *Sci. Rep.*, vol. 6, Apr. 2016, doi: 10.1038/srep24772.

[38] O. Aftab, M. Fryknäs, U. Hammerling, R. Larsson, and M. G. Gustafsson, "Detection of cell aggregation and altered cell viability by automated label-free video microscopy: A promising alternative to endpoint viability assays in high-throughput screening," *J. Biomol. Screen.*, vol. 20, no. 3, pp. 372–381, Mar. 2015, doi: 10.1177/1087057114562158.

[39] A. D. Roth et al., "Docetaxel (Taxotere)-cisplatin (TC): an effective drug combination in gastric carcinoma. Swiss Group for Clinical Cancer Research (SAKK), and the European Institute of Oncology (EIO)," *Ann. Oncol. Off. J. Eur. Soc. Med. Oncol.*, vol. 11, no. 3, pp. 301–306, 2000, doi: 10.1023/A:1008342013224.

[40] J. Picus and M. Schultz, "Docetaxel (Taxotere) as monotherapy in the treatment of hormone-refractory prostate cancer: preliminary results.," *Semin. Oncol.*, vol. 26, no. 5 Suppl 17, pp. 14–18, Oct. 1999, Available: https://europepmc.org/article/med/10604263, PMID. 10604263.

[41] J. E. Cortes and R. Pazdur, "Docetaxel," *J. Clin. Oncol.*, vol. 13, no. 10, pp. 2643–2655, 1995, doi: 10.1200/JCO.1995.13.10.2643.

[42] J. Follet *et al.*, "The association of statins and taxanes: an efficient combination trigger of cancer cell apoptosis," *Br. J. Cancer*, vol. 106, no. 4, pp. 685–692, Feb. 2012, doi: 10.1038/bjc.2012.6.

[43] C. J. Lovitt, T. B. Shelper, and V. M. Avery, "Advanced cell culture techniques for cancer drug discovery," *Biology (Basel).*, vol. 3, pp. 345–367, 2014, doi: 10.3390/biology3020345.

[44] A. G. Souza *et al.*, "Comparative assay of 2d and 3d cell culture models: proliferation, gene expression and anticancer drug response," *Curr. Pharm. Des.*, vol. 24, no. 15, pp. 1689–1694, May 2018, doi: 10.2174/1381612824666180404152304.

[45] H. Karlsson, M. Fryknäs, R. Larsson, and P. Nygren, "Loss of cancer drug activity in colon cancer HCT-116 cells during spheroid formation in a new 3-D spheroid cell culture system," *Exp. Cell Res.*, vol. 318, no. 13, pp. 1577–1585, Aug. 2012, doi: 10.1016/J.YEXCR.2012.03.026.

[46] K. Räsänen and A. Vaheri, "Activation of fibroblasts in cancer stroma," *Experimental Cell Research*, vol. 316, no. 17, pp. 2713–2722, Oct. 2010, doi: 10.1016/j.yexcr.2010.04.032.

[47] A. P. Thrift and H. B. El-Serag, "Burden of gastric cancer," *Clin. Gastroenterol. Hepatol.*, vol. 18, no. 3, pp. 534–542, Mar. 2020, doi: 10.1016/j.cgh.2019.07.045.

[48] A. Ocana, A. Pandiella, L. L. Siu, and I. F. Tannock, "Preclinical development of molecular-targeted agents for cancer," *Nat. Rev. Clin. Oncol.,* vol. 8, no. 4, pp. 200–209, Apr. 2011, doi: 10.1038/nrclinonc.2010.194.

[49] M. Zanoni *et al.*, "3D tumor spheroid models for in vitro therapeutic screening: a systematic approach to enhance the biological relevance of data obtained OPEN," *Sci. Rep.*, vol. 6, Jan. 2015, doi: 10.1038/srep19103.

[50] A. Riedl *et al.*, "Comparison of cancer cells in 2D vs 3D culture reveals differences in AKT-mTOR-S6K signaling and drug responses," *J. Cell Sci.,* vol. 130, no. 1, pp. 203-218, Jan. 2017, doi: 10.1242/jcs.188102.

[51] C. Wenzel et al., "3D high-content screening for the identification of compounds that target cells in dormant tumor spheroid regions," *Exp. Cell Res.*, vol. 323, no. 1, pp. 131–143, Apr. 2014, doi: 10.1016/J.YEXCR.2014.01.017.

[52] S. Ghosh *et al.*, "Three-dimensional culture of melanoma cells profoundly affects gene

expression profile: A high density oligonucleotide array study," *J. Cell. Physiol.*, vol. 204, no. 2, pp. 522–531, Aug. 2005, doi: 10.1002/jcp.20320.

[53] S. L'Espérance, M. Bachvarova, B. Tetu, A. M. Mes-Masson, and D. Bachvarov, "Global gene expression analysis of early response to chemotherapy treatment in ovarian cancer spheroids," *BMC Genomics*, vol. 9, no. 1, pp. 1–21, Feb. 2008, doi: 10.1186/1471-2164-9-99.

[54] Y. Imamura *et al.*, "Comparison of 2D- and 3D-culture models as drug-testing platforms in breast cancer," *Oncol. Rep.*, vol. 33, no. 4, pp. 1837–1843, Apr. 2015, doi: 10.3892/or.2015.3767.

[55] P. Longati *et al.*, "3D pancreatic carcinoma spheroids induce a matrix-rich, chemoresistant phenotype offering a better model for drug testing," *BMC Cancer*, vol. 13, Feb. 2013, doi: 10.1186/1471-2407-13-95.

[56] D. S. Tan, R. Agarwal, and S. B. Kaye, "Mechanisms of transcoelomic metastasis in ovarian cancer," *Lancet Oncology*, vol. 7, no. 11, pp. 925–934, Nov. 2006, doi: 10.1016/S1470-2045(06)70939-1.

[57] B. Krušlin, M. Ulamec, and D. Tomas, "Prostate cancer stroma: An important factor in cancer growth and progression," *Bosn. J. Basic Med. Sci.,* vol. 15, no. 2, 2015, doi: 10.17305/bjbms.2015.449.

[58] H. Shoval et al., "Tumor cells and their crosstalk with endothelial cells in 3D spheroids," *Sci. Rep.*, vol. 7, no. 1, pp. 1–11, Sep. 2017, doi: 10.1038/s41598-017-10699-y.

[59] B. W. Huang and J. Q. Gao, "Application of 3D cultured multicellular spheroid tumor models in tumor-targeted drug delivery system research," *J. Control. Release*, vol. 270, pp. 246–259, Jan. 2018, doi: 10.1016/J.JCONREL.2017.12.005.

[60] R. Straussman *et al.*, "Tumour micro-environment elicits innate resistance to RAF inhibitors through HGF secretion," *Nature*, vol. 487, no. 7408, pp. 500–504, Jul. 2012, doi: 10.1038/nature11183.

[61] T. Eder *et al.*, "Cancer-associated fibroblasts modify the response of prostate cancer cells to androgen and anti-androgens in three-dimensional spheroid culture," *Int. J. Mol. Sci.*, vol. 17, no. 9, p. 1458, Sep. 2016, doi: 10.3390/ijms17091458.

[62] O. I. Hoffmann, C. Ilmberger, S. Magosch, M. Joka, K. W. Jauch, and B. Mayer, "Impact of the spheroid model complexity on drug response," *J. Biotechnol.*, vol. 205, pp. 14–23, Jul. 2015, doi: 10.1016/j.jbiotec.2015.02.029.

[63] N. Yang *et al.*, "A co-culture model with brain tumor-specific bioluminescence demonstrates astrocyte-induced drug resistance in glioblastoma," *J. Transl. Med.*, vol. 12, no. 1, p. 278, Dec. 2014, doi: 10.1186/s12967-014-0278-y.

[64] S. Goulitquer *et al.*, "Consequences of blunting the mevalonate pathway in cancer identified by a pluri-omics approach," *Cell Death Dis.*, vol. 9, no. 7, p. 745, Jul. 2018, doi: 10.1038/s41419-018-0761-0.

[65] C. Pourreyron *et al.*, "Age-dependent variations of human and rat colon myofibroblasts in culture: Influence on their functional interactions with colon cancer cells," *Int. J.*

Cancer, vol. 104, no. 1, pp. 28–35, Mar. 2003, doi: 10.1002/ijc.10898.

Acknowledgments: We thank Dr Olivier Mignen and Christophe Brigaudeau for giving access to the IncuCyte™ live imaging and analysis system. We thank Dr Gaelle Marenne for her help with statistical analysis and Pr Pascale Marcorelles for giving us access to the technical facility and support of the Pathological Anatomy and Cytology Department. George Alzeeb received a fellowship from Brest University ("Contrat Doctoral d'Etablissement"). This work was supported by grants from the INSERM, from Brest University and from the Ligue Contre le Cancer, Comité du Finistère (n° RAB18153NNA and n° RAB19101NNA to Catherine Le Jossic-Corcos and Laurent Corcos, respectively) and from the ERAPerMed GRAMMY project IRSTB111/L3P2131. Laurent Corcos was partially appointed by Brest University Hospital.

Author Contributions: Conceptualization, GA, LC and CLJC; Investigation, GA, DA, VT, MT and CLJC; Methodology, GA; Supervision, LC and CLJC; Writing – original draft, GA; Writing – review & editing, LC, CLJC.

Disclosures: The authors declare no conflicts of interest.

IV.3. General Conclusions

Cancer cells have the peculiarity to become rapidly resistant to single therapeutic agents. Combinations of drugs targeting different pathways can provide a more lasting benefit against tumor cells. However, it takes an average of 15 years and 800 million US Dollars to develop a novel drug targeting additional pathways in cancer cells. In this work, we proposed a drug repurposing approach based on the use of a non-oncological drug, lovastatin, in combination with a chemotherapeutic agent, docetaxel, to treat GC cell lines.

It is now clear that small improvements in predictive preclinical models can result in large progress in drug discovery. Standard 2D cell cultures have contributed to the development of many cancer therapies, but this model, by and large, fails to resume tumor complexity and pathophysiology. This may be one of the most important causes that mitigates the rate of cancer drugs entering early clinical trials. Novel preclinical models, such as 3D cultures described in this work, are likely more predictive than standard 2D cultures for molecule-based cancer therapy research. In addition, culturing cells in 3D modifies their sensitivity to cytotoxic agents and usually makes them more resistant to treatment compared to cells in 2D cultures.

Recently, high-throughput image microscopy has been developed as a powerful method for measuring drug effects on the size and viability of spheroids. Standard automation equipment available for high-throughput screening could facilitate the practical implementation of such models.

It is important to use real-time monitoring of 3D tumor spheroids growth, viability and apoptosis to validate optimal drugs. Indeed, 3D-based screening assays likely improve the efficiency of drug screening. The combined used of a repurposed drug, such as lovastatin, deserves much consideration. One potential advantage of the combination therapy with lovastatin and docetaxel is its potential as an innovative anti-cancer strategy against GC. Taken altogether, our data advocate in favor of associating lovastatin with docetaxel in the treatment of patients with GC.

Version en français

Les cellules cancéreuses ont la particularité de devenir rapidement résistantes à des agents thérapeutiques uniques. Des combinaisons de médicaments ciblant différentes voies peuvent offrir un avantage plus durable contre les cellules tumorales. Cependant, il faut en moyenne 15 ans et 800 millions de dollars américains pour développer un nouveau médicament ciblant des voies supplémentaires dans les cellules cancéreuses. Dans ce travail, nous avons proposé une approche de repositionnement thérapeutique basé sur l'utilisation d'un médicament non oncologique, la lovastatine, en combinaison avec un agent chimiothérapeutique, le docétaxel, pour traiter les lignées cellulaires de cancer gastrique.

Il est maintenant clair que de petites améliorations dans les modèles précliniques prédictifs peuvent entraîner de grands progrès dans la découverte de médicaments. Les cultures cellulaires 2D ont contribué au développement de nombreuses thérapies anticancéreuses, mais ce modèle ne parvient pas à reproduire la complexité et la physiopathologie de la tumeur. C'est peut-être l'une des causes les plus importantes qui diminue le taux de médicaments anticancéreux entrant dans les premiers essais cliniques. Les nouveaux modèles précliniques, telles que les cultures 3D décrites dans ce travail, sont probablement plus prédictifs que les cultures 2D pour la recherche de nouvelles thérapies du cancer. De plus, la culture des cellules en 3D modifie leur sensibilité aux agents cytotoxiques et les rend généralement plus résistantes au traitement par rapport aux cellules en cultures 2D.

Récemment, la microscopie d'image à haut débit a été développée comme une méthode puissante pour mesurer les effets des médicaments sur la taille et la viabilité des sphéroïdes. L'équipement d'automatisation standard disponible pour le criblage à haut débit pourrait faciliter la mise en œuvre pratique de tels modèles.

Il est important d'utiliser le suivi en temps réel de la croissance, de la viabilité et de l'apoptose des sphéroïdes tumoraux 3D pour valider les composés médicamenteux optimaux, permettant une meilleure caractérisation des effets des médicaments. L'utilisation combinée d'un médicament repositionné, telle que la lovastatine, mérite qu’on y prête attention, nos données plaidant en faveur de l'association de lovastatine et de docétaxel dans le traitement des patients atteints de cancer gastrique.

Chapter V
Gastric Cancer Multicellular Spheroids Analysis by Two-Photon Microscopy

V.1. General Introduction

This chapter presents the second research work from this thesis. It was performed in collaboration with the OPTIMAG Team from Brest University. It aims at analyzing the organization of gastric cancer (GC) spheroids, especially in bicellular models, using bi-photonic microscopy. The obtained results were assembled in a research paper and is in revision for publication in *Biomedical Optics Express* journal (*January 2022*).

The results will be shown under their submission form to the journal, including different parts of the article: introduction, discussion, materials and method, supplementary data and references in the section below*: V.2. Research Article 2.*

Aim of this work

Fibroblasts are among the most important stromal signaling partners found within the various forms of cancers (see Chapter II). It has been traditionally difficult to develop co-cultures of cells in order to study the role of direct interactions between cancer cells and stromal cells. The developments of 3D cell culture models have facilitated culturing different cell types in the same environment. In recent years, both the culture of cancer cells in 3D and their culture with other cell types have been described in various studies (see Chapter III).

In the present work, we developed bicellular spheroids from GC cells and cancer-associated fibroblasts (CAF). We report on their structural organization by 3D imaging using laser microscopy.

While live 3D high-resolution microscopy techniques are rapidly developing, their use in biological applications is limited by practical difficulties. Here, we propose a simple method to determine the spatial organization of cells contained in spheroids with easy manipulation steps adapted to live 3D bio-imaging. We developed an imaging slide based on a hanging-drop method that can be readily implemented in the lab.

Clarifying spatial patterning of spheroids formed from different cell types would enable physiologically relevant GC co-culture models to be created for a better understanding of GC

biology and selecting improved therapies. The focus of this work is thus to understand the self-organization of cells in 3D.

3D imaging

The common sentence "*seeing is believing"* is often cited when we try to understand new phenomena in cell physiology. Optical 3D microscopy plays a central role in biology allowing sample imaging at high spatial resolution and providing the opportunity to detect structures in depth. Fluorescence imaging is one of the most widely used imaging technologies in the biomedical field [1]. Using a variety of fluorescent indicators that can be personalized with specificity to target proteins or lipids was the biggest step through to survey cell physiology. It presents multiple advantages such as multiple signal acquisition capability and high sensitivity. Briefly, the process of fluorescence involves the absorption of light energy (photon) by an indicator followed by the emission of part of this light energy (as another photon) a few nanoseconds later. The emitted photon has less energy than the absorbed one because some energy is lost in this process. The separation of absorbed and emitted light is achieved by the use of optical filters selected with respect to the indicators being used [2].

However, a certain challenge persists due to restricted tissue penetration depth. Certain tools to overcome these limitations exist. During this thesis, we used the two-photon microscopy, which is a fluorescence imaging technique that allows imaging of 3D structures. Unlike traditional fluorescence microscopy, two-photon imaging requires excitation with longer wavelengths than the emitted light using near-infrared excitation light that reduces scattering in the biological sample. This process can only be achieved by having a very high spatial and temporal density of photons, because the two absorbed photons must arrive simultaneously onto the sample. This requires a relatively specialized, high-powered, pulsed laser. Due to the multi-photon absorption, the background signal is strongly suppressed. The excitation lasers used are absorbed and scattered in 3D samples to a lesser extent compared to visible light, enabling the imaging of deeper portions of the structure. Two-photon microscopy is a superior alternative to standard confocal microscopy since it enables efficient light detection and deeper tissue penetration that is important for imaging 3D structures with high thickness [3].

The interest in using two-photon microscopy is the possibility to image cells based on their endogenous fluorophores in long-term studies of living cells (auto-fluorescence or stable fluorescent protein transfection). In addition, it provides the possibility to image stained samples and to detect the second harmonic generation (SHG) of certain biological structures such as collagen [4]. Two-photon microscopy can thus perform precise, multicolor fluorescence imaging that is useful for thin living samples and *in vitro* cultured cells [5].

During this work, we applied the two-photon microscopy methodology to study the organization of our 3D culture model generated by cancer cell lines and cancer associated fibroblasts.

References

[1] L. Bacic, A. Sabantsev, and S. Deindl, “Recent advances in single-molecule fluorescence microscopy render structural biology dynamic,” *Curr. Opin. Struct. Biol.*, vol. 65, pp. 61–68, Dec. 2020, doi: 10.1016/J.SBI.2020.05.006.

[2] M. J. Sanderson, I. Smith, I. Parker, and M. D. Bootman, “Fluorescence Microscopy,” *Cold Spring Harb. Protoc.*, vol. 2014, no. 10, Oct. 2014, doi: 10.1101/PDB.TOP071795.

[3] T. Nemoto, R. Kawakami, T. Hibi, K. Iijima, and K. Otomo, “Two-photon excitation fluorescence microscopy and its application in functional connectomics,” *Microscopy*, vol. 64, no. 1, pp. 9–15, Feb. 2015, doi: 10.1093/JMICRO/DFU110.

[4] Y. J. Hwang *et al.*, “Multi-photon imaging of actin filament formation and mitochondrial energetics of human acbt gliomas,” *Photochem. Photobiol.*, vol. 87, no. 2, p. 408, Mar. 2011, doi: 10.1111/J.1751-1097.2010.00873.X.

[5] M. Drobizhev, N. S. Makarov, S. E. Tillo, T. E. Hughes, and A. Rebane, “Two-photon absorption properties of fluorescent proteins,” *Nat. Methods*, vol. 8, no. 5, p. 393, May 2011, doi: 10.1038/NMETH.1596.

Version en Français

Ce chapitre présente le deuxième travail de recherche de ma thèse. Il a été réalisé en collaboration avec l'équipe OPTIMAG de l'Université de Brest. Il s'intéresse à l'analyse de l'organisation des sphéroïdes de cancer gastrique notamment dans le modèle bicellulaire en utilisant la microscopie bi-photonique. Les résultats obtenus ont été rassemblés dans un article de recherche qui est en révision pour publication dans le journal *Biomedical Optics Express* journal (*Janvier 2022*).

Les résultats seront présentés sous leur forme de soumission au journal, comprenant différentes parties de l'article : introduction, discussion, matériel et méthodes, données supplémentaires et références dans la section ci-dessous : *V.2. Research Article 2*.

Objectif de ce travail

Les fibroblastes sont parmi les plus importants partenaires de signalisation stromale que l'on retrouve dans les différentes formes de cancers (voir chapitre II). Il n'est pas toujours aisé de réaliser des modèles de co-cultures de cellules afin d'étudier le rôle des interactions directes entre les cellules cancéreuses et les cellules stromales. Le développement de modèles de culture cellulaire en 3D a facilité la culture de différents types de cellules dans le même environnement. Ces dernières années, la culture de cellules cancéreuses en 3D et leur culture avec d'autres types de cellules ont été décrites dans diverses études (voir chapitre III).

Dans le présent travail, nous avons développé des sphéroïdes bicellulaires à partir de cellules de cancer gastrique et de fibroblastes associés au cancer (CAF). Nous avons étudié leur organisation structurelle par imagerie 3D en utilisant la microscopie bi-photonique.

Bien que les techniques de microscopie 3D en direct à haute résolution se développent rapidement, leur utilisation dans des applications biologiques est limitée par des difficultés pratiques. Ici, nous proposons une méthode simple pour déterminer l'organisation spatiale des cellules contenues dans des sphéroïdes avec des étapes de manipulation faciles et adaptées à la bio-imagerie 3D en direct. Nous avons mis en place une lame d'imagerie basée sur une méthode de suspension qui peut être facilement mise en œuvre dans le laboratoire.

La démonstration de la configuration spatiale des sphéroïdes formés à partir de différents types de cellules permettrait de créer des modèles de co-culture de cancer gastrique physiologiquement pertinents pour mieux comprendre la biologie de ces cancers et sélectionner des thérapies améliorées. L'objectif de ce travail est donc de comprendre l'auto-organisation des cellules en 3D.

Imagerie en 3D

Le proverbe "voir, c'est croire" est souvent cité lorsque nous essayons de comprendre de nouveaux phénomènes en physiologie cellulaire. La microscopie optique 3D joue un rôle central en biologie, permettant l'imagerie d'échantillons à haute résolution spatiale et offrant la possibilité de détecter des structures en profondeur. L'imagerie par fluorescence est l'une des technologies d'imagerie les plus utilisées dans le domaine biomédical. L'utilisation d'une variété d'indicateurs fluorescents qui peuvent être personnalisés pour cibler spécifiquement des protéines ou des lipides a été le plus grand pas en avant pour étudier la physiologie cellulaire. Elle présente de multiples avantages tels que la capacité d'acquisition de signaux multiples et une sensibilité élevée. En bref, le processus de fluorescence implique l'absorption d'énergie lumineuse (photon) par un indicateur, suivie de l'émission d'une partie de cette énergie lumineuse (sous forme d'un autre photon) quelques nanosecondes plus tard. Le photon émis a moins d'énergie que le photon absorbé car une partie de l'énergie est perdue dans ce processus. La séparation de la lumière absorbée et de la lumière émise est obtenue par l'utilisation de filtres optiques sélectionnés en fonction des indicateurs utilisés.

Cependant, un certain défi persiste en raison de la profondeur de pénétration limitée des tissus associée à cette technique. Certains outils permettant de surmonter ces limitations existent. Au cours de cette thèse, nous avons utilisé la microscopie à deux photons, qui est une technique d'imagerie par fluorescence permettant l'imagerie de structures 3D. Contrairement à la microscopie à fluorescence traditionnelle, l'imagerie à deux photons nécessite une excitation avec des longueurs d'onde plus grandes que la lumière émise en utilisant une lumière d'excitation proche de l'infrarouge qui réduit la diffusion dans l'échantillon biologique. Ce processus ne peut être réalisé qu'en ayant une très haute densité spatiale et temporelle de photons, car les deux photons absorbés doivent arriver simultanément sur l'échantillon. Cela nécessite un laser pulsé relativement spécialisé et de

grande puissance. En raison de l'absorption multi-photonique, le signal de fond est fortement supprimé. Les lasers d'excitation utilisés sont absorbés et diffusés dans les échantillons 3D dans une moindre mesure par rapport à la lumière visible, ce qui permet d'imager des parties plus profondes de la structure. La microscopie à deux photons est une alternative supérieure à la microscopie confocale standard car elle permet une détection efficace de la lumière et une pénétration plus profonde des tissus, ce qui est important pour l'imagerie de structures 3D très épaisses.

L'intérêt de l'utilisation de la microscopie à deux photons tient à la possibilité d'imager des cellules en fonction de leurs fluorophores endogènes dans le cadre d'études à long terme de cellules vivantes (autofluorescence ou transfection de protéines fluorescentes stables). En outre, elle permet d'imager des échantillons colorés et de détecter la génération de seconde harmonique (SHG) de certaines structures biologiques telles que le collagène. La microscopie à deux photons peut donc réaliser une imagerie de fluorescence précise et multicolore, utile pour les échantillons vivants minces et les cellules cultivées *in vitro*.

Au cours de ce travail, nous avons appliqué la méthodologie de la microscopie à deux photons pour étudier l'organisation de notre modèle de culture 3D généré par des lignées de cellules cancéreuses et des fibroblastes associés au cancer.

V.2. Research Article 2: Gastric Cancer Multicellular Spheroids Analysis by Two-Photon Microscopy

Authors: George Alzeeb[1], Matthieu Dubreuil[2*], Danielle Arzur[1], Sylvain Rivet[2], Laurent Corcos[3,4], Yann Le Grand[2,a] and Catherine Le Jossic-Corcos[1,a]

[1]Université de Bretagne Occidentale, Genetics, functional genomics and biotechnology INSERM UMR 1078, IBSAM, 22 avenue Camille Desmoulins, Brest, 29238, France
[2]Université de Bretagne Occidentale, Laboratory of Optics and Magnetism OPTIMAG EA 938, IBSAM, 6 avenue Le Gorgeu, Brest, 29238, France
[3]Inserm, Univ Brest, EFS, UMR 1078, GGB, F-29200 Brest, France
[4]CHU de Brest, INSERM, Univ Brest, EFS, UMR 1078, GGB, F-29200 Brest, France
**Correspondence:* matthieu.dubreuil@univ-brest.fr
[a]: Equal contribution

In Revision for publication in the journal 'Biomedical Optics Express': January 2022

Abstract: Gastric cancer (GC) is highly deadly, despite improved treatment efficacy. Early therapeutic developments partly relied on *in vitro* cell systems grown in two-dimensions (2D). However, it has become clear that the surrounding stromal cell environment may also play a role on cell responses. Cancer-associated fibroblasts (CAF) are one such partner in tumors where they may either promote or restrain the proliferation of epithelial cancer cells, invasion and drug resistance. Recently, three-dimensional (3D) *in vitro* culture systems, known as spheroids, have been developed to circumvent some of the limits of 2D cell models. We established a standardized procedure for establishing monocellular spheroids from HGT-1 and AGS human gastric cancer cell lines, and bicellular spheroids of HGT-1 or AGS cells mixed with human primary CAF in a scaffold-free setting. To analyze spheroid spatial organization, we used two-photon microscopy, enabling large depth imaging of uncleared samples and providing low photodegradation. These bicellular associations made the cells firmly attached to each other, generating compact spheroids. While CAF in AGS/CAF spheroids clustered in the center of the spheroids, they were dispersed throughout in HGT-1/CAF spheroids. Such differences may reflect clonal specificities of these GC cell lines and/or the differential influence of CAF on 3D organization.

This article will be presented in this thesis as its submitted format to Biomedical Optics Express.

1. Introduction

Gastric cancer (GC) represents the fifth most common malignancy in the world and the third leading cause of cancer-related deaths in both sexes. It is often diagnosed at a late stage; hence it is a highly deadly disease [1]. Consequently, it is mandatory to develop novel therapeutic strategies aimed at identifying early disease and drug-response markers. One approach to this need is to use three-dimensional (3D) culture models, such as spheroids [2,3]. Indeed, tumor complexity and direct pathophysiology relevance are missing in two-dimensional (2D) cell cultures [4]. By contrast, 3D cell culture models make cell-cell interactions possible. Under such conditions, cells are submitted to more realistic oxygen and nutrient gradients. Spheroids were established as a relevant *in vitro* model for drug testing in oncology, due to their ability to reproduce the main features of *in vivo* solid tumors, *i.e.* cellular heterogeneity, cell-cell signaling, growth kinetics, gene expression and drug resistance. In addition, the responses to treatment in 3D models could be closer to *in vivo* situations [5]. 3D tumor spheroids are mostly composed of tumor cells only, thus partially mimic realistic *in vivo* conditions, particularly because of the lack of extra cellular matrix (ECM) deposition and the absence of tumor-stromal cell interactions. Cancer-associated fibroblasts (CAF) are one of the major stromal cell populations in solid tumors. Their role in tumor growth and drug resistance is essential [6,7]. Accordingly, recent studies focus on the analysis of multicellular spheroids as 3D co-culture models associating epithelial cancer cells and CAF [8].

The development of 3D cell culture models has coincided with the progress of 3D optical imaging methods able to fully characterize the spatial organization of cells in 3D with cellular spatial resolution [9]. Among these methods, confocal fluorescence, light-sheet and two-photon microscopies, are powerful techniques enabling, in association with optimized sample preparation processes, high-throughput visualization of spheroids [10]. Confocal fluorescence microscopy [11-14] is the most widespread modality employed to perform depth-resolved structural analysis of spheroids. However, this technique has some limitations for imaging deep layers, typically located at more than a few tens of µm beyond the surface of large spheroids because of strong light scattering. In addition, photo-degradation of the samples due to short excitation wavelengths can make 3D imaging challenging. Optical clearing [12,13] is often used before imaging to reduce light scattering and recover relevant visualization of the interior of the spheroids (up to 150-200 µm beyond the surface) but this requires

additional sample preparation. Light-sheet microscopy [15] is a good alternative to confocal microscopy as it enables visualization in 3D of large spheroids at high speed with low photodamage. However, observation with a light sheet microscope requires laborious sample mounting for light excitation and detection at orthogonal directions. Two-photon microscopy enables reaching larger imaging depth in uncleared samples relative to confocal microscopy and triggers less photodegradation, making it a good compromise for the structural analysis of large spheroids. To this date, only few studies using two-photon microscopy to analyze 3D cell culture models in cancer research have been performed [16-19], and no structural analysis of GC multicellular spheroids made of tumor cells and CAF has been reported, this may be an important limitation of the model. It is known that mechanical forces, which are likely contributed by cell-cell interactions, are also important to drive cancer progression towards metastasis. In this article, we report on the structural analysis by two-photon microscopy of living GC multicellular spheroids made from tumor cells and CAF. We have minimized sample preparation steps and the spheroids were directly manipulated. Imaging was performed at different times after spheroids formation, enabling the monitoring of the organization between CAF and epithelial cancer cells from two different human GC cell lines, HGT-1 and AGS. Strikingly, our results revealed different spatial organizations of tumor cells and CAF according to the GC cell line.

2. Materials and Methods

Cell culture, staining and spheroids formation

HGT-1 and AGS human GC cells were grown at 37°C under a humidified atmosphere with 5% CO_2 in Dulbecco's modified Eagle's medium (DMEM) (Corning, MA, USA), containing 4.5 g/L glucose and supplemented with 5 or 10% fetal bovine serum (FBS) (Gibco-Invitrogen, Cergy-Pontoise, France) without antibiotics (complete medium).

CAF were obtained from a GC patient-ablated tumor after tissue dissociation with collagenase and growth in culture in complete medium with 10% FBS. After about 10 days in culture, no more epithelial cells adhered to the dish and fibroblasts emerged and kept growing. The population that emerged was apparently homogenous and displayed a characteristic fibroblast morphology. The patient had given informed consent and use of tumor-derived cells was granted by the Ethics Committee of Brest University Hospital.

HGT-1 and AGS sub-populations labeled with eGFP (enhanced green fluorescent protein) or TdTomato (red) fluorescent tags, respectively, were generated using lentiviral infection. Briefly, self-inactivating HIV-1-based lentiviral vector, pRRL-sin-MND-GFP-IRES-Puro and pRRL-sin-MND-Tomato-IRES-Puro were purchased from VectUB (vectorology platform, University of Bordeaux, France). The vectors express TdTomato or eGFP under control of the MND promoter and co-express the puromycin resistance gene. Forty thousand cells were infected with lentiviruses (at a multiplicity of infection of 2) and selected with puromycin (1 µg/mL). We obtained eGFP fluorescent HGT-1 populations and TdTomato fluorescent AGS populations.

To generate spheroids, 2D cultured HGT-1, AGS and CAF were collected and seeded (in 200 µL complete medium) in ultra-low attachment (ULA) 96-well round bottom microplates (Corning, Amsterdam, Netherlands) allowing the formation of uniformly sized spheroids in a scaffold-free model. A single spheroid was formed in each well. To obtain the same size range of 6 days-old spheroids, we generated AGS spheroids by seeding 500 cells/well but only 250 cells/well for HGT-1 cells. Incubation for 4 days was sufficient to form tightly packed spheroids (Supplementary Figure V.1).

To obtain bicellular spheroids, cells of each type were added together in 1:1 ratio (250 HGT-1 + 250 CAF or 500 AGS + 500 CAF) in 200 µL complete medium in ULA 96-well round bottom microplates.

Two-photon imaging setup

The imaging setup consisted of a two-photon microscope based on a confocal laser scanning unit (FV300, Olympus) mounted on an upright microscope body (BX51WI, Olympus) and a Ti:Sapphire laser oscillator (Chameleon Vision II, Coherent) that can be tuned between 700 nm and 1050 nm, and equipped with a dispersion pre-compensation unit. Light was focused on the samples by a 20X/0.75NA microscope objective (UPlanSApo, Olympus). The microscope objective has a 0.65 mm working distance and is corrected for 0.17 mm-thick glass coverslips. The lateral and axial resolutions (FWHM) were respectively ~0.5 µm and ~1.7 µm. Two-photon excitation fluorescence (TPEF) light was epi-collected and detected through BG39 bandpass filters and a 570 nm dichroic mirror (FV300, DM570, Olympus) by two internal photomultiplier tubes (R928, Hamamatsu). Channel 1 and 2 were associated to the detection channels placed below ("green") and above ("red") the cut-off frequency of the dichroic mirror (570 nm), respectively. TPEF images were acquired with 12-bit intensity resolution and 1024x1024 pixel definition. The pixel dwell time was set to the maximum value of 8 µs, resulting in an acquisition time of 9.4 s for a 1024x1024 pixel image. The field of view for the images was 710x710 µm. Z-stack acquisitions were made on some samples for 3D rendering with 1 µm step and 512x512x150 pixel definition.

Imaging of spheroids

Two-photon excitation/emission fluorescence spectra of eGFP and TdTomato were taken from [20] and displayed in Supplementary Figure V.2. eGFP exhibits maximum two-photon absorption at 920 nm and produces maximum fluorescence emission around 510 nm. TdTomato exhibits maximum two-photon absorption at 1050 nm and produces maximum fluorescence emission around 580 nm. Cancer-associated fibroblasts (CAF) were not stained because they exhibit strong autofluorescence when excited at 750 nm. In addition, the fluorescence emission spectra of CAF was broad enough to produce, approximately, the same intensity on both detection channels. The following process was thus employed to image HGT-1/CAF and AGS/CAF co-culture spheroids.

For HGT-1/CAF bicellular spheroids, imaging of HGT-1 cells labelled with eGFP was first performed at 920 nm excitation wavelength and fluorescence light was detected on channel 1. At this excitation wavelength, autofluorescence of CAF is negligible. Imaging of CAF was

then realized at 750 nm excitation wavelength and fluorescent light was detected on channel 2 because small residual excitation of eGFP at 750 nm does not produce significant fluorescent light in this channel.

For AGS/CAF bicellular spheroids, imaging of AGS cells stained with TdTomato was first realized at 1000 nm excitation wavelength and fluorescence light was detected on channel 2. At this excitation wavelength, autofluorescence of CAF is also negligible. Imaging of CAF was then realized at 830 nm excitation wavelength and fluorescence light was detected on channel 1 where TdTomato does not produce significant fluorescence light, whereas the autofluorescence from CAF is still conveniently detectable. The excitation wavelength for CAF imaging was not set to 750 nm as for HGT-1/CAF spheroids because for AGS/CAF co-culture, two-photon excitation of higher electronic transitions of TdTomato starts to produce detectable fluorescence signal on both channels (Supplementary Figure V.2).

Laser excitation power was controlled by a Glan polarizer and a zero-order half wave plate (WPHSM05-830, Thorlabs) and was measured at the sample plane with a microscope slide thermal sensor (S175C, Thorlabs). The laser excitation power was adjusted to ~100 mW for all experiments and all excitation wavelengths, which gives the best signal-to-noise ratio in the images, while avoiding photo degradation of the samples. The spheroids were stable enough to ensure successive 3D imaging at two different excitation wavelengths.

Images were displayed while encoding the different cell types in selected false colors that produced optimal contrast. For HGT-1/CAF bicellular spheroids, HGT-1 cells were encoded in green and CAF in yellow. For AGS/CAF bicellular spheroids, AGS cells were encoded in red and CAF in yellow.

A custom process for spheroids deposition was implemented (Figure V.1). Approximately 50 µL of medium containing one spheroid was directly collected by aspiration with a micropipette equipped with a glass tip, and gently deposited onto a 0.17 mm-thick glass coverslip stuck on a metallic slide with a large central empty hole. A plastic cuvette was stuck under the metallic slide in order to avoid liquid evaporation. The slide was then quickly reversed and placed on the microscope translation stage. The spheroid was thus stably maintained in a liquid droplet close to the coverslip, enabling 3D imaging with minimal aberrations. The deposition process for one spheroid takes no longer than 2-3 min. Spheroids were kept under standard culture conditions until exploring time.

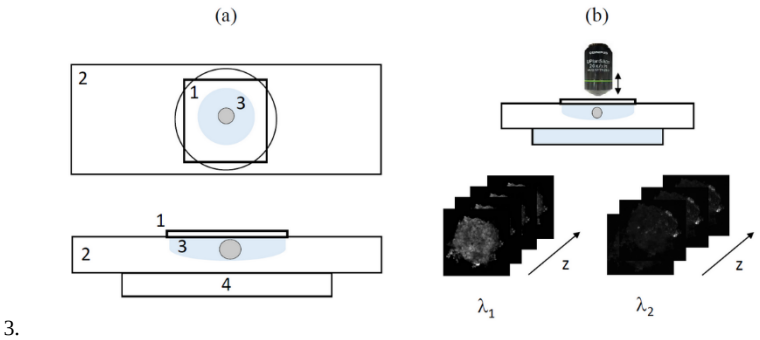

3.

Figure V.1. Process for two-photon imaging of multicellular spheroids.
(a) Schematic representation of the sample holder, composed of 1: 0.17 mm-thick glass coverslip, 2: metallic slide with an central empty hole, 3: liquid, 4: plastic cuvette. The spheroid is represented in gray. (b) 3D image acquisition with the two-photon microscope at two successive excitation wavelengths.

3. Results

HGT-1/CAF spheroids growth monitoring

HGT-1 cancer cells labelled with e-GFP were seeded alone or with CAF in ULA plates, and spheroids growth, structure and organization were analyzed over time. Spheroids were initiated at day 0 and were used successively at each time point (4, 6, 8 and 11 days thereafter) for imaging. They were manipulated and imaged readily without any additional fixation or staining steps. Spheroid images showed single plane TPEF images taken 40 to 50 µm from the top of the spheroid (Figure V.2 and Figure V.3). The growth of CAF was much slower, compared to that of HGT-1 cells, hence bicellular spheroids were mainly composed of GC cells after 4 days of culture. We explored the effects of different ratios of GC cells to CAF: 1:1, 1:2, 1:5 and 1:9 on the growth of spheroids. Spheroid organization was similar between all cell ratios. Therefore, we fixed the ratio to 1:1. Bicellular HGT-1/CAF spheroids were more densely packed in comparison to monocellular HGT-1 spheroids at each time point, from 4 to 11 days after spheroid initiation (Figure V.2, Supplementary Figure V.3). The count of eGFP-labelled HGT-1 cells, recovered from mono- or bicellular spheroids, showed no significant difference between both types of spheroids at the same age (Supplementary Figure V.4). Bi-photonic depth imaging of living 4 and 6 days-old HGT-1/CAF spheroids showed a characteristic spatial cell organization with CAF in a crown around the compacted HGT-1 cells and somewhat dispersed in between them (Figure V.2 and Figure V.3). CAF were less present in 8 days-old HGT-1/CAF spheroids, while virtually no more CAF could be seen in 11 days-old spheroids.

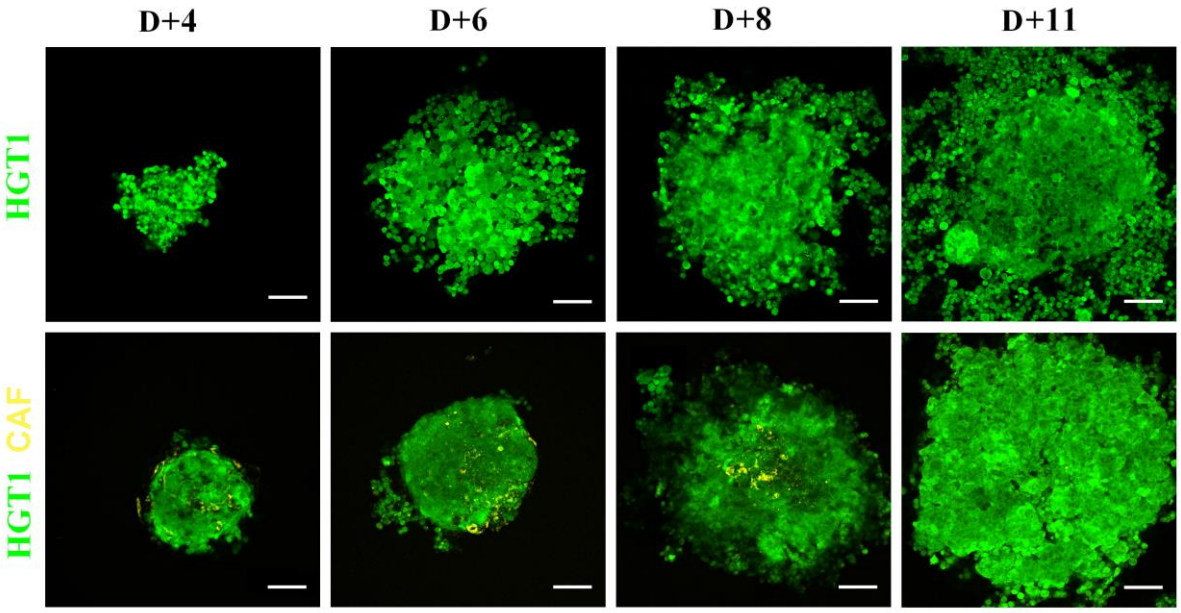

Figure V.2. Single plane TPEF images of HGT-1 and HGT-1/CAF spheroids.
Single plane TPEF images of (upper row) monocellular (HGT-1 cells) and (lower row) HGT-1/CAF spheroids at different days (D) after initiation of spheroid formation. HGT-1 cells were labelled with eGFP and appear in green. CAF were detected from their autofluorescence and appear in yellow. Imaging planes were typically located between 40 to 50 µm beyond the top of the spheroids. Scale bar : 100µm.

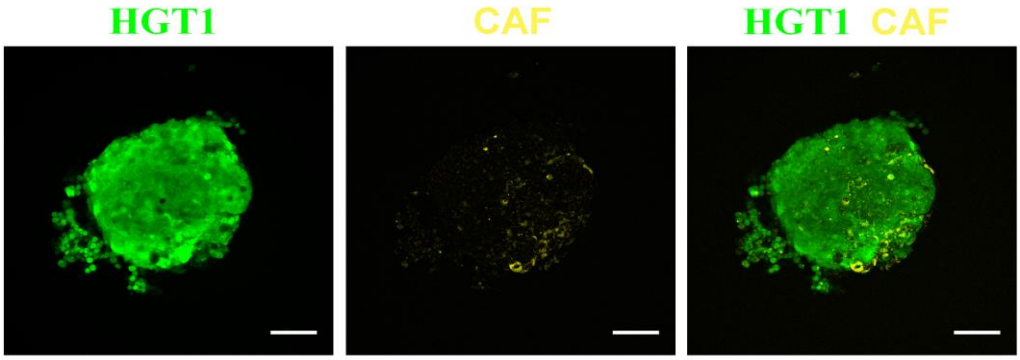

Figure V.3. Single plane TPEF images of HGT-1 cells and CAF in 6 days-old HGT-1/CAF spheroid.
Left : HGT-1 cells (eGFP display). Middle : CAF (autofluorescence display). Right : both HGT-1 cells and CAF are displayed. Scale bar : 100µm.

AGS/CAF spheroids growth monitoring

We next generated spheroids using the TdTomato-labelled AGS GC cell line. As for HGT-1 cells, AGS cells were seeded alone or with CAF in ULA plates, and spheroids growth, structure and organization were analyzed over time. Spheroid images show single plane TPEF images taken 40 to 50 µm from the top of the spheroid (Figure V.4 and Figure V.5). We next explored the effects of different ratio of AGS cells to CAF: 1:1, 1:2, 1:5 and 1:9 on spheroid's growth and organization. No structural changes were observed between those different ratios. Hence, we fixed the ratio to 1:1 with 500 AGS + 500 CAF. Bicellular AGS/CAF spheroids were very compact compared to monocellular spheroids at each time point, going from 4 to 11 days after spheroid formation (Figure V.4, Supplementary Figure V.3). Like for HGT-1/CAF spheroids, cells from AGS/CAF spheroids were firmly attached to each other and were hard to dissociate by mechanical force. We counted TdTomato-labelled AGS cells recovered from mono- and bicellular spheroids, but we observed no significant difference between both types of spheroids at the same age (Supplementary Figure V.4). Two-photon depth imaging of AGS/CAF spheroids showed a characteristic spatial cell organization with CAF in the central core surrounded by compacted AGS cells (Figure V.4, Figure V.5).

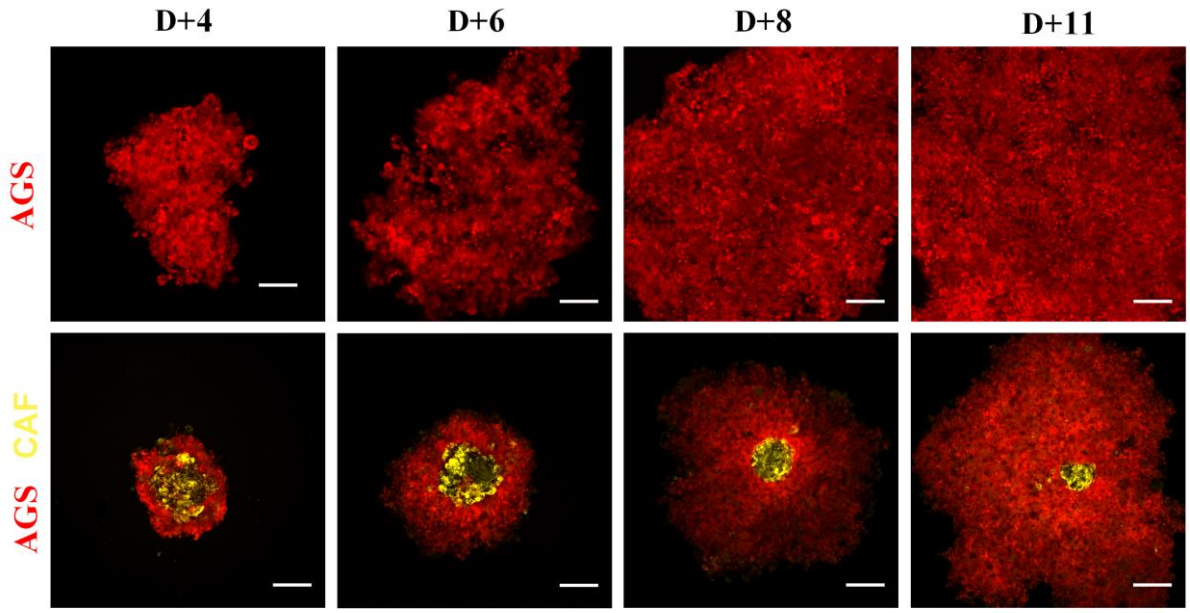

Figure V.4. Single plane TPEF images of AGS and AGS/CAF spheroids.
Single plane TPEF images of AGS spheroids (upper row) and bicellular AGS/CAF spheroids (lower row) at different days (D) after initiation of spheroid formation. AGS cells were labelled with TdTomato and displayed in red. CAF were detected from their autofluorescence and were displayed in yellow. Imaging planes were typically located between 40 to 50 µm beyond the top of the spheroids. Scale bar : 100 µm.

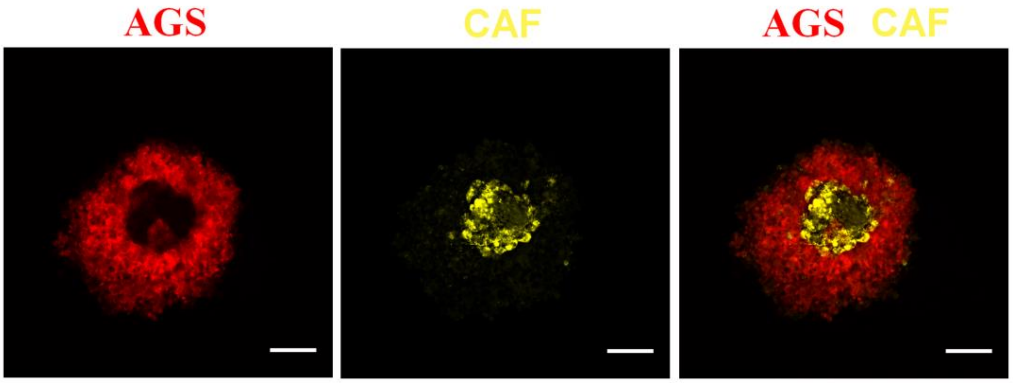

Figure V.5. Single plane TPEF images of AGS cells and CAF in 6 days-old AGS/CAF spheroid. Left : Only TdTomato-labelled AGS cells are displayed. Middle : Only CAF are displayed (autofluorescence). Right : both AGS cells (in red) and CAF (in yellow) are displayed. Scale bar : 100 µm.

3D rendering of spheroids

In order to explore the entire volume of the spheroids, we performed 3D TPEF imaging by acquiring several 512x512 pixel images at different foci incremented by 1 µm. 3D images were reconstructed using the ICY software and are displayed for 6 days-old spheroids (Figure V.6). We were able to generate the 3D shape of the imaged part of the spheroids (Figure V.6 and supplementary data Media 1 and Media 2). However, spheroids contained a large number of aggregated cells and thus produced strong light scattering, resulting in difficulties to image at focus planes above 120 to 170 µm beyond the surface, or about 1/2 to 1/3 of the spheroid lateral dimension. One should also note that the spheroids could not keep their regular spherical shape because of the manipulation and deposition process on the microscope slide. Nerveless, without clearing manipulation, we can image 3D spheroid and report cells self-organization in such structure. Figure V.6(a) and supplementary data Media 1 confirms the organization of CAF in bi-cellular HGT-1/CAF spheroids, located in crown of a densely packed cancer cell spheroid, as revealed by single plane imaging (Figure V.5). Supplementary Media 2 confirms the organization of CAF in bicellular AGS/CAF spheroids, located in a central core with cancer cell around it. This organization was not revealed by Figure V.6(b) because the core of CAF is located beneath the surface of the spheroid.

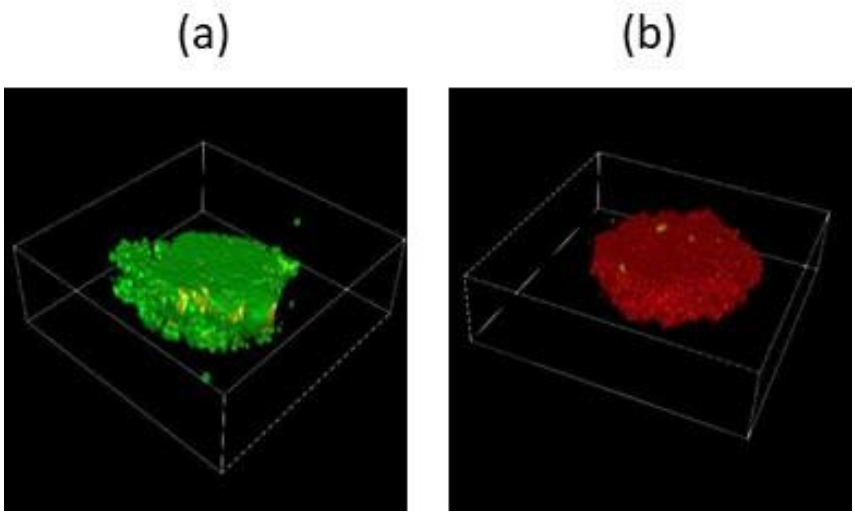

Figure V.6. 3D representation of bicellular spheroids.
(a) HGT-1/CAF: HGT-1 cells were displayed in green (eGFP). (b) AGS/CAF: AGS cells were displayed in red. CAF were displayed in yellow. The size of the boxes are (a) 710x710x170 µm and (b) 710x710x120 µm.

Infiltration assay

In order to endorse the different spatial cell distributions between GC cell lines, we performed an infiltration assay. Monocellular CAF spheroids were first generated. After 6 days, CAF spheroids were formed and 250 HGT-1 cells or 500 AGS cells were added. Spheroid organization was analyzed by bi-photonic depth imaging after 6 days. Images showed the characteristic spatial cell organization of dispersed CAF between HGT-1 cells (Figure V.2), whereas AGS cells surrounded CAF spheroids (Figure V.7), as observed during the formation of AGS/CAF spheroids in (Figure V.4).

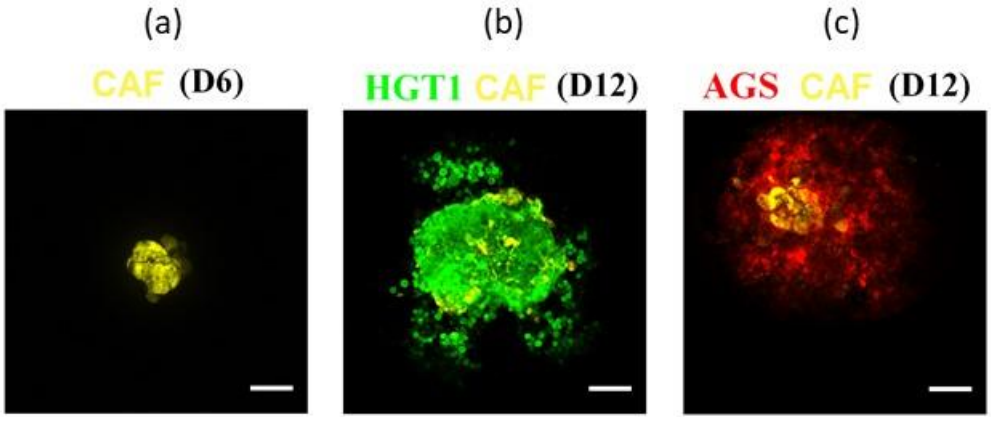

Figure V.7. Spheroids infiltration assay.
Single plane TPEF images of : (a) monocellular CAF spheroids 6 days after the beginning of spheroid formation (CAF were detected by their autofluorescence and displayed in yellow); (b) bicellular HGT-1/CAF spheroids 6 days after addition of HGT-1 cells to 6 days-old CAF spheroids (HGT-1 cells were labelled with eGFP and displayed in green and CAF were detected from their autofluorescence and displayed in yellow); (c) bicellular AGS/CAF spheroids 6 days after addition of AGS cells to 6-days old CAF spheroids (AGS cells were labelled with TdTomato and displayed in red and CAF were detected from their autofluorescence and displayed in yellow). Imaging planes were typically located between 40 to 50 µm beyond the top of the spheroids. Scale bar : 100 µm.

4. Discussion

Cancer cells are strongly influenced by their microenvironment, which modulates local tumor progression and metastasis, and has a significant impact on drug response [21-22]. CAF are one of the major types of stroma cells and play a crucial role in tumor development and survival [23], through their ability to express a variety of growth factors promoting cancer cell proliferation and mediating modifications in ECM composition [24]. The drug resistance phenotype acquired by solid tumors may result, at least in part, from interactions between CAF and tumor cells, which makes the epithelial cancer cells-CAF interaction a promising target for GC therapy [25].

Standard 2D cell cultures have contributed to the development of many cancer therapies. However, this model lacks tumor complexity and direct pathophysiology relevance, which may be one of the main causes of the poor rate of cancer drugs entering early clinical trials, and becoming marketed drugs [26]. Novel preclinical models, such as 3D cell cultures, can reproduce key factors of tumors, such as cellular organization and cell-cell interactions, and may be more predictive than 2D cell cultures for cancer therapy research [27]. Co-cultured spheroids provide even a closer resemblance to the *in vivo* tumors [28]. Aiming to explore such a model, we have developed here a 3D co-culture model of epithelial GC cells and CAF well suited to perform 3D optical imaging. Since several optical systems suffer from photodegradation or optical clearing and depend on sample preparation, we set up a simplified method to monitor growth and organization of live spheroids. We used two-photon microscopy, a non-invasive imaging technique well suited to analyze spheroid development and structure in an automated medium-throughput format [29]. Indeed, two-photon fluorescence microscopy generates higher signal-to-noise ratio images, compared to classical confocal fluorescence microscopy, by reducing excitation attenuation and background signals due to the multiphoton absorption process. The low phototoxicity permits longer exposure times that are mandatory for 3D imaging of multicellular spheroids. Applying this method, we were able to image samples containing two different cell types without any additional manipulation.

In this study, we have generated spheroids in a scaffold-free model, using two different human GC cell lines, carrying a specific fluorescent marker, in combination with human primary CAF that are naturally auto-fluorescent. Scaffold-free models make cultures independent of

matrixes (natural hydrogels or synthetic polymers) that have several disadvantages like somewhat uncontrollable composition, a poor reproducibility, and the difficulty to access and harvest single spheroids. These limitations require additional treatments (chemical or physical), which are often time consuming [2]. The organization of single cells within the spheroid itself remain ill defined, due to the lack of amenability for in-depth microscopy of such opaque structures.

Our results showed that this approach was appropriate to monitor spheroids growth and structural evolution between day 4 and day 11. It also appeared that cells from bicellular spheroids were more tightened, generating more compact spheroids than single cell type spheroids (Figure V.2, Figure V.4 and Supplementary Figure V.3). Interestingly, we observed a different spatial distribution of cells between GC cell lines. In HGT-1/CAF spheroids, a more diffuse distribution of HGT-1 cells was observed with a domination of CAF at the periphery, both when the two cell types were mixed at the beginning or when HGT-1 cells were added when CAF spheroids were already assembled. In contrast, in AGS/CAF spheroids, fibroblasts were concentrated in the central zone leaving cancer cells at the periphery, as previously reported in the context of breast cancer [30]. When added after CAF spheroids were formed, AGS cells also stayed on the surface like when added at the same time with CAF (Figure V.7). Such distinctive behaviors of both cell lines are suggestive of a different migratory / invasive and malignant potential of these GC cell lines, as reported for other tumor cells [30]. In favor of this hypothesis, experiments conducted in 2D cultures showed a stronger ability of HGT-1 cells to repair a scratch in a wound-healing assay than AGS cells (data not shown). This difference could be explained by distinct propensities to undergo epithelial-to-mesenchymal transition progression [31].

Three-D multicellular tumor models, with the co-culture of cancer and stromal cells, have proven well suited to study tumor microenvironments. However, technical complexities restrict the exploration of such models. We used here two-photon fluorescence microscopy to analyze the spatial organization of bicellular spheroids from two different GC lines, which showed marked differences in structure and behavior when combined with CAF. Two-photon microscopy could also be used in additional applications, such as real-time monitoring of drug response of 3D tumor spheroids. We surmise that such approaches could be applied as well to organoids, *in vitro* 3D culture models assembled from patients' primary cancer cells [32].

5. Supplementary Figures

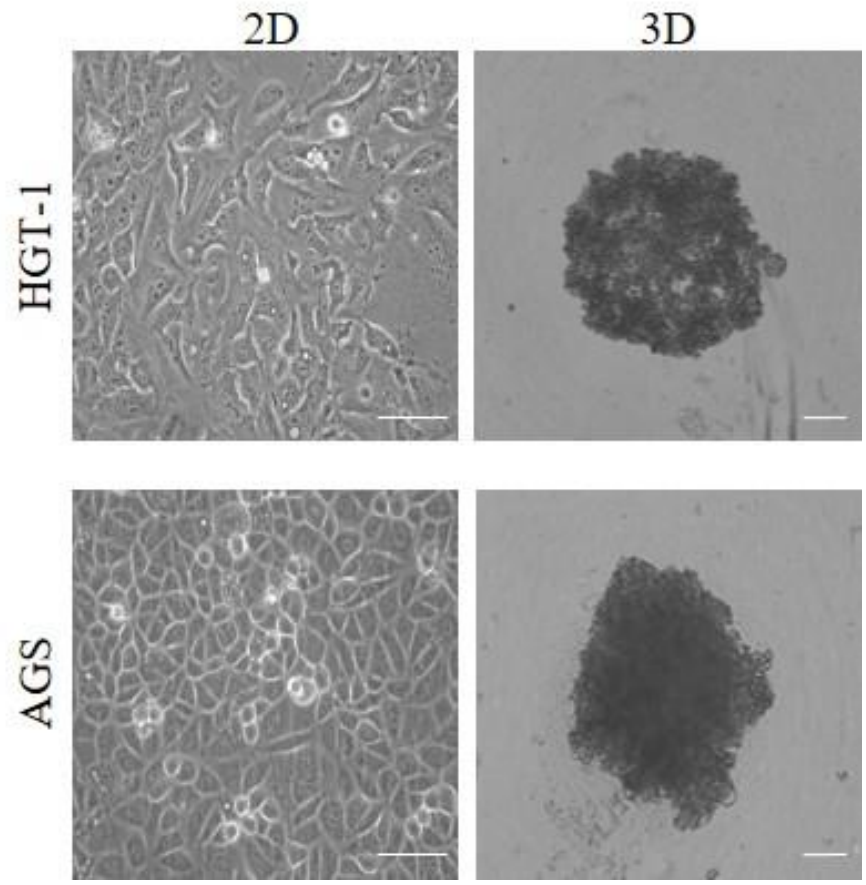

Supplementary Figure V.1. Bright field photographs of HGT-1 and AGS human GC cell lines in 2D or 3D cultures.
Scale bar: 100µm.

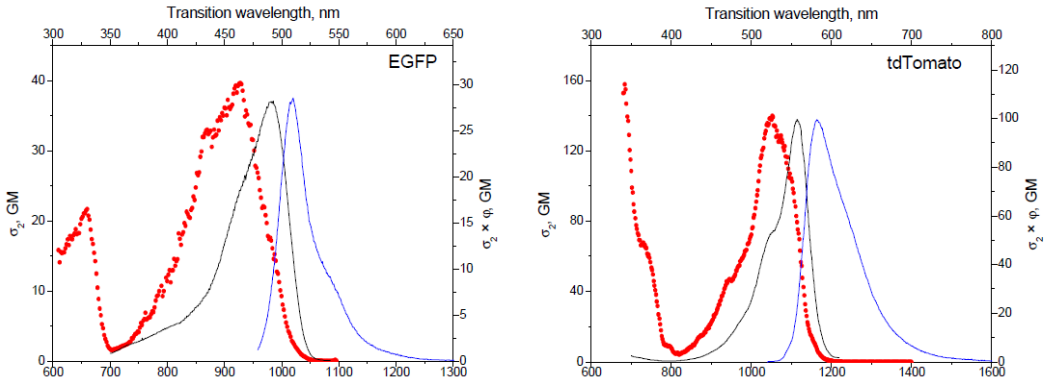

Supplementary Figure V.2. Fluorescence excitation/emission spectra of eGFP and TdTomato.

Two-photon absorption spectra (red symbols), fluorescence emission (blue line) and one-photon fluorescence excitation (black line) of eGFP (left) and TdTomato (right). The left vertical scale shows the two-photon absorption cross section. The scale on the right represents two-photon brightness. One-photon excitation and emission spectra are shown in arbitrary units. From [20].

	HGT-1	HGT-1/CAF	P.Value
D4	210 ± 16	251 ± 8	0.0078
D6	468 ± 36	332 ± 24	0.0242
D8	685 ± 67	546 ± 31	0.0138
D11	898 ± 33	640 ± 21	0.0044

	AGS	AGS/CAF	P.Value
D4	315 ± 11	242 ± 22	0.0035
D6	526 ± 23	288 ± 15	0.0038
D8	785 ± 13	531 ± 45	0.0083
D11	1050 ± 59	616 ± 54	0.0023

Supplementary Figure V.3. Spheroids size monitoring.

Spheroids diameter was measured from TPEF images using the ImageJ software. Monocellular spheroid generated from 250 HGT-1 cells and bicellular spheroid generated from 250 HGT-1 + 250 CAF are represented in the first table. Monocellular spheroid generated from 500 AGS cells and bicellular spheroid generated from 500 AGS + 500 CAF are represented in the second table. Each measure was repeated on independent three spheroids and data are shown as mean ± SD, the third column showed the P.value, Student's t.test.

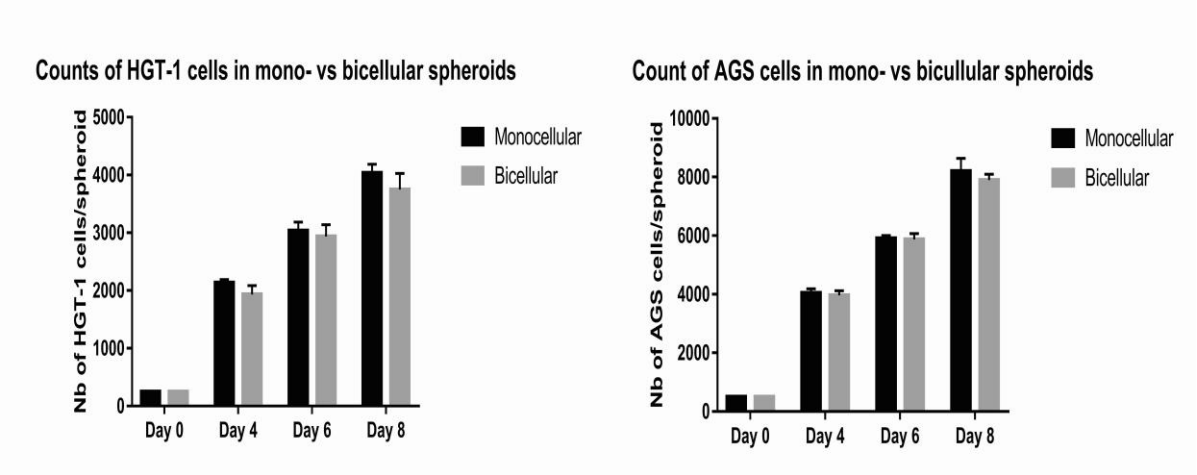

Supplementary Figure V.4. Counting cells recovered from spheroids.
Fluorescent cells were counted after recovering from mono- and bicellular (HGT-1/CAF) spheroids (right) and from mono- and bicellular (AGS/CAF) spheroids (left). Each experiment was repeated independently three times. Data are shown as the mean ± SD.

6. Supplementary Media

Supplementary media files will be available with the thesis manuscript

Media 1. 3D dynamic presentation of HGT-1/CAF spheroid

3D dynamic presentation was reconstructed with the ICY software from 512x512 pixel images acquired at different foci (incremented by 1 µm) in HGT-1/CAF spheroids. Scale: x, y: 700 µm, z: 100 µm.

Media 2. 3D dynamic presentation of AGS/CAF spheroid

3D dynamic presentation was reconstructed with the ICY software from 512x512 pixel images acquired at different foci (incremented by 1 µm) in AGS/CAF spheroids. Scale: x, y: 700 µm, z: 100 µm.

7. References

[[1] E. C. Smyth, M. Nilsson, H. I. Grabsch, N. C. van Grieken, and F. Lordick, “Gastric cancer,” *The Lancet*, vol. 396, no. 10251, pp. 635–648, Aug. 2020, doi: 10.1016/S0140-6736(20)31288-5.

[2] G. Alzeeb, J. P. Metges, L. Corcos, and C. Le Jossic-Corcos, “Three-dimensional culture systems in gastric cancer research,” *Cancers*, vol. 12, no. 10, pp. 1–20, Oct. 2020, doi: 10.3390/cancers12102800.

[3] D. V. LaBarbera, B. G. Reid, and B. H. Yoo, “The multicellular tumor spheroid model for high-throughput cancer drug discovery,” *Expert Opin. Drug Discov.,* vol. 7, no. 9, pp. 819–830, Sep. 2012, doi: 10.1517/17460441.2012.708334.

[4] C. Jensen and Y. Teng, “Is it time to start transitioning from 2D to 3D cell culture?,” *Front. Mol. Biosci.,* vol. 7, Mar. 2020, doi: 10.3389/fmolb.2020.00033.

[5] S. Thippabhotla, C. Zhong, and M. He, “3D cell culture stimulates the secretion of in vivo like extracellular vesicles,” *Sci. Rep.*, vol. 9, no. 1, Dec. 2019, doi: 10.1038/s41598-019-49671-3.

[6] S.-Y. Jeong, J.-H. Lee, Y. Shin, S. Chung, and H.-J. Kuh, “Co-culture of tumor spheroids and fibroblasts in a collagen matrix-incorporated microfluidic chip mimics reciprocal activation in solid tumor microenvironment,” *PLoS One*, vol. 11, no. 7, p. e0159013, Jul. 2016, doi: 10.1371/JOURNAL.PONE.0159013.

[7] H. Shoval *et al.*, “Tumor cells and their crosstalk with endothelial cells in 3D spheroids,” *Sci. Rep.*, vol. 7, no. 1, pp. 1–11, Sep. 2017, doi: 10.1038/s41598-017-10699-y.

[8] H. Shao, M. Moller, D. Wang, A. Ting, M. Boulina, and Z. J. Liu, “A novel stromal fibroblast-modulated 3D tumor spheroid model for studying tumor-stroma interaction and drug discovery,” *J. Vis. Exp.*, vol. 2020, no. 156, p. e60660, Feb. 2020, doi: 10.3791/60660.

[9] L. Teodori, A. Crupi, A. Costa, A. Diaspro, S. Melzer, and A. Tarnok, “Three-dimensional imaging technologies: a priority for the advancement of tissue engineering and a challenge for the imaging community,” *J. Biophotonics*, vol. 10, no. 1, pp. 24–45, Jan. 2017, doi: 10.1002/JBIO.201600049.

[10] E. C. Costa, A. F. Moreira, D. de Melo-Diogo, V. M. Gaspar, M. P. Carvalho, and I. J. Correia, “3D tumor spheroids: an overview on the tools and techniques used for their analysis,” *Biotechnol. Adv.*, vol. 34, no. 8, pp. 1427–1441, Dec. 01, 2016, doi: 10.1016/j.biotechadv.2016.11.002.

[11] J. F. Dekkers *et al.*, “High-resolution 3D imaging of fixed and cleared organoids,” *Nat. Protoc.*, vol. 14, no. 6, pp. 1756–1771, May 2019, doi: 10.1038/s41596-019-0160-8.

[12] M. E. Boutin, T. C. Voss, S. A. Titus, K. Cruz-Gutierrez, S. Michael, and M. Ferrer, “A high-throughput imaging and nuclear segmentation analysis protocol for cleared 3D culture models,” *Sci. Rep.*, vol. 8, no. 1, pp. 1–14, Jul. 2018, doi: 10.1038/s41598-018-29169-0.

[13] E. Steinberg *et al.*, “Rapid clearing for high resolution 3D imaging of ex vivo pancreatic cancer spheroids,” *Int. J. Mol. Sci.*, vol. 21, no. 20, pp. 1–18, Oct. 2020, doi:

10.3390/IJMS21207703.

[14] E. Leary, C. Rhee, B. T. Wilks, and J. R. Morgan, “Quantitative live-cell confocal imaging of 3D spheroids in a high-throughput format,” *SLAS Technol.*, vol. 23, no. 3, pp. 231–242, Jun. 2018, doi: 10.1177/2472630318756058.

[15] F. Pampaloni, N. Ansari, and E. H. K. Stelzer, “High-resolution deep imaging of live cellular spheroids with light-sheet-based fluorescence microscopy,” *Cell Tissue Res.*, vol. 352, no. 1, pp. 161–177, Feb. 2013, doi: 10.1007/S00441-013-1589-7.

[16] S. K. Baek, A. R. Makkouk, T. Krasieva, C. H. Sun, S. J. Madsen, and H. Hirschberg, “Photothermal treatment of glioma; An in vitro study of macrophage-mediated delivery of gold nanoshells,” *J. Neurooncol.*, vol. 104, no. 2, pp. 439–448, Sep. 2011, doi: 10.1007/S11060-010-0511-3/FIGURES/8.

[17] Y. J. Hwang *et al.*, “Multi-photon imaging of actin filament formation and mitochondrial energetics of human ACBT gliomas,” *Photochem. Photobiol.*, vol. 87, no. 2, p. 408, Mar. 2011, doi: 10.1111/J.1751-1097.2010.00873.X.

[18] T. D. Rane and A. M. Armani, “Two-photon microscopy analysis of gold nanoparticle uptake in 3D cell spheroids,” *PLoS One*, vol. 11, no. 12, p. e0167548, Dec. 2016, doi: 10.1371/JOURNAL.PONE.0167548.

[19] C. Frongia, C. Lorenzo, F. Gianni, G. P. Prevost, B. Ducommun, and V. Lobjois, “3D imaging of the response to CDC25 inhibition in multicellular spheroids,” *Cancer Biol. Ther.,* vol. 8, no. 23, pp. 2228–2234, Dec. 2009, doi: 10.4161/CBT.8.23.9984.

[20] M. Drobizhev, N. S. Makarov, S. E. Tillo, T. E. Hughes, and A. Rebane, “Two-photon absorption properties of fluorescent proteins,” *Nat. Methods*, vol. 8, no. 5, p. 393, May 2011, doi: 10.1038/NMETH.1596.

[21] B. Krušlin, M. Ulamec, and D. Tomas, “Prostate cancer stroma: An important factor in cancer growth and progression,” *Bosn. J. Basic Med. Sci.,* vol. 15, no. 2, 2015, doi: 10.17305/bjbms.2015.449.

[22] Y. Mao, E. T. Keller, D. H. Garfield, K. Shen, and J. Wang, “Stromal cells in tumor microenvironment and breast cancer,” *Cancer and Metastasis Rev.*, vol. 32, no. 1–2, pp. 303–315, Jun. 2013, doi: 10.1007/s10555-012-9415-3.

[23] L. Tao, G. Huang, H. Song, Y. Chen, and L. Chen, “Cancer associated fibroblasts: An essential role in the tumor microenvironment (review),” *Oncol. Lett.*, vol. 14, no. 3, pp. 2611–2620, 2017, doi: 10.3892/ol.2017.6497.

[24] M. Yashiro and K. Hirakawa, “Cancer-stromal interactions in scirrhous gastric carcinoma,” *Cancer Microenviron.*, Dec. 2010, vol. 3, no. 1, pp. 127–135, doi: 10.1007/s12307-010-0036-5.

[25] A. Ocana, A. Pandiella, L. L. Siu, and I. F. Tannock, “Preclinical development of molecular-targeted agents for cancer,” *Nat. Rev. Clin. Oncol.*, vol. 8, no. 4, pp. 200–209, Apr. 2011, doi: 10.1038/nrclinonc.2010.194.

[26] D. Anton, H. Burckel, E. Josset, and G. Noel, “Three-dimensional cell culture: A breakthrough in vivo,” *Int. J. Mol. Sci.*, vol. 16, no. 3, pp. 5517–5527, Mar. 2015, doi:

10.3390/ijms16035517.

[27] M. Zanoni *et al.*, “3D tumor spheroid models for in vitro therapeutic screening: a systematic approach to enhance the biological relevance of data obtained,” *Sci. Rep.*, vol. 6, 2016, doi: 10.1038/srep19103.

[28] C. P. Liao, H. Adisetiyo, M. Liang, and P. Roy-Burman, “Cancer-associated fibroblasts enhance the gland-forming capability of prostate cancer stem cells,” *Cancer Res.*, vol. 70, no. 18, pp. 7294–7303, Sep. 2010, doi: 10.1158/0008-5472.CAN-09-3982.

[29] A. Diaspro, G. Chirico, and M. Collini, “Two-photon fluorescence excitation and related techniques in biological microscopy,” *Q. Rev. Biophys.*, vol. 38, no. 2, pp. 97–166, May 2005, doi: 10.1017/S0033583505004129.

[30] C. Angelucci *et al.*, “Epithelial-stromal interactions in human breast cancer: effects on adhesion, plasma membrane fluidity and migration speed and directness,” *PLoS One*, vol. 7, no. 12, p. e50804, Dec. 2012, doi: 10.1371/journal.pone.0050804.

[31] A. Wells, Y. L. Chao, J. Grahovac, Q. Wu, and D. A. Lauffenburger, “Epithelial and mesenchymal phenotypic switchings modulate cell motility in metastasis,” *Front. Biosci.*, vol. 16, no. 3, pp. 815–837, Jan. 2011, doi: 10.2741/3722.

[32] K. Werner, J. Weitz, and D. E. Stange, “Organoids as model systems for gastrointestinal diseases: tissue engineering meets genetic engineering,” *Curr. Pathobiol. Rep.*, vol. 4, no. 1, pp. 1–9, Mar. 2016, doi: 10.1007/s40139-016-0100-z.

Acknowledgments. GA received a fellowship from Brest University (“Contrat Doctoral d’Etablissement”). MD, SR and YLG acknowledge the Ministère de l'Économie et des Finances and the Région Bretagne (CPER STIC&ONDES). This work was supported by grants from the INSERM, from Brest University and from the Ligue Contre le Cancer, Comité du Finistère (n° RAB18153NNA and n° RAB19101NNA to CLJC and LC, respectively) and from the ERAPerMed GRAMMY project IRSTB111/L3P2131. All authors acknowledge IBSAM (Institut Brestois Santé Agro Matière) for financial support. All authors thank G. Leroux for technical assistance.

Disclosures. The authors declare no conflicts of interest.

Data availability. Data underlying the results presented in this paper are not publicly available at this time but may be obtained from the authors upon reasonable request.

V.3. General Conclusions

In this study, we have generated bicellular spheroids, using two different human GC cell lines in association with human primary CAF. We reported the cellular arrangement within the spheroid using in-depth microscopy. Confocal fluorescence microscopy, one of the main tools for 3D imaging, presents several limitations such as those leading to photobleaching and phototoxicity of live cells. Here, we used two-photon microscopy to overcome these issues. Our results showed a different spatial distribution of cells between the GC cell lines. In HGT-1/CAF spheroids, a diffuse distribution of both cell types was observed with CAF enriched at the periphery. In contrast, in AGS/CAF spheroids, CAF were concentrated in the central area, leaving AGS cells in the periphery.

Cell-cell and cell-matrix interactions are critical for tumor development. However, it is quite challenging to understand the influence of the tumor microenvironment (TME) and its potential role as a therapeutic target. CAF have been shown to enhance the inflammatory environment, promote tumor progression and lead to drug resistance. Classical studies to analyze the dynamic interactions between cancer cell and CAF rely on mouse models, but such models are technically demanding and not compatible with 3D imaging. We developed in this work a 3D cellular model adaptable to the microscopy platform. Bicellular spheroids have proven useful to study tumor physiology, especially with respect to cell organization and interactions. A complexification of such models can be foreseen by adding other stroma components to the spheroid such as immune cells, stem cells or endothelial cells. Turning to organoids could thus enlight further the intimacy of tumor organization and functional adaptations.

Version en Français

Dans cette étude, nous avons généré des sphéroïdes bicellulaires, en utilisant deux lignées cellulaires GC humaines différentes, en association avec des CAF primaires d'origine humaine. Nous avons observé l'arrangement cellulaire dans le sphéroïde en utilisant la microscopie en profondeur. La microscopie confocale à fluorescence, l'un des principaux outils d'imagerie 3D, présente plusieurs limites telles que celles conduisant au photoblanchiment et à la phototoxicité vis-à-vis des cellules vivantes. Ici, nous avons utilisé la microscopie à deux photons pour surmonter ce problème. Nos résultats ont montré une distribution spatiale différente des cellules entre les lignées cellulaires GC. Dans les sphéroïdes HGT-1/CAF, une distribution diffuse des deux types cellulaires a été observée avec des CAF localisés à la périphérie. En revanche, dans les sphéroïdes AGS/CAF, les CAF étaient concentrés dans la zone centrale, laissant les cellules AGS à la périphérie.

Les interactions cellule-cellule et cellule-matrice sont essentielles au développement tumoral. Cependant, il est assez difficile de comprendre l'influence du microenvironnement tumoral (TME) et son rôle potentiel en tant que cible thérapeutique. Il a été démontré que les CAF améliorent l'environnement inflammatoire, favorisent la progression tumorale et conduisent à une résistance aux médicaments. Les études classiques pour analyser les interactions dynamiques entre les cellules cancéreuses et les CAF reposent sur des modèles murins, mais ces modèles sont techniquement exigeants et non compatibles avec l'imagerie 3D. Nous avons développé dans ce travail un modèle cellulaire 3D adaptable à la plateforme de microscopie. Les sphéroïdes bicellulaires se sont avérés utiles pour étudier la physiologie des tumeurs, en particulier en ce qui concerne l'organisation et les interactions cellulaires. Une complexification de ces modèles peut être envisagée en ajoutant d'autres composants du stroma au sphéroïde tels que des cellules immunitaires, des cellules souches ou des cellules endothéliales. Se tourner vers de tels organoïdes pourrait ainsi éclairer plus finement l'organisation tumorale et ses adaptations fonctionnelles.

Chapter VI
General Conclusions and Perspectives

According to data from Global Cancer Statistics 2020, gastric cancer (GC) is ranked fifth amongst the most common cancers and is the fourth most common cause of cancer-related deaths worldwide. The treatment of GC remains a major challenge and its survival rate remains low. This underscores the imperative need to better understand cancer development and to develop innovative therapies.

The two-dimensional (2D) monolayer culture model is the most widely used *in vitro* model for identifying new diagnostic markers and developing new therapeutic strategies. Nevertheless, 2D cultures imperfectly represent tissue complexity, and in particular the typology of interactions between cells, due to the attachment of cells to a solid substratum.

On the contrary, three-dimensional (3D) culture systems are of growing interest in cancer research, allowing to better recapitulate some of the functional aspects of tumors. This results from: i) the organization of cells in layers with different proliferation rates, ii) the formation of diffusion gradients for nutrients, oxygen and metabolic waste, iii) the specificities of cell-cell interactions, iv) the expression of specific genes and v) the induction of chemoresistance. Several 3D culture models have been reported. In particular, the work in this thesis focused on mono- or bicellular spheroid models. Spheroid production falls into two broad categories: i) scaffold-based models that take advantage of various types of materials to mimic tumor-extracellular matrix (ECM) interactions *in vivo* and ii) suspension-based models, which primarily include non-adherent cultures that prevent cells from attaching to the scaffold forcing them to aggregate and to form spheroids.

The aim of this thesis was to establish a flexible 3D GC culture model that could be useful to address different basic cancer research-related questions, such as the mechanisms that operate in cancer progression or in structure formation, and to develop transcriptomic and metabolomic analyses with an *in vivo*-like model. Ultimately, this should help bring to light novel therapeutic strategies.

Cytotoxicity applications

In a previous study, our team demonstrated that lovastatin induced massive apoptosis of 2D-grown HGT-1 GC cells in a dose- and time-dependent manner. This effect was more than additive to that of docetaxel. In the present work (Chapter IV), the study was extended to 3D level [1]. Using the IncuCyte™ real-time microscopy imaging and cell analysis system, in addition to other apoptosis and cell viability assays, the combination of docetaxel and lovastatin proved highly efficient at inducing GC cell death.

It was important to confirm the effect of this drug combination in a more complex model, *i.e.* the 3D culture model, beyond its effect in 2D for several reason detailed in Chapter III. The results from both mono- and bicellular 3D models, presented in this thesis, demonstrated that such a drug combination appeared quite realistic as a plausible option to treat cancer patients. These results are in favor of promoting the docetaxel/lovastatin combination to enter the earlier phase of clinical trials. Indeed, the use of already existing and approved drugs to treat complex pathologies like GC can clearly reduce the cost and the time usually required to develop novel drugs. Furthermore, since both lovastatin and docetaxel are already marketed drugs, their toxicity profiles are well known, which suppresses the need for extensive and costly analyses of these compounds.

The establishment and the analysis of 3D tumor spheroids generated in 96-well U-bottomed ultra-low attachment (ULA) microplates allowed an important technical improvement in the drug discovery field [2]. For example, the culture of lung cancer cell spheroids in ULA microplates altered the responses of lung cancer cells towards drugs compared to 2D culture conditions [3]. Such culture conditions showed morphologies and immuno-histochemical staining similar to that of spheroids grown in a scaffold manner. In addition, they could be used for tumor cell migration and invasion assays [4]. This model enables to specifically target certain cell behaviors in drug discovery by enhancing cell motility, inducing cell dormancy, promoting cell differentiation (for stem-cells) and proposing a metastatic-like microenvironment.

It is important to consider that the effects of the drugs vary not only among cell lines, but also with the surrounding microenvironment. The response to therapeutic agents may range from high sensitivity to drug resistance based on the spheroids composition. This makes usage of

bi- or multicellular spheroids, for instance associating fibroblasts to stromal cells, an important and more relevant model in preclinical drug discovery experiments. We will next elaborate tri-cellular spheroids, mixing cancer cells, CAF and mesenchymal stem cells (MSC).

Now that our 3D model is well characterized, additional cytotoxicity tests remain to be done using different drugs (oxaliplatin, 5-FU… with or without statins). Thanks to the use of 96 well culture plates, the effect of molecules from the "Prestwick" chemical library (composed of already marketed drugs from different categories available in the lab) will be tested in order to search for new molecules of potential therapeutic interest (Auranofin, Doxorubicin, Haloprogin, Topotecan...). In addition, CAF have been recently shown as important therapeutic targets (Chapter II).

3D spatial organization approach

The structural analysis of mono- and bicellular spheroids were then reported by two-photon microscopy enabling large depth imaging of uncleared samples and providing less photodegradation. All assays demonstrated that when cells were mixed with CAF, in a 3D culture model, they were straightened and firmly attached, generating more compact spheroids. In depth images showed a different and characteristic spatial distribution of cancer cells and CAF, distinctively between HGT-1 and AGS GC cell lines. We were able to image 2 different cell types in the same sample without any staining after formation of the spheroid.

Detailed fluorescent microscopic visualization and evaluation of complex 3D structures face many technical challenges: 3D preparation methods are not usually adapted to microscopy, manipulating 3D spheroids or organoids is not straightforward, and living cells are usually unstable facing fluorescent laser [5]. Here, our system allows light to penetrate at a depth, up to 120 µm, without any clearing techniques, and holds promise for the analysis of samples with simple preparation steps, high resolution and multichannel fluorescence acquisition. However, in our study, we faced some limitations depending on culture in ULA microplates with round bottom that was not adapted for direct imaging of the spheroid in the well. Additionally, our 3D imaging system was not equipped with an immersion objective limiting light penetration. To bypass the microplate limitation, we set in motion a simple system based on the hanging drop method, as described in Chapter V.

We will work to clear our spheroids so that we could capture the entire 3D shape. Many clearing methods exist, aqueous or solvent-based, and can be an important addition for in depth imaging of large samples such as spheroids or organoids (RapidClear, 80 % glycerol...) [6].

The self-organization of cells in the spheroids could reflect the migratory and the invasive potential of the cells. Several additional studies are currently in progress to address this question [7]. During this thesis, we reported the characterization of expression of genes encoding adhesion molecules such as E-cadherin, epithelial cell adhesion molecule (EpCam), integrin beta 1 (ITGB1) and integrin beta 3 (ITGB3) in HGT-1 and AGS cells. Clear differences were observed between these two cell lines. In order to determine the contribution of these genes in the spatial organization, cells were transfected by siRNA to inhibit the expression of these genes. Quite strikingly, preliminary results have indicated that inhibition of ITGB3 in HGT-1 cells in bicellular HGT-1/CAF spheroids showed an organization resembling that of AGS cells in AGS/CAF spheroids. Cell migration assays in 2D showed a larger migration capacity of HGT-1 cells compared to AGS cells. This capacity was significantly reduced after the inhibition of ITGB3, reducing their migratory potential close to that of 2D AGS cells. Additional assays have to be carried out to confirm the role of ITGB3 and identify its underlying mechanism of action, especially in 3D-grown cells. The potential roles of other integrins will be tested as well to determine the specificity of ITGB3 in controlling the migratory potential.

Genes involved in the formation of spheroids

Similarly to the possible role of ITGB3 in the organization of bicellular spheroids, the expression of several genes has been reported to control the capacity of the cell lines to generate spheroids [9–11]. Understanding the implication of such genes in the formation and growth of spheroids is important to identify cancer driver genes and potential novel therapy targets. Hence, we will develop molecular analyses in order to identify markers responsible for the formation of these 3D structures and to understand the underlying mechanisms (such as E-cadherin, COX2...). This approach should provide a better understanding of the biophysical and biochemical mechanisms associated with the formation of these structures assembled in absence of scaffold and with the response of GC cells to chemotherapy treatments.

Several studies showed that in 3D cultures, expression of stem cell markers in spheroid cells is enhanced [12] (Chapter III). Using RNA from AGS and HGT-1 spheroids, we analyzed the expression of genes specifically expressed in GC stem cells and we compared their expression level to that of cells cultured in a 2D model. Spheroids generated using different numbers of cancer cells (500-1000) and spheroids from different ages (4, 6, 8, 12, 17 days-old) were tested in order to potentially enrich the spheroids with stem cells. Regardless of the experimental condition, we did not observe differences in the expression of the stem cell markers LGR5, OCT4, ALDH1, CD44, and ABCG2 between 2D and 3D cultured cells. Additional modifications of culture parameters and conditions (several passaging in 3D culture, limiting initial cell number, specific culture media …) will be applied later to increase the presence of GC stem cells in our model.

Transcriptomic profiles

Recently, high-throughput new generation sequencing technologies revealed important findings regarding the genomic, epigenetic and transcriptomic diversity of cancers that would not be captured by histological analysis only [13]. As mentioned in Chapter III, gene expression profiles of GC spheroids are not yet well described. Understanding the cell biology of 3D structures is important for a more complete appreciation of *in vivo* tissue function. Several studies showed that within 3D models, cell lines demonstrate different functional phenotypes compared to 2D models, depending on the physical environment (spheroid size, CO_2 level, necrotic center…), which are controlled by gene expression programs [14]. Epigenetics and alternative splicing are parts of the mechanisms that can regulate transcriptional responses in 3D structures [15]. The presence of a specific microenvironment could also have an impact on cancer cells transcriptomic profiles. Hence, it was demonstrated that CAF can dictate the transcription level of different genes implicated in several pathways of cancer cells growth and invasion [16]. The establishment of a transcriptomic profile of our model in mono- and bicellular conditions will allow us to investigate the variability and the complexity of gene expression, to trace the origin of cancer cells and uncover the mechanisms leading to the development of resistance to anticancer drugs. Such studies should be ideally supplemented with transcriptomic analyses at the level of the single cell.

Taken together, studying the motility of cancer cells using 3D platforms in association with modern imaging tools and new generation transcriptomic tools can provide a high level of integration of information about cancer cell behavior. Such approaches will help investigate unresolved issues, including the interplay between metastasis and drug resistance.

Cancer cells metabolism

The metabolism of cancer cells is characterized by multiple alterations adapted to their specific needs. Numerous observations have documented this aspect, mainly in relation to the avidity of these cells for glucose, glutamine and, more recently, for lipids. Blockade of the mevalonate pathway by statins (inhibition of HMG-CoA Reductase, see Chapter IV) leads to a shortage of several intermediate metabolites, in particular farnesyl pyrophosphate (FPP) and geranylgeranyl pyrophosphate (GGPP), which are necessary for the functionalization (prenylation) of GTPases of the ras and rho families.

In order to clarify the nature of the biochemical differences induced by the treatments (docetaxel, lovastatin or both) in HGT-1 cells, our team has conducted an untargeted metabolomic analysis with the aim of obtaining a multifaceted understanding of drug - cells interactions. This study showed that the levels of more than 100 metabolites and several lipid families were modified after the treatments, especially in the presence of lovastatin. The level of L-glutamine was the most increased, demonstrating a significant metabolic adaptation of cancer cells. Glutamine is an important energy source for epithelial cells and for fast growing cells such as tumor cells, including HGT-1 and AGS cells. It is also an important substrate for lipid synthesis and contributes to the regulation of the expression of key enzymes in this biosynthetic pathway.

Based on these results, during this thesis preparation, an analytical study was performed by measuring intracellular and secreted glutamine to determine whether the modification recorded in the 2D earlier study also occurred in 3D, and to decipher the role of glutamine accumulation in the cells after treatment with lovastatin. Analyses were performed in collaboration with the NMR platform of Brest University to quantify glutamine. The first results revealed a reversal of the intracellular glutamine/glutamate ratio with an accumulation of glutamine and a decrease of glutamate levels following treatment with CB-839, an inhibitor of the glutaminase enzyme. Cell viability assays (MTT assay) showed that CB-839 increased

the cytotoxic effect of lovastatin treatment of AGS cells (by 20%), but had no effect on HGT-1 cells. Additional experiments will be required to understand the effects of glutamine accumulation in cells on apoptosis and viability after treatment with lovastatin.

In order to better understand the important cytotoxic effect of lovastatin on GC cell lines, as an agent blunting the mevalonate pathway, a collaboration with the MetaToul platform (Toulouse) was initiated during this thesis. MetaToul developed a pipeline for the metabolomic analysis of the early steps of the cholesterol synthesis pathway. It was possible to quantify a set of central metabolites (Acetyl-CoA, succinyl-CoA, ketoglutarate, ATP, AMP...) in GC cell lines and in the extracellular medium. This encouraging data indicates that it is possible to follow the evolution of such metabolites, as well as those generated by the glutamine pathway (glutamate, succinate, isocitrate...).

Taking advantage of the development of a sensitive analytical system by improving detection limits in MetaToul lab, metabolomic analyses of 3D cultures (HGT-1 or AGS spheroids) are in progress. This approach, thanks to its high sensitivity, permits the analysis of metabolomic profiles from the cells contained in single spheroids. Low amounts of biological materials are required with as little as 6000 cells/spheroid. As previously mentioned (Chapter III), culture conditions can deeply impact the metabolomic profiles of the cells.

Can we imagine a single-cell metabolomic approach in association with the 3D culture model to better understand the heterogeneity of such complex model [17]? For that perspective, we have to push the limit of detection (sensitivity) to investigate subcellular compartments and to sample live single cells in their 3D microenvironment, which represent their *in vivo* living conditions.

The switch from 2D to 3D cultures generates different gradients in the spheroids (nutriments, oxygen, lactate…) enabling major adjustments of the cells' metabolome. Such metabolomic modifications can have an important impact on many cellular mechanisms, gene expression and cell activity, in addition to their role in the responses to drug treatment and the outcome of therapy. These experiments might enable the identification of potential GC biomarkers and potentially lead to the identification of novel drug targets. However, since metabolism is a highly dynamic process, such that the metabolites are continuously transformed and

exchanged, it may be quite challenging to capture significant changes that occur within the fluxome.

During this thesis, a fluxomic analysis was also initiated by substituting ^{14}C-glucose in culture media by ^{13}C-glucose in both 2D and 3D cells, both as mono- and bicellular spheroids, the results of which are currently under analysis with our partners from MetaToul.

From spheroids to organoids

Progress in 3D culture technologies open new opportunities in the development of novel modeling systems, referred to as organoids (Chapter III). Since 2020, our team has been participating in the European "GRAMMY" project that comprises an experimental axis devoted to the analysis of GC fragments amenable to the construction of organoids. Illustrating the genetic heterogeneity of primary tumors, organoids are a powerful *in vitro* method offering new means of investigating tumor treatment responses. This model will be used as an efficient drug-testing platform to analyze the effect of the docetaxel / lovastatin combination, in addition to the search for other active molecules from chemical library screening. Furthermore, the spatial organization of such organoids will be approached by bi-photonic microscopy. Such an analysis holds a special interest, as organoids may be far more complex than spheroids in their richness in distinct cell types that compose tumors.

To conclude

Depending on the type of scientific questions, especially those related to the effects of drugs, 3D cultures might be better suited than 2D cultures. Since the procedures to establish 3D cultures of spheroids can be highly standardized, we believe that these should constitute the future "gold standard" in the drug discovery pipeline. Nevertheless, these should be ideally supplemented with 3D imaging and omics approaches and, why not, at the single cell level when technologies permit it. This combination requires novel techniques and bioinformatic tools. It also allows the exploration of the central dynamics of the cells with more comprehensive perspective and eventually favour a deep understanding of *in vivo* cell biology.

References

[1] G. Mazzoleni, D. Di Lorenzo, and N. Steimberg, "Modelling tissues in 3D: the next future of pharmaco-toxicology and food research?," *Genes Nutr.*, vol. 4, no. 1, p. 13, Mar. 2009, doi: 10.1007/S12263-008-0107-0.

[2] S. Breslin and L. O'Driscoll, "Three-dimensional cell culture: The missing link in drug discovery," *Drug Discov. Today*, vol. 18, no. 5–6, pp. 240–249, Mar. 2013, doi: 10.1016/j.drudis.2012.10.003.

[3] J. E. Ekert *et al.*, "Three-dimensional lung tumor microenvironment modulates therapeutic compound responsiveness in vitro - Implication for drug development," *PLoS One*, vol. 9, no. 3, Mar. 2014, doi: 10.1371/journal.pone.0092248.

[4] M. Vinci *et al.*, "Advances in establishment and analysis of three-dimensional tumor spheroid-based functional assays for target validation and drug evaluation," *BMC Biol.*, vol. 10, no. 1, pp. 1–21, Mar. 2012, doi: 10.1186/1741-7007-10-29/FIGURES/8.

[5] H. U. Dodt *et al.*, "Ultramicroscopy: three-dimensional visualization of neuronal networks in the whole mouse brain," *Nat. Methods*, vol. 4, no. 4, pp. 331–336, Mar. 2007, doi: 10.1038/nmeth1036.

[6] W. Li, R. N. Germain, and M. Y. Gerner, "Multiplex, quantitative cellular analysis in large tissue volumes with clearing-enhanced 3D microscopy (Ce3D)," *Proc. Natl. Acad. Sci. U. S. A.*, vol. 114, no. 35, pp. E7321–E7330, Aug. 2017, doi: 10.1073/PNAS.1708981114/-/DCSUPPLEMENTAL.

[7] C. Angelucci *et al.*, "Epithelial-stromal interactions in human breast cancer: effects on adhesion, plasma membrane fluidity and migration speed and directness," *PLoS One*, vol. 7, no. 12, p. e50804, Dec. 2012, doi: 10.1371/journal.pone.0050804.

[8] S. Blacher *et al.*, "Cell invasion in the spheroid sprouting assay: a spatial organisation analysis adaptable to cell behaviour," *PLoS One*, vol. 9, no. 5, p. e97019, May 2014, doi: 10.1371/JOURNAL.PONE.0097019.

[9] N. Oue *et al.*, "Induction of KIFC1 expression in gastric cancer spheroids," *Oncol. Rep.*, vol. 36, no. 1, pp. 349–355, Jul. 2016, doi: 10.3892/or.2016.4781.

[10] T. Imai *et al.*, "Overexpression of KIF11 in gastric cancer with intestinal mucin phenotype," *Pathobiology*, vol. 84, no. 1, pp. 16–24, Sep. 2017, doi: 10.1159/000447303.

[11] E. Taha, "Studies on the facts of the loss of MMP3 on tumoroid formation and the integrity of extracellular vesicles," *thesis*, Sep. 2020. Available: http://ousar.lib.okayama-u.ac.jp/60940.

[12] M. E. Han *et al.*, "Cancer spheres from gastric cancer patients provide an ideal model system for cancer stem cell research," *Cell. Mol. Life Sci.*, vol. 68, no. 21, pp. 3589–3605, Nov. 2011, doi: 10.1007/s00018-011-0672-z.

[13] V. H. Teixeira *et al.*, "Deciphering the genomic, epigenomic, and transcriptomic landscapes of pre-invasive lung cancer lesions," *Nat. Med.*, vol. 25, no. 3, pp. 517–525, Jan. 2019, doi: 10.1038/S41591-018-0323-0.

[14] E. Gheytanchi *et al.*, "Morphological and molecular characteristics of spheroid formation in HT-29 and Caco-2 colorectal cancer cell lines," *Cancer Cell Int.*, vol. 21, no. 1, pp. 1–16, Dec. 2021, doi: 10.1186/S12935-021-01898-9/TABLES/2.

[15] C. Branco da Cunha *et al.*, "CD44 alternative splicing in gastric cancer cells is regulated by culture dimensionality and matrix stiffness," *Biomaterials*, vol. 98, pp. 152–162, Aug. 2016, doi: 10.1016/j.biomaterials.2016.04.016.

[16] T. Simon and B. Salhia, "Cancer associated fibroblast subpopulations with diverse and dynamic roles in the tumor microenvironment," *Mol. Cancer Res.*, p. molcanres.0282.2021, Oct. 2021, doi: 10.1158/1541-7786.MCR-21-0282.

[17] R. Liu and Z. Yang, "Single cell metabolomics using mass spectrometry: Techniques and data analysis," *Anal. Chim. Acta*, vol. 1143, pp. 124–134, Jan. 2021, doi: 10.1016/J.ACA.2020.11.020.

Annex I
Récapitulatif de la Thèse

Version en Français

Développement d'un Modèle Cellulaire Flexible Tridimensionnel : Un Focus sur le Cancer Gastrique

Thèse préparée par George Alzeeb

Sous la direction de Dr. Laurent Corcos et Dr. Catherine Le Jossic-Corcos

Cette annexe synthétise les travaux réalisés durant cette thèse. EIle a été préparée en Français à la demande de l'Ecole Doctorale Biologie Santé (EDBS), en raison de notre choix de présenter l'essentiel du manuscrit de thèse en anglais. C'est pour cette même raison que nous avons fait figurer, dans le corps du manuscrit, en français également, les introductions et les conclusions des Chapitres III, IV et V.

Résumé

Le cancer gastrique (CG) est le cinquième cancer le plus fréquent dans le monde et est la quatrième cause de décès par cancer en 2020. Le pronostic du CG est mauvais et la plupart des formes avancées de la maladie sont incurables. Il est donc urgent de développer de nouvelles thérapies. Notre équipe a démontré que la combinaison de statine et de taxane induit fortement l'apoptose des cellules du CG en 2 dimensions (2D). Néanmoins, la culture en 2D représente imparfaitement la complexité tissulaire, et en particulier le rôle des interactions entre cellules. L'une des stratégies qui permettent d'améliorer la réussite des nouveaux médicaments anticancéreux en clinique repose sur l'utilisation de modèles de culture cellulaire tridimensionnelle (3D). Ces modèles montrent un intérêt croissant dans la recherche sur le cancer, permettant de mieux rétablir certains des aspects fonctionnels des tumeurs. Nous avons ainsi généré des sphéroïdes monocellulaires de cellules cancéreuses gastriques humaines (HGT-1 ou AGS), ainsi que des sphéroïdes bicellulaires associant ces cellules à des fibroblastes issus de tumeurs (CAF, Cancer Associated Fibroblasts), selon une méthodologie robuste, qui prévient leur attachement à une matrice. Nous avons étudié la cytotoxicité induite par le docétaxel et la lovastatine (test MTT). De plus, nous avons utilisé le système d'imagerie et d'analyse en temps réel IncuCyte^{TM} pour suivre la croissance des sphéroïdes et la réponse apoptotique. Ces tests ont montré une toxicité importante, majorée en cas d'association des deux molécules, comme observé en 2D. Nous avons entrepris l'analyse de l'organisation du modèle 3D bicellulaire par microscopie laser à 2 photons. Nos résultats montrent une organisation distinctive des sphéroïdes bicellulaires selon la lignée de cellules épithéliales cancéreuses, HGT-1 ou AGS. Cette organisation pourrait s'expliquer par des différences de capacité migratoire / invasive des cellules de CG. Dans le cadre du programme européen GRAMMY, nous envisagerons une application de ces approches sur des organoïdes de tumeurs issues de patients.

Le cancer gastrique

(Chapitre I)

Le cancer gastrique (CG) est le cinquième cancer le plus fréquent dans le monde avec plus d'un million nouveaux cas, c'est la quatrième cause de décès par cancer (768 793 décès), selon les données de ''Global Cancer Statistics'' en 2020 [1]. La classification de Lauren est largement utilisée pour classer les adénocarcinomes gastriques en un sous-type intestinal associé à des facteurs environnementaux (infections à Helicobacter pylori, l'alimentation et le mode de vie) et un sous-type diffus souvent associé à des anomalies génétiques [2]. L'incidence de la maladie varie considérablement d'une région à l'autre : elle est la plus élevée en Asie centrale et orientale, suivie de l'Amérique latine et de l'Europe de l'Est. Bien que l'Europe occidentale présente des taux intermédiaires à faibles de CG, avec 28 490 nouveaux cas en 2020, le taux de mortalité reste élevé avec environ 18 000 décès en 2020 (taux de létalité : 63 %) [3]. L'infection par Helicobacter pylori est le principal facteur de risque du CG (associée à 78 % de tous les CG), car elle provoque une inflammation de la muqueuse gastrique. Le facteur alimentaire (les aliments salés, fumés ou additionnés de conservateurs chimiques), le tabagisme et la consommation d'alcool, l'infection par le virus d'Epstein-Barr (EBV), sont tous considérés comme des facteurs de risque de CG. En outre, 1 à 3 % des cancers gastriques sont liés à des syndromes familiaux [4]. Le pronostic du CG est mauvais et la plupart des formes avancées de la maladie sont incurables. Les principaux traitements du CG reposent sur la résection chirurgicale comme première modalité curative [5], la chimiothérapie [6] et la thérapie ciblée viennent par la suite [7, 8]. Bien que l'efficacité des traitements se soit améliorée au cours de la dernière décennie, les taux de survie des patients atteints de CG restent faibles. Il est donc urgent de développer de nouvelles thérapies.

Le modèle de culture cellulaire en trois dimensions

(Chapitre III)

Le modèle de culture cellulaire traditionnel en cancérologie des tumeurs solides est celui de la culture de lignées cellulaires cancéreuses en monocouche à 2-dimensions (2D). Ce modèle continue de jouer un rôle important pour la compréhension des mécanismes fondamentaux de la tumorigenèse grâce à sa facilité de manipulation, sa reproductibilité et son faible coût [9]. Toutefois, la culture en 2D impose des contraintes géométriques et mécaniques non physiologiques en raison de la nécessaire adhésion des cellules à un support solide artificiel (généralement en polystyrène). Une telle culture affecte la polarité des cellules et donc, potentiellement, les phénotypes tumoraux caractéristiques des tumeurs d'origine [10]. Par conséquent, l'utilisation des modèles animaux, plus physiologiques, s'est intensifiée, augmentant ainsi la durée et le coût global du processus de découverte et de développement des médicaments. La xénogreffe de fragments de tumeurs, appelé *'patient-derived xenograft'* (PDX), chez la souris immunodéprimée, est la plus utilisée pour étudier le développement des cancers humains et leurs réponses aux traitements chez l'animal [11].

Au cours des dernières décennies, de nouvelles techniques de modélisation des tumeurs solides ont été développées. Celles-ci reposent sur la culture de cellules maintenues dans un environnement tridimensionnel (3D), grâce à l'utilisation de substrats (boîtes/flacons de culture) à faible adhésivité cellulaire. Ainsi, la culture en 3D permet d'utiliser, *in vitro*, des échantillons complexes ou des mini-organes dans un environnement contrôlé [12]. Ces modèles ont également l'avantage de mimer le comportement tumoral, qui dépend de signaux environnementaux, et des interactions cellule-cellule et cellule-matrice extracellulaire (MEC). Il est rapporté que les agents cytotoxiques sont généralement plus actifs dans les cultures en 2D qu'en 3D, conduisant à sans doute surévaluer leur activité par l'utilisation de la 2D uniquement [13, 14]. En revanche, la culture en 3D permettrait de mieux anticiper les phénomènes de résistance. Outre la résistance aux agents anticancéreux, les modèles de culture en 3D peuvent également aider à prévoir la pénétration des médicaments dans les tumeurs, une limite importante, et souvent négligée, à l'origine d'échappement thérapeutique. Deux modèles de culture cellulaire en 3D sont principalement utilisés : les sphéroïdes et les organoïdes (Figure 1). Durant cette thèse nous nous sommes intéressés à la culture des sphéroïdes [15].

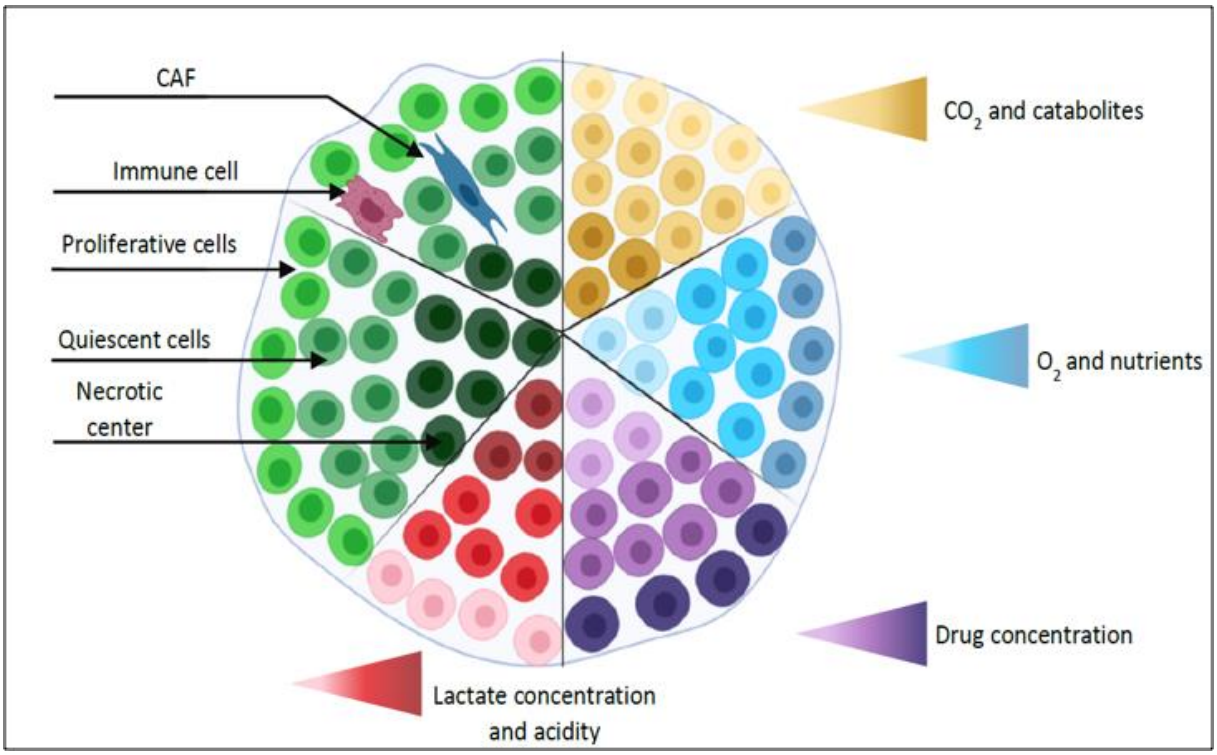

Figure 1. Représentation simplifiée d'un sphéroïde avec ses différentes couches cellulaires : une couche externe prolifératives, une couche intermédiaire de cellules en quiescence et un centre nécrotique. L'ensemble est soumis à différents gradients (oxygène, nutriments, CO_2, catabolites et concentration en médicaments). Le sphéroïde en co-culture : addition des fibroblastes-associés au cancer (CAF) et des cellules immunitaires. *Alzeeb, 2020* [15].

Afin de reproduire l'hétérogénéité cellulaire des tumeurs solides et de mieux prendre en compte les phénomènes de résistance aux traitements, dont ceux qui pourraient être majorés, voire causés, par les interactions cellules cancéreuses-cellules stromales, des sphéroïdes pluricellulaires peuvent être assemblés. Ils associent des cellules épithéliales cancéreuses et des cellules stromales, comme les fibroblastes associés au cancer, dénommés *« cancer-associated fibroblasts »* (CAF), les cellules endothéliales ou les cellules immunitaires. Les interactions cellules-cellules au sein des sphéroïdes affectent leur prolifération, leur survie et les réponses aux traitements. Les sphéroïdes constitués de cellules tumorales et de CAF, le type cellulaire le plus abondant dans la Transition Epithélio-Mésenchymateuse (TEM), sont largement utilisés pour tester des candidats médicaments [16, 17]. Actuellement, il n'est pas possible d'utiliser une nomenclature unique, basée sur des marqueurs partagés et des fonctions similaires, pour définir les CAF. On doit distinguer deux cas de figures, d'une part l'utilisation des CAF dérivées de la tumeur du patient et d'autre part les fibroblastes présents

au site métastatique pour les tumeurs avancées mais cette seconde situation n'est pas aisément exploitable car il est moins fréquent d'opérer les métastases par rapport aux tumeurs primaires [18, 19].

Les organoïdes sont des structures complexes souvent formées à partir des cellules cancéreuses primaires ou des cultures de biopsies tissulaires ; ils feront l'objet d'études futures. De nombreuses caractéristiques ont encouragé l'utilisation des organoïdes comme modèles du cancer puisqu'ils sont issus directement des patients et ne sont donc pas limités par les différences entre espèces, ce qui est le principal inconvénient des modèles animaux [20, 21]. En outre, les organoïdes peuvent également être produits en quantité et cryo-conservés, ce qui permet de créer des bibliothèques d'organoïdes représentatives de différents types et sous-types de cancers, en en faisant un outil extrêmement utile pour les études précliniques [22] (Figure 2).

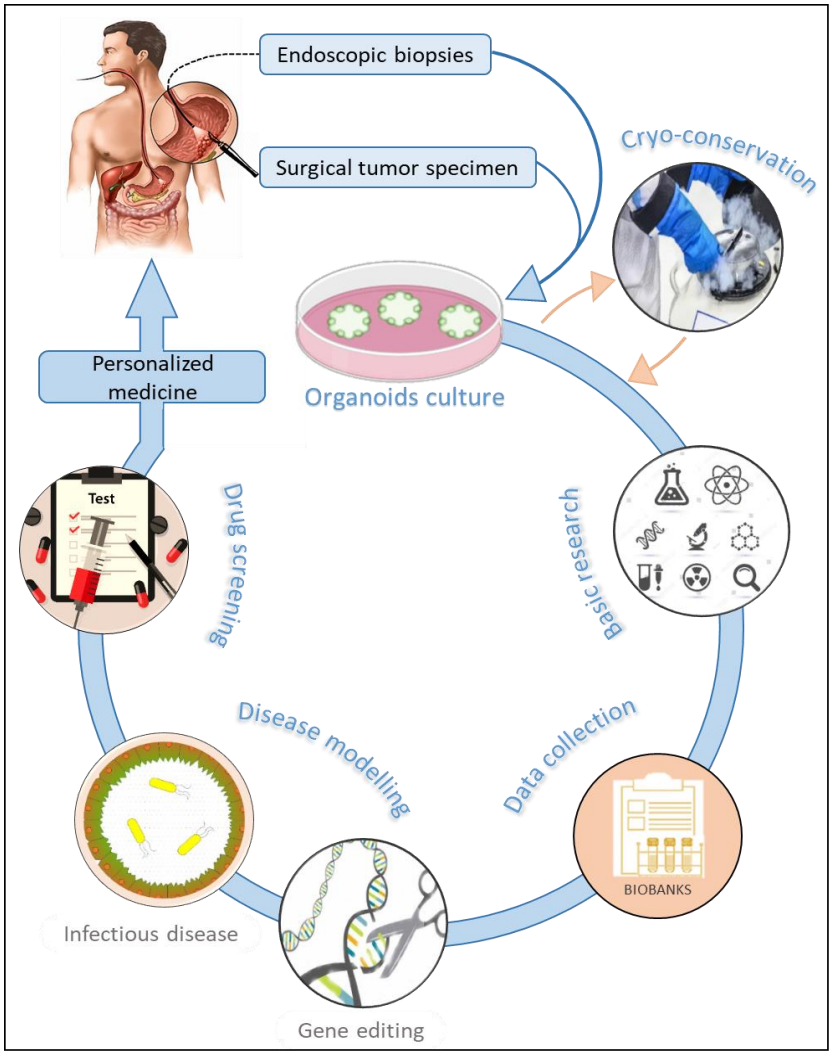

Figure 2. Représentation graphique des applications des organoïdes gastriques et de leur implication dans la médecine personnalisée. *Alzeeb, 2020* [15].

Ce domaine en évolution rapide vise à fournir une alternative *in vivo* au système PDX, assez exigeant et coûteux. Les sphéroïdes sont donc bien adaptés pour analyser les interactions entre les cellules qui composent la tumeur, y compris les cellules souches, les CAF, les cellules immunitaires et les cellules endothéliales. En tant que tels, ils sont également appropriés pour analyser les effets des médicaments cytotoxiques, ainsi que pour identifier de nouveaux biomarqueurs. Cependant, l'harmonisation des techniques est nécessaire pour garantir une meilleure reproductibilité des données issues de l'utilisation des modèles 3D, avant que ceux-ci ne puissent être considérés comme le modèle standard pour le criblage préclinique des molécules thérapeutiques contre le CG.

Analyse de l'effet des agents médicamenteux sur la mort cellulaire dans des sphéroïdes de cancer gastrique par l'imagerie cellulaire en temps réel

(Chapitre IV)

Bien que l'efficacité des traitements se soit améliorée au cours de la dernière décennie, les taux de survie au CG restent faibles. Cela pointe l'urgence de développer de nouvelles thérapies. Le repositionnement des médicaments est devenu une stratégie alternative puissante et efficace pour la découverte de nouvelles options thérapeutiques, en particulier dans un contexte adjuvant.

Dans une étude précédente, notre équipe a montré que l'association de lovastatine, normalement utilisée pour le traitement de l'hypercholestérolémie, en raison de sa capacité à inhiber de manière compétitive la 3-hydroxy-3-méthyl-glutaryl-coenzyme-A réductase (HMG-CoA Red), et le docétaxel, un taxane anticancéreux utilisé pour traiter le CG et d'autres tumeurs solides, a induit une réponse apoptotique plus qu'additive dans la lignée cellulaire humaine HGT-1 de GC cultivée en 2D. Comme mentionné dans la partie précédente, il a été démontré que les systèmes de culture 3D prédisent efficacement l'efficacité *in vivo* des agents thérapeutiques. Dans cette partie du travail, notre objectif était de demander si les observations précédentes faites dans des cellules cultivées en 2D, seraient toujours valables pour les cellules cultivées en 3D.

Nous avons ainsi généré des sphéroïdes monocellulaires de cellules HGT-1 ou AGS, deux lignées cellulaires immortalisées du CG (Figure 3), ainsi que des sphéroïdes bicellulaires associant ces cellules cancéreuses à des fibroblastes associés au cancer (''Cancer-associated fibroblasts'' CAF), selon une méthodologie robuste, qui restreint leur attachement à une matrice.

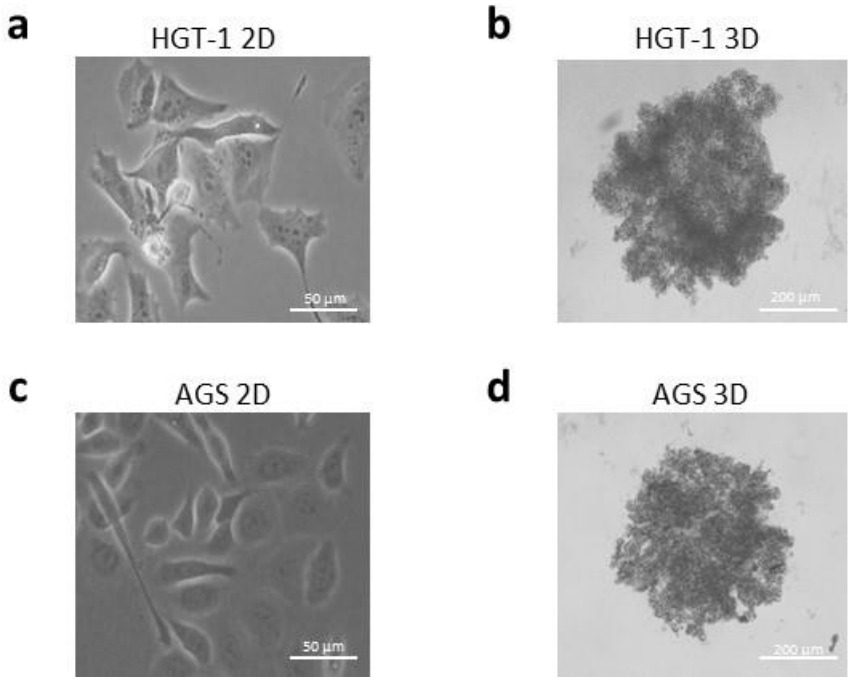

Figure 3. Photographies en contraste de phase des cellules HGT-1 (a : 2D, b : 3D-après 6 jours de culture) et AGS (c : 2D, d : 3D-après 6 jours de culture).

Nous avons utilisé le système d'imagerie et d'analyse en temps réel, IncuCyte^{TM} pour déterminer la croissance, la cytotoxicité ou l'induction de l'apoptose par la lovastatine et le docétaxel. Le module sphéroïde de l'IncuCyte^{TM} permet la visualisation en temps réel et l'analyse automatisée de la croissance des sphéroïdes. Ainsi, une visualisation complète de la morphologie des sphéroïdes, de la compaction intercellulaire (agrégats fragiles ou sphéroïdes compacts) et de la taille caractéristique de chaque type de cellule peut être obtenue. Ce sont des paramètres d'intérêt pour caractériser la viabilité des cellules formant la structure 3D. Ces tests ont montré une toxicité importante, majorée en cas d'association des deux molécules, comme il avait été obtenu en 2D (Figure 4).

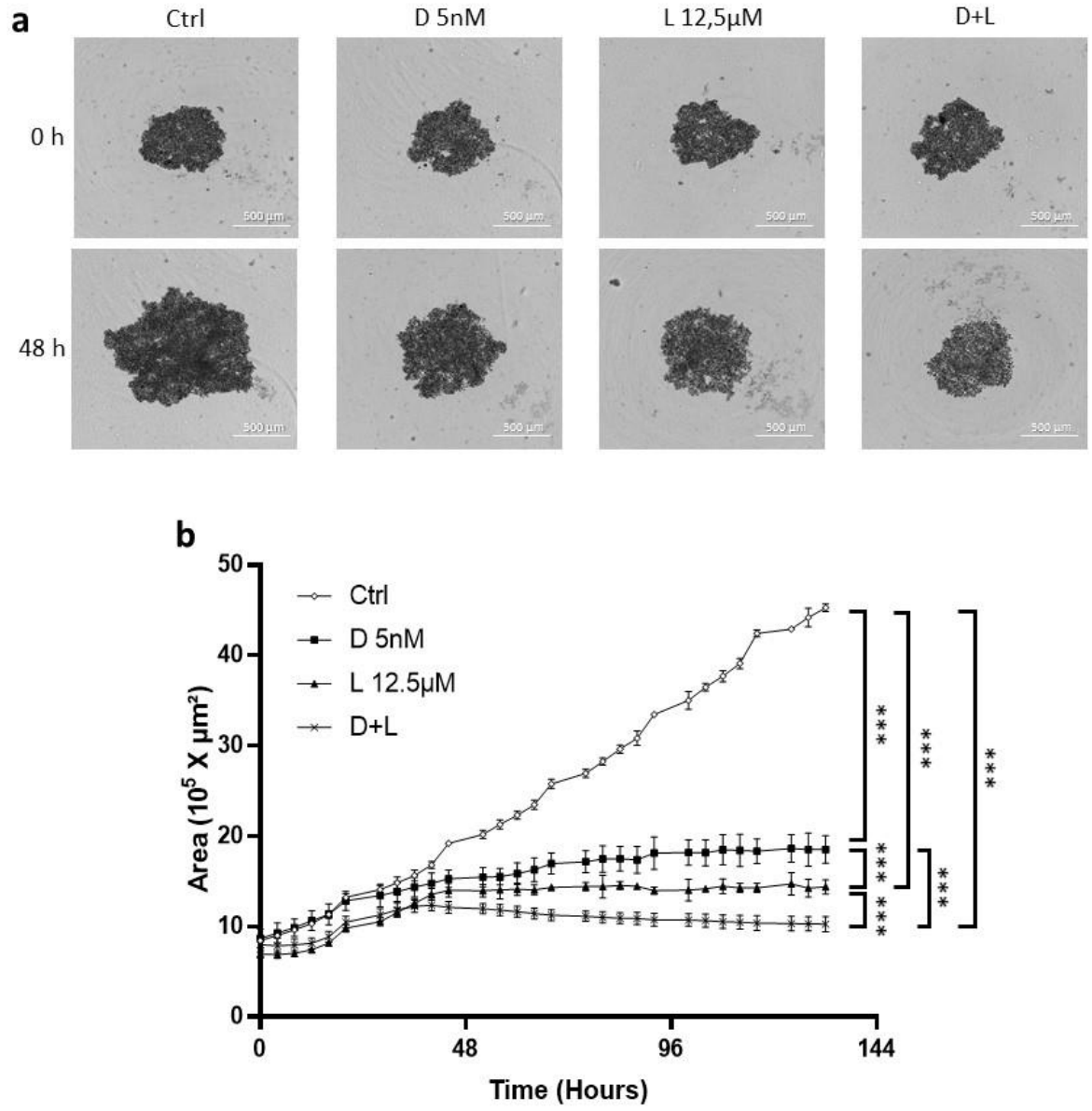

Figure 4. Effets des traitements par docétaxel et lovastatine sur la croissance des sphéroïdes HGT-1.

(a) Photographies en contraste de phase des sphéroïdes HGT-1 âgés de 6 jours à 0 h et 48 h de traitement par 5nM de docétaxel (D 5nM), 12,5µM de lovastatine (L 12,5µM) et 5nM de docétaxel + 12,5µM de lovastatine (D+L), capturées par l'IncuCyte™. (b) Suivi de croissance en temps réel (surface 10^5 x μm^2) des sphéroïdes HGT-1, réalisé par l'IncuCyte™. Des sphéroïdes âgés de six jours (commençant par 0 sur le graphique) étaient traités par D 5nM (carrés noirs), L 12,5µM (triangles noirs) ou D+L (X noir) pendant une durée allant jusqu'à 144 h. Le contrôle (Ctrl) est représenté par des losanges blancs. Les résultats sont présentés comme la moyenne ± ET de n=3 expériences indépendantes avec quatre réplicats techniques dans chacune. ***p ≤ 0,001, one-way ANOVA suivie d'une analyse de Tukey.

Les cellules cancéreuses sont fortement influencées par leur microenvironnement, qui module la progression de la tumeur et a un impact important sur la réponse à la thérapie. La co-culture de cellules tumorales avec des CAF permet de reproduire, en partie, les interactions entre les différents types de cellules, qui sont connues pour affecter la progression de la maladie et l'efficacité des thérapies anticancéreuses. Ici, nous avons développé un modèle de co-culture (directe) en 3D en associant des cellules de CG aux CAF. Dès le deuxième jour de la co-culture, les sphéroïdes ont pris une forme plus compacte, par rapport aux sphéroïdes en monocultures. Cela n'a pas eu d'impact négatif sur la réponse aux médicaments, la combinaison de docétaxel et de lovastatine a montré également une forte cytotoxicité dans cette configuration (Figure 5).

Le suivi en temps réel de la réponse au médicament des sphéroïdes tumoraux 3D s'est avéré être une approche assez sensible et fiable pour déterminer la toxicité globale, à la fois dans les sphéroïdes mono- et bicellulaires. Transposés à une configuration clinique, ces résultats peuvent conduire à proposer l'association de lovastatine et de docetaxel pour le traitement des patients atteints de CG. Un avantage évident de cette thérapie combinée serait d'utiliser des doses de médicaments plus faibles que celles habituellement utilisées, réduisant ainsi les effets secondaires toxiques potentiels, comme ceux qui ont été rapportés chez les patients cancéreux subissant une thérapie anticancéreuse aux taxanes.

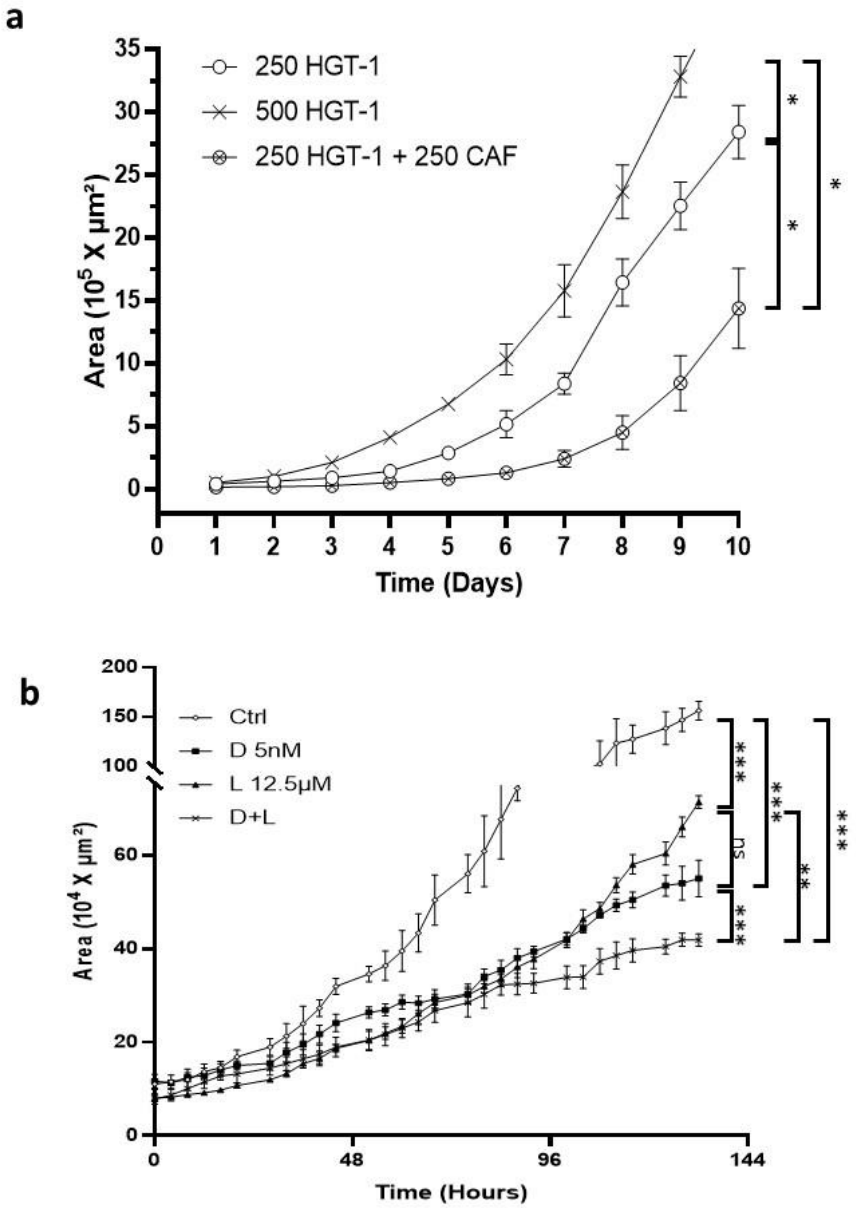

Figure 5. Sphéroïdes bicellulaires.
(a) Suivi de croissance en temps réel (surface 10^5 x µm²) effectué en utilisant l'IncuCyte™. Les sphéroïdes monocellulaires générés à partir de : i) 250 cellules HGT-1 sont représentés par des cercles blancs, ii) 500 cellules HGT-1 sont représentées par un symbole X noir et iii) les sphéroïdes bicellulaires générés à partir de 250 HGT-1 + 250 CAF sont représentés par des X à l'intérieur des cercles. (b) Suivi de croissance (surface 10^4 x µm²) des sphéroïdes bicellulaires formés de 250 HGT-1 + 250 CAF réalisé à l'aide de l'IncuCyte™. Des traitements simples avec 5nM de docétaxel (D 5nM) (carrés noirs), 12,5µM de lovastatine (L 12,5µM) (triangles noirs) et un traitement combiné avec 5nM de docétaxel + 12,5µM de lovastatine (D+L) (X noir) ont été appliqués sur des sphéroïdes âgés de 6 jours et comparés au contrôle (losanges blancs). Les résultats sont présentés comme la moyenne ± ET de n=3 expériences indépendantes avec quatre réplicats techniques dans chacune. ns $p > 0.05$; *$p \leq 0.05$ **$p \leq 0.01$; ***$p \leq 0.001$, one-way ANOVA suivie d'une analyse de Tukey.

Analyse des sphéroïdes multicellulaires du cancer gastrique par microscopie à deux photons

(Chapitre V)

Ces travaux ont été réalisés en collaboration avec le laboratoire OPTIMAG de l'Université de Brest. Ce laboratoire s'intéresse est spécialisé dans la microscopie, et en particulier la microscopie laser à 2 photons.

Le proverbe "voir, c'est croire" est souvent cité lorsque nous essayons de comprendre de nouveaux phénomènes en physiologie cellulaire. La microscopie optique 3D joue un rôle central en biologie, permettant l'imagerie d'échantillons à haute résolution spatiale et offrant la possibilité de détecter des structures en profondeur. Ici, nous proposons une méthode simple pour déterminer l'organisation spatiale des cellules contenues dans des sphéroïdes avec des étapes de manipulation faciles et adaptées à la bio-imagerie 3D en direct.

Les fibroblastes sont parmi les plus importants partenaires de signalisation stromale que l'on retrouve dans les différentes formes de cancers. Le développement de modèles de culture cellulaire en 3D a facilité la culture de différents types de cellules dans le même environnement. Dans notre travail, nous avons développé des sphéroïdes bicellulaires à partir de cellules de CG et de CAF et nous avons étudié leur organisation par imagerie 3D.

Plusieurs systèmes optiques souffrent de limitations comme la photodégradation ou l'éclaircissement optique et dépendent de la préparation de l'échantillon. Pour contourner certaines de ces limitations, nous avons développé une méthode simplifiée pour suivre la croissance et l'organisation de sphéroïdes vivants, en utilisant la microscopie à deux photons, une technique d'imagerie non invasive bien adaptée à l'analyse du développement et de la structure des sphéroïdes dans un format automatisé à moyen débit. En effet, la microscopie de fluorescence à deux photons a prouvé qu'elle générait des images au rapport signal / bruit plus élevé que la microscopie confocale à fluorescence classique. La faible phototoxicité permet des temps d'exposition plus longs qui sont requis pour l'imagerie tridimensionnelle de sphéroïdes multicellulaires [23, 24].

Nos résultats ont montré que cette approche était appropriée pour suivre la croissance et la structure des sphéroïdes. Il est également apparu que les cellules de ces sphéroïdes

bicellulaires étaient plus serrées, générant des sphéroïdes plus compacts que les sphéroïdes monocellulaires (Figure 6).

	HGT-1	HGT-1/CAF	P.Value
D4	210 ± 16	251 ± 8	0.0078
D6	468 ± 36	332 ± 24	0.0242
D8	685 ± 67	546 ± 31	0.0138
D11	898 ± 33	640 ± 21	0.0044

	AGS	AGS/CAF	P.Value
D4	315 ± 11	242 ± 22	0.0035
D6	526 ± 23	288 ± 15	0.0038
D8	785 ± 13	531 ± 45	0.0083
D11	1050 ± 59	616 ± 54	0.0023

Figure 6. Mesure de la taille des sphéroïdes.
Le diamètre des sphéroïdes est mesuré à partir des images TPEF (Two-photon excitation fluorescence) à l'aide du logiciel ImageJ. Les sphéroïdes monocellulaires générés à partir de 250 cellules HGT-1 et les sphéroïdes bicellulaires générés à partir de 250 HGT-1 + 250 CAF sont représentés dans le premier tableau. Les sphéroïdes monocellulaires générés à partir de 500 cellules AGS et les sphéroïdes bicellulaires générés à partir de 500 AGS + 500 CAF sont représentés dans le second tableau. Chaque mesure est réalisée sur trois sphéroïdes indépendants et les données sont présentées sous forme de moyenne ± ET, la troisième colonne indique la *P.value, Student's t.test*.

De manière intéressante, nous avons observé une distribution spatiale différente des cellules entre les lignées cellulaires de CG. Dans les sphéroïdes HGT-1/CAF, une distribution plus diffuse des deux types de cellules est observée avec une majoration des CAF en périphérie. En revanche, dans les sphéroïdes AGS/CAF, les fibroblastes sont concentrés dans la zone centrale, laissant les cellules cancéreuses à la périphérie (Figure 7).

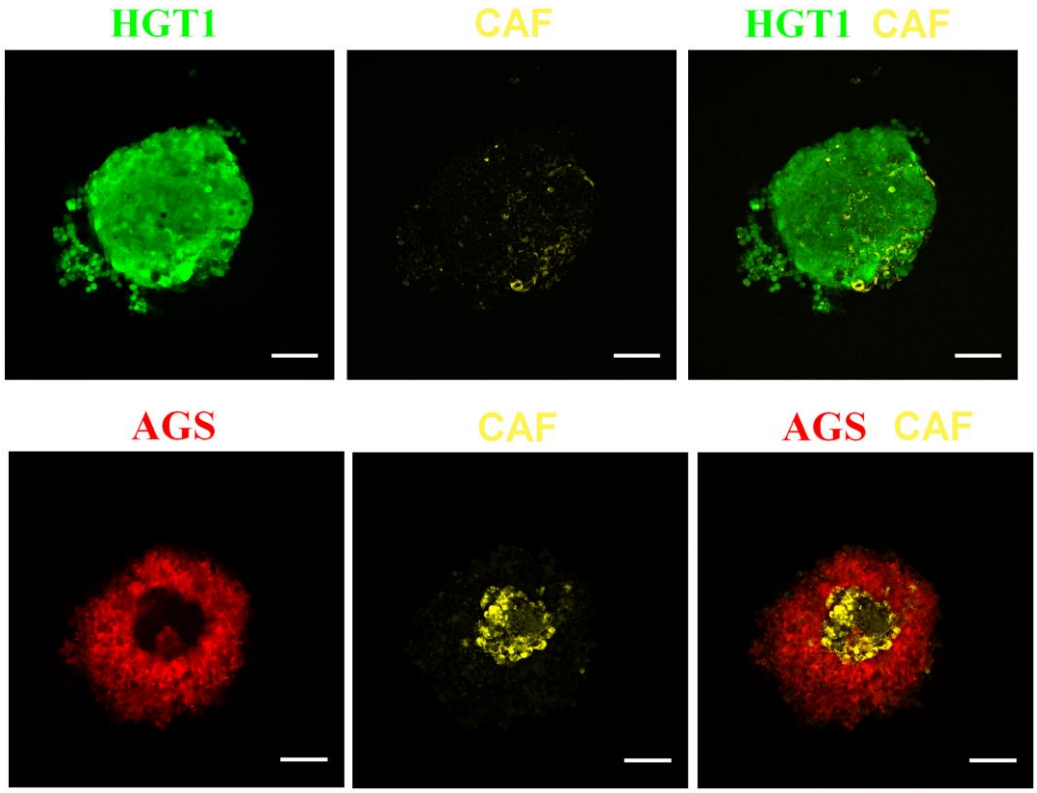

Figure 7. Distribution des cellules dans les sphéroïdes bicellulaires.
Partie supérieure : images TPEF (Two-photon excitation fluorescence) à plan unique d'un sphéroïde HGT-1/CAF âgés de 6 jours. A gauche : cellules HGT-1 (affichage eGFP - vert). Au milieu : CAF (autofluorescence - jaune). A droite : les cellules HGT-1 et les CAF sont affichés. Partie inférieure : images TPEF à plan unique d'un sphéroïde AGS/CAF âgés de 6 jours. A gauche : cellules AGS marquées (affichage TdTomato – rouge). Au milieu : CAF (autofluorescence – jaune). A droite : les cellules AGS et CAF sont affichées. Barre d'échelle : 100 µm.

En outre, l'addition différée de cellules HGT-1 à des sphéroïdes constitués uniquement de CAF a montré que les cellules HGT-1 pouvaient pénétrer dans ces sphéroïdes et récapituler l'organisation spatiale des sphéroïdes HGT-1/CAF. Au contraire, les cellules AGS restaient à la surface des sphéroïdes de CAF. Ces comportements distincts suggèrent l'existence de différences propres à chacune des lignées dans leur aptitude migratoire / invasive, comme cela a été rapporté pour d'autres cellules tumorales.

Ainsi, nous avons étudié l'expression des gènes codant pour des molécules d'adhésion telles que la E-cadhérine, la molécule d'adhésion des cellules épithéliales (EpCam), l'intégrine bêta 1 (ITGB1) et l'intégrine bêta 3 (ITGB3) dans les cellules HGT-1 et AGS. De nettes différences

étaient observées entre ces deux lignées cellulaires. Afin de déterminer la contribution de ces gènes dans l'organisation spatiale des cellules cultivées en 3D, nous avons inhibé l'expression de l'ITGB3 par siRNA dans les cellules HGT-1. Les résultats préliminaires ont montré une organisation des cellules dans les sphéroïdes bicellulaires HGT-1/CAF ressemblant à celle des sphéroïdes AGS/CAF suite cette l'inhibition. En outre, les tests de migration cellulaire en 2D ont montré une plus grande capacité migratoire des cellules HGT-1 par rapport aux cellules AGS. Cette capacité est considérablement réduite après l'inhibition de l'ITGB3 dans les cellules HGT-1, ramenant leur potentiel migratoire à un niveau proche de celui des cellules AGS. D'autres essais doivent être réalisés pour confirmer le rôle de l'ITGB3 et identifier son mécanisme d'action. Les rôles potentiels d'autres intégrines seront également testés afin de déterminer la spécificité ou non de l'ITGB3 dans le contrôle du potentiel migratoire et de l'organisation cellulaire des sphéroïdes.

Conclusion générale

Dans une étude précédente, notre équipe a démontré que la lovastatine induisait une apoptose massive des cellules de CG cultivées en 2D. Cet effet était plus qu'additif à celui du docétaxel. Dans le présent travail, l'étude est étendue aux cultures en 3D. En utilisant le système d'imagerie et d'analyse cellulaire par microscopie en temps réel l'IncuCyte^{TM}, en plus d'autres tests d'apoptose et de viabilité cellulaire, l'association docétaxel et lovastatine s'est avérée très efficace pour induire la mort des cellules de CG. Maintenant que notre modèle 3D est bien caractérisé, il fera l'objet de prochains tests de cytotoxicité en utilisant différents médicaments (oxaliplatine, 5-FU... avec ou sans statines) et des molécules de la chimiothèque "Prestwick" (composée de médicaments déjà commercialisés de différentes catégories, disponible au laboratoire) afin de rechercher de nouvelles molécules d'intérêt thérapeutique potentiel.

L'analyse structurale des sphéroïdes mono- et bicellulaires a été conduite par microscopie à deux photons permettant une imagerie en profondeur des échantillons. Les images ont montré une distribution spatiale différente et caractéristique des cellules cancéreuses et des CAF, de manière distinctive entre les lignées cellulaires de CG, HGT-1 et AGS. Nous avons été en mesure d'imager 2 types de cellules différentes dans un même échantillon sans aucune coloration après la formation du sphéroïde. En effet, des sous-populations HGT-1 et AGS marquées par des protéines fluorescentes eGFP (vert) ou TdTomato (rouge), respectivement, ont été générées par infection lentivirale et utilisées pour produire des sphéroïdes avec des CAF qui ont présenté une forte autofluorescence sans aucun marquage.

Selon la question scientifique, notamment en ce qui concerne les effets des médicaments, les cultures en 3D pourraient être plus adaptées que les cultures en 2D. Étant donné que les procédures d'établissement de cultures 3D de sphéroïdes peuvent être standardisées, nous pensons que celles-ci devraient constituer le futur "modèle standard" pour la découverte de médicaments. Néanmoins, elles devraient idéalement être complétées par des approches d'imagerie 3D et d'analyse ''-omiques''. Cette combinaison nécessite des techniques et des outils bioinformatiques novateurs permettant de simplifier l'analyse des données générées par les outils biologiques au niveau ''-omiques'' et surtout de profiter de la grande quantité de données générées pour essayer de comprendre les mécanismes physiopathologiques d'un

modèle qui représentent mieux l'*in vivo*. Avec ces outils nous pourrons passer à l'analyse au niveau de simple cellule que ce soit en transcriptomique, mais aussi en métabolomique. Profitant du développement d'un système analytique sensible par l'amélioration des limites de détection dans le laboratoire de MetaToul (Toulouse-France), des analyses métabolomiques des sphéroïdes HGT-1 ou AGS ont été initiées. Ces approches, grâce à leur haute sensibilité, permettent l'analyse des profils métabolomiques des cellules contenues d'un seul sphéroïde.

Références

[1] H. Sung *et al.*, "Global cancer statistics 2020: GLOBOCAN estimates of incidence and mortality worldwide for 36 cancers in 185 countries," *CA. Cancer J. Clin.*, vol. 71, no. 3, pp. 209–249, May 2021, doi: 10.3322/caac.21660.

[2] P. Lauren, "The two histological main types of gastric carcinoma: diffuse and so-called intestinal-type carcinoma. An attempt at a histo-clinical classification.," *Acta Pathol. Microbiol. Scand.*, vol. 64, pp. 31–49, 1965, doi: 10.1111/apm.1965.64.1.31.

[3] M. Balakrishnan, R. George, A. Sharma, and D. Y. Graham, "Changing trends in stomach cancer throughout the world," *Curr. Gastroenterol. Rep.*, vol. 19, no. 8., Aug. 2017, doi: 10.1007/s11894-017-0575-8.

[4] P. Rawla and A. Barsouk, "Epidemiology of gastric cancer: global trends, risk factors and prevention," *Przegląd Gastroenterol.*, vol. 14, no. 1, p. 26, 2019, doi: 10.5114/PG.2018.80001.

[5] S. S. Lee, H. Y. Chung, O. K. Kwon, and W. Yu, "Long-term quality of life after distal subtotal and total gastrectomy symptom-and behavior-o riented con sequences," *Ann. Surg.*, vol. 263, no. 4, pp. 738–744, 2016, doi: 10.1097/SLA.0000000000001481.

[6] K. Fujitani *et al.*, "Gastrectomy plus chemotherapy versus chemotherapy alone for advanced gastric cancer with a single non-curable factor (REGATTA): a phase 3, randomised controlled trial," *Lancet Oncol.*, vol. 17, no. 3, pp. 309–318, Mar. 2016, doi: 10.1016/S1470-2045(15)00553-7.

[7] L. L. Gunderson, R. Bruce Hoskins, A. C. Cohen, S. Kaufman, W. C. Wood, and R. W. Carey, "Combined modality treatment of gastric cancer," *Int. J. Radiat. Oncol.*, vol. 9, no. 7, pp. 965–975, Jul. 1983, doi: 10.1016/0360-3016(83)90383-8.

[8] S. E. Al-Batran *et al.*, "Histopathological regression after neoadjuvant docetaxel, oxaliplatin, fluorouracil, and leucovorin versus epirubicin, cisplatin, and fluorouracil or capecitabine in patients with resectable gastric or gastro-oesophageal junction adenocarcinoma (FLOT4-AIO): results from the phase 2 part of a multicentre, open-label, randomised phase 2/3 trial," *Lancet Oncol.*, vol. 17, no. 12, pp. 1697–1708, Dec. 2016, doi: 10.1016/S1470-2045(16)30531-9.

[9] J.-P. Gillet, S. Varma, and M. M. Gottesman, "The clinical relevance of cancer cell lines," *J. Natl. Cancer. Inst.*, vol. 105, pp. 452–458, 2013, doi: 10.1093/jnci/djt007.

[10] L. M. McCaffrey and I. G. Macara, "Epithelial organization, cell polarity and tumorigenesis," *Trends Cell Biol.*, vol. 21, no. 12, pp. 727–735, Dec. 2011, doi: 10.1016/J.TCB.2011.06.005.

[11] J. Jung, H. S. Seol, and S. Chang, "The generation and application of patient-derived xenograft model for cancer research," *Cancer Res. Treat.*, vol. 50, no. 1, pp. 1–10, Jan. 2018, doi: 10.4143/crt.2017.307.

[12] F. Sensi, E. D'Angelo, S. D'Aronco, R. Molinaro, and M. Agostini, "Preclinical three-dimensional colorectal cancer model: The next generation of in vitro drug efficacy evaluation," *J. Cell. Physiol.*, vol. 234, no. 1, pp. 181–191, Jan. 2018, doi: 10.1002/jcp.26812.

[13] P. Longati *et al.*, "3D pancreatic carcinoma spheroids induce a matrix-rich, chemoresistant phenotype offering a better model for drug testing," *BMC Cancer*, vol. 13, Feb. 2013, doi: 10.1186/1471-2407-13-95.

[14] A. I. Minchinton and I. F. Tannock, "Drug penetration in solid tumours," *Nat. Rev. Cancer*, vol. 6, no. 8, pp. 583–592, Aug. 2006, doi: 10.1038/nrc1893.

[15] G. Alzeeb, J. P. Metges, L. Corcos, and C. Le Jossic-Corcos, "Three-dimensional culture systems in gastric cancer research," *Cancers*, vol. 12, no. 10, pp. 1–20, Oct. 2020, doi: 10.3390/cancers12102800.

[16] Z. Lao *et al.*, "Improved methods to generate spheroid cultures from tumor cells, tumor cells & fibroblasts or tumor-fragments: microenvironment, microvesicles and miRNA," *PLoS One*, vol. 10, no. 7, p. e0133895, Jul. 2015, doi: 10.1371/JOURNAL.PONE.0133895.

[17] J. SY, L. JH, S. Y, C. S, and K. HJ, "Co-culture of tumor spheroids and fibroblasts in a collagen matrix-incorporated microfluidic chip mimics reciprocal activation in solid tumor microenvironment," *PLoS One*, vol. 11, no. 7, Jul. 2016, doi: 10.1371/JOURNAL.PONE.0159013.

[18] M. V. Plikus *et al.*, "Fibroblasts: origins, definitions, and functions in health and disease," *Cell*, vol. 184, no. 15, pp. 3852–3872, Jul. 2021, doi: 10.1016/J.CELL.2021.06.024.

[19] E. Sahai *et al.*, "A framework for advancing our understanding of cancer-associated fibroblasts," *Nat. Rev. Cancer*, vol. 20, no. 3, pp. 174–186, Jan. 2020, doi: 10.1038/S41568-019-0238-1.

[20] T. Sato *et al.*, "Long-term expansion of epithelial organoids from human colon, adenoma, adenocarcinoma, and Barrett's epithelium," *Gastroenterology*, vol. 141, no. 5, pp. 1762–1772, 2011, doi: 10.1053/j.gastro.2011.07.050.

[21] K. Werner, J. Weitz, and D. E. Stange, "Organoids as model systems for gastrointestinal diseases: tissue engineering meets genetic engineering," *Curr. Pathobiol. Rep.*, vol. 4, no. 1, pp. 1–9, Mar. 2016, doi: 10.1007/s40139-016-0100-z.

[22] H. H. N. Yan *et al.*, "A comprehensive human gastric cancer organoid biobank captures tumor subtype heterogeneity and enables therapeutic screening," *Cell Stem Cell*, vol. 23, no. 6, pp. 882-897, Dec. 2018, doi: 10.1016/J.STEM.2018.09.016.

[23] M. Drobizhev, N. S. Makarov, S. E. Tillo, T. E. Hughes, and A. Rebane, "Two-photon absorption properties of fluorescent proteins," *Nat. Methods*, vol. 8, no. 5, p. 393, May 2011, doi: 10.1038/NMETH.1596.

[24] T. Nemoto, R. Kawakami, T. Hibi, K. Iijima, and K. Otomo, "Two-photon excitation

fluorescence microscopy and its application in functional connectomics," *Microscopy*, vol. 64, no. 1, pp. 9–15, Feb. 2015, doi: 10.1093/JMICRO/DFU110.

Annex II
PML Hyposumoylation Is Responsible For The Resistance of Pancreatic Cancer

This annex will contain a research paper of some of the work done during my Masters internship at the 'Centre de Recherche en Cancerologie de Marseille –CRCM', 'Institut Paoli-Calmettes', Inserm UMR1068, Aix-Marseille University. This study was published in *The FASEB Journal* in *2019*.

This work explores the resistance mechanisms of pancreatic cancer relying on the post-translational modifications (PTMs) of involved proteins. This approach pointed at an alteration of Promyelocytic Leukemia protein (PML) sumoylation associated with both gemcitabine and oxaliplatin resistance.

PML hyposumoylation is responsible for the resistance of pancreatic cancer

Mirna Swayden,* George Alzeeb,* Rawand Masoud,* Yolande Berthois,* Stéphane Audebert,* Luc Camoin,* Laurent Hannouche,† Hortense Vachon,† Odile Gayet,* Martin Bigonnet,* Julie Roques,* Françoise Silvy,* Alice Carrier,* Nelson Dusetti,* Juan L. Iovanna,* and Philippe Soubeyran*,[1]

*Centre de Recherche en Cancérologie de Marseille (CRCM), Centre National de la Recherche Scientifique (CNRS), Institut Paoli-CalmettesCentre de Recherche en Cancérologie de Marseille (CRCM), and †Transcriptomique and Génomique Marseille Luminy (TGML), Théories et Approches de la Complexité Génomique (TAGC), INSERM, Aix-Marseille University, Marseille, France

ABSTRACT: The dismal prognosis of pancreatic ductal adenocarcinoma (PDAC) is mainly due to its rapidly acquired resistance to all conventional treatments. Despite drug-specific mechanisms of resistance, none explains how these cells resist the stress induced by any kind of anticancer treatment. Activation of stress-response pathways relies on the post-translational modifications (PTMs) of involved proteins. Among all PTMs, those mediated by the ubiquitin family of proteins play a central role. Our aim was to identify alterations of ubiquitination, neddylation, and sumoylation associated with the multiresistant phenotype and demonstrate their implications in the survival of PDAC cells undergoing treatment. This approach pointed at an alteration of promyelocytic leukemia (PML) protein sumoylation associated with both gemcitabine and oxaliplatin resistance. We could show that this alteration of PML sumoylation is part of a general mechanism of drug resistance, which in addition involves the abnormal activation of NF-κB and cAMP response element binding pathways. Importantly, using patient-derived tumors and cell lines, we identified a correlation between the levels of PML expression and sumoylation and the sensitivity of tumors to anticancer treatments.—Swayden, M., Alzeeb, G., Masoud, R., Berthois, Y., Audebert, S., Camoin, L., Hannouche, L., Vachon, H., Gayet, O., Bigonnet, M., Roques, J., Silvy, F., Carrier, A., Dusetti, N., Iovanna, J. L., Soubeyran, P. PML hyposumoylation is responsible for the resistance of pancreatic cancer. FASEB J. 33, 12447–12463 (2019). www.fasebj.org

KEY WORDS: chemoresistance · post-translational modification · ubiquitin family · promyelocytic leukemia protein · sumoylation

Pancreatic cancer at present is the fourth leading cause of cancer-related death worldwide (1). Pancreatic ductal adenocarcinoma (PDAC) makes up 90% of pancreatic cancer, with a poor prognosis and an overall 5-yr survival rate of only 8% (2). Surgery is often considered to be the main cure for PDAC; however, 80% of patients with PDAC cannot be resected at the time of diagnosis. Adjuvant chemotherapies using a combination of cytotoxic drugs such as the FOLFIRINOX protocol (3) or gemcitabine-nab-paclitaxel (4) may in some cases successfully reduce tumor size or improve the prognosis but their efficiency remains limited and, most of the time, relapse occurs. This is due to the fact that PDAC is characterized by an extraordinary resistance toward all anticancer treatments. Although drug-specific mechanisms have been studied for each treatment (5), the general mechanisms of resistance of PDAC cells remain poorly known, although they represent clinically important therapeutic targets to be used in combination with current chemotherapies.

Chemotherapeutic drugs used in clinics are heavy cellular-stress inducers, which are expected to provoke the death of cancer cells. However, PDAC cells have extremely efficient stress responses that enable them to survive in these conditions. Stress-response pathways rely on constituent proteins whose activities are tightly regulated by their post-translational modifications (PTMs) that enable

ABBREVIATIONS: AGC, automatic gain control; ALDH1A1, aldehyde dehydrogenase 1 family member A1; CREB, cAMP response element binding; FBS, fetal bovine serum; FWHM, full width at half maximum; GFP, green fluorescent protein; GTF, gene transfer format; i.d., interior diameter; IPA, Ingenuity Pathway Analysis; NB, nuclear body; Nedd8, neural precursor cell expressed developmentally down-regulated 8; PDAC, pancreatic ductal adenocarcinoma; PDX, patient-derived xenograft; PML, promyelocytic leukemia; PTM, post-translational modification; R-Gem, gemcitabine resistant; R-Ox, oxaliplatin resistant; RNA-seq, RNA sequencing; ROC, receiver operating characteristic; ROS, reactive oxygen species; SENP, SUMO-specific peptidase; siRNA, small interfering RNA; SUMO, small Ubl modifier; TBS, Tris-buffered saline; Ubl, ubiquitin-like; WT, wild type

[1] Correspondence: Centre de Recherche en Cancérologie de Marseille, CRCM, INSERM UMR1068, CNRS UMR7258, Université U105, Institut Paoli-Calmettes, Parc Scientifique de Luminy, 163, Avenue de Luminy, 13288 Marseille Cedex 9, France. E-mail: philippe.soubeyran@inserm.fr

doi: 10.1096/fj.201901091R
This article includes supplemental data. Please visit *http://www.fasebj.org* to obtain this information.

the activation or inactivation of these pathways. Thus, overactivation of stress responses in PDAC is a potential consequence of alterations of PTMs regulating the overall process. This is not surprising because PTMs are involved in the control of all biologic functions and, consequently, alterations of PTMs are always involved in cancer development and progression (6). This has also been shown for PTMs by ubiquitin-like (Ubl) proteins, which are known to control a wide range of physiologic processes in eukaryotic cells (7) and are often described in cancer diseases (8).

Ubiquitin is a 76-aa protein with a MW of 8.5 kDa (9). Ubiquitylation is the formation of an isopeptide bond between the COOH group of the C-terminal glycine of ubiquitin and the NH_2 group of a lysine residue of the target protein (10). Ubiquitylation is carried out by the successive activity of 3 enzymes (E1, E2, and E3) (11), whose actions are reversed by deubiquitylating enzymes (12). Ubiquitin itself can be conjugated to another ubiquitin through 1 of its 7 lysine residues or through its N-terminal methionine, resulting in the formation of 8 different types of polyubiquitin chains. These different types of ubiquitylation orchestrate the functions of a protein through the regulation of different properties such as its interactions, localization, activity, and degradation (13). This large variety of ubiquitin functions is widened by the existence of 17 Ubl proteins, which share the same structure and follow the same successive scheme of conjugation with their own set of enzymes (14, 15). Because of their central role in maintaining cellular homeostasis, deregulation of Ubl-mediated PTMs plays a role in many human pathologies, including cancer, representing a valuable source of new therapeutic targets or cotargets when dealing with resistance mechanisms (16, 17).

Looking for alterations of PTMs associated with PDAC, we have previously shown that such alterations induced by gemcitabine treatment can favor cell survival in response to chemotherapy (18). Our goal in this study was to identify general mechanisms of resistance of PDAC cells (*i.e.*, alterations of PTMs found in resistance to different treatments). We generated the profiles of proteins modified by ubiquitin, neural precursor cell expressed developmentally down-regulated 8 (Nedd8), and small Ubl modifier (SUMO) 1 in PDAC gemcitabine-resistant (R-Gem) cells or oxaliplatin-resistant (R-Ox) cells. Comparison with parental cells led us to the identification of resistance-specific alterations of PTMs. The comparison of these alterations allowed us to identify common PTM substrates, among which was promyelocytic leukemia (PML), a protein well known for its role in acute PML (19) as well as in other cancers (20) but whose sumoylation has never been described in resistance mechanisms or in PDAC until now. Our results clearly showed that the decrease of PML sumoylation resulted in the alteration of its functions and played a significant role in the resistance of pancreatic cancer cells through mechanisms involving NF-κB- and cAMP response element binding (CREB)–dependent pathways. Importantly, we could correlate the level of expression and sumoylation of PML in PDX (patient-derived xenograft) samples with their sensitivity to anticancer treatments. Thus, by searching for alterations of PTMs associated with a resistant phenotype of pancreatic cancer cells, we were able to identify a new mechanism of multiresistance that had not been detected so far by standard genomic and transcriptomic approaches.

MATERIALS AND METHODS

Cell lines, antibodies, and reagents

MiaPaCa-2 and HEK-293T cell lines were maintained and manipulated following American Type Culture Collection (Manassas, VA, USA) recommendations. MiaPaCa-2 cell lines resistant to 20 μM oxaliplatin and 20 μM gemcitabine were produced by gradually increasing the concentration of both drugs by 50% after each subcultivation starting from a minimum concentration of 10 nM up to 20 μM. Parental cells were grown in parallel without treatment to produce control cells. The following antibodies and reagents were used: mouse monoclonal anti-Flag (M2; MilliporeSigma, Burlington, MA, USA), mouse monoclonal anti-PML (sc-966; Santa Cruz Biotechnology, Dallas, TX, USA), Lipofectamine 2000 (11668-019; Thermo Fisher Scientific, Waltham, MA, USA), PrestoBlue (A13262; Thermo Fisher Scientific), Ni2+-NTA agarose beads (Qiagen, Hilden, Germany), imidazole (I2399; MilliporeSigma), anti-flag M2 agarose beads (A2220; MilliporeSigma), Flag peptide (F3290; MilliporeSigma), and Alexa Fluor 568 donkey anti-mouse IgG (A10037; Thermo Fisher Scientific). Anti-SUMO1 (21C7) and anti-SUMO-2/3 (8A2) hybridomas were obtained from Dr. Bossis (IGMM, Montpellier, France), and antibodies were produced using Celline Classic bioreactor flask CL (MilliporeSigma) following the manufacturer's instructions. NF-κB activator SRI-22782 (6090784; Chembridge, San Diego, CA, USA), NF-κB inhibitor BMS-345541 (B9935; MilliporeSigma), CREB inhibitor 666-15 (5661; Tocris Bioscience, Bristol, United Kingdom), cAMP activator Forskolin (F6886; MilliporeSigma). PML4 wild type (WT) and triple lysine to arginine mutant 3K ($K_{65,160,490}R$) in pCMVtag2B-Flag mammalian expression vector have been previously described.

Lentiviral infection of MiaPaCa2 cells with 6HF-Ubl constructs

A tandem 6-His and Flag tag was introduced into an empty pCCL-WPS-mPGK lentiviral vector at the 5′ end of the multicloning sites portion to produce the pCCL-6HF vector. The full-length cDNA for human ubiquitin, Nedd8, and SUMO1 were subcloned into this vector using *Sma*I and *Eco*RV restriction sites for ubiquitin, *Bam*HI and *Eco*RV for Nedd8, and *Bam*HI for SUMO1. Each plasmid was verified by DNA sequencing. Lentiviral particles were generated by transfecting 293T cells with a mix of 1/3 pCCL construct [ubiquitin, Nedd8, SUMO1, or green fluorescent protein (GFP)], 1/3 δ Helper (carries sequence necessary for viral assembly of lentivirus), and 1/3 pVsVg (expresses the vesicular stomatitis virus envelop glycoprotein G pseudotype) using Lipofectamine reagent and following manufacturer's recommendations. At 24 h post-transfection, the medium was replaced. At 24 h later, the medium was changed again, and viruses containing medium were collected, filtered through a 0.2-μm filter, and added on 40% confluent MiaPaCa2 R-Gem cells and MiaPaCa2 R-Ox cells seeded in 25-cm^2 flasks. This step was repeated 24 h later to perform a second infection. At 5 d after infection, expression of GFP was verified by fluorescence microscopy, and ubiquitin, Nedd8, and SUMO1 expression was controlled by Western blot.

The 2-step purification of 6His-flag-ubiquitin, -Nedd8, and -SUMO1 conjugates

MiaPaCa-2 parental and resistant cells expressing the 6HF-Ubl constructs or GFP were seeded in 150-mm dishes at 10^6 cells per dish, and when they reached 70% confluence, ~100

(MiaPaCa-2-6HF-ubiquitin and -SUMO1) or 150 mg (MiaPaCa-2-6HF-Nedd8) of proteins was used to isolate modified substrates. For each dish of parental or resistant cells, 2 ml of buffer 1 (6 M guanidinium-HCl, 0.1 M Na_2HPO_4/ NaH_2PO_4, pH 8.0 and 0.5% Triton X-100) was added directly to the cell monolayer. Lysates were sonicated 3 times for 30 s, with a 1-min break between pulses to reduce viscosity. Protein concentration was adjusted between untreated and treated samples using Protein Assay (Bio-Rad, Hercules, CA, USA), and Ni2+-NTA agarose resin (Qiagen) was added with a ratio of 2 μl resin for 1 mg proteins. Samples were rotated at room temperature for 2 h 30 min, and beads were then washed once with 1 ml of buffer 1 and twice with 1 ml of prechilled buffer 2 (50 mM NaH_2PO_4, 150 mM NaCl, 1% Tween 20, 5% Glycerol, pH 8.0) and 10 mM imidazole. Purified proteins were eluted for 2 h at 4°C in 600 μl of buffer 2 and 250 mM imidazole. Eluted proteins were then incubated with 50 μl anti-flag M2 agarose beads (MilliporeSigma) and rotated at 4°C for 2 h 30 min. Beads were then washed twice with 500 μl prechilled buffer 2. Purified proteins were eluted in 100 μl buffer 2 containing 0.1 μg/μl flag peptide by rotating at 4°C for 1 h 30 min. Eluted proteins were collected and analyzed by mass spectrometry.

Mass spectrometry analysis

Protein extracts were loaded on NuPAGE 4−12% Bis-Tris acrylamide gels according to the manufacturer's instructions (Thermo Fisher Scientific). Running was stopped as soon as proteins stacked in a single band. Protein-containing bands were stained with Imperial Blue (Thermo Fisher Scientific), cut from the gel, and digested with high-sequencing-grade trypsin (Promega, Madison, WI, USA) before mass spectrometry analysis. Mass spectrometry analysis was carried out by liquid chromatography and tandem mass spectrometry using an LTQ Velos Orbitrap or a Q Exactive Plus Hybrid Quadrupole-Orbitrap (Thermo Fisher Scientific) online with a nanoLC Ultimate 3000 RSLC chromatography system (Thermo Fisher Scientific). A total of 5 μl corresponding to one-fifth of the whole sample was injected in triplicate on the system. After preconcentration and washing of the sample on an Acclaim PepMap 100 C18 Column [2 cm × 100 μm interior diameter (i.d.) 100 Å, 5 μm particle size; Thermo Fisher Scientific), peptides were separated on an Acclaim PepMap RSLC C18 Column (15 cm × 75 μm i.d., 100 Å, 2 μm particle size; Thermo Fisher Scientific) at a flow rate of 300 nl/min, a 2-step linear gradient (4−20% acetonitrile and H_2O, 0.1% formic acid for 90 min, and 20−45% acetonitrile/H_2O; 0.1% formic acid for 30 min). For peptide ionization in the nanospray source, spray voltage was set at 1.9 kV, and the capillary temperature at 275°C. All samples were measured in a data-dependent acquisition mode. Each run was preceded by a blank MS run to monitor system background. The peptide masses were measured in the LTQ Velos Orbitrap in a survey full scan (scan range 300−1700 *m/z* with 30 K full width at half maximum (FWHM) resolution at *m/z* = 400, target automatic gain control (AGC) value of 1.00×10^6, and maximum injection time of 200 ms). In parallel to the high-resolution full scan in the Orbitrap, the data-dependent collision-induced dissociation (CID) scans of the 10 most-intense precursor ions were fragmented and measured in the linear ion trap (normalized collision energy of 35%, activation time of 10 ms, target AGC value of 1×10^4, maximum injection time 100 ms, and isolation window 2 Da). Parent masses obtained in the Orbitrap analyzer were automatically calibrated on 445.1200 locked mass. Dynamic exclusion was implemented with a repeat count of 1 and exclusion duration of 30 s.

In the Q Exactive Plus Hybrid Quadrupole-Orbitrap, the peptide masses were measured in a survey full scan (scan range 375–1500 *m/z*, with 70 K FWHM resolution at *m/z* = 400, target AGC value of 3.00×10^6, and maximum injection time of 100 ms). Following the high-resolution full scan in the Orbitrap, the 10 most-intense data-dependent precursor ions were successively fragmented in HCD cells and measured in Orbitrap (normalized collision energy of 25%, activation time of 10 ms, target AGC value of 1.00×10^3, intensity threshold 1.00×10^4, maximum injection time 100 ms, isolation window 2 *m/z*, 17.5 K FWHM resolution, scan range 200–2000 *m/z*). Dynamic exclusion was implemented with a repeat count of 1 and exclusion duration of 20 s.

Raw files generated from mass spectrometry analysis were processed using Proteome Discoverer v.1.4.1.14 (Thermo Fisher Scientific). This software was used to search data *via* an in-house Mascot server (v.2.3.0; Matrix Science, London, United Kingdom) against the human database subset of the SwissProt database (v.2017.03, 20184 human entries; *https://www.uniprot.org/*). A database search was done using the following settings: a maximum of 2 trypsin miscleavages allowed, methionine oxidation and protein *N*-acetylation as dynamic modification, and cysteine carbamidomethylation as fixed modification. A peptide mass tolerance of 6 ppm and a fragment mass tolerance of 0.8 Da were allowed for search analysis. Only peptides identified with a false discovery rate <1% were used for protein identification.

Mass spectrometry data processing to generate PTM profiles

To process raw data coming from mass spectrometry based on a peptide counting approach, we have used the following formulas in which, for each identified protein, v_1 corresponds to the number of peptides in parental value sample, v_2 corresponds to the number of peptides in resistant value sample, k_1 corresponds to the number of peptides in parental control sample, and k_2 corresponds to the number of peptides in resistant control sample.

Normalization

We have normalized values between parental and resistant cells for ubiquitin, Nedd8, SUMO1, and GFP control. Normalized $v = V$ and normalized $k = K$.

$$V_1 = v_1 \times \left(\sum v_1 + \sum v_2\right)/\left(2 \times \sum v_1\right)$$

$$V_2 = v_2 \times \left(\sum v_1 + \sum v_2\right)/\left(2 \times \sum v_2\right)$$

$$K_1 = k_1 \times \left(\sum k_1 + \sum k_2\right)/\left(2 \times \sum k_1\right)$$

$$K_2 = k_2 \times \left(\sum k_1 + \sum k_2\right)/\left(2 \times \sum k_2\right)$$

Specific to background values

To get a value for the specific number of identified peptides per protein (V'_1 and V'_2) and for each protein, we subtracted the number of peptides identified in control samples (GFP) from values (ubiquitin, Nedd8, and SUMO1)

$$V'_1 = V_1 - K_1 \text{ if } V_1 - K_1 \geq 0; V'_1 = 0 \text{ if } V_1 - K_1 < 0$$

$$V'_2 = V_2 - K_2 \text{ if } V_2 - K_2 \geq 0; V'_2 = 0 \text{ if } V_2 - K_2 < 0$$

Variation of PTM

To obtain a rate for positive and negative variations of PTMs induced by acquiring the resistant phenotype, we used the following formula where the difference between the parental and resistant specific values was divided by the sum of all peptides

including those in control (to penalize proteins identified with peptides in control sample) and multiplied by 100.

$$\mathrm{Var} = (V'_2 - V'_1)/(V_1 + K_1 + V_2 + K_2) \times 100$$
$$-100 < \mathrm{Var} < +100$$

Variations were considered as significant if they were below −50 or above 50.

Confidence in percentage

To obtain a confidence value between 0 and 100%, we used the following formula. The first part of the formula takes into account the proportion of peptides in control samples, and the second part further reduces the final value of proteins identified with few peptides.

$$\left((V_1 + V_2)^2/(1 + V_1 + V_2 + K_1 + K_2)^2\right) \times 100$$
$$- 100/(1 + V'_1 + V'_2); = 0 \text{ if } < 0$$

Immunoprecipitation

MiaPaCa-2 cells, controls, or R-Gem or R-Ox cells expressing 6HF-SUMO1 or GFP were plated in 10-cm^2 dishes. When they reached 80% confluence, cells were lysed on ice using HEPES-based lysis buffer containing 10 mM *N*-ethylmaleimide (04259; MilliporeSigma) and a cocktail of proteases inhibitor (1:200, P8340; MilliporeSigma). Lysates were centrifuged for 10 min at 14,000 rpm at 4°C. Protein concentration of the supernatant was determined using Protein Assay (Bio-Rad), and equal amounts of total protein were used to incubate with 50 μl anti-flag M2-coated beads and rotated for 2 h at 4°C. Beads were then washed 3 times with cold lysis buffer, and proteins were eluted using 250 μl HEPES lysis buffer containing 0.1 μg/μl of Flag peptide for 90 min while rotating at 4°C. After a short spin, the supernatant was recovered using Hamilton syringe. Protein samples were then concentrated using Amicon Ultra-0.5 Centrifugal Filter devices (MilliporeSigma) according to manufacturer's instructions prior to proceeding to SDS-PAGE.

Western blotting

Proteins were resolved by SDS-PAGE and transferred to nitrocellulose membranes for 1 h. Then, membranes were blocked 1 h at room temperature with Tris-buffered saline (TBS) and 5% bovine serum albumin and blotted overnight in TBS 5% bovine serum albumin containing primary antibodies at 1:500. After extensive washes in TBS 0.1% Tween 20, membranes were incubated for 1 h at room temperature with horseradish peroxidase–conjugated secondary antibodies at 1:5000 before being revealed with ECL. Acquisition was performed with a Fusion FX7 Imager (Vilber Lourmat, Collégien, France). Alternatively, SNAP i.d. Protein Detection System (MilliporeSigma) was used following the manufacturer's instructions.

Immunofluorescence

Cells grown on coverslips were fixed with formalin for 10 min and then blocked with 50 mM NH_4Cl in PBS for 10 min. After that, cell permeabilization was carried out by PBS and 0.2% Triton X-100 for 10 min. Blocking was performed with PBS and 5% fetal bovine serum (FBS) for 1 h and 30 min, and then cover slips were incubated for 2 h with anti-PML antibody in PBS and 5% FBS (1:50). Cover slips were incubated for 1 h with Alexa Fluor 568 donkey anti-mouse IgG as a secondary antibody in PBS and 5% FBS (1:50), then washed with PBS, covered with Vectashield mounting medium (H-1200; Vector Laboratories, Burlingame, CA, USA), and placed on microscopic slides.

Cell viability assay and caspase-3/7 assay

MiaPaCa-2 cells were seeded in a 96-well plate at a density of 20,000 cells per well and allowed to attach for 24 h. On the second d, Lipofectamine was used to transfect these cells with the plasmid encoding for GFP as a control, PCMCV-Tag2B flag-PML4 plasmid encoding WT PML and PCMCV-Tag2B flag-PML4 3MAS plasmid encoding mutant PML. On the third d, cells were treated with 1, 10, and 100 μM gemcitabine or oxaliplatin. After 72 h of incubation, 10 μl PrestoBlue was added to measure cell viability. For caspase-3/7 assay, 100 μl of substrate of the Caspase-Glo 3/7 Kit from Promega (G8093) was added according to manufacturer's directions. After 3 h of incubation with substrates, a Tristar LB 941 apparatus (Berthold Technologies, Bad Wildbad, Germany) was used to measure the fluorescence and emitted luminescence.

RNA sequencing

MiaPaCa-2 cells (control, R-Gem, and R-Ox) were grown is 10-cm Petri dishes and were transfected with GFP, PML-WT, or PML-3K expression vectors when reaching 40–50% confluence. At 48 h post-transfection, total RNA was isolated from the 9 samples and was used for the RNA sequencing (RNA-seq) library preparation using TruSeq mRNA-seq Stranded v2 Kit sample preparation (Illumina, San Diego, CA, USA). Libraries were paired-end sequenced on the Illumina NextSeq 500 sequencer. Reads with a phred score <20 and shorter than 25 bp were removed using Sickle (v.1.33) (*https://codeload.github.com/najoshi/sickle/tar.gz/v1.33*). Quality of trim reads was checked using multiQC (v1.0, *https://github.com/ewels/MultiQC.gitcd MultiQC*). Trim reads were aligned using STAR aligner (v.2.7.0d, *https://github.com/alexdobin/STAR.git*) with arguments "outFilterMismatchNoverLmax" and "outFilterMultimapNmax" set to 0.08 and 1, respectively. Transcripts discovery was performed using Cufflinks (v.2.2.1, *http://cole-trapnell lab.github.io/cufflinks/releases/v2.2.1*) with the "library-type" argument set to fr-firstrand, and a gene transfer format (GTF) file obtained from Gencode (Comprehensive gene annotation, vM1) provided as the genomic annotation. The GTF files produced for each sample by Cufflinks were combined using Cuffmerge. The class code assigned to each transcript by Cuffmerge was used to defined unknown transcripts (class code "u"). Only *de novo* transcripts with counts >0 in ≥1 RNA-seq sample were kept for subsequent analyses. These *de novo* transcripts were combined with the Gencode GTF file to produce the final genomic annotation that was provided to FeatureCounts (v.1.6.1, *http://subread.sourceforge.net*) for quantification. Differential gene expression was performed using Fisher test between 2 samples in all conditions. To create bigwig files, reads from Watson and Crick strands were selected using SAMtools (v.1.9, *https://sourceforge.net/projects/samtools/files/samtools/1.9*) and provided to the bam2wig.py script from the RseQC program suite (v.2.6.4, *https://sourceforge.net/projects/rseqc/files/RSeQC-2.6.4.tar.gz/download*). RNA-seq profiles were visualized using the Integrative Genomics Viewer genome browser. The Fisher differential expression data were used in Ingenuity Pathway Analysis (IPA; Qiagen) to identify which pathways were affected either positively or negatively (*z* score) by the acquisition of the resistant phenotype and by the expression of WT or 3K mutant PML.

Reactive oxygen species and superoxide anions staining and measurement by flow cytometry

MiaPaCa-2 parental cells, R-Gem cells, or R-Ox cells were seeded in a 12-well plate at a density of 5×10^5 cells per well. Cells were allowed to attach for 24 h, and then the cells were treated with 10 μM gemcitabine or oxaliplatin. After 24 h, 500 μl of 2.5 mM CellRox or 5 mM of MitoSox stain (Thermo Fisher Scientific) was added to each well, and the plates were incubated for 30 min for ROX stain and 20 min for SOX stain at 37°C. Cells were washed 1 time with hot PBS, and then 200 μl accutase was added to detach the cells. After that, the cells were homogenized with 1 ml DMEM and centrifuged for 5 min at 1500 rpm. The supernatant was discarded, and the pellet was resuspended with 200 μl HBSS. Samples were read by MACSQuant VYB flow cytometer (Miltenyi Biotech, Bergisch Gladbach, Germany).

Generation of PDXs

A total of 3 expert clinical centers collaborated on this project after receiving ethics review board approval. Patients were included in this project under the Paoli-Calmettes Institute clinical trial number 2011-A01439-32. Consent forms of informed patients were collected and registered in a central database. The tumor tissues used for xenograft generation were deemed excess to that required for the patient's diagnosis. PDAC tissue from surgical samples was fragmented, mixed with 100 ml Matrigel (BD Biosciences, Franklin Lakes, NJ, USA), and implanted with a trochar (10 gauge; Innovative Research of America, Sarasota, FL, USA) in the subcutaneous right upper flank of an anesthetized and disinfected male NMRI-nude mouse. Samples obtained from endoscopic ultrasound-guided fine needle aspiration were mixed with 100 ml Matrigel and injected in the upper-right flank of a male nude mouse [Swiss Nude Mouse Crl:NU(lco)-Foxn1nu; Charles River Laboratories, Wilmington, MA, USA] for the first implantation. When xenografts reached 1 cm, these were removed and passed to NMRI-nude mice in the same manner as surgical samples. In total, 30 xenografts from 29 different patients were generated, and early passages were used for large-scale molecular profiling.

Production of PDX primary cell lines

Primary cell cultures were obtained from xenografts. Tissues were split into several small pieces and processed in a biosafety chamber. After a fine mincing, they were treated with collagenase type V (ref C9263; MilliporeSigma) and trypsin-EDTA (ref 25200-056; Thermo Fisher Scientific) and suspended in DMEM supplemented with 1% penicillin-streptomycin (Thermo Fisher Scientific) and 10% FBS (Lonza, Basel, Switzerland). After centrifugation, cells were resuspended in serum-free ductal medium. without antibiotics and incubated at 37°C in a 5% CO_2 incubator.

Small interfering RNA interference

Small interfering RNA (siRNA) transfections were performed using Interferin reagent (Polyplus transfection, Illkirch, France) following the manufacturer's instructions. siRNA of SUMO-specific peptidase (SENP) 1, 2, and 6 were synthetized by Eurofins Scientific (Luxembourg, Luxembourg).

RNA extraction

Total RNA was purified from MiaPaCa-2 cells using Trizol Reagent (Thermo Fisher Scientific) according to the manufacturer's instructions. Briefly, cells were lysed with 1 ml Trizol followed by a single step of phenol-chloroform purification. Total RNA was quantified using the Epoch Microplate Spectrophotometer (BioTek Instruments, Winooski, VT, USA), and the quantity and purity of RNA was determined by optical density 260/280 reading using an Epoch Microplate Spectrophotometer.

Quantitative RT-PCR

cDNA synthesis was performed using the GoScript Reverse Transcription Kit (Promega) according to the manufacturer's protocol. Then, quantitative RT-PCR was performed in a MX3005P machine (Agilent Technologies, Santa Clara, CA, USA) using the SYBR Premix Ex Taq and Rox reference dye (Takara Bio, Kusatsu, Japan). Primers were synthetized by Eurofins Scientific.

Statistical analysis

The significance of differences between means from ≥3 independent experiments was established using the Student's *t* test for unpaired samples. Values of $P < 0.05$ were considered statistically significant. MedCalc (MedCalc Software, Ostend, Belgium) was used to generate receiver operating characteristic (ROC) curves and dot diagrams following the manual's instructions. We used the STRING online tool (*http://string-db.org*) in order to identify which of the alterations were included in functional interacting networks. ACSN (Atlas of Cancer Signaling Networks: */acsn.curie.fr*) database was used to identify signaling networks ImageJ from National Institutes of Health was used to quantify bands of western blot.

RESULTS

Alterations of PTM profiles induced by acquired resistance to gemcitabine or to oxaliplatin by pancreatic cancer cells

We have generated R-Gem and R-Ox PDAC cells (Supplemental Fig. S1) (see Materials and Methods for details), and, as we previously described (18), we used lentiviruses to produce stable cells expressing a 2-tagged (6his and Flag) version of ubiquitin, Nedd8, or SUMO1. We then generated the ubiquitylation, neddylation, and sumoylation profiles of R-Gem cells as well as control cells (**Fig. 1*A*, *B***, Supplemental Fig. S2*A*, and **Table 1**). These profiles were composed of 342 ubiquitylated, 189 neddylated, and 387 sumoylated proteins, among which 70 ubiquitylations, 50 neddylations, and 92 sumoylations were significantly altered (either increased or decreased) in resistant cells (Table 1). Comparing the list of ubiquitylated, neddylated, and sumoylated proteins together, we observed an important overlap between the 3 different kinds of PTM because 161 proteins may be modified by either ubiquitin, nedd8, or SUMO1 (Supplemental Fig. S3*A*). Focusing on resistance-associated PTM alterations, we noticed that most of them involved only 1 type of PTM (57 ubiquitylations, 32 neddylations, and 73 sumoylations) compared with 5, 11, and 6 double alterations (Fig. 1*A*). Only 2 proteins displayed an alteration of the 3 PTMs: aldehyde dehydrogenase 1 family member A1 (ALDH1A1) and glucosamine (UDP-*N*-acetyl)-2-epimerase/*N*-acetylmannosamine kinase (Supplemental Fig. S3*B*). We used the Search Tool for the Retrieval of

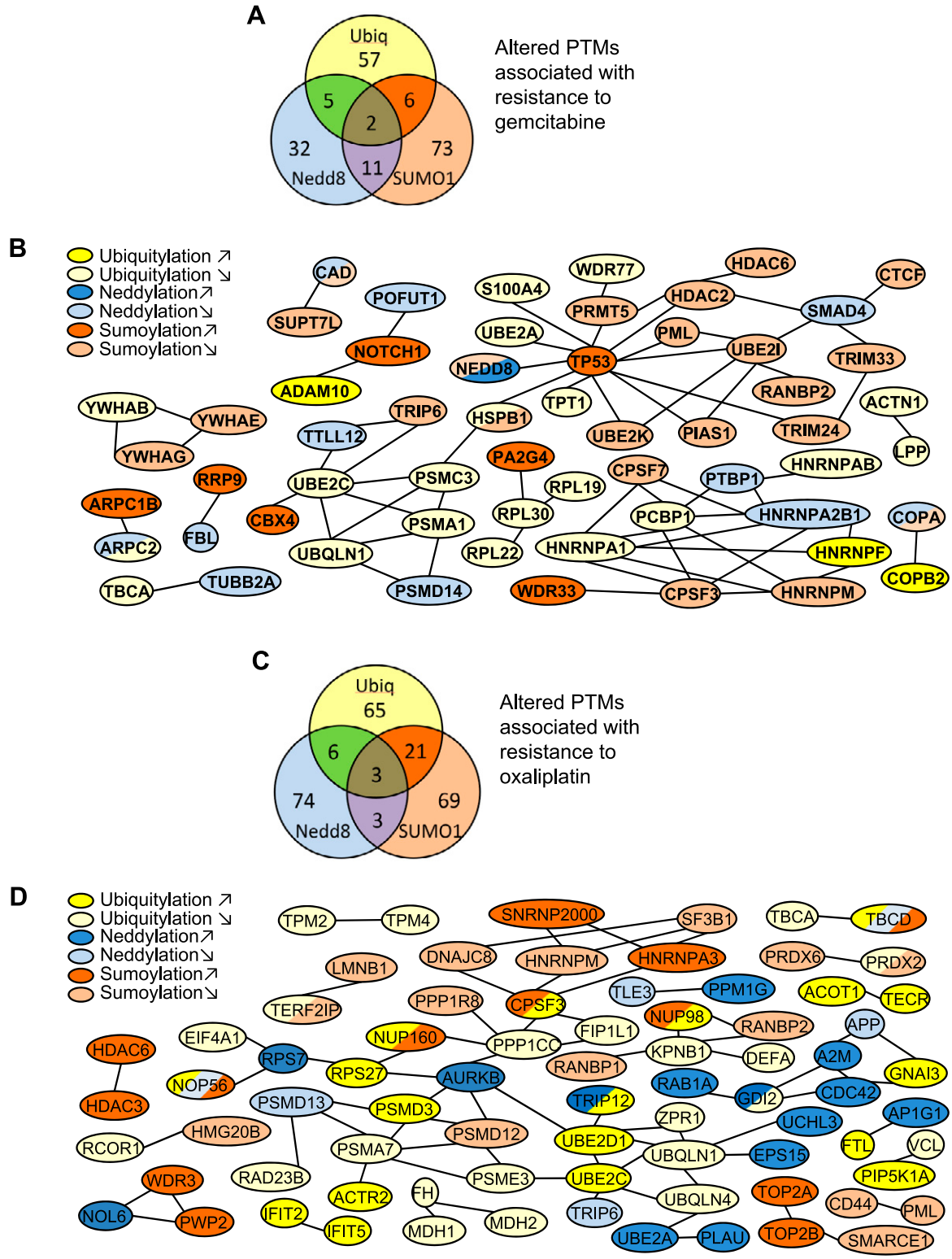

Figure 1. Gemcitabine and oxaliplatin resistance induced alterations of PTM profiles. *A*) Venn diagram showing the proportions of proteins with gemcitabine resistance–induced alteration of PTMs by 1, 2, or all 3 modifiers (total 186). *B*) Physical and functional interaction network of proteins with gemcitabine resistance–induced alteration of PTMs. A total of 59 of 186 proteins were found to interact with at least another 1. *C*) Venn diagram showing the proportions of proteins with oxaliplatin resistance–induced alteration of PTMs by 1, 2, or the 3 modifiers (total 241). *D*) Physical and functional interaction network of proteins with oxaliplatin resistance–induced alteration of PTMs. A total of 77 out of 241 proteins were found to interact with at least another 1.

Interacting Genes/Proteins (STRING) database (*http://string-db.org*) in order to identify which of the alterations were included in functional interacting networks. We observed that approximately one-third of them (59 out of 186) were already known to interact physically, and among them, we found an important node composed of

TABLE 1. *Proteins identified as ubiquitylated, neddylated, and sumoylated in control and R-Gem cells and the number of proteins with altered PTMs found in R-Gem cells compared with parental cells*

Gemcitabine	Total	↑	↓	→
Ubiquitylation	342	14	56	272
Neddylation	189	6	44	139
Sumoylation	387	33	59	295

TP53 and regulation of apoptosis, subnetworks with function in RNA splicing, Notch and TGF-β signaling pathways, and proteins involved in mesenchymal cell development (Fig. 1*B*).

We used the same strategy to generate the PTM profiles of R-Ox cells (Fig. 1*C, D*, Supplemental Fig. S2*B*, and **Table 2**), and we identified 393 ubiquitylated, 1040 neddylated, and 363 sumoylated proteins in both parental and R-Ox cells and 95, 86, and 96 alterations of ubiquitylation, neddylation, and sumoylation, respectively, associated with the R-Ox phenotype (Table 2). Studying the repartition of the 3 types of modifications, we observed (as before) an important proportion (123) of proteins modified by the 3 modifiers or by 2 of them (Supplemental Fig. S3*C*). Similar to gemcitabine resistance, PTM alterations associated with oxaliplatin resistance concerned mainly 1 type of modification (Fig. 1*C*), and only 3 proteins (cap methyltransferase 2, nucleolar protein 56, and tubulin folding cofactor D) displayed an alteration of ubiquitination, neddylation, and sumoylation (Supplemental Fig. S3*D*). Here as well, approximately one-third of oxaliplatin resistance–induced alterations of PTMs were found in functional interacting networks involved in the regulation of programmed cell death, response to stress, ubiquitin proteasome system, cell cycle, RNA processing, and DNA damage response (Fig. 1*D*).

Alterations of PTMs provoked by the acquisition of resistance involve common and drug-specific cancer signaling networks

We used the Atlas of Cancer Signalling Networks (*https//acsn.curie.fr*) database to identify which signaling networks are affected by the gain of resistance to gemcitabine and oxaliplatin (**Fig. 2**). Alterations of ubiquitination induced by both resistances targeted common and specific networks. Sonic hedgehog, PI3K, WNT, and TNF pathways were identically affected by gemcitabine and oxaliplatin resistance. Interestingly, oxaliplatin resistance specifically affected ubiquitinations in several DNA repair processes (homologous recombination, nucleotide excision repair, base excision repair, and nonhomologous end joining) and some cell cycle checkpoints, whereas gemcitabine resistance specifically altered ubiquitination in the caspase network and translesion bypass (Fig. 2*A*). Similar findings were observed with altered neddylation and altered sumoylation. Regarding neddylation, some signaling pathways were altered by both gemcitabine and oxaliplatin resistance such as AKT, MAPK, or WNT, whereas TNF response and Sonic Hedgehog were specific to oxaliplatin (Fig. 2*B*). Altered neddylation by oxaliplatin resistance specifically affected cell cycle–related networks and translesion bypass. Finally, altered sumoylations induced by oxaliplatin resistance specifically touched cell cycle and DNA repair networks, whereas gemcitabine resistance led principally to alterations of apoptosis and DNA repair pathways (Fig. 2*C*).

Identification of impaired PML sumoylation as a general mechanism of resistance

To identify a potential general mechanism of resistance looked for targets common to both resistances, as shown in **Table 3**, we identified 9 proteins that displayed altered ubiquitylation with both resistances, 2 neddylations, and 7 sumoylations. Most of these common alterations were in the same direction of variations: induced or repressed in both R-Gem and R-Ox cells (**Table 4**). Considering the central role of PML in cells and its implication in other cancer types and because its sumoylation has not been linked to chemoresistance so far, we first decided to confirm that the resistant phenotype of PDAC cells was associated with a repressed sumoylation of PML. As shown in **Fig. 3*A***, whereas we observed a robust sumoylation of PML in control cells, both R-Gem and R-Ox cells displayed a strong decrease of sumoylated PML, although the expression level of PML was similar in all cell types. We next tested the effect of anticancer treatments on PML sumoylation and observed that under gemcitabine or oxaliplatin treatment, the sumoylation of PML strongly increased in control cells (Fig. 3*B*). Interestingly, this response was impaired in resistant cells because the sumoylation of PML in R-Gem cells was not induced upon treatment with gemcitabine or with oxaliplatin (Fig. 3*C*). The same result was obtained with R-Ox cells (Fig. 3*D*).

Impaired PML sumoylation is associated with impaired nuclear body formation

The majority of PML functions depend on its capacity to form and stabilize PML nuclear bodies (NBs). Therefore, we verified if the impaired PML sumoylation could also impair the formation of NBs in resistant PDAC cells. We performed immunofluorescence studies using anti-PML antibody in order to visualize PML-NBs (**Fig. 4*A***). As expected, we observed a significant decrease of the mean number of NBs per nucleus in resistant cells (Fig. 4*B*). In addition, we also noticed a statistically significant decrease of the overall size (fluorescence intensity) of NBs in resistant cells (−30% for R-Gem cells and −20% for R-Ox cells) (Fig. 4*C*). Moreover, NBs are dynamic structures that

TABLE 2. *Proteins identified as ubiquitylated, neddylated, and sumoylated in control and R-Ox cells and the number of proteins with altered PTMs in resistant cells compared with parental cells*

Oxaliplatin	Total	↑	↓	→
Ubiquitylation	393	45	50	298
Neddylation	1040	50	36	954
Sumoylation	363	54	42	267

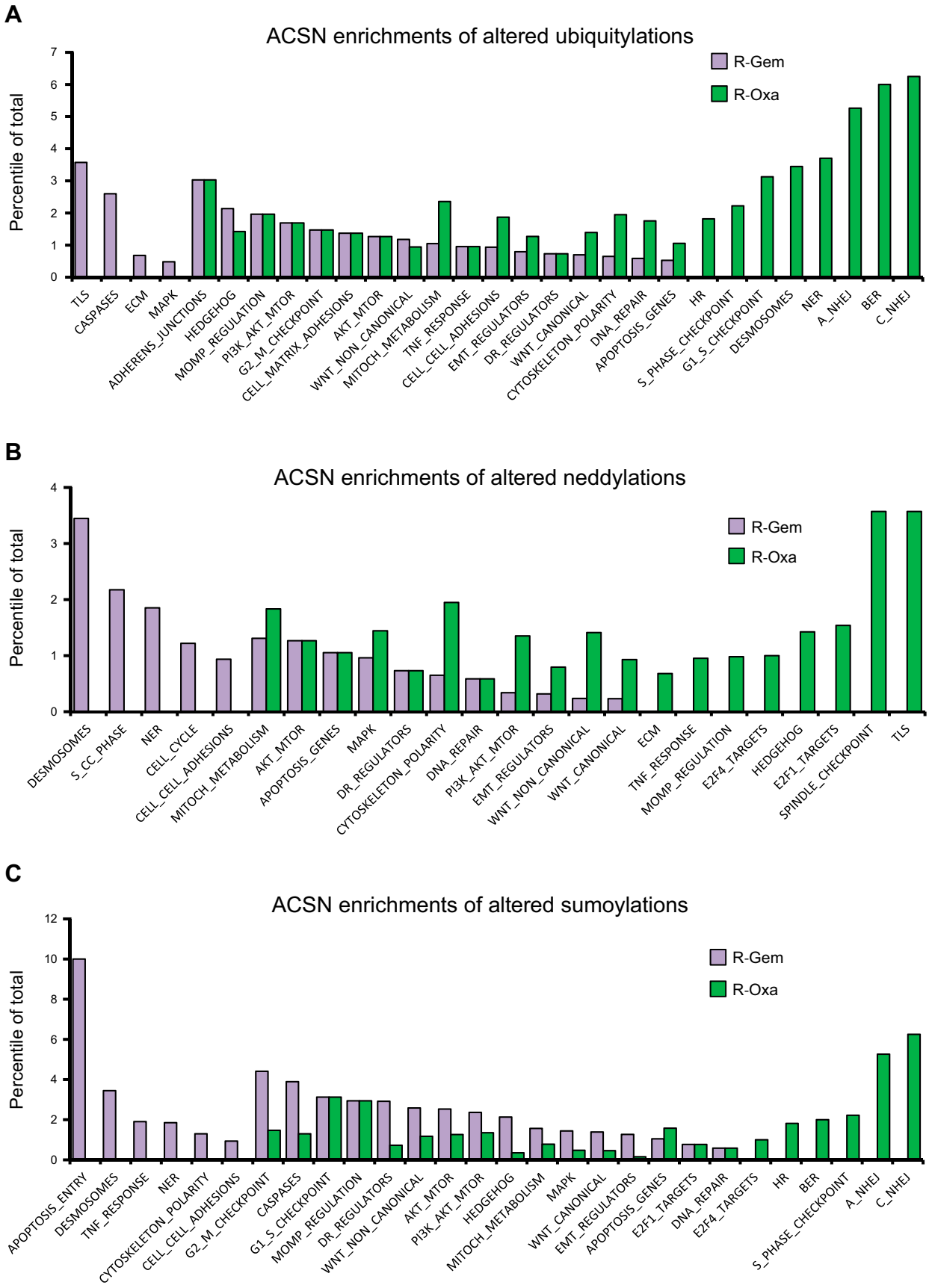

Figure 2. Cancer signaling networks in which resistance-induced alterations of ubiquitylation (*A*), neddylation (*B*), and sumoylation (*C*) are involved (according to the Atlas of Cancer Signalling Networks). BER, base excision repair; DR, DNA repair; ECM, extra-cellular matrix; EMT, endothelial mesechymal transition; HR, homologous recombination; MITOCH, mitochondria; MOMP, mitochondrial outer membrane permeabilization; NER, nucleotide excision repair; NHEJ, nonhomologous end joining; TLS, translesion bypass.

TABLE 3. *Number of altered PTMs that are common or specific to both gemcitabine and oxaliplatin resistance*

Altered PTM	R-Gem specific	R-Ox specific	Common
Ubiq	61	86	9
Nedd8	48	84	2
SUMO1	85	89	7

Ubiq, ubiquitin.

are known to respond to a variety of stresses (21). Therefore, we investigated the behavior of NBs in parental and resistant cells in response to treatments, and we observed a global increase of >100% of the size of NBs in the nucleus of cells when treated with either of the 2 drugs (Fig. 4*D*). By contrast, this induction was completely abolished in both resistant cells. Hence, not only the basal level of NBs was reduced in resistant cells but also their capacity to be activated in response to treatments.

Low-PML sumoylation is involved in PDAC cell resistance to chemotherapies

We next studied the impact of impaired PML sumoylation on the resistant phenotype of pancreatic cancer cells. To mimic the low sumoylation state of PML, we transfected cells with mammalian expression plasmids coding for either WT-PML protein or a sumoylation-deficient mutant PML-3K (22). Control cells were transfected with either 1 of the 2 PML vectors or a GFP-expressing vector as control (Supplemental Fig. S4) and then treated with either gemcitabine or oxaliplatin for 48 h. As shown in **Fig. 5*A***, cells expressing the WT PML were more sensitive to both gemcitabine and oxaliplatin treatments, whereas the sumoylation-deficient mutant PML expressing cells displayed a strong increase of survival. Importantly, the difference of cell survival between the WT and mutant PML was nearly 3 times with gemcitabine and almost 2 times with oxaliplatin (Fig. 5*A*). This higher survival of mutant PML–expressing cells compared with WT PML–expressing cells was associated with a decreased rate of apoptosis as assessed by caspase-3/7 activity (Fig. 5*B*). Taken together, these data show that a decreased sumoylation of PML was able to increase the resistance of PDAC cells to treatments.

We next wondered if increasing the sumoylation of PML could sensitize resistant cells to treatments. To address this question, we transfected R-Gem and R-Ox cells with the same vectors and studied their response to treatments. As expected, the survival of both resistant cell types was decreased when they overexpressed WT PML but not when overexpressing sumoylation-deficient PML (Fig. 5*C*). Indeed, although the decrease of cell survival between WT and mutant PML was only 30% for R-Gem cells and 25% for R-Ox cells, these differences were highly reproducible and statistically significant. Here as well, this decrease in cell viability by WT PML expression was correlated with a higher apoptotic rate (Fig. 5*D*). Hence, it seems that increasing the amount of WT PML in resistant cells made more PML available for sumoylation and partially restored its functions in resistant cells, leading to their increased sensitivity to treatments. Taken together, these data show that impaired sumoylation of PML in resistant PDAC cells is involved in the resistance mechanisms.

Resistance to gemcitabine and oxaliplatin involves NF-κB and CREB pathway activation, which is reversed by normal PML sumoylation

In order to decipher the mechanisms by which pancreatic cancer cells become resistant to gemcitabine or oxaliplatin treatment and, more importantly, to understand how PML sumoylation can interfere with these mechanisms to resensitize cells, we performed an RNA-seq study of control and resistant cells expressing GFP as unrelevant protein, or PML-WT or PML-3K. We used the DESeq2 fold change files to identify with IPA software to compare control *vs.* resistant and GFP *vs.* PML expression conditions, which pathways are significantly induced in gemcitabine and oxaliplatin resistance acquisition, and which are affected by PML-WT or PML-3K expression (Supplemental Fig. S5*A*, *B*). We focused our attention on the pathways induced (or repressed) by the resistance that are reversed by PML-WT expression but not by PML-3K mutant expression (**Fig. 6*A*, *D***) because they were most likely to explain the mechanism by which PML sumoylation could restore PDAC cell sensitivity to gemcitabine and oxaliplatin (Fig. 5). According to IPA, 1 of the most-activated pathways in R-Gem cells strongly inhibited by PML-WT and not affected by PML-3K expression was the NF-κB pathway (Fig. 6*A*). This finding was confirmed by the

TABLE 4. *Alterations of PTMs common to both gemcitabine and oxaliplatin resistance*

Altered PTM	R-Gem↗	R-Gem↘	R-Ox↗	R-Ox↘
Ubiq		GNAI2 MDH2 NME1 PGK1 RBM8A TBCA TPM4 UBE2C UBQLN1	GNAI2 UBE2C	MDH2 NME1 PGK1 RBM8A TBCA TPM4 UBQLN1
Nedd8 SUMO1	CCDC50	ALDH1A1 CPSF3 HDAC6 HISTH3A HNRNPM MSANTD4 PML RANBP2	CCDC50 CPSF3 HDAC6 HISTH3A	ALDH1A1 HNRNPM MSANTD4 PML RANBP2

ALDH1A1, aldehyde dehydrogenase 1 family member A1; CCDC50, coiled-coil domain-containing 50; CPSF3, cleavage and polyadenylation specific factor 3; GNAI2, G protein subunit α I2; HDAC6, histone deacetylase 6; HISTH3A, histone 3A; HNRNPM, heterogeneous nuclear ribonucleoprotein M; MDH2, malate dehydrogenase 2; MSANTD4, Myb/SANT DNA-binding domain containing 4 with coiled-coils; NME1, NME/NM23 nucleoside diphosphate kinase 1; PGK1, phosphoglycerate kinase 1; PML, promyelocytic leukemia protein; RanBP2, Ran-binding protein 2; RBM8A, RNA-binding motif protein 8A; TBCA, tubulin folding cofactor A; TPM4, tropomyosin 4; UBE2C, ubiquitin-conjugating enzyme E2 C; Ubiq, ubiquitin; UBQLN1, ubiquilin 1. Arrow up: PTM increased by the treatment. Arrow down: PTM decreased by the treatment.

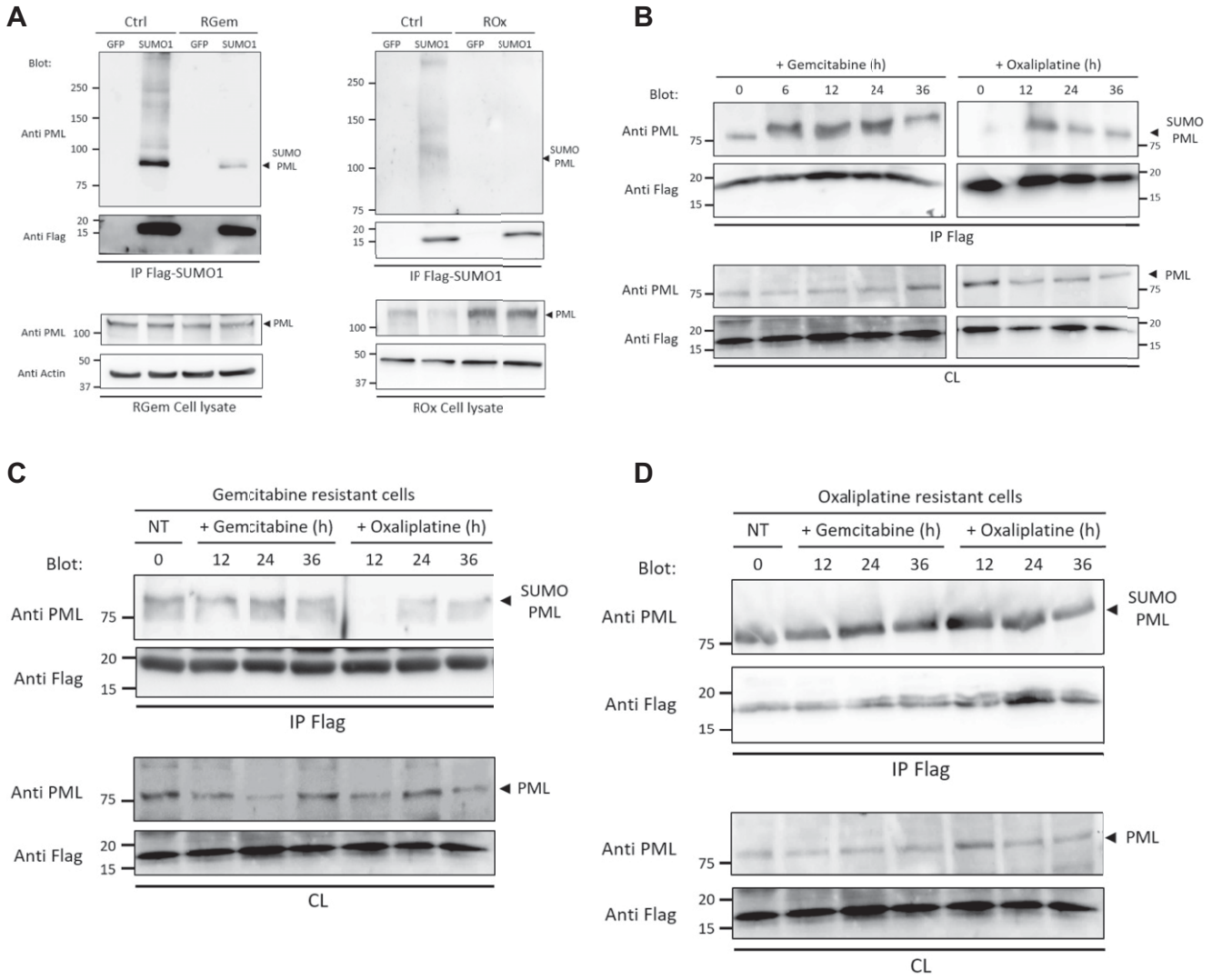

Figure 3. Identification of impaired PML sumoylation as a general mechanism of resistance. *A*) Left panel: Lysates from control and R-Gem cells were subjected to immunoprecipitation using anti-Flag antibody to isolate sumoylated proteins and membranes blotted using an anti-PML antibody to reveal the sumoylated form of PML. Right panel: as in left panel but using lysates from R-Ox cells. *B*) PML sumoylation kinetics in MiaPaCa-2 cells treated with either gemcitabine or oxaliplatin. After purification of sumoylated protein through immunoprecipitation using anti-Flag antibody, the amount of sumoylated PML was revealed by immunoblotting for PML. *C*) The previous process as in *B* but with R-Gem cells. *D*) The previous process as in *B* with R-Ox cells. CL, cell lysate; Ctrl, control; IP, immunoprecipitation; NT, non-treated.

constitutive overphosphorylation of the P65 subunit of NF-κB in resistant cells (Supplemental Fig. S5*C*). Indeed, the phosphorylation of P65, which forms the NF-κB complex with P50, is necessary for its nuclear translocation and is usually used as a parameter to detect activation of the NF-κB pathway (23). Using NF-κB–inhibiting and -activating drugs, we could validate that inhibiting NF-κB could block the antiapoptotic effect of PML hyposumoylation in control cells (Fig. 6*B*) and that NF-κB activation could limit the impact of PML-WT expression in R-Gem cells (Fig. 6*C*). Regarding oxaliplatin resistance, the most induced pathway strongly reversed by PML-WT but not sumoylation-deficient PML was the CREB pathway (Fig. 6*D*). This finding was confirmed by controlling the constitutive overexpression of P300, a well-known transcriptional target of the CREB pathway (24), in R-Ox cells compared with control cells (Supplemental Fig. S5*D*) As for NF-κB, we showed that inhibiting CREB function could limit the resistance of control cells expressing PML-3K (Fig. 6*E*) and, inversely, its activation in resistant cells could block the impact of PML-WT expression in resistant cells (Fig. 6*F*). All together, these data showed that restoring the normal sumoylation of PML in PDAC cells could decrease their resistance to different drugs through the control of different altered pathways (*i.e.*, the NF-κB pathway for gemcitabine and the CREB pathway for oxaliplatin).

The expression and sumoylation of PML correlates with resistance of patients with PDAC

In order to validate our findings at the clinical level, we used previously established PDXs (25) of patients with PDAC to monitor the expression of PML and to

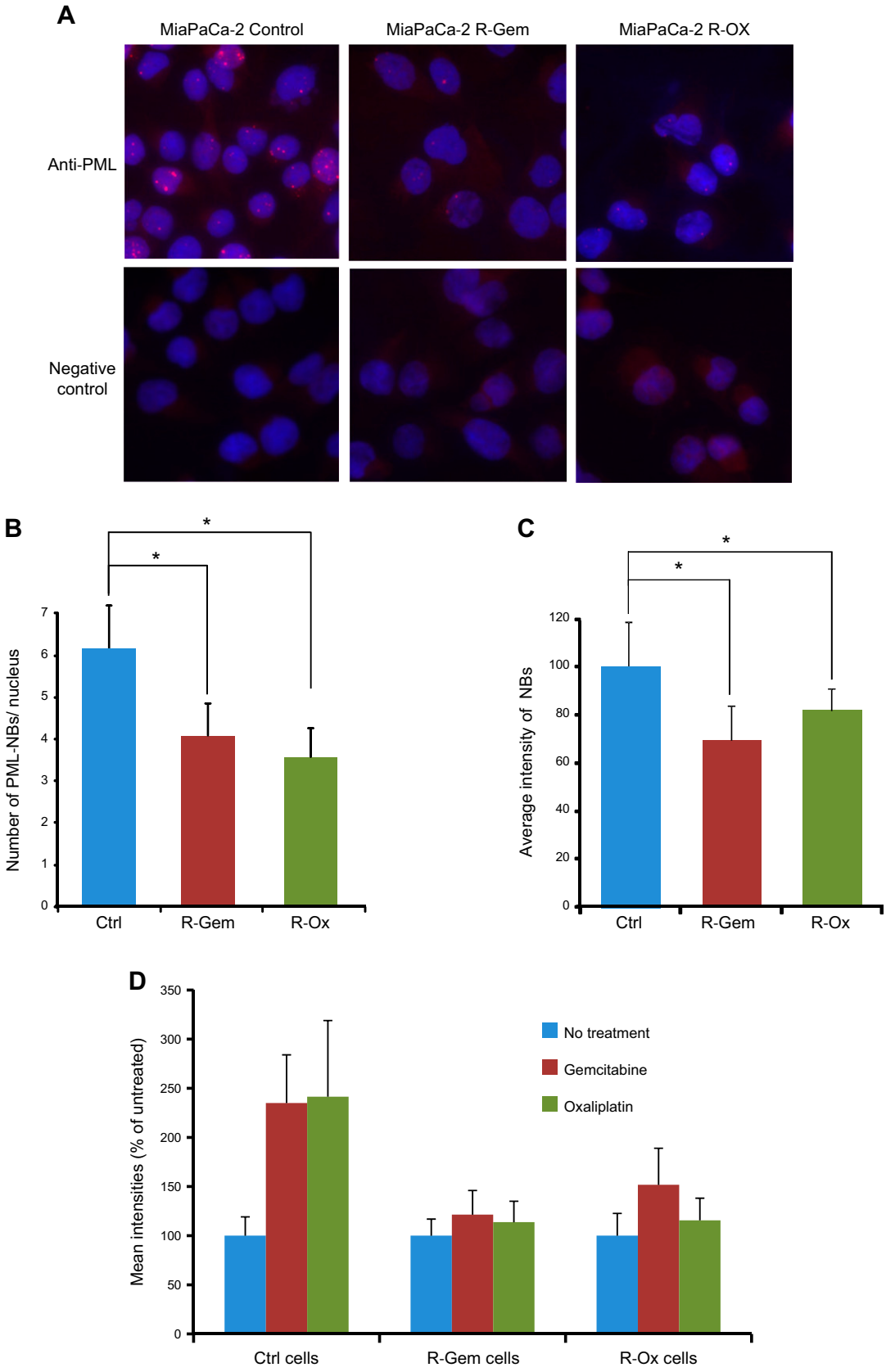

Figure 4. PML-repressed sumoylation in resistant cells alters NB formation. *A*) Representative pictures of immunofluorescence staining of the different MiaPaCa-2 cells in which PML-NBs appear as red spots within nuclei stained with DAPI. *B*) Quantification and comparison of the number of NBs per nucleus in the MiaPaCa-2 control cells (Ctrl) *vs.* R-Gem cells and R-Ox cells. *C*) Quantification and comparison of the mean intensity of NBs in the MiaPaCa-2 parental cells *vs.* MiaPaCa-2 R-Ox cells and MiaPaCa-2 R-Gem cells. *D*) Variation of NB intensity in control MiaPaCa-2 cells as well as in R-Gem and R-Ox cells after 24 h of treatment with 10 μM of each drug. $*P < 0.05$.

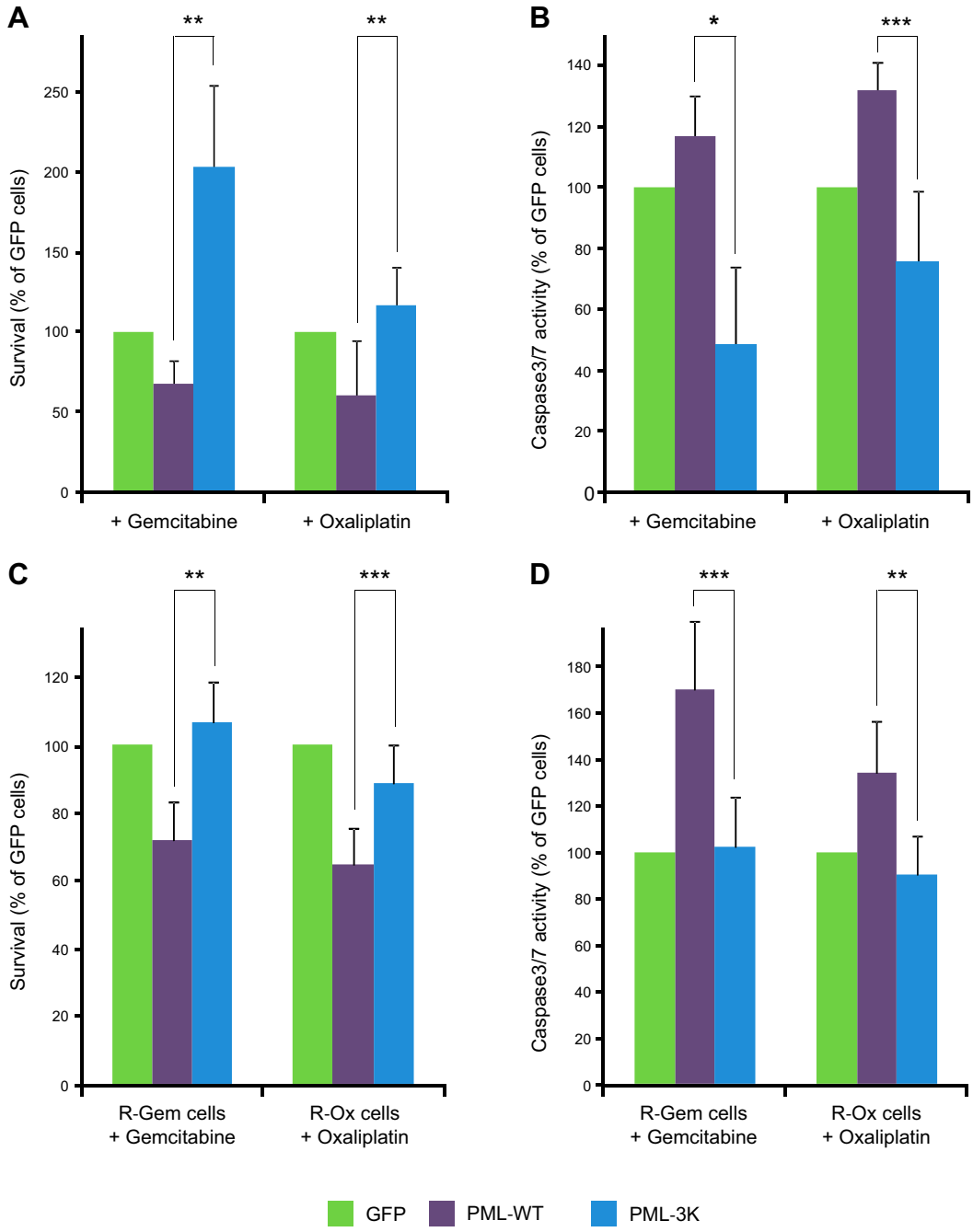

Figure 5. PML-repressed sumoylation is involved in chemoresistance of pancreatic cancer cells. *A*, *B*) Control MiaPaCa-2 cells were transfected with plasmids expressing WT PML or sumoylation-deficient mutant PML in which the 3 sumoylated lysine residues were changed to arginine or a GFP-expressing vector as a control. The day after transfection, cells were treated with 10 μM gemcitabine or oxaliplatin for an additional 72 h, and then their viability (*A*) and caspase-3/7 activity (*B*) were assessed as described in Material and Methods. *C*, *D*) MiaPaca-2 R-Gem cells or R-Ox cells were transfected as previously described and were treated with 100 μM gemcitabine or oxaliplatin. After 72 h of treatment, the cell viability (*C*) and caspase 3/7 activity (*D*) was assessed as previously described (*A*, *B*). Expression of transfected PML was controlled by Western blot (Supplemental Fig. S4).*$P < 0.05$, **$P < 0.02$, ***$P < 0.01$ (Student's *t* test analysis from ≥3 independent experiments).

evaluate its sumoylation (**Fig. 7*A***). We could observe an important heterogeneity of PML expression and of PML sumoylation between the PDXs studied, and there was no correlation between level of expression and level of sumoylation. However, we were able to combine these PML data with data of patients from whom PDXs were derived. Because patients with the most aggressive and multiresistant tumors are also those with shorter survival rates, we had the opportunity to study the potential correlation between PML expression and sumoylation and tumor resistance. As shown in Fig. 7*B*, the combination of both the level of PML protein and of its sumoylation (obtained by the multiplication of both values because both PML expression and PML sumoylation are positively affect survival) displayed a significant correlation with patients' survival.

Activation z-score

A

Pathway modulated by Gem resistance	Effect of PML-WT expression	Effect of PML-3K expression	Canonical Pathways
3.3	-1.342	0	Nf-kB Signaling
2.668	-0.447	0.447	Neuroprotective Role of THOP1 in Alzheimer's Disease
1.732	-0.447	0.816	Leukocyte Extravasation Signaling
1.134	-1.342	N/A	Osteoarthritis Pathway

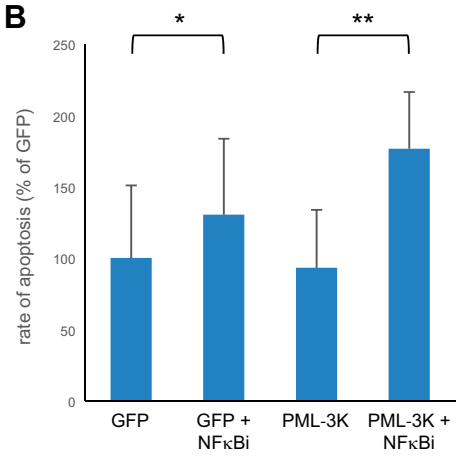

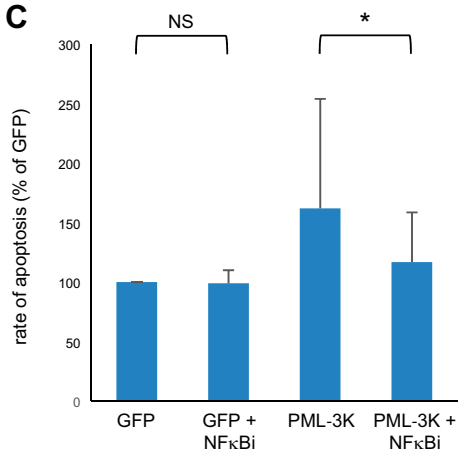

D

Pathway modulated by Ox resistance	Effect of PML-WT expression	Effect of PML-3K expression	Canonical Pathways
1.732	-1	N/A	CREB signaling in Neurons
0.577	-1	N/A	Sperm Motility
0.5	-1.342	0	Adrenomedullin signaling pathway
0.378	-2	N/A	Fcγ Receptor-mediated Phagocytosis in Macrophages and Monocytes
0.333	-1	N/A	Amyotropic Lateral Sclerosis Signaling
0.218	-1	0	Synaptic Long Term Depression
-0.302	2	-0.447	Gα1 Signaling
-0.6	2	0	cAMP-mediated signaling
-0.186	1	N/A	Protein Kinase A Signaling

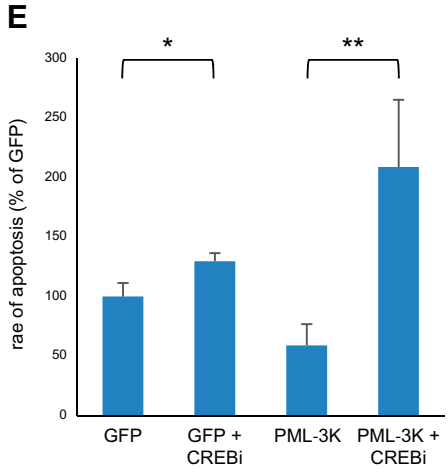

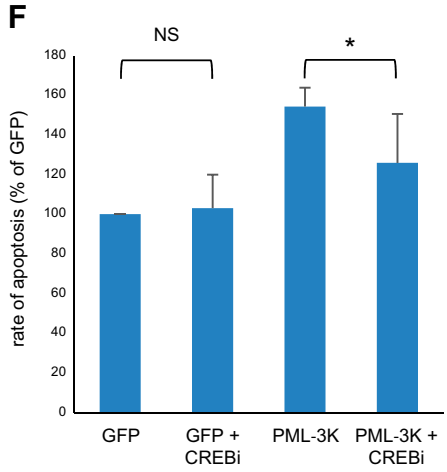

Figure 6. Pathways altered by gemcitabine and oxaliplatin resistances corrected by normal PML sumoylation. RNA-seq data from MiaPaCa-2 control and resistant cells expressing either GFP or PML-WT or PML-3K mutant were analyzed with the help of IPA to identify pathways altered by resistance acquisition to either gemcitabine (*A*) or oxaliplatin (*D*) and which is reversed by PML-WT but not by PML-3K expression. *A*) Table of the main pathways altered by gemcitabine resistance acquisition with the corresponding activation *z* scores (+ for activation, - for inhibition). *B*) Control cells were transfected with GFP or PML-3K

(*continued on next page*)

Hence, pancreatic tumors characterized by a high expression or high sumoylation level of PML are likely to be the most sensitive to the chemotherapies and represent a good prognosis for patients. We further evaluated the potential use of PML expression and sumoylation as a prognosis tool by studying its ability to distinguish between long-survival patients (>24 mo) and short-survival patients (<24 mo) (Fig. 7*C*). Indeed, Fig. 7*C* clearly shows the accuracy of this prognosis marker both for the specificity and sensitivity levels. Indeed, the area under the curve and the *P* value for the ROC curve were 0.953 and <0.001, respectively. Fig. 7*C* shows that this test had a sensitivity of 100 and specificity of 87.5.

PDX-derived cell lines were developed and used *in vitro* to generate chemograms to different drugs commonly used in PDAC treatment (25). The secretomes (all proteins secreted in the culture medium) of 40 of these cell lines were recently studied by mass spectrometry, leading to the identification of thousands of proteins (unpublished results), including PML. We wondered if a correlation could exist between the amount of secreted PML and the resistance to each tested drug. By comparing the level of secreted PML between the 10 most-sensitive and 10 most-resistant PDX cell lines for each drug, we observed a correlation for most of them (Fig. 7*D*). This was particularly evident for gemcitabine ($P = 0.006$) but also for docetaxel ($P = 0.025$) and for irinotecan ($P = 0.031$) and its active product, 7-ethyl-10-hydroxycamptothecin ($P = 0.045$).

Identifying the molecular mechanism responsible for PML hyposumoylation

We next tried to identify the mechanisms responsible for the decrease of PML sumoylation. Because oxidative stress affects PML functions (26), we measured the reactive oxygen species (ROS) level and observed that the acquisition of resistance was associated with an increase in intracellular ROS (Supplemental Fig. S6*A*, *B*). This result suggests that, whereas acute oxidative stress induces PML sumoylation and NB formation, a mechanism associated with resistance leads to maintaining PML sumoylation at the lowest level, even in the presence of constitutive high ROS content. Because ROSs can inhibit the sumoylation machinery (27), this could account for low-PML sumoylation, but this was not the case because reducing the ROS content did not restore the normal sumoylation of PML (Supplemental Fig. S6*C*). Another possibility could come from the abnormal activity of 1 or several desumoylating enzymes. A total of 3 of them are known to desumoylate PML (28, 29), and 1 (SENP1) is known to be overexpressed in PDAC (30). Therefore, we used siRNAs to silence these SENPs in resistant cells, and we were indeed able to observe an increased sumoylation of PML with all SENPs regarding gemcitabine resistance and mainly with SENP1 siRNA for oxaliplatin resistance (Supplemental Fig. S7*A*). However, studying the expression levels of these enzymes in our cellular model (Supplemental Fig. S7*B*), no difference could be observed between chemoresponsive and chemoresistant cells. In PDX-derived cell lines of patients with long or short survival rates (Supplemental Fig. S8), we did not observe any significant difference or correlation of expression. Therefore, at present, the mechanism responsible for PML hyposumoylation in resistant PDAC cells remains elusive.

DISCUSSION

PDAC has the particularity to be or to become rapidly resistant to all anticancer therapies. This suggests that tumor cells, which make up these tumors, possess specific mechanisms that help them to survive any kind of stress. This could be due to the specific nature of the tissue from which they arise because ductal and acinar cells have to protect themselves from the cocktail of digesting enzymes they produce and drive to the intestine or due to the fact that pancreatic tumors are usually detected at a late and advanced stage (2). It is established that PTMs play major roles in cellular response to stress like a therapeutic treatment. PTMs mediated by the ubiquitin family of proteins are involved in almost all cellular processes, including stress-response pathways, and consequently may be altered when cells become resistant to any anticancer treatment. We showed previously that treating pancreatic cancer cells with gemcitabine provokes an important rebuilding of the ubiquitination, neddylation,l and sumoylation profiles (18). Here, we demonstrate that the acquisition of resistance to gemcitabine and to oxaliplatin, another important drug used in the FOLFIRINOX protocol of PDAC treatment (3), was associated with the constitutive remodeling of part of the PTM profile modifomes. Indeed, both resistances led to profound changes in the ubiquitination, neddylation, and sumoylation profiles of our cellular model (Fig. 1 and Tables 1–3). Most of these alterations were drug specific regarding the targeted proteins and also the cellular functions they are involved in (Figs. 1 and 2), but as expected, some of these alterations were common to both resistances, representing a potential common mechanism and therefore a general mechanism of resistance (Table 4). Among them, PML represented a good candidate because of its already well-known role in acute PML (19), a pathology in which PML is fused to retinoic acid receptor α, and in oncogenic processes in

expression plasmids and treated or not with 5 μM BMS-345541, an NF-κB inhibitor (NF-κBi). *C*) R-Gem cells transfected with either GFP or PML-WT expression plasmids were treated with gemcitabine 100 ± 1 μM of SRI-22782, an NF-κB activator (NF-κBa). *D*) Like in *A*, table of the main pathways altered by oxaliplatin resistance acquisition with the corresponding *z* scores. *E*) Control cells were transfected with GFP or PML-3K expression plasmids and treated or not with 0.5 μM of 666-15, a CREB pathway inhibitor (CREBi). *F*) R-Ox cells transfected with either GFP or PML-WT expression plasmids were treated with oxaliplatin 100 ± 10 μM of Forskolin, a CREB pathway activator (CREBa). For each graph, the rate of apoptosis was quantified using caspase 3/7 activity over the cell viability. NS, no statistical significance. Results are expressed as percentile of GFP nontreated cells, and bars show means ± SD. $*P < 0.05$, $**P < 0.01$ (Student's *t* test).

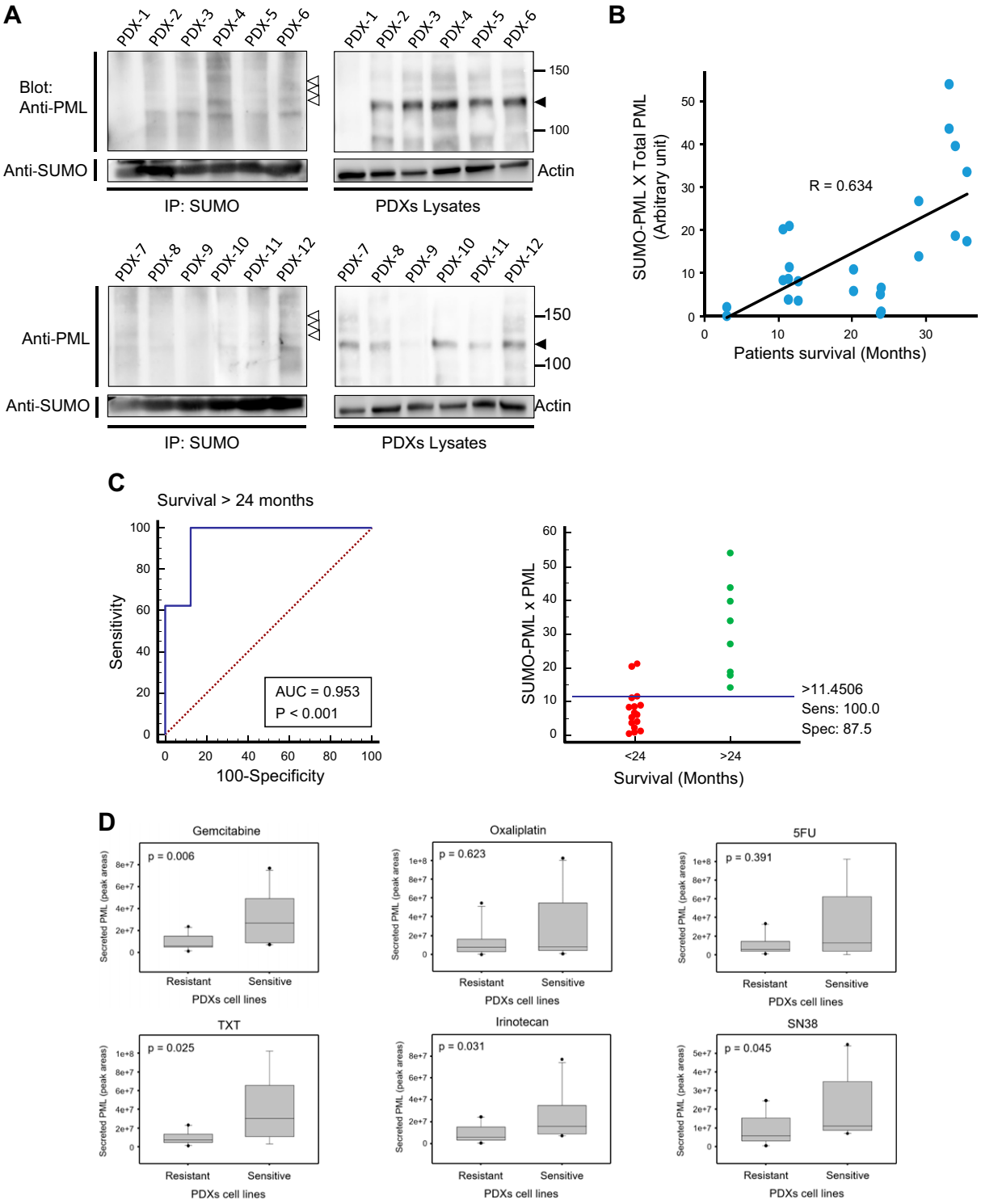

Figure 7. PML expression and sumoylation correlates with resistance in patients. *A*) Lysates from PDXs were subjected to immunoprecipitation using a combination of anti-SUMO1 and anti-SUMO2/3 antibodies followed by PML Western blot analysis. Expression level of PML has also been evaluated by Western blot in lysates. Black arrow: PML; white arrow: sumoylated PML. *B*) Signals from 2 independent experiments were quantified by densitometry using ImageJ, and PML values were temporized by SUMO values in IP (relative amount of sumoylated PML) or by actin values in lysates (total amount of PML). These values were used to evaluate the correlation between PML sumoylation and expression with patients' survival. *C*) The accuracy of PML expression and sumoylation to distinguish patients' survival rates more or less than 24 mo was tested by an ROC curve (left) and a dot diagram (right). *D*) Correlation of PML in secretomes of PDX-derived cell lines with their resistant phenotype. The secretion profiles (secretome) as well as the resistant profiles to 6 different chemotherapeutic drugs of a large number of PDX-derived cell lines (chemograms) have been established [(25) and unpublished results]. For each considered drug, the amount of secreted PML protein in the 10 most sensitive cell lines and the 10 most resistant cell lines was quantified by mass spectrometry. 5FU, 5 Fluorouracil; AUC, area under the curve; IP, immunoprecipitation; Sens, sensitivity; SN38, 7-ethyl-10-hydroxycamptothecin; Spec, specificity; THOP1, thimet oligopeptidase 1; TXT, docetaxel. Values are presented in box plots with result from Student's *t* test analysis.

general (31). Importantly, its role in resistance mechanisms remains poorly described, relying mainly on its expression level, which can correlate either positively or negatively with resistance depending on the cancer type (20). Until now, the role of its sumoylation in these processes was unknown. In our cellular model, acquisition of resistance to any of the drugs we used did not affect the protein expression level of PML. However, its basal sumoylation level was indeed decreased in both resistant cells, and, importantly, the induction of PML sumoylation in response to gemcitabine or oxaliplatin treatment was completely abolished (Fig. 3*C, D*). These data suggest that PML could no longer fulfill its function in resistant cells and probably could not favor cell death in response to anticancer treatment. Because the main SUMO dependent regulation of PML functions is through the generation and stabilization of PML-NBs (21), it was important to show that, indeed, the NB dynamic in resistant cells was altered both at the basal level and in response to stress induced by both drugs (Fig. 4). Yet, although the function of PML seemed to be altered in resistant cells, we had to show that this defect in PML sumoylation really played a role regarding the resistant phenotype. We tried to mimic the impact of a sumoylated and nonsumoylated PML on cell survival by overexpressing WT (normally sumoylated) or triple lysine to arginine mutant (not sumoylated) PML. This approach has been successful because we have been able to increase the resistance of control cells with the expression of mutant, nonsumoylated PML (Fig. 5*A, B*) and to resensitize resistant cells by expressing the WT, sumoylated PML (Fig. 5*C, D*).

Despite our attempts to detail the mechanism responsible for lower sumoylation of PML in resistant cells, it still remains elusive. Indeed, restoring a normal ROS level in resistant cells did not significantly recover normal sumoylation of PML (Supplemental Fig. S6). In addition, whereas we could restore part of the PML sumoylation by inhibiting the expression of desumoylases, we could not observe any significant alteration of their expression in resistant cells compared with control cells (Supplemental Fig. S7) or a correlation of their expression with survival in patients' derived material (Supplemental Fig. S8). Other mechanisms need to be explored, and among them, we will need to test the activity of these enzymes as well as their interactions with PML. Indeed, studying protein levels may not be relevant regarding their activity and affinity for their substrates. Surprisingly, our attempts to identify by which mechanisms PML sumoylation is involved in modulating pancreatic cancer cells resistance was more fruitful. RNA-seq study revealed that acquisition of resistance to gemcitabine or oxaliplatin were associated with alterations of specific and distinct pathways (Fig. 6*A, D*). Importantly, several of these altered pathways were efficiently corrected by restoring a normal sumoylation of PML, thereby restoring chemosensitivity of cells to these drugs (Fig. 6). In fact, the large repertoire of regulatory functions of PML enable it to affect pathways involved in both types of resistance. Hence, PML is a common point through which it is possible to go in order to block chemoresistance, no matter the drug.

To go beyond our *in vitro* cellular model, we have been interested in studying PML and its sumoylation in patient-derived material. This led us to realize the large variability of PML sumoylation between patients as well as the diversity of protein levels (Fig. 7*A*). Importantly, we identified a good correlation between PML expression and sumoylation in PDXs and the survival of patienst (Fig. 7*B*), meaning that both high levels of PML expression and PML sumoylation are required to favor patients' survival and tumor sensitivity to treatments. This predictive tool was confirmed by testing its ability to distinguish between long and short survival (24 mo) using an ROC curve and dot diagram (Fig. 7*C*). Of note, PML protein levels did not correlate with mRNA levels, evaluated by microarray analysis of PDXs (32), which were relatively equivalent between all PDXs tested (Supplemental Fig. S9).

Lately, proteomic analysis of tumor cells' secretomes by mass spectrometry was used as an efficient tool for the identification of diagnostic and prognostic biomarkers. In our study, we detected a correlation between the presence of PML in secretomes of PDX-derived cell lines and the resistance to diverse drugs (Fig. 7*D*). To our knowledge, this is the first study identifying secreted PML in PDAC-derived cell lines, although PML was previously identified in the secretomes of other cancer cells as a component of extracellular vesicles (33–35). Interestingly, these secreted extracellular vesicles can play important roles in tumor progression, metastasis, and drug resistance (36). Taken together, our data validated the role of PML as a new mechanism of resistance of PDAC that could be targeted to improve treatments efficacy and thereby patients' survival.

In summary, we have identified 1 new common and therefore potentially generic mechanism of pancreatic cancer cell resistance, which is driven by the abnormal PTM of a protein (*i.e.*, PML hyposumoylation, an alteration that could not have been detected previously by usual genomic and transcriptomic approaches). In this work, we have focused our attention on PML, but several other important targets common to both types of resistance represent additional potential mechanisms that could be exploited in the future. There is no doubt that the list of altered PTMs implicated in multiresistance mechanisms will grow and will perhaps highlight even more valuable candidates. FJ

ACKNOWLEDGMENTS

The authors thank Dr. Arkaitz Carracedo (Center for Cooperative Research in Bioscience, Spain) for providing PML constructs and to Dr. Guillaume Bossis (IGMM, Montpellier, France) for providing anti-SUMO1 and anti-SUMO2/3 hybridomas. High-throughput sequencing was performed at the Transcriptomique and Génomique Marseille Luminy (TGML) Platform and supported by grants from INSERM, GIS Infrastructures en Biologie Santé et Agronomie (IBiSA), Aix-Marseille Université, and ANR-10-INBS-0009-10. This work was supported by La Ligue Contre le Cancer, Association pour la Recherche sur le Cancer (ARC), Institute National du Cancer (INCa), Cancéropôle Provence-Alpes-Côte d'Azur (PACA), and INSERM. Proteomic analyses were done using the mass spectrometry facility of Marseille Proteomics (*marseille-proteomique.univ-amu.fr*) and were supported by IBiSA, Plateforme Technologique Aix-Marseille, Cancéropôle PACA, the Institut Paoli-Calmettes, and the Centre de Recherche en Cancérologie de Marseille. The authors declare no conflicts of interest.

AUTHOR CONTRIBUTIONS

P. Soubeyran designed the research; M. Swayden, G. Alzeeb, R. Masoud, Y. Berthois, F. Silvy, and P. Soubeyran performed the research; S. Audebert and L. Camoin performed the mass spectrometry analysis; L. Hannouche and H. Vachon performed the RNA sequencing experiment and analysis; O. Gayet, M. Bigonnet, J. Roques, and N. Dusetti provided material and help with patient-derived xenograft–related data; R. Masoud and A. Carrier helped in designing, performing, and analyzing the redox reaction state of cells; J. L. Iovanna and P. Soubeyran directed the work; M. Swayden, J. L. Iovanna, and P. Soubeyran analyzed the data; and M. Swayden and P. Soubeyran wrote the manuscript.

REFERENCES

1. Schneider, G., Siveke, J. T., Eckel, F., and Schmid, R. M. (2005) Pancreatic cancer: basic and clinical aspects. *Gastroenterology* **128**, 1606–1625
2. Siegel, R. L., Miller, K. D., and Jemal, A. (2018) Cancer statistics, 2018. *CA Cancer J. Clin.* **68**, 7–30
3. Conroy, T., Desseigne, F., Ychou, M., Bouché, O., Guimbaud, R., Bécouarn, Y., Adenis, A., Raoul, J. L., Gourgou-Bourgade, S., de la Fouchardière, C., Bennouna, J., Bachet, J. B., Khemissa-Akouz, F., Péré-Vergé, D., Delbaldo, C., Assenat, E., Chauffert, B., Michel, P., Montoto-Grillot, C., and Ducreux, M.; Groupe Tumeurs Digestives of UnicancerPRODIGE Intergroup. (2011) FOLFIRINOX versus gemcitabine for metastatic pancreatic cancer. *N. Engl. J. Med.* **364**, 1817–1825
4. Von Hoff, D. D., Ervin, T., Arena, F. P., Chiorean, E. G., Infante, J., Moore, M., Seay, T., Tjulandin, S. A., Ma, W. W., Saleh, M. N., Harris, M., Reni, M., Dowden, S., Laheru, D., Bahary, N., Ramanathan, R. K., Tabernero, J., Hidalgo, M., Goldstein, D., Van Cutsem, E., Wei, X., Iglesias, J., and Renschler, M. F. (2013) Increased survival in pancreatic cancer with nab-paclitaxel plus gemcitabine. *N. Engl. J. Med.* **369**, 1691–1703
5. Adamska, A., Elaskalani, O., Emmanouilidi, A., Kim, M., Abdol Razak, N. B., Metharom, P., and Falasca, M. (2018) Molecular and cellular mechanisms of chemoresistance in pancreatic cancer. *Adv. Biol. Regul.* **68**, 77–87
6. Krueger, K. E., and Srivastava, S. (2006) Posttranslational protein modifications: current implications for cancer detection, prevention, and therapeutics. *Mol. Cell. Proteomics* **5**, 1799–1810
7. Hochstrasser, M. (2009) Origin and function of ubiquitin-like proteins. *Nature* **458**, 422–429
8. Hoeller, D., and Dikic, I. (2009) Targeting the ubiquitin system in cancer therapy. *Nature* **458**, 438–444
9. Goldstein, G., Scheid, M., Hammerling, U., Schlesinger, D. H., Niall, H. D., and Boyse, E. A. (1975) Isolation of a polypeptide that has lymphocyte-differentiating properties and is probably represented universally in living cells. *Proc. Natl. Acad. Sci. USA* **72**, 11–15
10. Pickart, C. M., and Eddins, M. J. (2004) Ubiquitin: structures, functions, mechanisms. *Biochim. Biophys. Acta* **1695**, 55–72
11. Ye, Y., and Rape, M. (2009) Building ubiquitin chains: E2 enzymes at work. *Nat. Rev. Mol. Cell Biol.* **10**, 755–764
12. Nijman, S. M. B., Luna-Vargas, M. P. A., Velds, A., Brummelkamp, T. R., Dirac, A. M. G., Sixma, T. K., and Bernards, R. (2005) A genomic and functional inventory of deubiquitinating enzymes. *Cell* **123**, 773–786
13. Yau, R., and Rape, M. (2016) The increasing complexity of the ubiquitin code. *Nat. Cell Biol.* **18**, 579–586
14. Cappadocia, L., and Lima, C. D. (2018) Ubiquitin-like protein conjugation: structures, chemistry, and mechanism. *Chem. Rev.* **118**, 889–918
15. Vertegaal, A. C. O. (2011) Uncovering ubiquitin and ubiquitin-like signaling networks. *Chem. Rev.* **111**, 7923–7940
16. Hietakangas, V., Anckar, J., Blomster, H. A., Fujimoto, M., Palvimo, J. J., Nakai, A., and Sistonen, L. (2006) PDSM, a motif for phosphorylation-dependent SUMO modification. *Proc. Natl. Acad. Sci. USA* **103**, 45–50
17. Bedford, L., Lowe, J., Dick, L. R., Mayer, R. J., and Brownell, J. E. (2011) Ubiquitin-like protein conjugation and the ubiquitin-proteasome system as drug targets. *Nat. Rev. Drug Discov.* **10**, 29–46
18. Bonacci, T., Audebert, S., Camoin, L., Baudelet, E., Bidaut, G., Garcia, M., Witzel, I. I., Perkins, N. D., Borg, J. P., Iovanna, J. L., and Soubeyran, P. (2014) Identification of new mechanisms of cellular response to chemotherapy by tracking changes in post-translational modifications by ubiquitin and ubiquitin-like proteins. *J. Proteome Res.* **13**, 2478–2494
19. De Thé, H., Lavau, C., Marchio, A., Chomienne, C., Degos, L., and Dejean, A. (1991) The PML-RAR α fusion mRNA generated by the t(15;17) translocation in acute promyelocytic leukemia encodes a functionally altered RAR. *Cell* **66**, 675–684
20. Gurrieri, C., Capodieci, P., Bernardi, R., Scaglioni, P. P., Nafa, K., Rush, L. J., Verbel, D. A., Cordon-Cardo, C., and Pandolfi, P. P. (2004) Loss of the tumor suppressor PML in human cancers of multiple histologic origins. *J. Natl. Cancer Inst.* **96**, 269–279
21. Lallemand-Breitenbach, V., and de Thé, H. (2018) PML nuclear bodies: from architecture to function. *Curr. Opin. Cell Biol.* **52**, 154–161
22. Shen, T. H., Lin, H. K., Scaglioni, P. P., Yung, T. M., and Pandolfi, P. P. (2006) The mechanisms of PML-nuclear body formation. *Mol. Cell* **24**, 331–339
23. Maguire, O., Collins, C., O'Loughlin, K., Miecznikowski, J., and Minderman, H. (2011) Quantifying nuclear p65 as a parameter for NF-κB activation: correlation between imagestream cytometry, microscopy, and western blot. *Cytometry A* **79**, 461–469
24. Yuan, L. W., and Gambee, J. E. (2001) Histone acetylation by p300 is involved in CREB-mediated transcription on chromatin. *Biochim. Biophys. Acta* **1541**, 161–169
25. Duconseil, P., Gilabert, M., Gayet, O., Loncle, C., Moutardier, V., Turrini, O., Calvo, E., Ewald, J., Giovannini, M., Gasmi, M., Bories, E., Barthet, M., Ouaissi, M., Goncalves, A., Poizat, F., Raoul, J. L., Secq, V., Garcia, S., Viens, P., Iovanna, J., and Dusetti, N. (2015) Transcriptomic analysis predicts survival and sensitivity to anticancer drugs of patients with a pancreatic adenocarcinoma. *Am. J. Pathol.* **185**, 1022–1032
26. Tessier, S., Martin-Martin, N., de Thé, H., Carracedo, A., and Lallemand-Breitenbach, V. (2017) Promyelocytic leukemia protein, a protein at the crossroad of oxidative stress and metabolism. *Antioxid. Redox Signal.* **26**, 432–444
27. Bossis, G., and Melchior, F. (2006) Regulation of SUMOylation by reversible oxidation of SUMO conjugating enzymes. *Mol. Cell* **21**, 349–357
28. Best, J. L., Ganiatsas, S., Agarwal, S., Changou, A., Salomoni, P., Shirihai, O., Meluh, P. B., Pandolfi, P. P., and Zon, L. I. (2002) SUMO-1 protease-1 regulates gene transcription through PML. *Mol. Cell* **10**, 843–855
29. Hattersley, N., Shen, L., Jaffray, E. G., and Hay, R. T. (2011) The SUMO protease SENP6 is a direct regulator of PML nuclear bodies. *Mol. Biol. Cell* **22**, 78–90
30. Ma, C., Wu, B., Huang, X., Yuan, Z., Nong, K., Dong, B., Bai, Y., Zhu, H., Wang, W., and Ai, K. (2014) SUMO-specific protease 1 regulates pancreatic cancer cell proliferation and invasion by targeting MMP-9. *Tumour Biol.* **35**, 12729–12735
31. Wang, Z. G., Delva, L., Gaboli, M., Rivi, R., Giorgio, M., Cordon-Cardo, C., Grosveld, F., and Pandolfi, P. P. (1998) Role of PML in cell growth and the retinoic acid pathway. *Science* **279**, 1547–1551
32. Bian, B., Bigonnet, M., Gayet, O., Loncle, C., Maignan, A., Gilabert, M., Moutardier, V., Garcia, S., Turrini, O., Delpero, J. R., Giovannini, M., Grandval, P., Gasmi, M., Ouaissi, M., Secq, V., Poizat, F., Nicolle, R., Blum, Y., Marisa, L., Rubis, M., Raoul, J. L., Bradner, J. E., Qi, J., Lomberk, G., Urrutia, R., Saul, A., Dusetti, N., and Iovanna, J. (2017) Gene expression profiling of patient-derived pancreatic cancer xenografts predicts sensitivity to the BET bromodomain inhibitor JQ1: implications for individualized medicine efforts. *EMBO Mol. Med.* **9**, 482–497
33. Tauro, B. J., Greening, D. W., Mathias, R. A., Mathivanan, S., Ji, H., and Simpson, R. J. (2013) Two distinct populations of exosomes are released from LIM1863 colon carcinoma cell-derived organoids. *Mol. Cell. Proteomics* **12**, 587–598
34. Silvers, C. R., Miyamoto, H., Messing, E. M., Netto, G. J., and Lee, Y.-F. (2017) Characterization of urinary extracellular vesicle proteins in muscle-invasive bladder cancer. *Oncotarget* **8**, 91199–91208
35. Hurwitz, S. N., Rider, M. A., Bundy, J. L., Liu, X., Singh, R. K., and Meckes, D. G., Jr. (2016) Proteomic profiling of NCI-60 extracellular vesicles uncovers common protein cargo and cancer type-specific biomarkers. *Oncotarget* **7**, 86999–87015
36. Zhang, C., Ji, Q., Yang, Y., Li, Q., and Wang, Z. (2018) Exosome: function and role in cancer metastasis and drug resistance. *Technol. Cancer Res. Treat.* **17**, 1533033818763450

Received for publication April 29, 2019.
Accepted for publication July 23, 2019.

Annex III
Trainings And Communications

Trainings

1. Second seasonal school of the 'Réseau Francophone de Métabolomique et Fluxomique' junior. *November 2018*, Toulouse-France.

2. Galaxy initiation: Biological station of Roscoff. *May 2019*, Roscoff-France.

3. Introduction to scientific integrity: URFIST- Rennes. *May 2019*, Online session

4. R-initiation: Biological station of Roscoff. *June 2019*, Roscoff-France.

5. R statistics analysis: Biological station of Roscoff. *June 2019*, Roscoff-France.

6. IncuCyte application and analysis: Sartorius. *January 2020*, Brest-France.

7. Metabolomic network: Corsaire. *November 2020*, Online session.

8. Workshop Imaging Organoids, From the bench to the microscope: GDR ImaBio, Université de Bordeaux. *September 2021*, Bordeaux-France.

Oral communications

1. George Alzeeb, *et al.*: 'Modèle de culture en 3D du cancer gastrique: analyse des interactions physiques et biochimiques'. IBSAM. *June 2019*, Brest-France.

2. George Alzeeb, *et al.*: 'Modélisation de l'action des médicaments anticancéreux: de la 2D à la 3D'. Niches and epigenetics of tumors network, Cancéropôle grand ouest. *July 2020,* E-conference.

3. George Alzeeb, *et al.*: 'Apoptosis, chemotherapy and metabolism: from 2D to a 3D gastric cancer model'. Journée d'animation scientifique de l'Axe Analyse Structurale et Métabolomique, BiogenOuest. *October 2020*, E-conference.

4. George Alzeeb, *et al.*: 'Apoptosis, chemotherapy and metabolism: from 2D to a 3D gastric cancer model'. 14èmes Journées du Cancéropôle Grand Ouest. *October 2020*, Angers-France.

5. George Alzeeb, *et al.*: 'Development of a flexible high-throughput 3D model'. IBSAM. *June 2021*, Brest-France.

6. George Alzeeb, *et al.*: 'Development of a flexible three-dimensional culture model: A focus on gastric cancer'. Workshop Imaging Organoids. *September 2021*, Bordeaux-France.

Poster communications

1. George Alzeeb, *et al.*: 'Mechanisms of gastric cancer suppression by taxanes and statins using a pluri-omics approach'. Second seasonal school of the Réseau Francophone de Métabolomique et Fluxomique junior. *November 2018*, Toulouse-France.

2. George Alzeeb, *et al.*: 'Mechanisms of gastric cancer suppression by taxanes and statins using a pluri-omics approach'. IBSAM. *June 2019*, Brest-France.

3. George Alzeeb, *et al.*: 'Modèle de culture en 3D du cancer gastrique : analyse des interactions physiques et biochimiques'. 13èmes Journées du Cancéropôle Grand Ouest. *July 2019*, Tours-France.

Titre : Développement d'un Modèle Cellulaire Flexible Tridimensionnel : Un Focus sur le Cancer Gastrique

Mots clés : Cancer gastrique, culture cellulaire en 3D, sphéroïdes, cytotoxicité, microscopie en 3D

Résumé : Le cancer gastrique (CG) est le cinquième cancer le plus fréquent dans le monde et est la quatrième cause de décès par cancer en 2020. Le pronostic du CG est mauvais et la plupart des formes avancées de la maladie sont incurables. Il est donc urgent de développer de nouvelles thérapies. Notre équipe a démontré que la combinaison de statine et de taxane induit fortement l'apoptose des cellules du CG en deux dimensions (2D). Néanmoins, la culture en 2D représente imparfaitement la complexité tissulaire, et en particulier le rôle des interactions entre cellules. L'une des stratégies qui permettent d'améliorer la réussite des nouveaux médicaments anticancéreux en clinique repose sur l'utilisation de modèles de culture cellulaire tridimensionnelle (3D). Ces modèles montrent un intérêt croissant dans la recherche sur le cancer, permettant de mieux rétablir certains des aspects fonctionnels des tumeurs. Nous avons ainsi généré des sphéroïdes monocellulaires de cellules cancéreuses gastriques humaines (HGT-1 ou AGS), ainsi que des sphéroïdes bicellulaires associant ces cellules à des fibroblastes issus de tumeurs (CAF, Cancer Associated Fibroblasts), selon une méthodologie robuste, qui prévient leur attachement à une matrice. Nous avons étudié la cytotoxicité induite par le docétaxel et la lovastatine (test MTT). De plus, nous avons utilisé le système d'imagerie et d'analyse en temps réel IncuCyteTM pour suivre la croissance des sphéroïdes et la réponse apoptotique. Ces tests ont montré une toxicité importante, majorée en cas d'association des deux molécules, comme observé en 2D. Nous avons entrepris l'analyse de l'organisation du modèle 3D bicellulaire par microscopie laser à deux photons. Nos résultats montrent une organisation distinctive des sphéroïdes bicellulaires selon la lignée de cellules épithéliales cancéreuses. Cette organisation pourrait s'expliquer par des différences de capacité migratoire / invasive des cellules de CG. Dans le cadre du programme européen GRAMMY, nous envisagerons une application de ces approches sur des organoïdes de tumeurs issues de patients.

Title : Development of a Flexible Three-Dimensional Culture Model: Focus on Gastric cancer

Keywords : Gastric cancer, 3D cell culture, spheroids, cytotoxicity, 3D microscopy

Abstract : Gastric cancer (GC) is the fifth most common cancer in the world and is the fourth leading cause of cancer death in 2020. The prognosis of GC is poor and most advanced forms of the disease remain incurable. It is therefore urgent to develop innovative therapies. Our team has demonstrated that the combination of statin and taxane strongly induces apoptosis of GC cells in two-dimensions (2D). Nevertheless, 2D culture imperfectly represents tissue complexity, and in particular the role of cell-cell interactions. One strategy to improve the success of new anticancer drugs in the clinic is the use of three-dimensional (3D) cell culture models. These models are of growing interest in cancer research, allowing to better restore some of the functional aspects of tumors. We have generated monocellular spheroids of human GC cells (HGT-1 or AGS), as well as bicellular spheroids associating these cells with cancer-associated fibroblasts (CAF), using a robust methodology, which prevents their attachment to a matrix. We studied cytotoxicity induced by docetaxel and lovastatin (MTT assay). In addition, we used the IncuCyteTM real-time imaging and analysis system to monitor spheroids growth and apoptotic response. These tests showed significantly increased toxicity when the two molecules were combined, such as was reported in 2D. In addition, we characterized the cellular distribution of the 3D bicellular model by bi-photonic microscopy. Our results show a distinctive formation of the bicellular spheroids as well as a specific spatial organization depending on the nature of the cancer epithelial cells. This distinctive organization could be explained by differences in the migratory/invasive potential between the two GC cell lines. As part of the GRAMMY European program, we will extend these approaches to patients' tumor organoids.